Industrialization of a dual-phase steel stamped component

Process optimization using AutoForm software

Maria Alexandre Cavaleiro Ferraz de Carvalho

Master Dissertation

Supervisors: Prof. Marco Paulo Lages Parente
Eng. João Carlos Matos de Sousa Pinto

U. PORTO
FEUP FACULDADE DE ENGENHARIA
UNIVERSIDADE DO PORTO

Master in mechanical engineering

June 2023

To my family

Industrialization of a dual-phase steel stamped component

Abstract

Both material and process developments in sheet metal forming technology are dependent on the fulfillment of frequently incompatible demands and requirements in car manufacturing: better performance with lower fuel consumption and less hazardous emissions, improved safety and comfort features, more complex geometries and tighter tolerances. In the last decade, two main fields have developed to meet these needs. On the one hand, significant developments were observed in the application of advanced high-strength steels, being dual-phase steels one of the best examples. On the other hand, new finite element analysis codes, like AutoForm, have been created and perfected to cope with the formability challenges that arise due to the use of these new materials as well as the ever-shorter lead times and ever-tighter tolerances.

In this work, an industrial case study that involves these two investigation areas was considered. The main objective is to identify a possible cause for a thinning defect (i.e., crack) appearing with an irregular pattern in a complex dual-phase steel automotive component and then suggest, simulate, and implement alterations in the tool to eliminate this problem. This component consists of two symmetrical parts that are produced simultaneously in an also symmetrical tool.

Firstly, the industrialization process of the component was studied. This process includes the project of the combined progressive tool as well as the control gauge, and also the simulation of the current manufacturing process using AutoForm R10 software. The results of the simulation include formability (wrinkling, thinning, edge cracks) and springback prediction.

Secondly, trying to identify a cause for the production problem and also to characterize the raw material, uniaxial tensile tests were performed on samples from both left and right sides of two different coils. The tests allowed to conclude that no significant differences exist between sides of the same coil. However, they indicated severe differences between coils, establishing a solid relation between mechanical properties (total elongation and strength) and formability. The samples from the coil that produced more cracked parts have lower total elongation and higher strength than those from the coil that produced fewer cracked parts. The experimental results were used to edit the material model.

Knowing that the mechanical properties could fluctuate, several alterations to the tool were analyzed, simulated, and implemented in order to make it work against these variations in the raw material. Satisfactory results were obtained with solution 3 (removal of extra 1 mm in the critical zone) having 2 out of 3 productions with 0 cracked parts. Since the simulation of this solution did not indicate any risk of rupture, it was decided to perform uniaxial tensile tests on samples from the coil of the third production. Total elongation turned out to be much lower than the admissible and yield strength above the acceptable.

Therefore, a fourth solution was proposed so that the tool would be even more robust. This solution consists in a deeper alteration to the tool, leaving extra material in the critical zone during the trimming process that is only removed after stamping. In this way, not only the simulation indicates no risk of rupture, but also if it eventually occurs during the stamping phase, the cracked zone is posteriorly removed. This solution is yet to be implemented. Lastly, considering the cost of this last solution, the resolution of the production problem is evaluated economically.

Keywords: Sheet metal forming, stamping, numerical simulation, finite element method, advanced high-strength steels, dual-phase steels, automotive industry, constitutive modelling, yield criteria, formability, AutoForm R10

Resumo

Os desenvolvimentos de materiais e processos na tecnologia de conformação de chapas metálicas dependem do cumprimento de requisitos frequentemente incompatíveis no fabrico de automóveis: melhor desempenho com menor consumo de combustível e emissões menos perigosas, recursos aprimorados de segurança e conforto, geometrias mais complexas e tolerâncias mais apertadas. Na última década, dois campos desenvolveram-se para atender a essas necessidades. Por um lado, foram observadas evoluções significativas na aplicação de aços avançados de alta resistência, sendo os aços *dual-phase* um dos melhores exemplos. Por outro lado, novos códigos de análise de elementos finitos, como o software AutoForm, foram criados e aperfeiçoados para lidar com os desafios de conformabilidade que surgem devido ao uso desses novos materiais, bem como com os prazos de entrega cada vez mais curtos e tolerâncias cada vez mais apertadas.

Neste trabalho, foi considerado um caso de estudo industrial que envolve essas duas áreas de investigação. O objetivo principal é identificar uma possível causa para um defeito de afinamento (uma fissura) que aparece com um padrão irregular num componente automóvel complexo fabricado num aço *dual-phase* e, posteriormente, sugerir, simular e implementar alterações na ferramenta para eliminar esse problema. Este componente consiste em duas peças simétricas que são produzidas simultaneamente numa ferramenta também simétrica.

Em primeiro lugar, foi estudado o processo de industrialização do componente. Este processo inclui o projeto da ferramenta progressiva combinada, bem como a maquete de controlo, e também a simulação do processo de fabrico atual usando o software AutoForm R10. Os resultados da simulação incluem conformabilidade (enrugamento, redução de espessura, *edge cracks*) e previsão de retorno elástico.

Em segundo lugar, tentando identificar a causa do problema de produção e também caracterizar o material, foram realizados ensaios de tração uniaxial em amostras dos lados esquerdo e direito de duas bobines diferentes. Os testes permitiram concluir que não existem diferenças significativas entre lados de uma mesma bobine. No entanto, indicaram grandes diferenças entre bobines, estabelecendo uma relação sólida entre as propriedades mecânicas (alongamento total e resistência) e a conformabilidade. As amostras da bobine que produziu mais peças fissuradas têm menor alongamento total e maior resistência do que aquelas da bobine que produziu menos peças com fissura. Os resultados experimentais foram usados para editar o modelo de material.

Sabendo que as propriedades mecânicas poderiam oscilar, diversas alterações à ferramenta foram analisadas, simuladas e implementadas a fim de torná-la robusta a essas variações na matéria-prima. Foram obtidos resultados satisfatórios com a solução 3 (remoção de 1 mm extra de material na zona crítica) já que em 2 de 3 produções não existiram peças fissuradas. Como a simulação desta solução não indicou risco de rutura, optou-se por realizar ensaios de tração uniaxial em amostras da bobine da terceira produção. O alongamento total revelou-se muito inferior ao admissível e a tensão de rotura acima do aceitável.

Assim, uma quarta solução foi proposta para tornar a ferramenta ainda mais robusta. Esta solução consiste numa alteração mais profunda da ferramenta para permitir deixar material extra na zona crítica durante o processo de corte que só é removido após a estampagem. Desta forma, não só a simulação indica que não há risco de rotura, como também caso esta ocorra durante a fase de estampagem, a zona fissurada é posteriormente removida. Esta solução ainda não foi implementada. Por fim, considerando o custo desta última solução, avalia-se economicamente a resolução do problema de produção.

Palavras-chave: Conformação plástica, estampagem, simulação numérica, método dos elementos finitos, aços avançados de alta resistência, aços *dual-phase*, indústria automóvel, modelos constitutivos, critérios de cedência, conformabilidade, AutoForm R10

Ackowledgements

First and foremost, I would like to express my gratitude to everyone in Gestamp Cerveira for the warm welcome and for their constant availability and patience. I deeply appreciate the opportunity and all the resources provided through the internship. A special thanks to my supervisor, Eng. João Pinto, and to my department colleagues, Eng. Tiago Rocha, Eng. Tiago Gomes, Eng. Pedro Mina, Eng. João Duro, and Eng. Miguel Docamiño.

To Professor Marco Parente thanks for the availability, support, suggestions, and critical spirit during the weekly meetings.

I would also like to thank Eng. Rui Silva from the LET laboratory in FEUP that conducted the experimental tests.

Finally, the present work would not be possible without the help and support of my family and friends. A special thanks to my mother, my father, my sister, and my four-legged friend for the everyday love, support, and precious moments throughout life.

Contents

1 Introduction........1
    1.1 Context and motivation........2
    1.2 Gestamp Cerveira........3
        1.2.1 Production Department........6
            1.2.1.1 Stamping........7
            1.2.1.2 Welding........8
        1.2.2 Tooling Department........9
        1.2.3 Quality Department........10
        1.2.4 Projects/Engineering Department........10
    1.3 Objectives........11
    1.4 Methodology........12
    1.5 Structure and layout........14

2 Technologies and materials........15
    2.1 Stamping technology........15
        2.1.1 Deformation modes........16
        2.1.2 Project of a stamped component........16
        2.1.3 Experimental strain analysis and forming limit curve........17
        2.1.4 Common defects........21
    2.2 Cutting technology........23
    2.3 Cutting and stamping tools........25
    2.4 Project of a strip for a progressive tool........28
    2.5 Dual-Phase steels........31
        2.5.1 Production........33
        2.5.2 Microstructure........34
        2.5.3 Groups and general properties........36
        2.5.4 Springback........36

3 Numerical modelling of sheet metal forming processes........39
    3.1 Constitutive material models........39
        3.1.1 Hardening behavior........40
        3.1.2 Yield criteria for anisotropic materials........42
            3.1.2.1 Anisotropy........43
            3.1.2.2 Principal of normality........44
            3.1.2.3 Yield criteria for isotropic material........45
            3.1.2.4 Yield criteria considering anisotropy........45
            3.1.2.5 Choice of yield criteria........46
    3.2 Simulation of cutting and stamping processes........47
        3.2.1 AutoForm presentation........49
        3.2.2 Implicit solution........50
        3.2.3 Finite elements........50
            3.2.3.1 Elasto-Plastic shell element........52
            3.2.3.2 Mesh refinement or adaptive mesh........53
            3.2.3.3 Adaptive time step........54
        3.2.4 Tools and support types........55
        3.2.5 Contact and friction........56
        3.2.6 Material generator and editor........57
            3.2.6.1 Hardening law........58
            3.2.6.2 Yield criterion........58
            3.2.6.3 Forming limit curve........59
        3.2.7 Formability results........60
            3.2.7.1 Formability and traditional FLC........60
            3.2.7.2 Advanced formability and advanced FLC........61
            3.2.7.3 Wrinkles and potential wrinkles........62
            3.2.7.4 Thickness variation........63
            3.2.7.5 Edge cracks........63
        3.2.8 Springback results........64

4 Industrialization of an automobile dual-phase steel component........67
    4.1 Description and characterization of the component........67
    4.2 Industrialization process of the component........69
        4.2.1 Feasibility study........70
            4.2.1.1 Study of the strip........70
            4.2.1.2 Simulation in AutoForm of current process........75
        4.2.2 Project of the tool........86
        4.2.3 Project of the control gauge........96

4.3 Problem in production 104

5 Experimental and numerical characterization of the material 107

5.1 Comparison between material models in AutoForm results 107

5.1.1 Barlat 89 107

5.1.2 Hill 48 108

5.1.3 Conclusions of the numerical characterization 109

5.2 Experimental characterization of the material 109

5.2.1 Comparison between sides of the same coil 111

5.2.2 Comparison between coils 113

5.2.3 True stress-strain curves and hardening law 114

5.2.4 Conclusions of the experimental characterization 115

5.3 Material model edition 117

6 Iterative numerical modelling and experimental implementation for problem solving 119

6.1 Solution 1: Removal of a label - experimental results 119

6.2 Solution 2: Smoothing radius - numerical and experimental results 120

6.3 Solution 3: Manufacturing new critical punches and dies on the right side - numerical and experimental results 122

6.4 Solution 4: New format with excess material in the critical zone for posterior 3D cutting – numerical results 125

6.5 Economical impact 126

7 Conclusions and future work 129

References 131

ANNEX A: Reference dates and respective achievements in Gestamp Cerveira's history 135

ANNEX B: General tolerances imposed by the client 137

ANNEX C: Results of the simulations of the current process considering the Hill 48 and the Barlat 89 yield criteria 139

ANNEX D: Experimental results 143

ANNEX E: Conditions and results of the uniaxial tensile tests from the coil used in the production of 3rd April 145

ANNEX F: Results of the numerical simulation with removal of 0.5 mm of material in the critical zone 149

Acronyms

AHSS	advanced high strength steels	**G/NG**	go/ no go
AFR	associated flow rule	**GUI**	graphical user interfaces
BCC	body-centered cubic	**HSLA**	high strength low alloyed
BEM	bending enhanced membrane	**HSS**	high strength steel
BH	bake hardening	**IF**	interstitial free steels
BIW	body-in-white	**MAG**	metal active gas
CAE	computer aided engineering	**MIG**	metal inert gas
CAL	continuous annealing line	**MUC**	material usage coefficient
$\boldsymbol{cof}$	coefficient of friction	**NAFR**	non-associated flow rule
CP	complex phase	**ND**	normal direction
CS	composite shell	**RD**	rolling direction
DFN	*définition numérique*	**TD**	transverse direction
DIC	digital image correlation	**TRB**	tailor rolled blank
DP	dual-phase	**TRIP**	transformation induced plasticity
EPS	elasto-plastic shell	**TS**	thick shell
FCC	face-centered cubic	**TWB**	tailor welded blank
FE	finite elements	**TWIP**	twinning induced plasticity
FEM	finite element method	**UAP**	*unidade autónoma de produção*
FLC	forming limit curve	**UTS**	ultimate tensile strength
FLD	forming limit diagram		

Nomenclature

A_t	total elongation
E	Young's modulus
e_0	initial thickness
e	final thickness
e	engineering strain
ε	true strain
$\varepsilon_1, \varepsilon_2, \varepsilon_3$	principal strains
ε_p	plastic strain
l_0	gage length or initial length
l_1, l_2	final length
r	Lankford or plastic anisotropic coefficient
r_b	biaxial anisotropic coefficient
R_m	ultimate tensile strength
R_c	shear strength
$Rp_{0.2}$	yield strength
S	engineering stress
σ	true stress
$\sigma_1, \sigma_2, \sigma_3$	principal stresses
σ_y	yield stress
ν	Poisson's ratio
Φ	yield condition

List of Figures

Figure 1 - Corporación Gestamp logos (Gestamp Cerveira 2023). 3
Figure 2 - Examples of products produced in Gestamp Cerveira (Gestamp Cerveira 2021). 4
Figure 3 - Evolution of human resources in Gestamp Cerveira (Gestamp Cerveira 2021). 4
Figure 4 - Certifications obtained by Gestamp Cerveira chronologically (Gestamp Cerveira 2021). 5
Figure 5 - Clients of Gestamp Cerveira (Gestamp Cerveira 2021). 5
Figure 6 - Evolution of billing in Gestamp Cerveira (Gestamp Cerveira 2021). 6
Figure 7 - Organization of the shop floor in Gestamp Cerveira (Gestamp Cerveira 2021). 6
Figure 8 - Spatial distribution of the UAP's (Gestamp Cerveira 2021). 7
Figure 9 - 1500 ton servo press in Gestamp Cerveira (Gestamp Cerveira 2023). 8
Figure 10 - Transfer tandem presses in Gestamp Cerveira (Gestamp Cerveira 2023). 8
Figure 11 - Welding equipment in Gestamp Cerveira (Gestamp Cerveira 2021). 9
Figure 12 - Remote welding cell (left) and hybrid welding cell (right) (Gestamp Cerveira 2023). 9
Figure 13 - Tooling department in Gestamp Cerveira (Gestamp Cerveira 2023). 9
Figure 14 - Quality department labs: metrology (left) and metallography (right) (Gestamp Cerveira 2023). 10
Figure 15 - Number of components analysed in the metrology lab (left) and metallography lab (right) (Gestamp Cerveira 2021) 10
Figure 16 - Gantt chart describing the tasks that must be done and their chronological distribution. .. 13
Figure 17 - Example of a simple stamping process (left) (Dias dos Santos, Ferreira Duarte, and Barata da Rocha 2005) and tool (right). 15
Figure 18 - Extension and expansion deformation modes (Dias dos Santos, Ferreira Duarte, and Barata da Rocha 2005). 16
Figure 19 - Grids for experimental analysis of deformations (Dias dos Santos, Ferreira Duarte, and Barata da Rocha 2005). 18
Figure 20 - Deformation of a circle into an ellipse. 18
Figure 21 - Plane stress state (Dias dos Santos, Ferreira Duarte, and Barata da Rocha 2005). 19
Figure 22 - Plane of principal stresses σ1, σ2 (Dias dos Santos, Ferreira Duarte, and Barata da Rocha 2005). 19
Figure 23 - Plane of principal strains ε1, ε2 (Dias dos Santos, Ferreira Duarte, and Barata da Rocha 2005). 20
Figure 24 - Forming limit curves (Bouaziz, Zurob, and Huang 2013), (Banabic et al. 2010). 21
Figure 25 - Defects of stamped parts (Gestamp Cerveira 2023) and (Dias dos Santos, Ferreira Duarte, and Barata da Rocha 2005). 22
Figure 26 - Cutting technology (Dias dos Santos, Ferreira Duarte, and Barata da Rocha 2003). 23
Figure 27 - Blanking (left) and punching processes (right) (Dias dos Santos, Ferreira Duarte, and Barata da Rocha 2003). 23
Figure 28 - Cutting surface analysis: distinction between pure shear and rupture in real part. 24
Figure 29 - Cutting surface analysis: distinction between crushed, pure shear and rupture in real part (Dias dos Santos, Ferreira Duarte, and Barata da Rocha 2003). 24
Figure 30 - Single (left), double (middle) and triple (right) acting tools (Dias dos Santos, Ferreira Duarte, and Barata da Rocha 2005). 25
Figure 31 - Simple tool for manual feeding in Gestamp Cerveira (Gestamp Cerveira 2023). 26
Figure 32 - Progressive tool and correspondent strip (Gestamp Cerveira 2023). 26

Figure 33 - Transfer mechanism (Gestamp Cerveira 2023). ... 27

Figure 34 - Typical zones of a strip: trimming (left), stamping (middle), and punching/separation (right) (Gestamp Cerveira 2023). ... 28

Figure 35 - Side rail with one sketch. ... 28

Figure 36 - Side rails. ... 29

Figure 37 - Central rails. ... 29

Figure 38 - Side and central rails. ... 29

Figure 39 - Rigid connection. ... 30

Figure 40 - Harmonium connections. ... 30

Figure 41 - Important distances to consider in a typical connection. ... 31

Figure 42 - Evolution and chronological appearance of some AHSS (Tisza and Lukács 2015). ... 31

Figure 43 - Overview of mechanical properties (tensile strength and elongation) of some steels (Granbom 2010). ... 32

Figure 44 - Usage of DP steels in a car (Granbom 2010). ... 32

Figure 45 - Typical microstructure of a DP steel (Granbom 2010). ... 33

Figure 46 - DP steel production line (Granbom 2010). ... 33

Figure 47 - Continuous annealing line and process temperature description in time (Granbom 2010). ... 34

Figure 48 - UTS of a DP steel as a function of martensite volume percentage and carbon content (Bouaziz, Zurob, and Huang 2013). ... 35

Figure 49 - Springback phenomenon (Tisza and Lukács 2015). ... 37

Figure 50 - Springback phenomenon in the same component made in DP600, DP800 and DP1000 (Peng, Koç, and Wenner 2008). ... 37

Figure 51 - Types of springback: angular change, twist and sidewall curl (Dezelak et al. 2014). ... 38

Figure 52 - Implementation complexity of different constitutive models with respect to the main purpose (Amaral 2020). ... 39

Figure 53 - Isotropic and kinematic hardening (Amaral 2020), (Banabic et al. 2010). ... 40

Figure 54 - Complex hardening behaviors during load reversal (Stadnicki and Wróbel 2015). ... 41

Figure 55 - Definition of the RD, TD and ND. ... 43

Figure 56 - Representation of stress and plastic strain increment direction applied to the von Mises yield surface (Amaral 2020). ... 44

Figure 57 - Different types of plastic flow directionality (Amaral 2020). ... 44

Figure 58 - Tresca and von Mises yield surfaces. ... 45

Figure 59 - Process flow before and after the use of numerical simulation. ... 48

Figure 60 – Generic triangular elements and its displacements. ... 51

Figure 61 - Refinement levels in AutoForm software. ... 54

Figure 62 - Refinement scheme in AutoForm software. ... 54

Figure 63 - Design process of FE models in AutoForm (Liao et al. 2015). ... 55

Figure 64 - Rectangular cup with uniform pressure (left), columns (middle) and with cushion pins (right). ... 56

Figure 65 - AutoForm material editor layout (Jadhav, Schoiswohl, and Buchmayr 2018). ... 57

Figure 66 - Input variables necessary to define the yield criteria models. ... 59

Figure 67 - Definition of the AutoForm parameter failure. ... 61

Figure 68 - Definition of the AutoForm parameter max failure. 61
Figure 69 - Visual explanation of the advanced forming limit curve concept. 62
Figure 70 - Color scale of the advanced forming limit curve. 62
Figure 71 - Definition of the AutoForm parameter wrinkles. 63
Figure 72 - Definition of the AutoForm parameter potential wrinkles. 63
Figure 73 - Necessary input parameters to determine edge cracks in AutoForm. 64
Figure 74 - Components from a project of a car model, highlighted those produced in Gestamp Cerveira and highlighted the component under study. 67
Figure 75 - Symbol that identifies a regulation part. 67
Figure 76 - Pair of parts of the component under study. 68
Figure 77 - Main dimensions of the RH component. 69
Figure 78 - Main dimensions of the sketch/format that will originate the stamped component. 71
Figure 79 - Optimal layout suggested by FormingSuite. 71
Figure 80 - Main dimensions of the strip and distances between parts. 72
Figure 81 - Main dimensions of the harmonium connections between the parts and the side rails. 72
Figure 82 - Resultant geometry after step 6. 73
Figure 83 - Resultant geometry after step 7. 74
Figure 84 - Resultant geometry after step 9. 74
Figure 85 - Resultant geometry after step 11. 74
Figure 86 - Resultant geometry after step 13. 75
Figure 87 - Resultant geometry after step 14 (final geometry). 75
Figure 88 - Complete stamping strip of this component. 75
Figure 89 – Hardening law (left), yield surface (middle) and FLC (right) of DP980. 77
Figure 90 - Sequence of AutoForm operation to model the manufacturing process of the component. 77
Figure 91 - Meshed geometries in each operation (left) and correspondent tool (right). 78
Figure 92 - Sequence of geometries obtained after each AutoForm operation. 79
Figure 93 - Dispersion of points over the FLC after operations F-30 (left) and F-40 (right). 79
Figure 94 - Advanced formability results after F-30. 80
Figure 95 - Advanced formability results after F-40. 81
Figure 96 - Final advanced formability results. 82
Figure 97 - Springback results after each operation. 83
Figure 98 - Geometries before and after springback in operations F-30 and F-40. 84
Figure 99 - Final deviation from the desired geometry. 84
Figure 100 - Complementary results: thickness variation, formation of wrinkles, and edge cracks. 85
Figure 101 - Existing defects in the stamped parts. 86
Figure 102 - General sectors of the stamping tool: trimming zone and stamping/punching/separation zone. 87
Figure 103 - Main dimensions of the tool in bottom dead center. 88
Figure 104 - Lower shoe of the tool. 89
Figure 105 - Lifter plate, gas spring, and start line. 89

Figure 106 - Trim dies and die retainer. 90
Figure 107 - Dies present in the tool and focus on the compensated stamping die. 91
Figure 108 - Step sensor. 91
Figure 109 - End of strip sensor. 92
Figure 110 - Type holders. 92
Figure 111 - Strip guides. 92
Figure 112 - Scrap guides. 93
Figure 113 - Lower tool. 93
Figure 114 – Stripper plate. 94
Figure 115 - Trimming punch (cuts critical zone). 94
Figure 116 - Punches present in the tool. 95
Figure 117 - Pilot. 95
Figure 118 - Upper tool. 95
Figure 119 - Orientation of the component in the control gauge. 96
Figure 120 - Identification of the references fixing and positioning points. 97
Figure 121 - Location tolerance (eMachineShop n.d.). 97
Figure 122 - Surface tolerance (GD&TBasics n.d.). 98
Figure 123 - Flatness tolerance (GD&TBasics n.d.). 98
Figure 124 - Holes to be analysed. 98
Figure 125 - Areas to be analysed. 100
Figure 126 - Control gauge for a first quality control of the components. 102
Figure 127 - Closer look at some control gauge details. 103
Figure 128 - Pin gauges used to control dimension and position. 103
Figure 129 – Close look at the cracks that appear in the component under study. 104
Figure 130 - Location of the crack in the component. 104
Figure 131 - Smoothened radii implemented as an attempt to reduce the cracks. 105
Figure 132 - Attempt to eliminate the cracks by approximating geometry resultant from the first stamping to the final geometry. 106
Figure 133 - Advanced formability final results using the Barlat 89 material model. 107
Figure 134 - Dispersion of the critical points over the FLC considering the BBC 2005 (left) and the Barlat 89 (right) criteria. 108
Figure 135 - Advanced formability final results using the Hill 48 material model. 108
Figure 136 - Dispersion of the critical points over the FLC considering the BBC 2005 (left) and the Hill 48 (right) criteria. 109
Figure 137 - Dimensions of the specimens (left) and group of specimens before testing (right). 110
Figure 138 - Uniaxial tensile test machine used. 111
Figure 139 - Experimental results that compare the left and right sides of the two coils. 112
Figure 140 - Experimental results that compare both coils from specimens of the same side. 113
Figure 141 - True stress-strain curves from the current model and obtained in the experimental tests. 114
Figure 142 - Tested specimens after rupture. 115

Figure 143 - True stress-strain curves from the current model, the obtained in the experimental tests and the new approximation model. 117

Figure 144 - Label located in the critical zone removed as an attempt to eliminate the cracks. 119

Figure 145 - Second stamping punch with highlighted smoothened radius in the critical zone as an attempt to eliminate the cracks. 120

Figure 146 - Advanced formability results and points over the FLC according to new geometry with smoothened radius. 121

Figure 147 - New sketch geometry cutting more material than necessary as an attempt to eliminate the cracks. 122

Figure 148 - Advanced formability results and points over the FLC according to new sketch geometry. 123

Figure 149 - New sketch geometry leaving extra material than necessary for posterior 3D cutting as an attempt to eliminate the cracks. 125

Figure 150 - Best studied location to implement 3D cutting tools. 125

Figure 151 - Advanced formability results and points over the FLC according to defined solution 4. 126

Figure B 1 - General tolerances imposed by the client. 137

Figure C 1 - Edge crack results of the simulation of the current process considering the Hill 48 yield criterion. 139

Figure C 2 - Thickness results of the simulation of the current process considering the Hill 48 yield criterion. 139

Figure C 3 - Springback results of the simulation of the current process considering the Hill 48 yield criterion. 140

Figure C 4 - Edge crack results of the simulation of the current process considering the Barlat 89 yield criterion. 140

Figure C 5 - Thickness results of the simulation of the current process considering the Barlat 89 yield criterion. 141

Figure C 6 - Springback results of the simulation of the current process considering the Barlat 89 yield criterion. 141

Figure D 1 - Results of the uniaxial tensile tests on the specimens from group A. 143

Figure D 2 - Results of the uniaxial tensile tests on the specimens from group B. 143

Figure D 3 - Results of the uniaxial tensile tests on the specimens from group C. 144

Figure D 4 - Results of the uniaxial tensile tests on the specimens from group D. 144

Figure E 1 - Dimensions of the specimen for the uniaxial tensile tests according to NP EN ISO 6892-1. 145

Figure E 2 - Uniaxial tensile tests machine. 145

Figure E 3 - Results of the uniaxial tensile tests performed in Gestamp during the iterative problem-solving phase. 146

Figure E 4 - Specimens after rupture. 147

Figure F 1 - Advanced formability results and dispersion of points over the FLC with removal of 0.5 mm of material in the critical zone. 149

List of Tables

Table 1 - Operations performed in each UAP. 7

Table 2 - Stamping presses available in Gestmap Cerveira. 7

Table 3 - Basic mechanical properties of some DP steels (ArcelorMittal n.d.) 36

Table 4 - Chemical composition of DP980. 68

Table 5 - Chemical composition of the coating. 68

Table 6 - Basic mechanical properties in RD of DP980. 68

Table 7 - Simulation parameters to input in AutoForm. 76

Table 8 - Parameters for the BBC 2005 model to characterize the yield surface of DP980. 76

Table 9 - Necessary forces for each operation. 86

Table 10 - Tolerances to be controlled when analysing the holes. 99

Table 11 - Tolerances to be controlled when analysing the areas. 101

Table 12 - Components of the control gauge. 102

Table 13 - Attempts to reduce the cracks until the beginning of this study. 106

Table 14 - Parameters for the Barlat 89 model to characterize the yield surface of DP980. 107

Table 15 - Parameters for the Hill 48 model to characterize the yield surface of DP980. 108

Table 16 - Test parameters. 110

Table 17 - Average mechanical properties obtained in the experimental results. 115

Table 18 - Swift/Hockett-Sherby parameters that approximate the worst-case scenario from the tests. 117

Table 19 - Important coefficients for the definition of the yield criteria. 118

Table 20 - Cracked parts obtained in the production of 15th Feb after implementation of solution 1. 120

Table 21 - Cracked parts obtained in the production of 6th Mar after implementation of solution 2. . 122

Table 22 - Cracked parts obtained in the production of 3rd Apr, 26th Apr and 15th May after implementation of solution 3. 124

Table 23 - Mechanical properties of the coil from production of 3rd April. 124

Table A 1 - Reference dates and respective achievements in Gestamp Cerveira 135

Table E 1 - Conditions of the uniaxial tensile tests. 146

1 Introduction

Over the past few years, a great technological revolution has been verified in all industry sectors. Nowadays, technological solutions spread quickly and industries evolve faster. The automotive sector, in particular, is very active in innovation due to the competition and the growing legal requirements and costumer demands. Moreover, this sector is the leading sector in many countries, having a huge weight in their economies.

The growing demand on lower fuel-consumption, safety, comfort, and ever reducing emission standards has been challenging vehicle development programs in almost all automotive companies, promoting an increase in productivity and a reduction in costs (Tisza and Lukács 2014). There are two major working areas in this field: the development of new materials and virtual manufacturing software. Both strategies attempt to improve the quality of the products and reduce the lead times.

Researchers used to state that the steels in the automotive industry would progressively be substituted by lighter metals like aluminum or even composites. And if it is true that a lighter structure is pursued, it is also a fact that new alternatives have been found in the world of steels keeping these as preferred by the majority of car manufacturers. The use of lightweight and high-strength materials is definitely one of the ways of practically handling improved fuel-economy requirements in developing auto-bodies with efficient crash-energy management (Ozsoy et al. 2014).

Contrary to what could be expected, the increasing implementation of advanced high strength steels (AHSS) should be mentioned first among recent material developments. They offer a practical means of reducing the vehicle's overall body weight while preserving structural stiffness and integrity. In many structural members, conventional steel grades have been supplanted with their AHSS counterparts over the past decade (Ozsoy et al. 2014).

As it was stated by Bouaziz et al. (2013), safety, lightening and formability are the three main driving forces that compose the logic of development of the automotive industry, namely new materials and consequently new features in sheet metal forming, the most important manufacturing process in this sector.

Regarding safety, it is known that there is a growing demand on safety. Compared to the conventional low strength steels, the components produced with AHSS can absorb greater kinetic energy from an accident and deter incursion better. To characterize the energy absorption and anti-intrusion capabilities of the materials, several statistical analysis of crash test results had to be performed.

The term lightening describes the process of reducing the weight of a component by using a thinner segment of steel with a higher yield or tensile strength. The requirement to lower CO_2 emissions ultimately drives lightening, which translates into the necessity to achieve outstanding crash performance with little additional vehicle weight.

Lastly, regarding formability, before the newly created steels are used in the automotive sector, they must first be shaped into potentially complex pieces, most of the times by stamping at room temperature. In the automobile sector, the idea of a forming limit diagram (FLD) or forming limit curve (FLC) has been established to evaluate the formability of a specific material. The range of permissible plastic strains that the material can experience without any localized necking is defined by these diagrams. Only below the critical strains outlined by the FLD can successful formation take place (Bouaziz, Zurob, and Huang 2013).

In spite of the great combination of characteristics that these new materials possess regarding strength and lightness, the increasing use of AHSS in sheet metal parts raises formability and shape distortion problems that cannot be easily solved compared to stamping processes with conventional highly formable steel grades. The relatively high strength-to-elastic modulus ratio of AHSS is considered to be one of the main factors leading to difficulties to achieve a defect-free stamped part within desired dimensional tolerances (Ozsoy et al. 2014).

The increased springback that occurs during the forming of high strength steels is one of the most significant technological challenges in the design and manufacture of sheet metal components with the necessary shape and dimensional accuracy (Tisza and Lukács 2014).

Complementing the development and implementation of these new materials and dealing with the challenges that they raise, the other major technological breakthrough is the development of new software that simulates the stamping process. A tool that is now constantly being used to deal with design problems related to the use of these new steels and to reduce the developing times is finite element (FE) simulation. By using special developed software for stamping processes, such as AutoForm, the manufacturing process of the stamped components can be simulated and optimized, making sure that the tools are designed to compensate springback and that the number and type of operations are suitable to the machinery available, always assuring the parts' dimensional and geometrical integrity. By using these powerful tools engineers avoid the old trial-and-error methods driven by experience that were used in the development of tools and new designs.

Explicit or implicit solution techniques, sophisticated plasticity models, and new breakthroughs in element technology are some of the hotspots in this area. The influence of numerical parameters and modelling techniques has been well understood, and with the accomplished developments in cyclic plasticity modelling, very accurate springback predictions were also obtained for various sheet metal geometries.

A lot of research has been made in constitutive models in other to accurately predict sheet metal forming processes. Industrially, to avoid more intricate material testing to determine the model parameters, libraries frequently include trustworthy models of a range of materials. The software libraries are highly helpful in this regard (Ozsoy et al. 2014).

Following the tendencies in these two broad fields of investigation, the car industry must quickly adapt itself and take advantage of this knowledge to solve the daily problems in order to save money and be more competitive. The project that led to this dissertation is a combination of these two topics. It involves a dual-phase (DP) steel stamped component and the use of AutoForm, a FE simulation software to solve as soon as possible a recurrent defect that is appearing during that components' production.

1.1 Context and motivation

Gestamp Cerveira, Lda. is a company that produces metallic cold stamped parts for several car manufacturers in the automotive industry. Therefore, it is in direct contact with the presented innovation and consequent challenges of this very competitive sector, namely the growing safety and environmental requirements that lead to a light-weight design using new materials. In parallel with these new challenges, new finite element simulation tools are used in the company, as in the sector, in order to provide a faster, cheaper and more accurate design.

When Gestamp Cerveira is contacted by a client or possible client to produce a new component, the engineers in the engineering department are responsible to make an offer. After negotiations, if the component is adjudicated to Gestamp, the engineers from the same department begin the industrialization process. This process is long and laborious and it ends when the stamping tool and control gauge are ready, tested, validated and handed to the production department to begin series production.

However, even after the end of the industrialization process, the engineering department may be called to solve problems related to the production of the parts. One of these problems can be the appearance of cracks or other defects. The sooner these defects are spotted the better.

Nevertheless, in the worst-case scenario, they can be detected only by the client, leading to claims, and damaging the image of the company.

This dissertation is the result of a study made in Gestamp Cerveira precisely about a crack that was only detected by the client and only after about six months of being in production. The parts where these cracks appeared are very complex and they are made in pairs, i.e., at each stroke of the combined progressive tool it comes out a pair of symmetrical parts, a left and a right. The tool in which these parts are made is, therefore, also symmetrical. The cracks appear with an irregular pattern, with different frequencies depending on the coil used, and apparently more frequently on the right-hand part.

Despite the possible responsibility of the coil's supplier, these types of problems are usually solved inside the company, acting on the tool to make it more robust and proof against small variations in sheet properties.

The appearance of defects, including the cracks in these parts, are never economically good for the company because once they start appearing and until it is proven that the problem is solved it is necessary to verify those parts one by one when leaving the press and again before shipping, called the classification stage.

The engineering department and the company responsible for the project of the tool were called to intervene and suggest solutions for the problem. These solutions have been sequentially implemented each time the part is in production.

Therefore, the aim of this dissertation is to understand and describe the industrialization process that led this particular component to production. This includes following the growing trend in the use of simulation tools, simulating the actual stamping process of the part using AutoForm, a stamping specialized finite element method (FEM) software used in the company. For this simulation it is necessary to model the material properly, a DP980 steel. Finally, after trying to identify the cause of the cracks using uniaxial tensile tests, numerical simulations were conducted, to test alternative solutions to minimize the risk of defects. If the rejection rate decreases, it is also an objective to estimate the economical savings for the company.

1.2 Gestamp Cerveira

Gestamp Cerveira is part of the Spanish group Corporación Gestamp. Three main companies are part of this group: Gonvarri Steel Industries, Gestamp Automoción and Gestamp Renewables, whose logos are represented in Figure 1. Their main activities are the production of steel, the production of metallic components for the automotive industry, and renewable energies, respectively. There is also another company related to the group called Gescrap that is responsible for the transportation and management of the scrap produced in the stamping factories of the group.

Figure 1 - Corporación Gestamp logos (Gestamp Cerveira 2023).

Gestamp Cerveira, specialized in stamping and welding, is one of the factories that are part of Gestamp Automoción which is responsible for more than 100 factories present in 24 countries. Its main activity consists in the production of body-in-white (BIW), chassis and mechanisms to be used in cars and its main objective, in line with the objective of the automotive industry in general, is to reduce the weight of the vehicles assuring the quality and safety of the components. Some examples of the components produced in Gestamp Cerveira are represented in Figure 2.

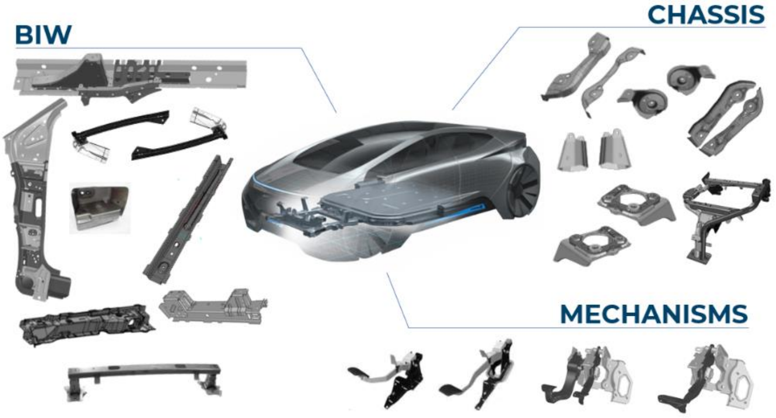

Figure 2 - Examples of products produced in Gestamp Cerveira (Gestamp Cerveira 2021).

This factory, located in Vila Nova de Cerveira, is extremely close to the northern border of Portugal. At the early stages of its development, from 1995 until 2008, Gestamp Cerveira (called Gestamp Portugal until 2013) was dependent on Gestamp Vigo. In 2008, after intern reorganization and the creation of the necessary departments, the factory became completely independent and autonomous, with independent administration and decision making. However, the relationship between the two factories remains close. In 2013, the name of the factory became Gestamp Cerveira instead of the old Gestamp Portugal since by that time there were already three Gestamp factories in Portugal: in Vila Nova de Cerveira, Vendas Novas and Aveiro.

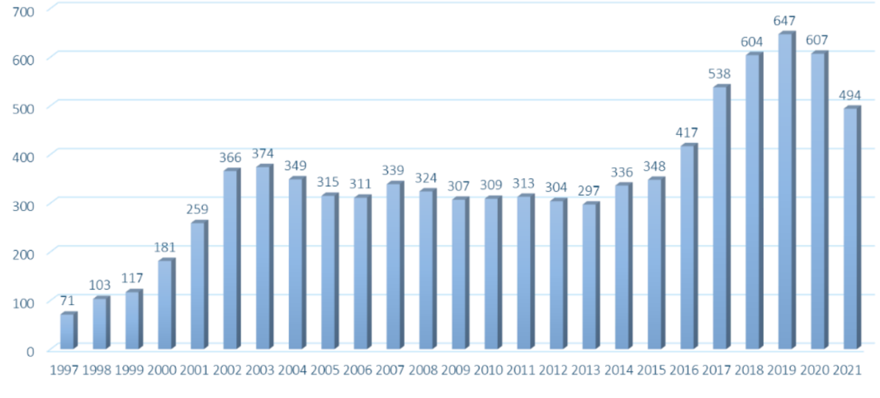

Figure 3 - Evolution of human resources in Gestamp Cerveira (Gestamp Cerveira 2021).

The evolution of the human resources is shown in Figure 3. By 2019, 647 people worked in Gestamp Cerveira. Due to the COVID-19 pandemic, by 2021 this number was reduced to 494 people. In spite of this reduction, this factory still plays an important role in the economy of the region. From the 494 workers, 44% are women and 56% are men.

This factory has been given certifications over the years as it can be seen in the diagram of Figure 4. Some of these are: ISO 9001, ISO/TS 16949, ISO 14001, EMAS, “Resíduo Zero” AENOR, and ISO 45001 certifications in the areas of health and safety, quality, and environment. It was also given the “Best Plant” prize by PSA– Peugeot Citröen S.A. (now Stellantis) in 2014, 2015, 2016 and 2017 (Gestamp Cerveira 2022).

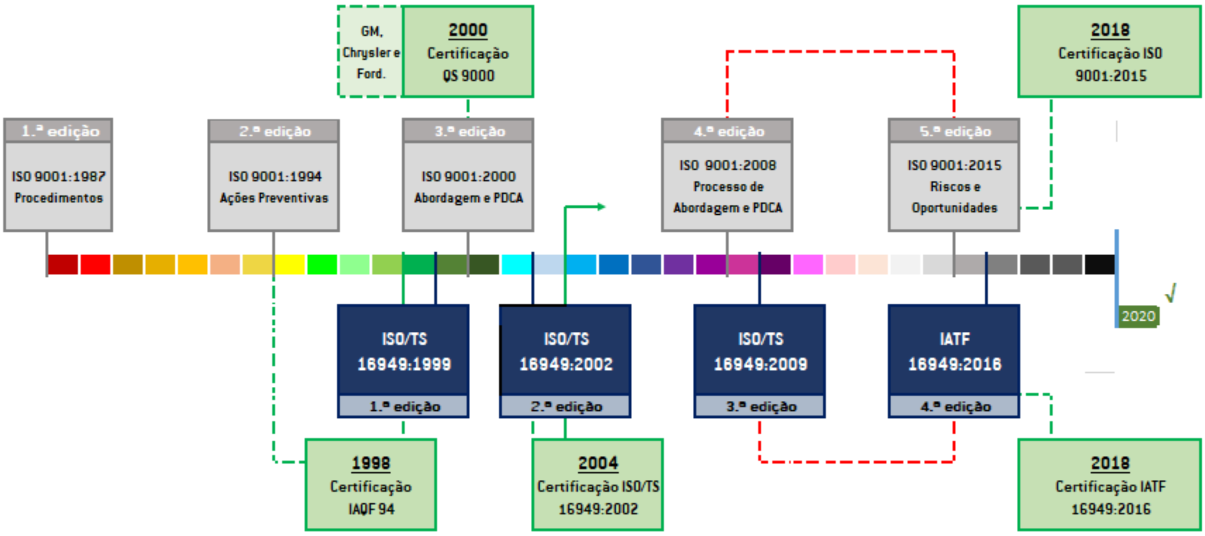
GM, Chrysler e Ford.
2000 Certificação QS 9000
2018 Certificação ISO 9001:2015
1.ª edição ISO 9001:1987 Procedimentos
2.ª edição ISO 9001:1994 Ações Preventivas
3.ª edição ISO 9001:2000 Abordagem e PDCA
4.ª edição ISO 9001:2008 Processo de Abordagem e PDCA
5.ª edição ISO 9001:2015 Riscos e Oportunidades
ISO/TS 16949:1999 1.ª edição
ISO/TS 16949:2002 2.ª edição
ISO/TS 16949:2009 3.ª edição
IATF 16949:2016 4.ª edição
2020
1998 Certificação IAQF 94
2004 Certificação ISO/TS 16949:2002
2018 Certificação IATF 16949:2016

Figure 4 - Certifications obtained by Gestamp Cerveira chronologically (Gestamp Cerveira 2021).

The main achievements and important marks in the history of Gestamp Cerveira are chronologically ordered and briefly described in Table A1 in Annex A.

The clients of Gestamp Cerveira can be classified as intern or extern. They respectively correspond to other Gestamp factories and other non-Gestamp factories such as Stellantis (former PSA), Renault/Nissan, Volkswagen, and others. The share of parts produced for each main client in the factory is exposed in Figure 5. It can be seen that a significant share of the production in Gestamp Cerveira does not go directly to the final client that assembles cars. In fact, 24% of this production goes to intern clients, i.e., other factories of the group Gestamp, to undergo other manufacturing or joining process.

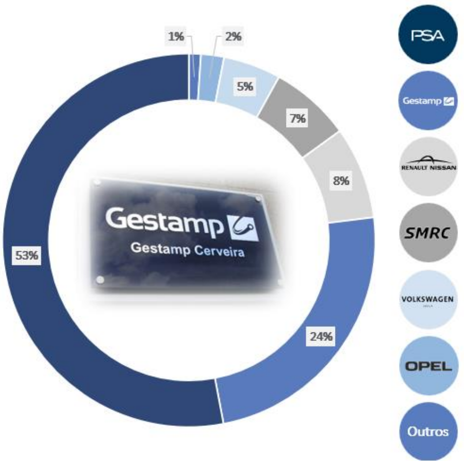

Figure 5 - Clients of Gestamp Cerveira (Gestamp Cerveira 2021).

Regarding billing, Gestamp Cerveira has constantly evolved reaching the highest billing volume in 2019 as it is stated in Figure 6. The decay in the following years is justified by the consecutive stops in the production due to the pandemic.

Regarding the layout of the factory, it is divided in three main sectors, called “naves”. The chronologically first sector, called “Nave 1”, is essentially dedicated to stamping processes, it is here where all the presses are located. However, one of the four production lines in this sector

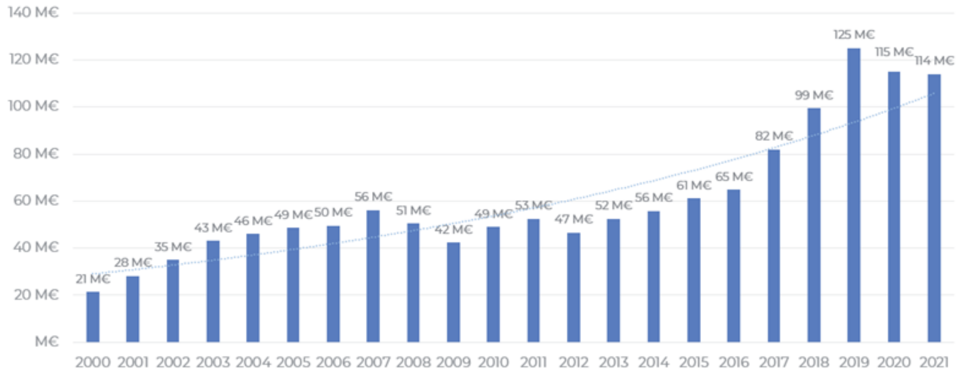

Figure 6 - Evolution of billing in Gestamp Cerveira (Gestamp Cerveira 2021).

is dedicated to welding, mainly resistance spot welding. Most part of the welding processes take place in “Nave 2”, namely manual welding using electrodes and robotized Metal Inert Gas/ Metal Active Gas (MIG/MAG) processes. In “Nave 3” are located some welding cells and the classification area.

The offices are located on the first floor of the building, and they are divided according to the different departments: projects/engineering, sales, financial, human resources, IT and management. The departments of logistics, quality, production, tooling, and maintenance are located on the shop floor. The organization of the factory that was just described is presented graphically in Figure 7.

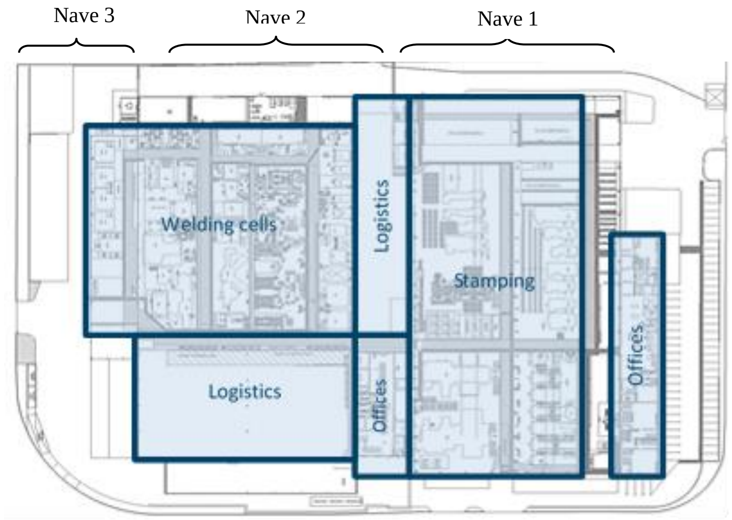

Figure 7 - Organization of the shop floor in Gestamp Cerveira (Gestamp Cerveira 2021).

1.2.1 Production Department

The production department is responsible to follow the projects in series production regarding scheduling the components that will be produced each day in each machine and dealing with problems in the machines. It is also responsible to manage the people working in each machine as well as their absence.

Spatially it is divided in eight production units called *Unidades Autónomas de Produção* (UAP) distributed as in Figure 8. The operations of stamping, welding and assembly of pedals are distributed by the UAP's according to the Table 1.

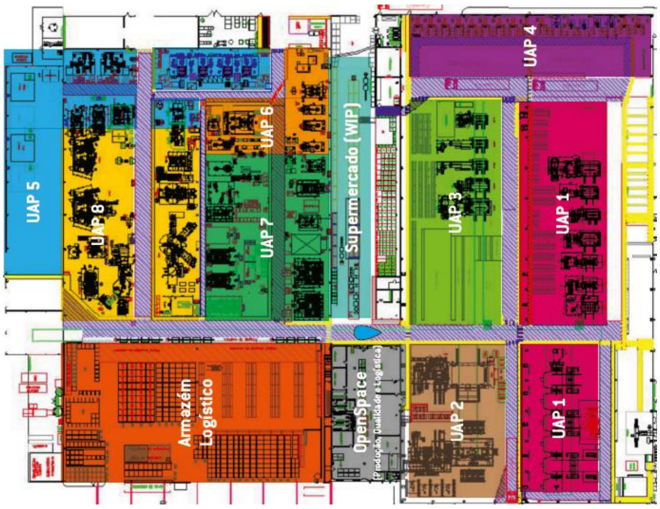

Figure 8 - Spatial distribution of the UAP's (Gestamp Cerveira 2021).

Table 1 - Operations performed in each UAP.

UAP	***Operations***
1, 2 and 3	Stamping processes
4	Manually fed welding cells (mainly resistance)
6	Assembly of pedals
5, 7 and 8	Welding cells (manual shielded metal arc welding, MIG/MAG automatized and robotized welding processes)

1.2.1.1 Stamping

Regarding the stamping processes, the factory possesses different types of mechanical presses that can be used according to the characteristics of the parts to be produced.

A press is a machine responsible for providing a tool, whose upper clamping shoe is fixed to the press slide, with the energy necessary for processes of sheet metal forming. This type of machine tool is characterized by its nominal force, which can be expressed in tons. They are essentially constructed by two parts: a structure or body and a movable system that animates one or more slides with an alternative linear movement that carries the upper part of the tool. In general, in a mass production environment mechanical presses are preferred since they allow faster operations. Therefore, there are manual, transfer, progressive and transfer tandem presses in the quantities shown in Table 2.

Table 2 - Stamping presses available in Gestmap Cerveira.

Press	***80 ton***	***125 ton***	***250 ton***	***300 ton***	***400 ton***	***630 ton***	***1250 ton***	***1500 ton***
Manual	1	1		2				
Progressive			3		4	3	1	2
Transfer						1		
Tandem				6				

The 1250 and 1500 ton presses can be adapted to work as progressive or transfer presses. The 1500 ton presses, one of them presented in Figure 9, are servo presses which means that they are driven by a servo motor, as opposed to a standard flywheel, clutch and brake. This allows for full power at any speed, but not at any point in the stroke (capacity is best near bottom dead center). Applications like metal forming that call for a variable slide velocity at various locations in the stroke profile are perfect candidates for servo presses. A servo press additionally offers a higher production volume compared to a hydraulic press. On a servo press, every stroke profile is entirely configurable as well (Stamtec n.d.).

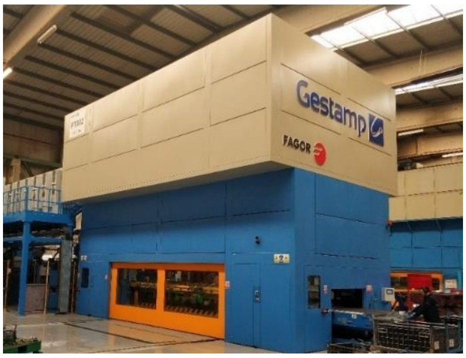

Figure 9 - 1500 ton servo press in Gestamp Cerveira (Gestamp Cerveira 2023).

The six transfer tandem presses are all implemented in the same robotized line of production (Figure 10) where an operation is performed in each press, after which the part is transferred to the next press by a robot.

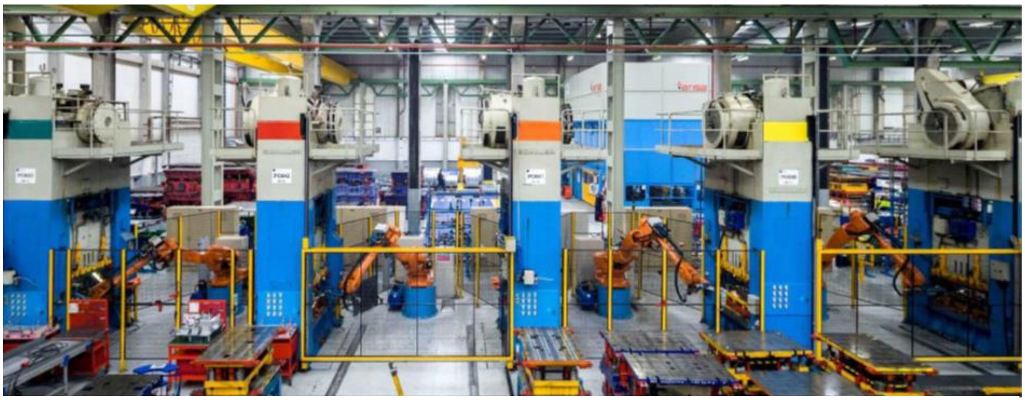

Figure 10 - Transfer tandem presses in Gestamp Cerveira (Gestamp Cerveira 2023).

With the existent equipment it is also possible to perform operations like automatic threading in press, automatic welding in press, stamping of aluminum parts, and Tailor Rolled Blank (TRB) and Tailor Welded Blank (TWB) parts, that respectively represent parts where the initial blank is shaped to have different thicknesses in the final component and parts that are obtained from different thicknesses formats welded together.

1.2.1.2 Welding

When it comes to the welding processes, Gestamp Cerveira also has a wide range of machines and equipment that allow manual or automated work to be performed, as it can be seen in Figure 11.

There are nine available welding cells that perform MIG/MAG and twelve cells that perform resistance spot welding. In these cells the welding processes are automatic. Nevertheless, it is also possible to perform these operations (resistance and MIG/MAG) manually.

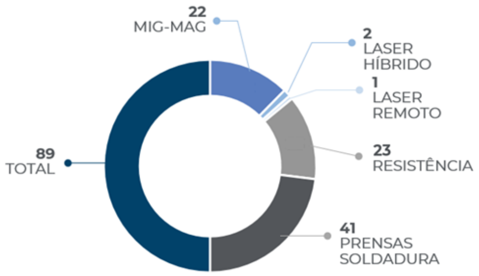

Figure 11 - Welding equipment in Gestamp Cerveira (Gestamp Cerveira 2021).

Besides these processes, it is also possible to perform laser welding operations either in a remote cell (left) or in a hybrid cell (right), Figure 12.

Attempting to better assess the welding beads, Gestamp Cerveira also possesses equipment in the quality department with high precision cameras that precisely analyze the beads and avoid that defective parts get to the client.

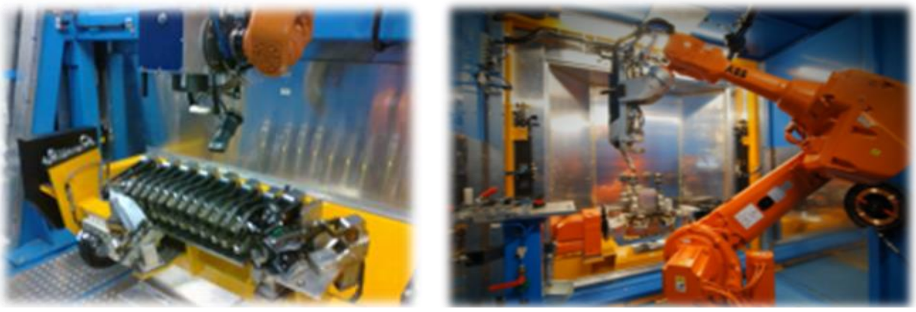

Figure 12 - Remote welding cell (left) and hybrid welding cell (right) (Gestamp Cerveira 2023).

1.2.2 Tooling Department

This department is responsible for all maintenance and repair of the tools, containing various types of processes, such as electro-erosion, manual and CNC turning, milling and grinding.

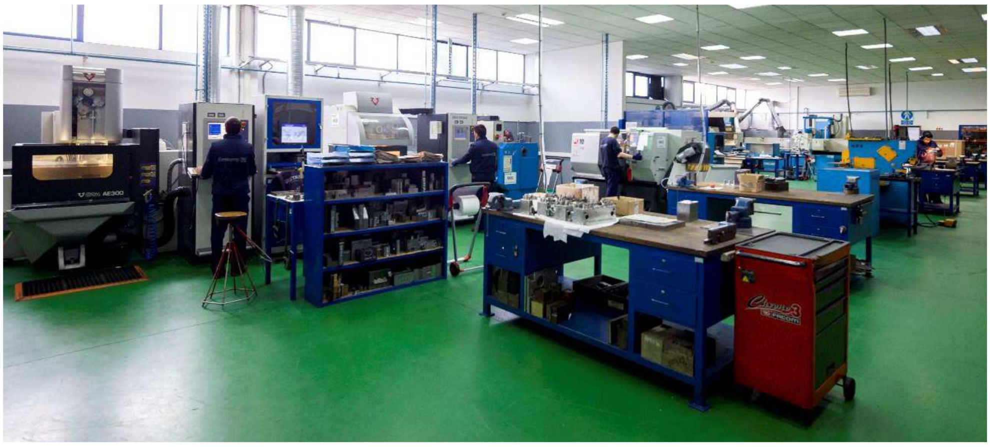

Figure 13 - Tooling department in Gestamp Cerveira (Gestamp Cerveira 2023).

For that purpose, in this department three electro-erosion machines can be found as well as three CNC, three automatic grinding and three turning machines (one CNC and two manual). Besides these machines used for cutting, machining, and finishing, there is also a small installation to perform heat treatments and a cleaning unit.

1.2.3 Quality Department

To evaluate the quality of the components it produces, Gestamp Cerveira has in its quality department instruments that allow the study and improvement of components. Some of these instruments are three 3D measuring machines (metrology laboratory), which are focused on measuring the components with great precision and compare them with the original project. It also has a laboratory for metallographic analysis (macrographs and micrographs), focused in analyzing welding beads, three ultrasonic testing machines, a destructive testing machine, as well as a reverse engineering tool.

Figure 14 - Quality department labs: metrology (left) and metallography (right) (Gestamp Cerveira 2023).

In Figure 15, it can be seen that both the number of components measured (done and programmed) and number of welding beads analyzed have been increasing (data was collected until mid 2018), demonstrating an increasing concern with the quality of the components sent to the client.

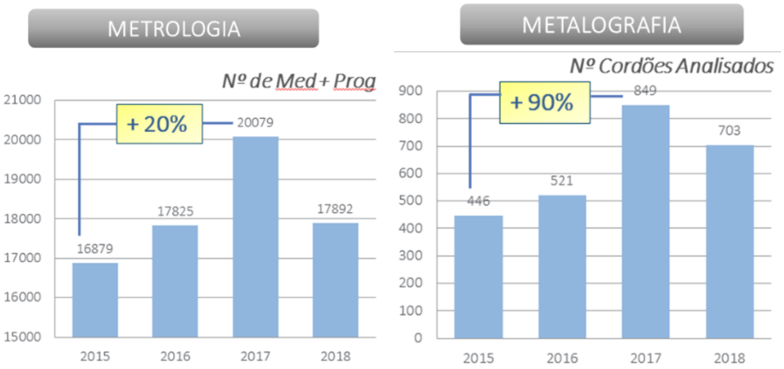

Figure 15 - Number of components analysed in the metrology lab (left) and metallography lab (right) (Gestamp Cerveira 2021)

1.2.4 Projects/Engineering Department

This dissertation was developed in the engineering department of the company. This department is responsible for the budgeting and industrialization process of the components produced in the factory. Being also responsible for accompanying the components in production, it is one of the departments called to solve problems when defective parts are found. Furthermore, it also studies and implements alterations in the components and technical economic savings, always trying to achieve better results with less costs.

When a client contacts Gestamp Cerveira to produce a certain part, the first analysis is done by this department. The engineers are responsible to check if the part is feasible or not through simulations of the stamping process using AutoForm and former experience. This first study also involves the study of the productive process through the project of the strip (a diagram that represents the sheet through the several stages of the stamping process). This process is important to define the size of the tool and the coil, the forces involved (that determine which press has to be used) and the number of workers needed. After this study, this department is responsible for making an offer to the client.

Then, if the client adjudicates this part to Gestamp Cerveira, this department is also responsible to project and adjudicate the tool and control gauge based on the geometry and tolerances.

1.3 Objectives

This work was mainly developed in Gestamp Cerveira. Being a dissertation written in industrial environment the main objective was to develop a complete, organized and useful study that could contribute for the success of the project and consequently help the company. Therefore, the main objective was to reduce or eliminate the appearance of cracks in the studied stamped part bringing economical savings to the company. To achieve this, several tasks were taken.

This industrial environment presents some extra challenges in the first place. So, the first task in the beginning of the internship was to deeply understand the company's structure, processes, clients, suppliers, organization, and the people that make everything work.

The project assigned to this dissertation had been concerning the engineers in the engineering department for some time. After being in production for about six months, a DP980 steel stamped component was currently giving problems since a crack was being found in some parts with a very irregular frequency. Some attempts had already been made to try to fix the problem, but none had been successful.

To fulfil the main objective of this thesis, the tasks or steps that were taken during this work were:

- Understand the complexity of stamping and cutting technologies and the working principles of the progressive combined tools.
- Identify the advantages and disadvantages of dual-phase steels, their composition, production, and main properties.
- Study the existing constitutive models to characterize the behavior of materials in general and particularly dual-phase steels in stamping processes, mainly regarding hardening, yield criteria considering anisotropy and formability.
- Understand the FEM software used in the company to simulate stamping processes – AutoForm. Be aware of its limitations and benefits. Study the implicit method, type of elements, material models available, possible output results, etc.
- Deeply understand, analyze, and describe the several steps of the industrialization process of a complex cold stamped DP980 component for the automotive industry, analyzing the strip, tool, and control gauge.
- Apply AutoForm in the simulation of the stamping process of the component whose industrialization process was described.
- Experimentally characterize the material used in real productions of this component and look for differences between both sides of the same coil and between different coils.
- Closely follow the productions of the component under study.
- Study possible alterations to the format or the tool to minimize the risk of splits using the software.
- Implement some of the alterations studied.
- Perform an economic analysis that states the impact of eliminating the cracks found.

1.4 Methodology

As it was said before, since this dissertation is developed in an industrial environment, the first weeks require a deep understanding of the company, namely its processes, clients, suppliers, departments, organization, and people in general.

After that, an even deeper knowledge of the engineering department must be gained. During this stage, the recent projects and the problems that the department has in hands have to be studied, mainly the problem that is the subject of the dissertation.

At the same time a structured and systematic review on stamping and cutting processes, stamping tools, and dual-phase steels should be carried out in order to fully understand the processes that are seen on the shop floor.

Once the component and its industrialization process and everything it involves are studied, it is necessary to get familiarized with AutoForm in order to be able to succeed in the stamping simulations both from the actual process and the implementation of possible solutions. To successfully perform the simulations, a literary review should also be carried out in order to understand the methods behind the software interface and the material models available.

Afterwards, an experimental characterization of the material used in different productions of the component using uniaxial tensile tests is made in order to identify a possible cause for the problem and identify the properties than can be influencing the most the appearance of cracks. The results can also be used to edit the material model used.

Throughout the development of this dissertation in the company, all the productions of this component must also be followed in order to implement or study the consecutive alterations that are suggested to minimize or eliminate the problem.

In Figure 16, a Gantt chart is displayed distributing in time the tasks that must be carried out.

In the first milestone, the theoretical chapters should be written, the problem must be well described, the technologies involved in the production of the component, dual-phase steels and constitutive models for sheet metals must be familiar. Also, the software, its methods and layout should be known.

In the second milestone, the industrialization process of the component must be understood and described including the strip, tool, and control gauge. Several experimental and/or simulated attempts to solve the problem must have been done and conclusions from each production withdrawn.

In the third milestone, the final document must be ready with the correct references and formatting.

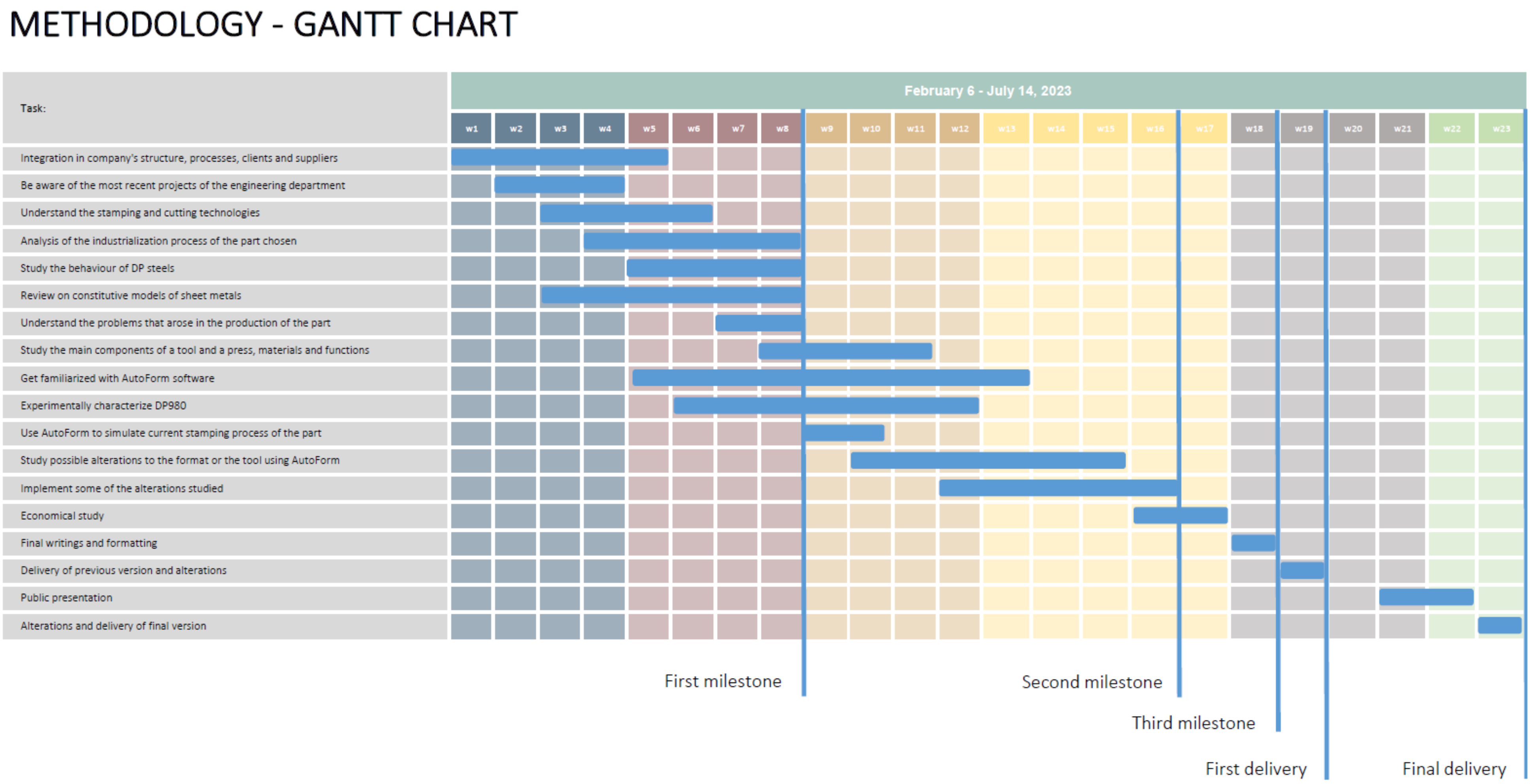

Figure 16 - Gantt chart describing the tasks that must be done and their chronological distribution.

1.5 Structure and layout

This thesis aims to describe the industrialization process of a DP980 steel (dual-phase steel with 980 MPa tensile strength) cold stamped component and apply the finite element method in the numerical simulation of the current sheet metal forming process using the commercial software AutoForm. Besides studying the present process, including the characterization of the material, it also intends to explore solutions in order to eliminate or reduce the cracks found in the production both through experimentation and numerical simulation.

In addition to the current chapter (Chapter 1), where a brief introduction to the company is done, the driving forces of the development in the automotive industry stated, and the latest breakthroughs in this sector presented, this thesis consists of other six chapters plus appendixes.

Chapter 2 presents some fundaments and basic concepts on the technologies that were studied during this thesis: stamping and cutting, and on the class of materials that will be used, DP steels.

Chapter 3 is focused on the numerical modelling of the sheet metal forming processes. A brief review on the most common constitutive models is carried out and a description of the characteristics and methods of the commercial software AutoForm is done.

Chapter 4 describes the industrialization process of the studied component namely regarding the strip, the tool, and the control gauge. This stage also includes the numerical simulation of the current process and the description and historic of the production problem.

Chapter 5 focuses on the material. First, some considerations about the yield criteria in the numerical model are analyzed. Then, the experimental characterization of the material of two coils is done and afterwards some adaptations to the previously used material model are considered.

In chapter 6, strategies for reducing or eliminating the appearance of cracks are studied. Numerical simulations are done in order to study the implementation of possible solutions to the problem. Achieving satisfactory results, it is also analyzed the economic impact of the elimination of the problem.

Chapter 7 presents the main conclusions of this thesis, along with some perspectives and suggestions for future work.

2 Technologies and materials

The process of metal forming by plastic deformation implies a permanent deformation of the material, that is, the load to be applied to the format during the process, must exceed the limit above which the material can no longer return to its initial geometry. One thing that characterizes plastic deformation is the non-linearity between stress and strain, being more difficult to predict the behavior of the material.

The technological processes of sheet metal forming by plastic deformation are characterized by the ability to obtain mechanical parts with high production cadences and by the almost integral use of the raw material, allowing to obtain the final or almost final part of the product. Since these high production cadences are attractive to production in series, these processes became very used in several industries such as the automotive.

The technologies in focus in this work, and that will be briefly described in this chapter mostly according to (Dias dos Santos, Ferreira Duarte, and Barata da Rocha 2003) and (Dias dos Santos, Ferreira Duarte, and Barata da Rocha 2005), are cutting and stamping of sheet metal, called sheet metal forming processes. These processes allow to obtain metallic parts from a coil or formats of sheet metal.

Also in this chapter, a succinct review on DP steels, its production, properties, microstructure, and main advantages and disadvantages, is carried out.

2.1 Stamping technology

Stamping is a technique of metal forming by plastic deformation that consists of obtaining mechanical parts whose geometry cannot be specified using flat patterns, from sheet metal, represented schematically in Figure 17. It is usually accepted that stamping can involve processes usually called as deep drawing, folding, crash forming, etc., depending on the geometry or on the way the sheet interacts with the tool binders. For the sake of simplicity and accordingly to what happens on an industrial level, the term stamping will be used to name the manufacturing process that globally includes all these processes. The plastic deformation imposed on the sheet, necessary to obtain the final shape, is achieved using a tool, illustrated schematically in Figure 17. In turn, the tool is mounted on a press, which provides the tool with the linear alternative movement necessary for the operation.

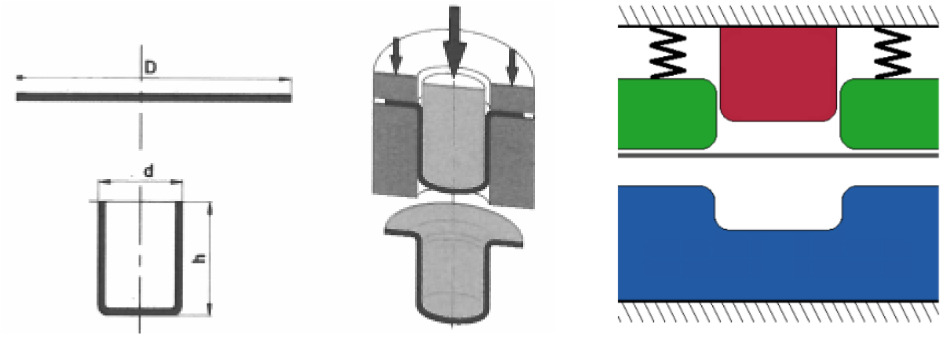

Figure 17 - Example of a simple stamping process (left) (Dias dos Santos, Ferreira Duarte, and Barata da Rocha 2005) and tool (right)

One of the main users of this technology is the automotive industry, responsible for high production volumes of complex stamped components. This sector represents a high economic share in developed countries, and it is responsible for the major innovations related to this technology: new materials, new forming methods, introduction of numerical simulation and augmented reality. Nevertheless, many other industries use this technology such as: domestic appliances, decorations, electronics, aeronautics, naval, etc.

2.1.1 Deformation modes

There are two fundamental deformation modes in stamping processes:

- Extension – the plate undergoes positive elongation (traction and increase in length) in one direction of the plate plane and a negative elongation (compression and length decrease) in the perpendicular direction to the previous one.
- Expansion – the plate undergoes positive elongations (traction and increase in length in all directions of the plate.

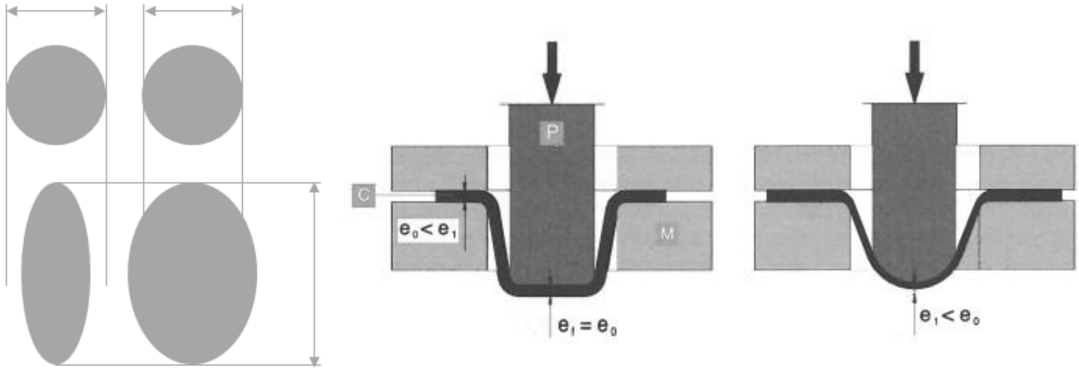

Figure 18 - Extension and expansion deformation modes (Dias dos Santos, Ferreira Duarte, and Barata da Rocha 2005).

The deformation modes depend directly on the action of the binder/blankholder, an element of the stamping tool whose function is to keep the plate against the die throughout the process, preventing that would cause defects in the final part. Thus, if there is no blankholder or its pressure is not sufficient (what happens in crash forming operations), the mode of deformation is fundamentally extension. If the pressure of the blankholder is sufficiently high to prevent the sliding of the plate between the die and the blankholder, the mode of deformation is expansion (common in deep drawings). To achieve the blocking effect, it is common to use, in addition to the pressure of the blankholder, drawbeads which can prevent the plate from sliding.

These two modes of deformation have a decisive influence on the final thickness of the product obtained. Thus, in the expanding mode the final thickness of the part is necessarily lower than that of the plate that gave rise to it.

2.1.2 Project of a stamped component

The automotive industry is associated with complex stamped components. The main difficulties when projecting the stamping processes of these components are the calculation of the blank format, the project of the simultaneous operations needed, the springback prediction, etc.

The main steps of the project of a stamped part are the analysis of the design of the part, evaluation of the production parameters (volume of production, material, thickness, quality, cadence, machines available), selection of the manufacturing methods, determination and characterization of the necessary steps (number of steps, sketch, calculation of forces), design, execution and tuning of the tool, quality control and production.

In the calculation of the sketch/format (the necessary sheet shape to be further stamped), several approaches may be taken, such as analytical calculation based on simplifying hypothesis, iterative trial and error experiments or calculation through software. Neither the first nor second approaches are viable in the project of automotive parts since their geometries are way too complex. The analytical method is also approximate since it considers that the thickness remains unchanged. The trial-and-error method is clearly too expensive.

Therefore, software like FomingSuite, that unlike analytical calculations have thickness variation into account, are precious to define the contour of the cut and consequently the step, width and layout of the contour in the strip that optimizes the use of material.

A material usage coefficient (MUC) is usually used to calculate the percentage of raw material that is actually being consumed in the final part and thus help to decide the best layout of the contour in the strip. This happens mainly for stamped components made in progressive tools. The closer the value to 100%, the less scrap or waste is produced, and the more efficient is the process. This value can be calculated as follows:

$$MUC = \frac{P_p}{W \times S \times T \times \rho} \times 100 \tag{2.1}$$

where P_p is the weight of the final part, W is the width of the strip, S is the step (distance that the strip moves forward at each press stroke), T the thickness and ρ the specific weight of the material.

Considering the automotive industry, values above 75% are considered very good, despite almost ¼ of the material being discarded as scrap. Values between 50 and 75% are satisfactory. Below this last range, the use of another manufacturing technology other than progressive tools, such as transfer presses or even tandem transfers using formats, begins to be considered.

The calculation of the number of steps that a part must undergo before its final geometry is obtained is also too complex to be done using analytical methods. The stamping of complex geometries with deep draws, side holes or 3D cuts requires large plastic deformations, which are only achieved with high forces, and complex elements incorporated in the tool. Since the maximum allowable force to run a stamping operation is limited and the distribution of components in the tool is also limited in space, it is usual to stamp a component in several steps, usually determined using former experience and software like AutoForm. In a progressive combined tool, it is usual to perform firstly the cutting operations in the first steps until the necessary format is obtained. Then, the stamping operations. And finally, the punching operations.

Regarding the determination of the forces necessary to perform the stamping operations, similarly to what happens in the calculation of the sketch and number of steps, it is impossible to calculate them precisely using analytical methods for complex geometries. They are, once again, determined with the help of specialized software like AutoForm. This force needs to have into account not only the theoretical stamping force, but also the friction forces.

2.1.3 Experimental strain analysis and forming limit curve

In an industrial stamped part, the value of the stresses installed at a given point is difficult to determine given the complexity of the geometry of most parts and the high level of plastic deformations imposed on the sheet. The high level of plastic deformations makes it impossible to adopt classical experimental techniques of stress analysis (extensometery or photoelasticity).

The experimental analysis of deformations in a stamping operation is conventionally carried out by previously printing a reference grid on the surface of the undeformed sheet. The plastic deformations imposed on the plate during conformation cause a distortion of this reference grid, and the value of the principal deformations at each point of the part can be determined by later comparing the deformed grid with the reference grid.

Figure 19 shows some reference grids correctly used in experimental analysis of deformations. The dimension of the pattern to be adopted does not depend on the dimensions of the part, but on the local deformation gradient at the critical points of the part.

The main printing techniques are scratch printing, ink printing, electrochemical printing, and photographic printing.

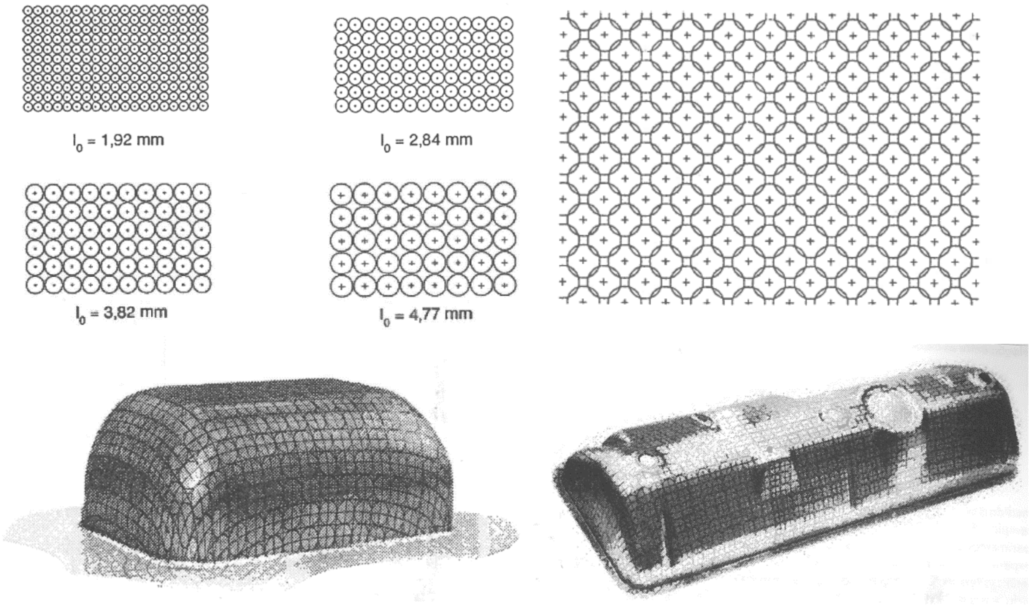

Figure 19 - Grids for experimental analysis of deformations (Dias dos Santos, Ferreira Duarte, and Barata da Rocha 2005).

The distortion of the reference grid during the plastic deformation of the sheet makes it possible to determine the principal directions of plastic deformation as well as the value of the principal deformations brought into play.

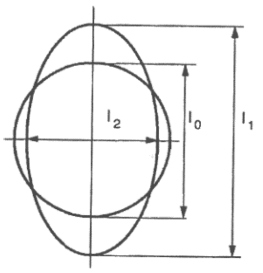

Figure 20 - Deformation of a circle into an ellipse.

The circles of the grid pattern are transformed into ellipses like shown in Figure 20 and the measurements of their axes make it possible to calculate the logarithmic deformations in the plane of the plate through the following expressions:

$$\varepsilon_1 = \int_{l_0}^{l_1} \frac{dl}{l} = ln\frac{l_1}{l_0} \text{ , } \varepsilon_2 = \int_{l_0}^{l_2} \frac{dl}{l} = ln\frac{l_2}{l_0} \text{ e } \varepsilon_3 = \int_{e_0}^{e} \frac{de}{e} = ln\frac{e}{e_0} \qquad (2.2)$$

with $\varepsilon_1 \geq \varepsilon_2$ and direction 3 perpendicular to the sheet plane and being the dimensions with index 0 before the forming operation.

It is common to also use the condition of incompressibility of the material during the forming process:

$$\varepsilon_1 + \varepsilon_2 + \varepsilon_3 = 0 \qquad (2.3)$$

This measurement, which requires a certain amount of experimental rigor given the size of the motif, is a long, tedious, and tiring operation for the experimenter. Recently, optical reference grid analyzers were developed, essentially composed of a video camera, an interface, and a microcomputer. However, this process has a price in line with its potential.

Theoretical and experimental analysis of the forming processes of sheet metals show that the principal stress of Cauchy σ_3, according to the direction perpendicular to the plane of the sheet, is in most cases insignificant, in view of the stresses installed in this plane (σ_1, σ_2), so that it is usually neglected in the calculations.

In a stamping operation, it is therefore usual to assume that the stress tensor at any point of the part corresponds to a plane stress state $(\sigma_3 = 0)$, like illustrated in Figure 21. The stress at a given point in the material can then be represented by the value of principal stresses σ_1 and σ_2. Considering that the evolution of the cartesian components of the stress tensor, from the undeformed state to the deformed state, is proportional (linear or proportional loading), that is:

$$\frac{d\sigma_2}{d\sigma_1} = constant \tag{2.4}$$

it is possible to associate a linear path of loading in the plane σ_1, σ_2 to each point of the part.

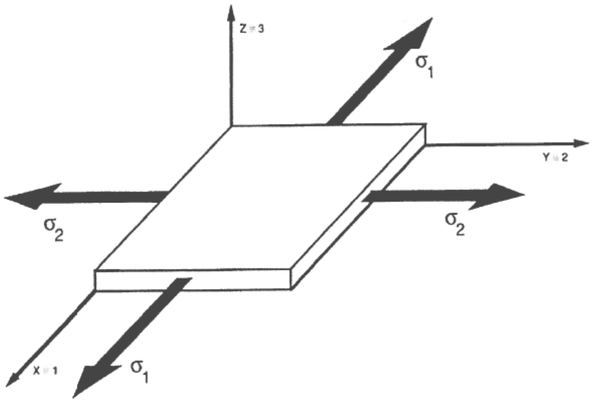

Figure 21 - Plane stress state (Dias dos Santos, Ferreira Duarte, and Barata da Rocha 2005).

All stress modes in stamping can thus be represented in the plane of principal stresses σ_1, σ_2. Figure 22 represents stress states commonly found in stamped parts. Each linear loading trajectory can be described through a parameter α representing the stress state:

$$\alpha = \frac{d\sigma_2}{d\sigma_1} = \frac{\sigma_2}{\sigma_1} = constant \tag{2.5}$$

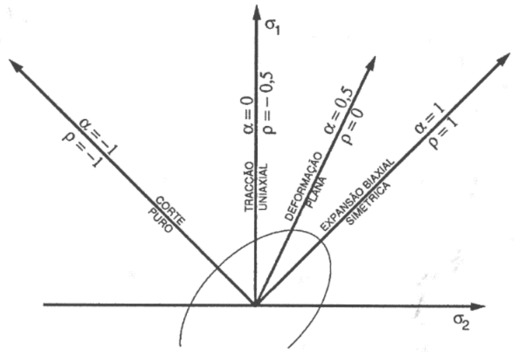

Figure 22 - Plane of principal stresses σ1, σ2 (Dias dos Santos, Ferreira Duarte, and Barata da Rocha 2005).

The representation of the deformation state in a diagram needs three variables, the logarithmic deformations ε_1, ε_2 and ε_3. However, the previously presented incompressibility condition reduces this space to two independent variables. It is thus possible, in the same way as for the stress state, to represent all strain modes in the plane of principal strains (Figure 23). Each linear strain trajectory can be described through a parameter ρ representative of the strain state and given by:

$$\rho = \frac{d\varepsilon_2}{d\varepsilon_1} \tag{2.6}$$

Assuming a linear load, we can say that the deformation trajectory of a point of a stamped part represents the geometric locus of the successive deformations of the point in question, throughout the forming operation. To each linear load path α corresponds a linear deformation path ρ. In the case of an isotropic material, this correspondence is given by the following equation deduced from the Levy-mises equations:

$$\rho = \frac{2\alpha - 1}{2 - \alpha} \tag{2.7}$$

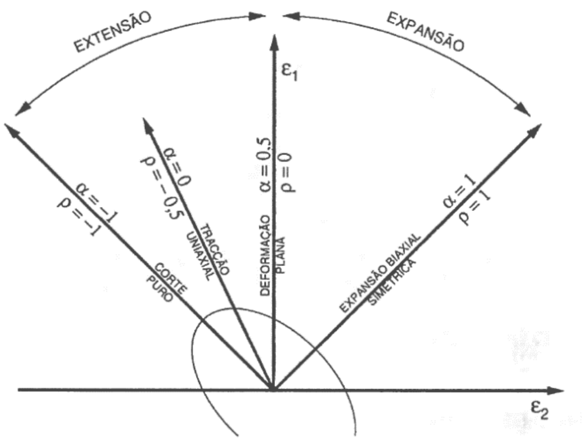

Figure 23 - Plane of principal strains ε₁, ε₂ (Dias dos Santos, Ferreira Duarte, and Barata da Rocha 2005).

In the stress and strain state diagrams, two domains corresponding to different stress modes are distinguished:

- Extension domain: this domain is comprised between the deformation trajectories corresponding to pure shear and plane deformation ($\varepsilon_2 < 0$).
- Expansion domain: this domain is comprised between the deformation trajectories corresponding to plane deformation and symmetric biaxial expansion ($\varepsilon_2 > 0$).

Formability can broadly be defined as the capability of sheet metal to undergo plastic deformation to a given shape without defects. In the study of the stamping process, the problem of the formability of thin plates, seen from the point of view of the user of the plate, involves many parameters: friction, gaps between punches and dies, lubricants, tool configuration, blank holder pressure, punch speed, etc. This fact explains the success of the concept of forming limit diagram or curve.

This concept was introduced by Keller and Goodwin in the 1960s to characterize the formability of thin sheets, that is, their aptitude for plastic deformation. These authors found that it was possible to define a curve in the plane of principal deformations $\varepsilon_1, \varepsilon_2$ separating the domain of admissible deformations from the domain of failure deformations. The forming limiting curve to failure therefore represents the limit deformations from which failure is reached. This curve is of little practical interest since the phenomenon of fracture is generally preceded by a plastic instability corresponding to the formation of a localized necking band. This necking manifests itself as a local thickness reduction of the material and is generally unacceptable for reasons of aesthetics, mechanical strength and corrosion resistance.

Currently, the high-quality standards make the appearance of a localized necking a sufficient condition to reject the stamped part. A second type of curve, the forming limit curve to necking, was then introduced to define the upper limit of drawing a sheet without producing localized plastic instability. This is the curve widely known as the forming limit curve.

This curve is of enormous importance in the study of the entire stamping process and today represents a precious tool at the disposal of anyone working with stamping. Indeed, the experimental measurement of the deformation in an industrial stamped part and its subsequent comparison with the forming limit curve allows quantitatively to be known: the safety margin of the stamping, the critical place where the necking or rupture will preferably occur, the selection of ideal working conditions, the quality of the plate necessary to guarantee the success of the operation, the influence of the properties of the plate on the safety margin of the stamping, the difficulty in obtaining the stamping.

Indeed, if through a numerical or analytical method, the deformations are determined at each point of the stamped part and the respective loading or deformation histories, it is possible not only to know if the part is feasible, but also to quantify the reliability of the operation through the position of the coordinate points $\varepsilon_1, \varepsilon_2$ relative to the FLC.

If, using a plasticity model, the FLC's are calculated numerically from the characteristics of the sheet, the success of a stamping operation can be judged without having to resort to experimental tests. This type of analysis lies within the scope of computer aided engineering (CAE) and represents the current trend in cutting-edge research in the field of sheet metal forming (computer aided sheet metal forming).

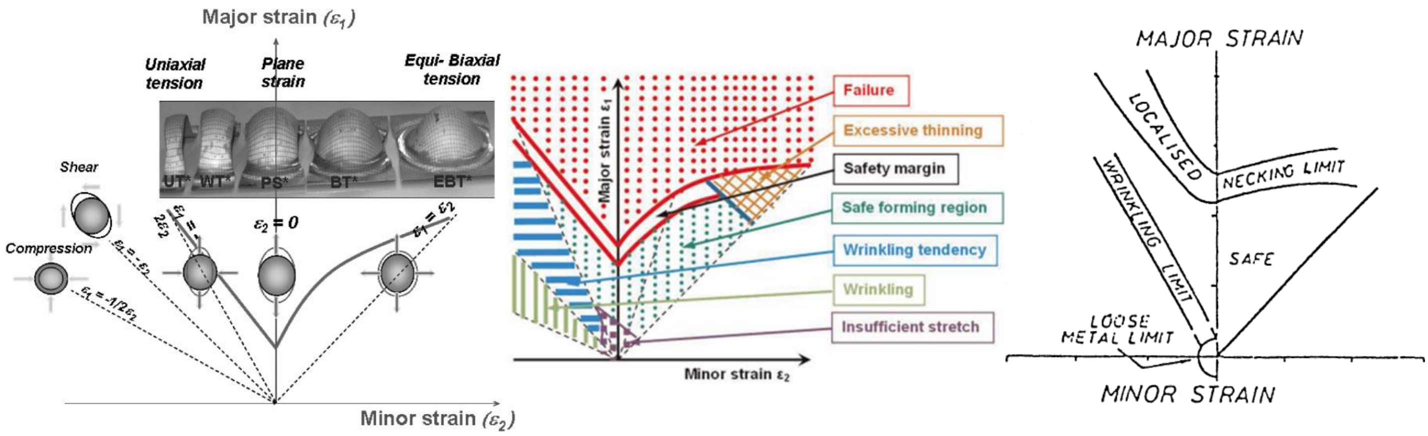
Major strain (ε_1)
Uniaxial tension
Plane strain
Equi- Biaxial tension
UT*
WT*
PS*
BT*
EBT*
Shear
Compression
$\varepsilon_1 = 2\varepsilon_2$
$\varepsilon_2 = 0$
$\varepsilon_1 = \varepsilon_2$
$\varepsilon_1 = -\varepsilon_2$
$\varepsilon_1 = -1/2\varepsilon_1$
Minor strain (ε_2)
Major strain ε_1
Minor strain ε_2
Failure
Excessive thinning
Safety margin
Safe forming region
Wrinkling tendency
Wrinkling
Insufficient stretch
MAJOR STRAIN
LOCALISED
NECKING LIMIT
WRINKLING LIMIT
SAFE
LOOSE METAL LIMIT
MINOR STRAIN

Figure 24 - Forming limit curves (Bouaziz, Zurob, and Huang 2013), (Banabic et al. 2010).

The experimental obtainment of the FLC is carried out from several simulation tests or formability tests in order to cover a wide range of deformation trajectories: uniaxial tensile, bulge-test, Nakajima, Erichsen, modified Erichsen, Olsen, Persoz, Guyot, Modified Guyot, Swift, Swift - IDDRG, AEG, FUKUI, KWI, flat cut, MIYAUCHI, among many others.

2.1.4 Common defects

One of the main challenges when projecting and producing stamped components is the appearance of defects. Engineers must be well aware of the most common defects and know what generally causes them so that they can act preventively or, if that cannot be done, correctively.

These defects can be divided in three classes: shape or sizing defects, defects on the surface and unsatisfactory properties. And the sources or causes of these defects can be defective base material, inadequate part design (drawing, choice of material) and incorrect procedure (machine, tools, process).

Most defects are detected through visual inspection, as the most frequent defects are related to surface or shape. Some examples are presented in Figure 25.

- Defect due to springback;

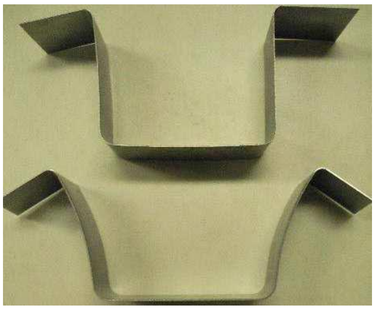

- Defect due to the presence of scrap;

- Defect due to poor positioning/pilotage;

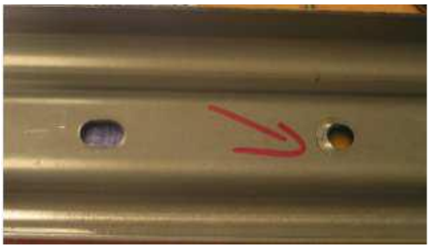

- Appearance of cracks or rupture;

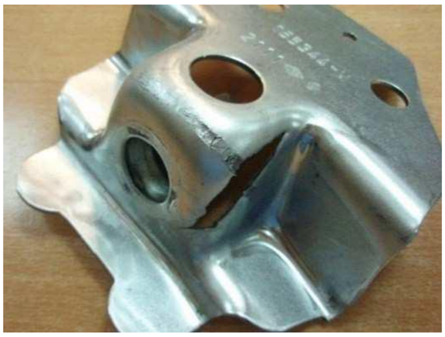

- Presence of burr.

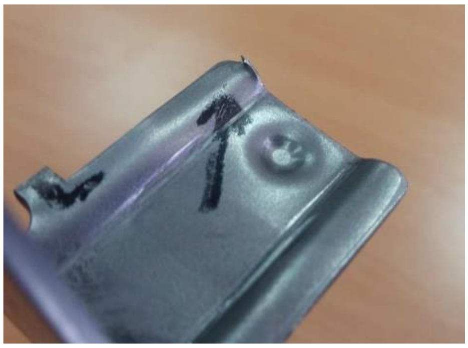

- Earring.

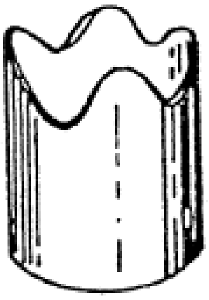

- Presence of wrinkles.

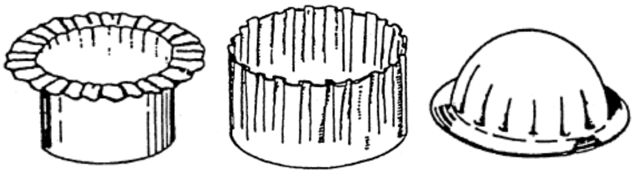

Figure 25 - Defects of stamped parts (Gestamp Cerveira 2023) and (Dias dos Santos, Ferreira Duarte, and Barata da Rocha 2005).

2.2 Cutting technology

What is usually described as a stamped component usually also involves cutting operations whether in the form of holes destined to lodge bolts and other fixing components or simply to obtain the initial blank format or sketch from which the part will be stamped. There are a few particularities in the cutting technology that should be explained.

The cutting technology consists of separating a contour from a flat product (a sheet format or sheet metal strip). The operation is carried out by a press, through a tool whose fundamental elements are punches and dies, Figure 26. In the case of a combined progressive tool that produces parts from a strip in a sequence of cutting, stamping, and punching operations, the cutting punches and dies are usually in the first steps of the tool.

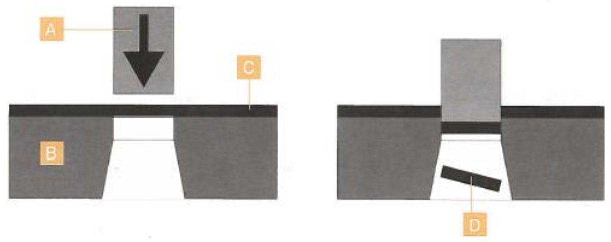

A – Punch B – Die C – Blank to be cut D – Scrap

Figure 26 - Cutting technology (Dias dos Santos, Ferreira Duarte, and Barata da Rocha 2003).

There are several types of cutting operations. The most used and that are usually integrated in the production of a stamped part are:

- Blanking – term referring to obtaining a part or format extracted from a strip or plate, following a closed contour. The format is rarely the final product, generally undergoing other forming operations (stamping, punching, bending, etc.).
- Punching – in punching there is the cut of the plate, however, the conserved part is the outside part.
- Notching – is based on cutting a partial zone on the edge of a plate or strip.

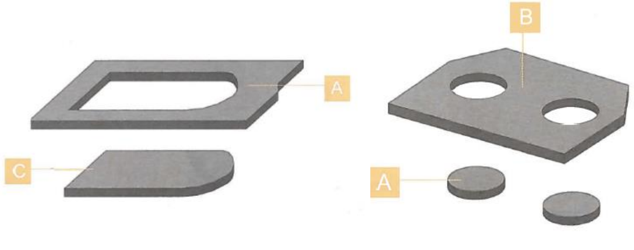

A – Scrap

B – Punched holes

C – Part

Figure 27 - Blanking (left) and punching processes (right) (Dias dos Santos, Ferreira Duarte, and Barata da Rocha 2003).

Analyzing now the mechanics of this processes, resulting from the interaction between die and punch, cutting operations can be divided into three distinct phases:

- Crushing – Before starting the cut, the punch touches the sheet, supported by the die, and crushes the material forcing it out through the die’s hole. At this stage elastic deformations develop in the plate, followed by complex plastic deformations on both sides of the plate, compressed between the die and the punch.

- Cutting – Continuing the descent of the punch, the material is subjected to a strong shear stress giving rise to the appearance of the pure shear surface (smooth and shiny zone) corresponding to the plastic deformation of the material.
- Rupture – Phenomenon that describes the separation of one metallic part from another.

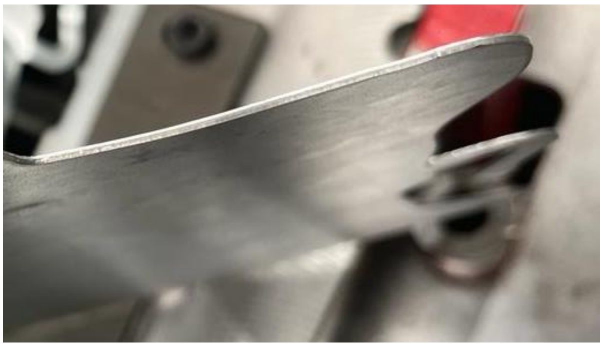

Figure 28 - Cutting surface analysis: distinction between pure shear and rupture in real part.

The cut surface makes an angle with the surface of the plate and presents, as shown in Figures 28 and 29, three main distinct zones: an almost invisible deformation band, a pure shear zone, the smoothest, most shiny area, and a rupture or ripping zone, the darkest and poorly finished area. The rupture area is therefore clearly more likely to have microcracks.

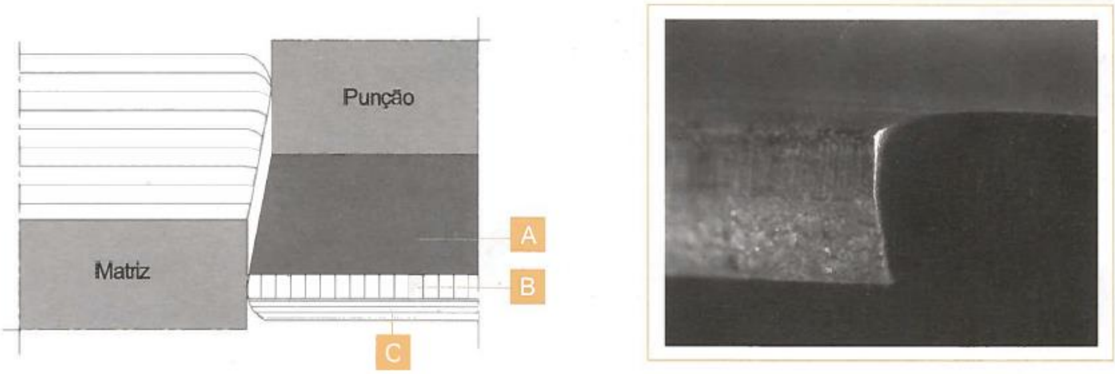

A – Rupture band B – Pure shear band C – Deformation band

Figure 29 - Cutting surface analysis: distinction between crushed, pure shear and rupture in real part (Dias dos Santos, Ferreira Duarte, and Barata da Rocha 2003).

The appearance of the cutting surface, namely the proportion of the thicknesses of the pure shear and rupture zones, depend on the properties of the sheet, the gap between punch and die, and the wear of the tool. Usually, the greater the hardness and the lower the ductility of the material, the greater the rupture area. Moreover, up to a certain limit, a decrease in the gap between the punch and die represents an increase in the thickness of the pure shear zone.

Precision in a cutting operation is directly linked to the type of tool used, the guiding of the tool and the operating state of the press, the state of wear of the tool, the gap (better precision with lower gap) and the distance between parts or between the part and the edge of the plate.

The gap is an important technical parameter in the cutting process, which directly controls the quality and appearance of the product, as well as the lifespan of the tools. It is generally observed that a gap that is too small causes a considerable increase in the wear rate of the tools, while an excessive gap causes a bow, a rupture angle and a burr that is too marked, in other words, a poor quality of the product. Radial gap is generally expressed as a percentage of the thickness of the material to be processed, with a value between 5 and 13% of the sheet thickness between the punch and the die being recommended but that can go up to 25%.

Regarding the calculation of the cutting forces, which is important for choosing the right press. These forces can be calculated using software such as AutoForm or through an empirical approximation expression:

$$F_c = L \times e \times R_c \tag{2.8}$$

where L is the perimeter of the contour needed, e is the thickness of the blank and R_c is the shear strength of the material. This latter value is usually calculated as:

$$R_c = 0.8 \times UTS \tag{2.9}$$

where UTS is the ultimate tensile strength of the material.

Several techniques may be used to lower the force that is simultaneously being exerted on the sheet. One of them is creating inclined punches that progressively contact with the sheet preventing an instantaneous contact with a large punch area. Another is a lag between punches, meaning that several punches contact the sheet at different times.

To facilitate the extraction of the scrap mainly in punching operations it is usual to have a small extractor on the top of the punch which is a small protrusion.

2.3 Cutting and stamping tools

The tools used in the automotive industry are usually combined tools, meaning that they are based on a set of elements (being the most important punches, dies and binders) designed to make cuts and shapes on a plate, in order to progressively obtain one or more parts. Therefore, these tools mix both technologies: cutting and stamping.

Before the project of a tool, it is essential to take the following aspects into account: the part geometry, production rate, and type of feed used, the type of material and its thickness, the size of the series to be produced, the required quality namely precision and appearance, and the tool maintenance.

The tools can essentially be classified according to two parameters of classification. The first being the number of simultaneous actions that can be exerted on the sheet and the second being the operations performed.

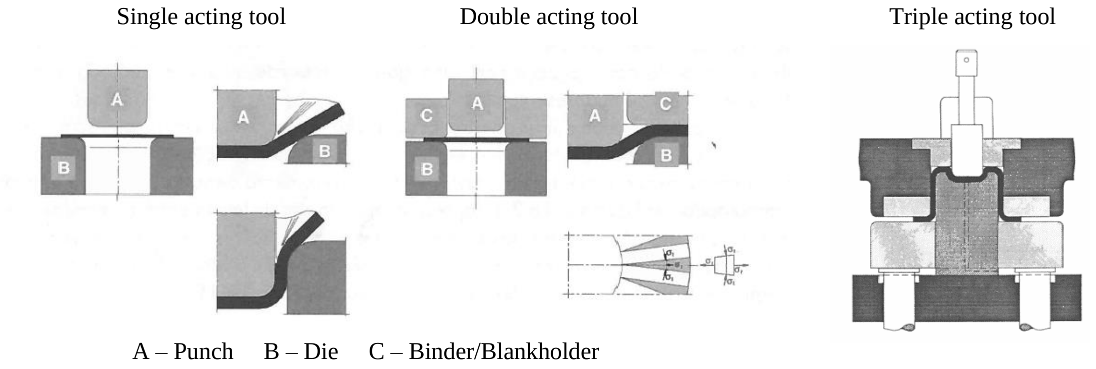
Single acting tool

Double acting tool

Triple acting tool

A – Punch B – Die C – Binder/Blankholder

Figure 30 - Single (left), double (middle) and triple (right) acting tools (Dias dos Santos, Ferreira Duarte, and Barata da Rocha 2005).

According to the first classification criteria the tools can be single, double or triple acting if they can perform one, two or three independent actions on the sheet. Single acting tools can be identified by the absence of binder/blankholder. Double acting tools are characterized by a second independent force exerted by the blankholder that is essentially responsible for stretching the metallic material, increasing rigidity, and lessening the springback effect during stamping processes, by reducing the material flow to the die cavity and providing more control to the process. Finally, the triple acting tools generally have one extra action on the lower part of the tool that allow inverted draws.

According to the second classification criteria they can be simple, progressive or transfer. Simple tools can be interpreted as tools that perform only one stroke on the part. The part can be done in one operation just in one tool or it can be done in several strokes and several operations making use of more than one tool, as is the case of the transfer tandem. These tools can be fed manually or by robots.

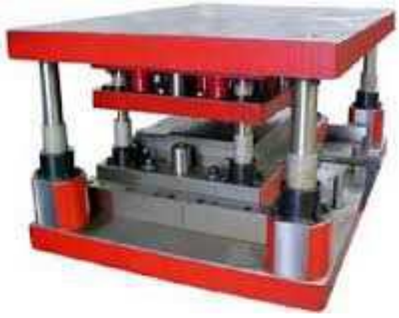

Figure 31 - Simple tool for manual feeding in Gestamp Cerveira (Gestamp Cerveira 2023).

Progressive tools are used to perform a sequence of trimming and stamping operations in one single tool. The sheet coil unrolls, and the strip moves into the tool step by step at each stroke. This way, there are several parts inside the tool at the same time but at different manufacturing stages. The part remains attached to the strip until the last operation. Generally, in the first steps are performed trimming operations followed by stamping and punching operations.

These sophisticated tools are characterized by high cadences but high costs being suitable for big series.

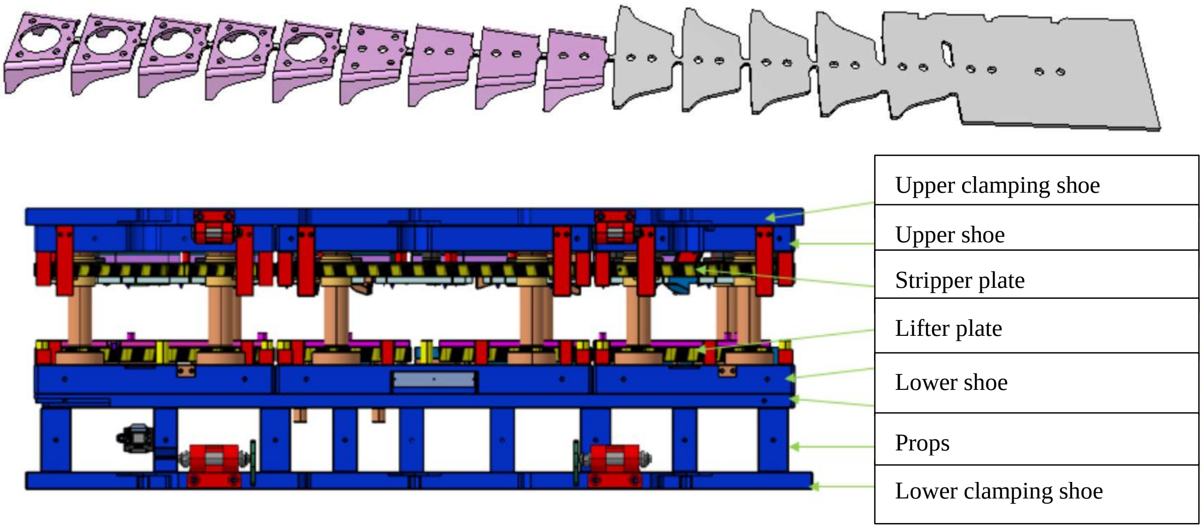

Figure 32 - Progressive tool and correspondent strip (Gestamp Cerveira 2023).

Transfer tools are the most robust tools allowing great precision and variety of possible geometries. Their functioning principle is similar to the progressive tools. Nevertheless, instead of the parts moving as a strip, they are moved from step to step using lateral clamps. Their work is inherently slower than the progressive. They are also very expensive, suitable for large productions. During their operation it is usually cut a large format, followed by the stamping and punching operations. In the last steps, the part is cut to its final geometry.

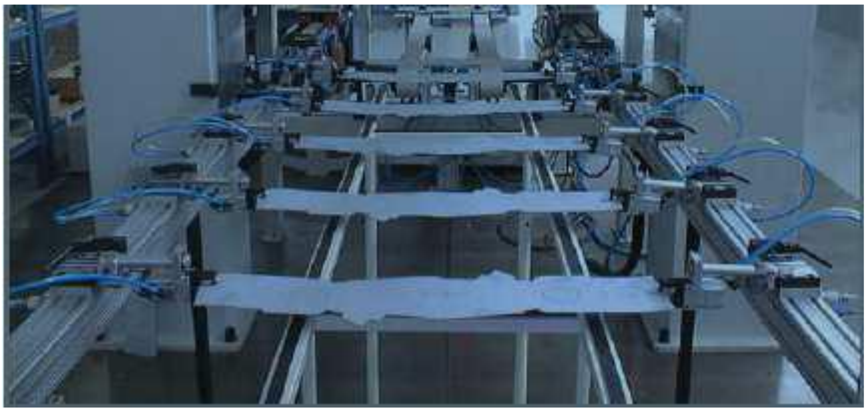

Figure 33 - Transfer mechanism (Gestamp Cerveira 2023).

Regarding some constructive aspects. The guiding of the tool is accomplished in three ways: the guiding of the press itself, the primary guiding between the upper and lower shoe using major columns and sleeves, and the secondary guiding between upper shoe and stripper plate and between lower shoe and lifter plate through minor columns and sleeves.

The intended component and the addendum necessary to sustain the initial blank typically impose the shape of the die. This means that the die cavity geometry determines the geometry of the punch by the application of an offset, establishing the gap between these two elements. It is an outside tool that applies the restraint force on the blank since the blankholder/binder is normally created by applying an offset to the addendum region of the die.

A general double acting tool as the one represented in Figure 32 is composed by two movable elements and two fixed elements. The lower and upper shoes are the fixed ones and are responsible for fixing the tool to the press. The movable elements, the lifter and stripper plates, are respectively connected to the lower and upper shoes through gas springs. The functioning principle of a double acting tool can be described in four steps that commonly occur regardless of the complexity of the tool. The first is the one in which the tool is completely opened. This is the moment when top dead center is reached. In this position, there is no contact between the upper part of the tool and the lower part. Both mobile elements (lifter plate and stripper plate) are opened, that is, the forces exerted by the gas springs make them positioned at the maximum possible level. This course is limited by the stoppers that keep the elements in the desired position. This is also the moment when the sheet metal moves forward, i.e., the process is fed. The feeder proceeds to an increment equivalent to the step in the case of a progressive tool. The strip contacts only with the lifter plate, the mobile element of the bottom part, and slides freely over it.

The second moment is characterized by the first contact between the upper and lower parts of the tool. At this moment, the lower movable plate (lifter plate) as well as the upper movable plate (stripper plat) make contact with the strip. The pilots enter the respective holes and the stripper plate touches the stops of the lifter plate. The existing gap between these plates corresponds to the thickness of the plate. Parallel to what happens on the strip, the guiding elements begin to exercise their function once the guiding columns enter the respective sleeves.

The third moment happens when the lower moving plate (lifter plate) descends. The lifter plate reaches its shortest course limited by the stops located at the lower shoe, while the stripper plate remains unchanged in relation to the upper shoe. This means that the lower gas springs are weaker than the upper ones. At this moment, the dies and binders are in contact with the strip, ready for the next moment in which work is carried out on the sheet (cutting and/or forming).

In the last moment, which is called bottom dead center, the tool is completely closed. This is the moment when the stripper plate moves upwards allowing the punches to act on the sheet making cuts and shapes. The scrap resulting from this action is stored in the drawers or guided to the scrap tunnel. All the stoppers are working, that is, they are several components in contact: lower shoe-lifter plate, lifter plate-stripper plate and stripper plate-upper shoe.

After this moment, the tool opens again and repeats the described cycle.

2.4 Project of a strip for a progressive tool

The strips represent the production process of a progressive tool, that is, they illustrate the various stages that the sheet goes through from the coil to the final part, providing information on the type of operation carried out at the different stations. Therefore, it is inevitable to talk about projecting a stamped part in a combined progressive tool without thinking and correctly defining the strip.

The characteristics that, in general, are shared by the strips of a progressive tool are the presence of connection elements (rails) between parts during the production process, pilot holes that ensure the correct position of the sheet in the different stages (generally 13 mm diameter holes), a notch on one side to ensure that the sheet advances through a sensor located in the second station of the tool, and finally a guillotine with the purpose of cutting the sheet at the end of each production, whether the coil is totally used or not.

Besides those characteristics, a strip can be divided into three zones, which can also be distinguished in a progressive tool: pilotage and trimming (area where the pilots and the necessary trims to get to the format holes are done), forming or stamping (area where stamping operations are performed giving the format its shape), and finally punching and separation (area where the holes are punched and the part is separated from the rails).

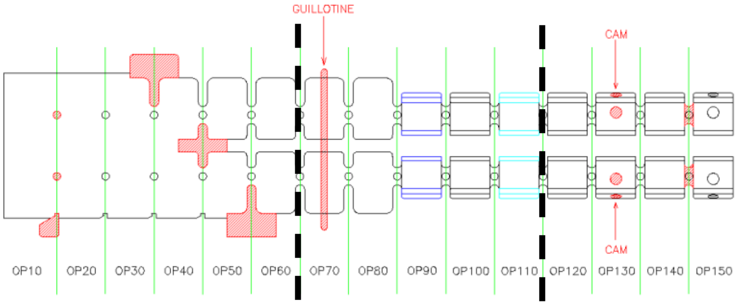

Figure 34 - Typical zones of a strip: trimming (left), stamping (middle), and punching/separation (right) (Gestamp Cerveira 2023).

Projecting a part to be made in a progressive tool generally is cheaper than in a transfer tool because cadences can be greater. However, these tools usually have lower MUC because of the rails. The rails aim to fix and guide the part from a tool's workstation to the next one until reaching the final operation where they are separated from the part and the remaining pieces are scrapped. There are mainly four types of rails:

- Side rail with one sketch – a simple side rail that is located on one of the sides of the sketch (Figure 35). This type of rails is used when the geometry of the parts does not allow the connection between them in the several stages, that is, when it is not possible to connect two sketches due to the lack of flat edges that facilitate the positioning without compromising the final separation.

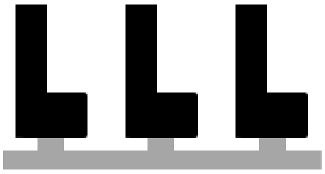

Figure 35 - Side rail with one sketch.

- Side rails – the side rails are present on both sides. Normally, this type of configuration is used for large parts, where fixing the piece at one end does not guarantee the correct positioning of the sheet in the tool. It can also be used in a left- and right-hand configuration as in Figure 36.

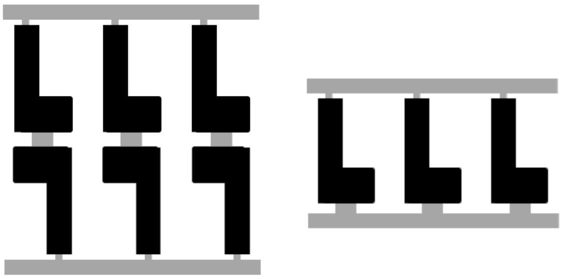

Figure 36 - Side rails.

- Central rails – there are two different types of central rails, one that can be located between sketches and other that crosses sketches for greater savings in sheet, Figure 37. However, this last scenario is only valid when it is not necessary to disproportionately increase the step to accommodate the pilot holes between parts.

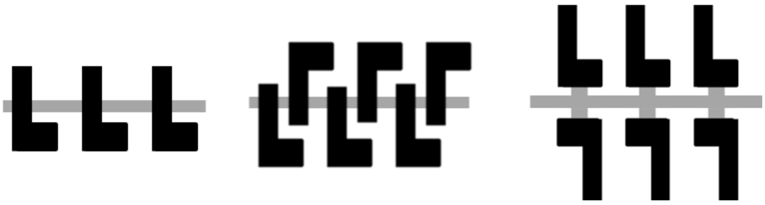

Figure 37 - Central rails.

- Side and central rails – the most rigid and expensive rails in terms of sheet metal consumption is the combination of the two previous examples, Figure 38. This is an extreme situation that produces a lot of scrap, and it is only feasible to apply in the case where the pieces to be produced are of large dimensions (or in the case of two hands being produced at the same time), having deep draws and folds with great complexity in order to increase the rigidity of the set and not allow oscillations, guaranteeing positioning.

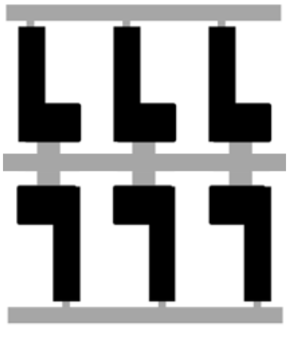

Figure 38 - Side and central rails.

Another important aspect when projecting a strip for a progressive tool is the type of connection between the parts and the rails. These can essentially be from two types. They can be simple rigid connections that have a basic geometry and, normally, do not allow the sheet to flow, Figure 39.

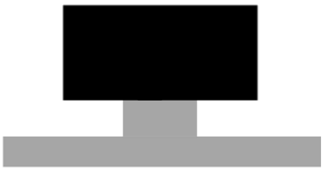

Figure 39 - Rigid connection.

The other type is usually called harmonium connection. It is a flexible connection that allows the sheet to flow, ideal for more complex applications like complex stampings that involve sheet flow. These connections allow the movement/flow of the plate in different axes, depending on the desired geometry. The most common configurations are shown in Figure 40.

Type 1 connections are normally used when the part has stamping operations perpendicularly to the strip. This configuration allows the blank to flow in that direction, accompanying the draws. The deformed configuration is also represented in Figure 40(1). It is also the configuration that produces the least scrap.

Connection 2, like the previous one, allows the sheet to flow perpendicularly to the production line, but with even deeper draws that require greater sheet flow. In addition to this characteristic, this configuration also allows for the displacement of the sketch vertically, that is, it allows the movement of the plate in three dimensions. Thus, the deformation of this connection corresponds to that shown in Figure 40(2).

The third connection is the most suitable for applications where there is a deep draw in the productive direction, not the perpendicular one like the previous. That requires the sheet to flow longitudinally instead of transversally like before. This makes the sketch shrink longitudinally and the connection to deform like in Figure 40(3).

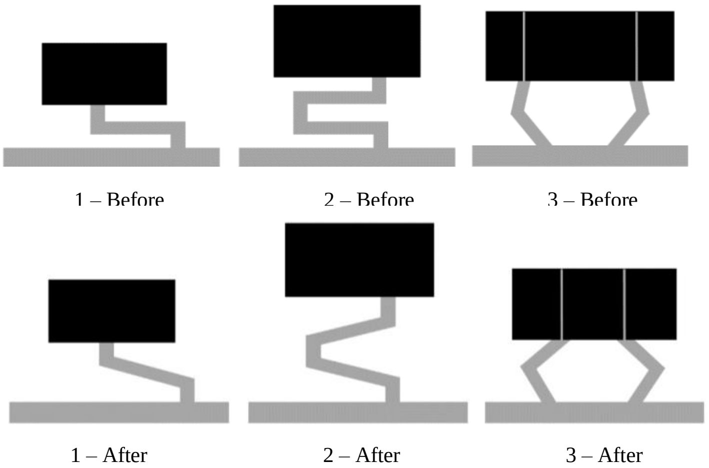

1 – Before 2 – Before 3 – Before

1 – After 2 – After 3 – After

Figure 40 - Harmonium connections.

The dimensions of the rails as well as the connections must follow rules to optimize the use of material and still confers the necessary rigidity for positioning and sliding conditions. These rules can be imposed by the clients or internally by Gestamp in this case. Taking as example the first type of rails (Figure 35) the more important dimensions that should be defined are the distance between parts (A), distance between the part and the edge of the strip (B), width of the rail (C), and the distance between rail and part (D), Figure 41.

The distance between parts (A) should never be inferior to 6 mm due to the slenderness of the punches. The distance between the edge of the band and the part (B) also has a defined minimum distance of 6 mm. Firstly, because the punches responsible for trimming the sketch (especially close to the edge of the strip) require some support otherwise they can break during these unbalanced trims. Secondly, because the edges of the coil are not completely straight lines, they can have deviations of about 2 mm that can also cause unbalances when trimming and consequently breaking punches. The width of the rail (C) depends on the thickness of the strip. For thicknesses lower than 1.5 mm, C must be 12 mm. For thicknesses greater than 1.5 mm, C must be 17 mm. These widths guarantee rigidity and good sliding conditions of the strip. The distance between the grid and the part (D) varies according to the type of connection desired. If this connection is ensured by a harmonium, this distance can reach 30 mm. However, if the connection is simple the distance can be 6 mm.

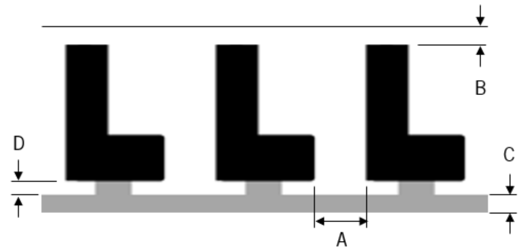

Figure 41 - Important distances to consider in a typical connection.

Other important dimensions include the width of central rails and the corresponding distance between rail and part, the width of the harmonium connection that must be at least 8 mm close to the part and to the side rail, and 4 mm along the connection, the width and length of the connection between two hands when there is not a central rail, etc.

2.5 Dual-Phase steels

In the second half of the 70’s and first half of the 80’s, some new materials have been developed to adapt to new demands of lighter but safer cars. Among these AHSS materials are dual-phase steels, tempered DP steels, complex phases (CP) steels, transformation induced plasticity (TRIP) steels(Tisza and Lukács 2015).

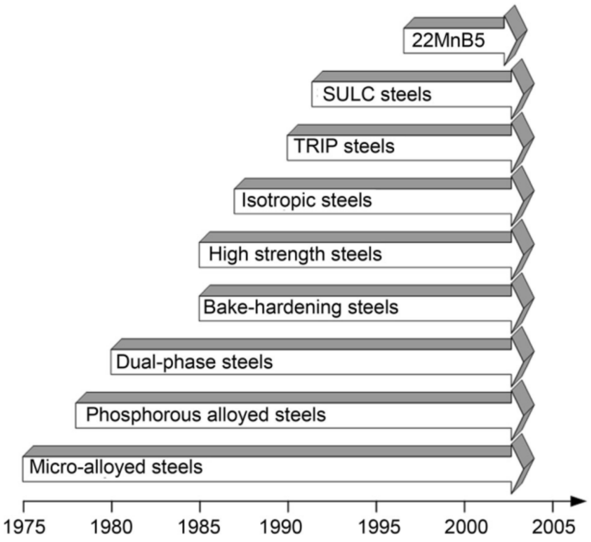

Figure 42 - Evolution and chronological appearance of some AHSS (Tisza and Lukács 2015).

The most developed and utilized AHSS in the automotive industry are dual-phase steels. In the 1980s they started being developed and in the 1990s, they started being produced industrially. These steels are, like the name suggests, made of two phases: a hard phase called martensite encased in a soft matrix phase called ferrite, which has a low strength and high ductility. It can also contain residual amounts of austenite and/or bainite. The Vicker’s hardness of ferrite is normally between 100 and 150 Hv, making it a soft material. Martensite is a hard phase and its hardness rises as the carbon content does (Bouaziz, Zurob, and Huang 2013).

The necessity for novel, high-strength steels that would not compromise formability or cost was what sparked this creation. Steel grades with high elongation to ensure formability, high tensile strength to establish fatigue and crash resistance, and low alloy content to assure weldability without affecting production cost have been specifically sought by the automotive sector (Granbom 2010). This combination of characteristics may be found in DP steels. However, some of these steels still present some challenges mainly regarding formability and distortion.

Nowadays, after more than thirty years of being on the market, there is still a high demand for DP steels since these materials may lower the weight of automobiles by combining high strength and good formability, allowing a reduction in the components' thickness, while having a positive environmental and financial impact. DP steels exhibit, therefore, superior qualities when compared to other high strength low alloy (HSLA) steels (Granbom 2010), as seen in Figure 43.

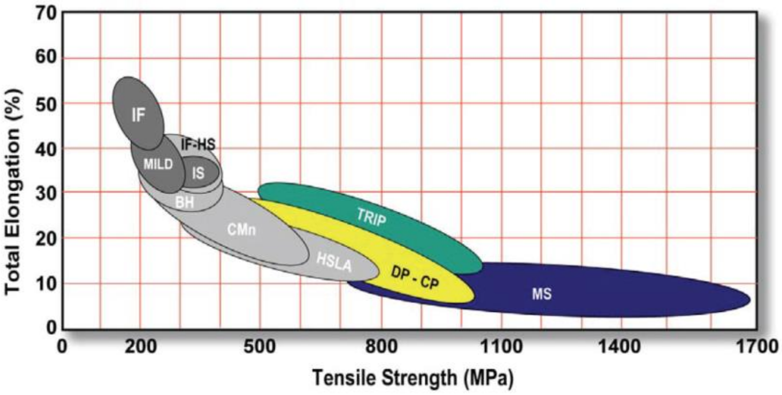

Figure 43 - Overview of mechanical properties (tensile strength and elongation) of some steels (Granbom 2010).

The automotive industry uses DP steels primarily for safety parts in car bodies, such as bumpers, B-pillars, side impact beams, etc., due to their combination of high strength, low cost, and high deformation hardening, which implies a high energy absorbing ability or "crashworthiness" (Granbom 2010), see Figure 44.

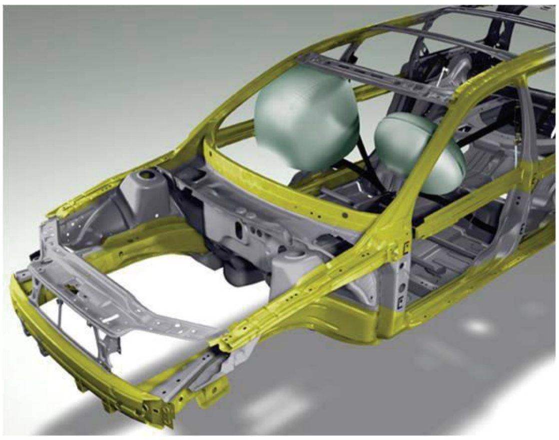

Figure 44 - Usage of DP steels in a car (Granbom 2010).

Nevertheless, the characteristics of DP steels are not all good. In spite of the efforts, one of the main technological challenges in designing and producing sheet metal parts with the necessary shape and dimensional precision using DP steels is the increased springback happening during the forming of high-strength steels, in addition to the significant changes in formability with increasing strength. These formability problems arise mostly in DP780, DP980 and DP1180 (Tisza and Lukács 2015).

Cold rolling of low alloy steels followed by intercritical annealing in a continuous annealing line, often known as CAL, is the most popular method for creating DP steels. The two-phase field of austenite/ferrite in the Fe-C diagram is referred to as intercritical. When quenched, the austenite phase will change to martensite if the steel hardens properly, and the cooling velocity is fast enough. The end outcome is a structure with hard martensite particles embedded within a soft continuous phase of ferrite. Figure 45 shows an illustration of a dual phase microstructure.

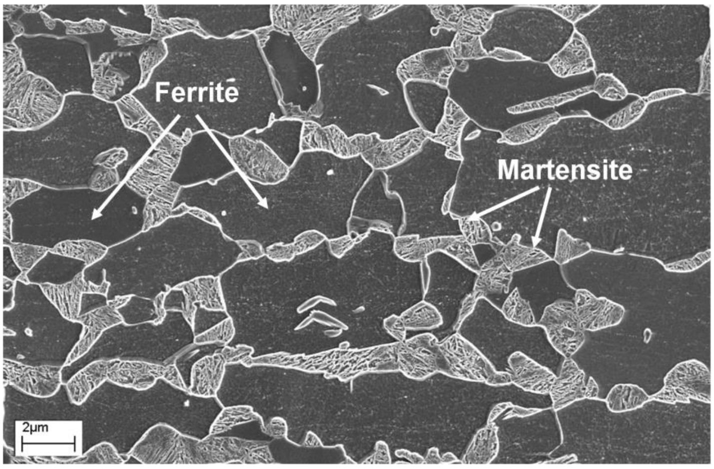

Figure 45 - Typical microstructure of a DP steel (Granbom 2010).

2.5.1 Production

Figure 46 describes a typical production line for DP steels and its description is based on the work of Granbom (2010).

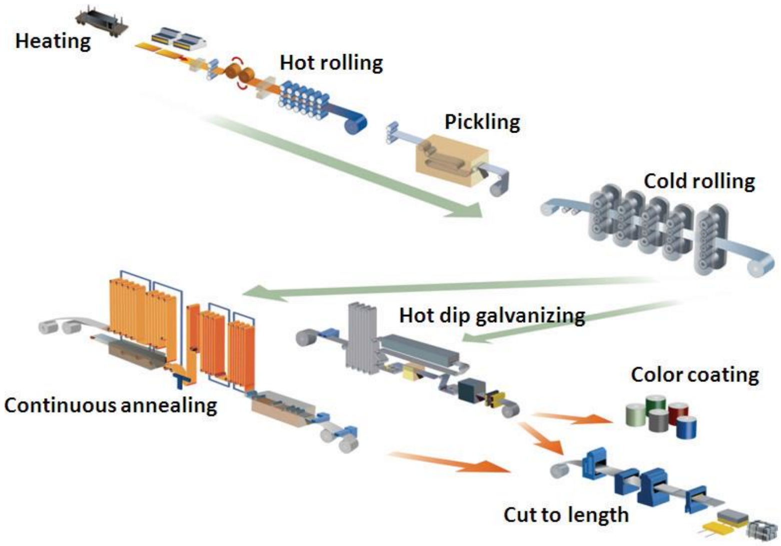

Figure 46 - DP steel production line (Granbom 2010).

Prior to the hot rolling mill, the temperature in the reheating furnaces reaches around 1200°C, and a fully annealed steel structure is obtained. Temperature and time in the reheating furnaces for micro alloyed steels are determined by the chemical composition of the steel grades in order to ensure the optimal dissolving of various particles. In order to create a ferrite-pearlitic structure with the correct grain size and particle distribution, the slabs are hot rolled in the temperature range in which the steel is austenitic and coiled. Dual phase steels have a typical chemical composition of 0.10-0.15C, 0.8-1.5Mn, 0.2-0.5Si, and sometimes, but not always, a tiny amount of the microalloying element Nb.

As the strip cools following hot rolling, oxide scales form on its surface. Before cold rolling, these must be eliminated to prevent surface flaws on the finished surface. Therefore, in the pickling line, oxide scale is removed using hot hydrochloric acid. The next process before annealing is the cold rolling line, which reduces the thickness and improves the surface quality. At this production stage, the conditions for further microstructural growth during annealing in the CAL are also established.

Figure 47 depicts a schematic representation of a CAL. Recrystallization and various phase transitions are the principal structural changes that occur in the CAL. The ferrite grains are distorted and extended in the rolling direction during cold rolling. The temperature at which the deformed structure begins to recrystallize is depending on the degree of deformation, chemical composition, and heating rate. In the soaking section, two major simultaneous processes occur: change of ferrite (α) to austenite (γ) and dissolution of carbide. The amount of austenite created is dependent on the soaking temperature, the soaking period, and the steel's chemical composition.

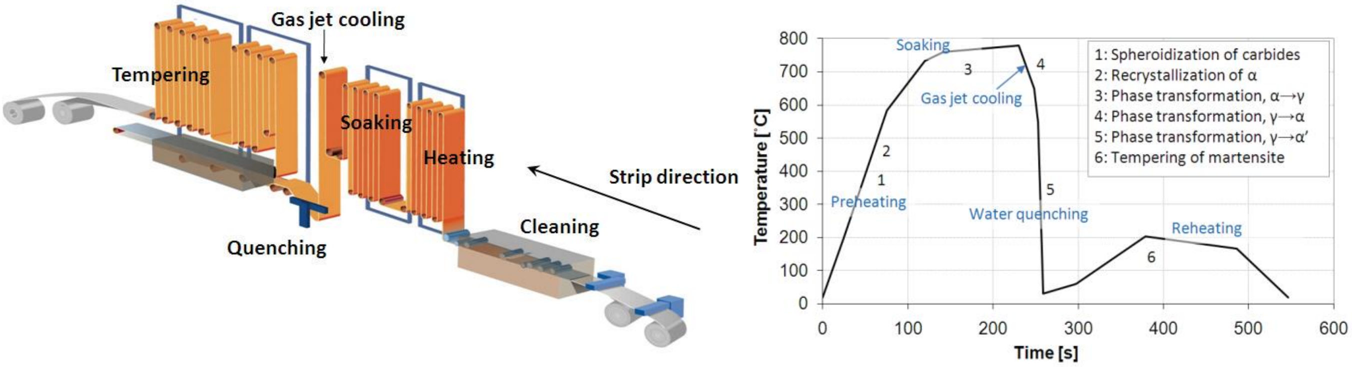
Gas jet cooling
Tempering
Soaking
Heating
Strip direction
Cleaning
Quenching
800
700
600
500
400
300
200
100
0
Temperature [°C]
Soaking
3
4
Gas jet cooling
2
1
Preheating
5
Water quenching
Reheating
6
1: Spheroidization of carbides
2: Recrystallization of α
3: Phase transformation, α→γ
4: Phase transformation, γ→α
5: Phase transformation, γ→α'
6: Tempering of martensite
0
100
200
300
400
500
600
Time [s]

Figure 47 - Continuous annealing line and process temperature description in time (Granbom 2010).

The material next passes into the gas-jet cooling stage, where the strip can be cooled with gas prior to water quenching. The passage in the gas-jet section always entails a retransformation from austenite to new ferrite, γ⟶α, due to a temperature reduction, even when the gas-jet cooling is turned off. The remaining austenite will then convert into martensite after being quenched in water. In the final portion of the CAL, the reheating zone, the martensite will be tempered.

2.5.2 Microstructure

There are still gaps in the knowledge of the physical metallurgy of the reactions leading to the DP structure as well as the plastic behavior of the material during deformation, despite the significant study that has been done in the subject of DP steels. The microstructure of the steel holds the key to understanding the mechanical behavior in major part. The chemical composition and production process parameters, in turn, influence the microstructure. A thorough work on the microstructure of dual-phase steels and its influence in the mechanical properties is made by (Güngör 2019) and summarized next.

When DP steels are subjected to uniaxial strain testing both phases begin to deform elastically. Due to its lower yield strength than the brittle martensite phase, the ductile phase, ferrite, then begins to yield first. Once the ferritic matrix begins to deform, martensite continues to elastically deform until it reaches its yield point. Martensite islands also start to yield above this yield point. Dual-phase steel's brittleness and strength are dependent on those properties of its martensitic phase.

An inter-granular plastic instability happens because the yield and ultimate tensile stress values between ferrite and martensite are so dissimilar. Localizations happen at the interface where martensite and ferrite meet because of this plastic instability. This local accumulation is crucial to the behavior of dual-phase steels during the hardening process.

A dual-phase steel's total mechanical response, particularly its strength and ductility, is greatly impacted by its ferrite grain size, martensite volume proportion, martensite carbon concentration, and martensite morphology.

In general, strength increases as the martensite volume percentage rises. However, it has a greater impact on ultimate tensile strength than yield strength. When opposed to ultimate tensile strength, martensite volume fraction has less of an impact on yield strength. The tensile strength and martensite volume fraction exhibit a roughly linear relationship. Higher martensite percentages boost the material's overall strength, however doing so is always unfavorable for ductility.

The strength of a DP steel is represented in Figure 48 as a function of martensite volume percentage and carbon content to emphasize the significance of reinforcing of the martensitic phase in this composite microstructure.

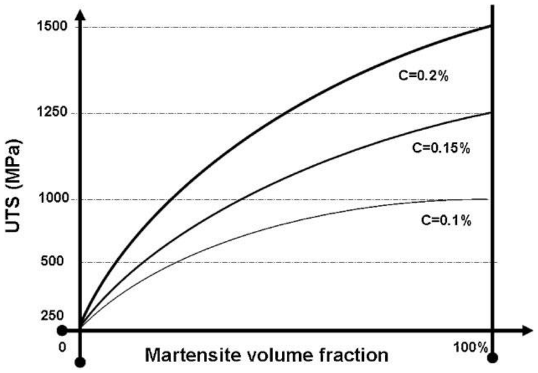

Figure 48 - UTS of a DP steel as a function of martensite volume percentage and carbon content (Bouaziz, Zurob, and Huang 2013).

In terms of the impact of martensite carbon content, a rise in carbon content increases the steel's strength and rate of hardening. The strongest martensite has the largest carbon concentration, but it has reduced ductility. As martensite with a higher carbon concentration exhibits brittle characteristics, it has been discovered that increased carbon content is unfavorable for material elongation.

Now regarding the effect of ferrite grain size. Lower carbon content percentages can be found in ferrite phase compared to martensite. As a result, the carbon concentration has a negligible impact on how ferrite flows. The main microstructural characteristic of ferrite that influences its own plastic behavior and, consequently, the strength and ductility of the DP steel is its grain size. The yield strength and the ultimate strength rise as the ferrite grain size decreases. Yet, it has been found that the ferrite grain size has a bigger impact on the DP steel's yield strength than on its ultimate tensile strength.

The final microstructural consideration is how the martensite morphology affects the strength and ductility of dual-phase steel. The strength and ductility of dual-phase steels are significantly influenced by the morphology (the form and distribution) of the martensite phase due to its contributions in microstructural properties including grain size and connectedness.

It is not quite obvious how the morphology and total strength are related. Equiaxed martensite particles are said to inhibit the plastic flow in the ferrite phase, causing strain hardening and an increase in yield and ultimate tensile strength.

2.5.3 Groups and general properties

Due to the ferrite–martensite structure, DP steels exhibit a mix of exceptional mechanical qualities, including high tensile strength, a high work hardening rate at early stages of plastic deformation, and good ductility, which distinguishes them from high strength low alloy steels. Due to the strain hardening process, dual-phase steels get stronger and achieve greater stress values during plastic deformation (Wu-rong et al. 2011).

In DP steels, the islands of martensite, dispersed in the ferritic matrix, act as an obstacle for dislocations and contribute to the improvement of resistance. The martensitic phase has a beneficial effect on fatigue life, as it can delay or prevent the growth of cracks.

These steels can essentially be formed as low strength steels. However, the parts produced have high resistance due to the high hardening coefficient. In addition, they have greater total elongation than any other high-strength or low-strength alloys steels of similar strength. The relatively high ductility presented by these steels is associated with the high plasticity of the ferrite phase. This occurs because the fissures in the martensite and the disconnection of the islands of martensite of the ferritic matrix occur for stresses higher than those found in the structures containing perlite (Du et al. 2007).

Thus, the main advantages of DP steels are high elongation, high strength, good formability, fatigue resistance, and crash resistance, in addition to being lightweight and economical. Nevertheless, this combination of excellent properties is not always verified for the strongest dual-phase steels. Namely, for DP steels with ultimate tensile strength above 780, total elongation is usually relatively low, affecting formability and possible defects.

Commercial names like DP600, DP750, and others denote the grade, and the number in the name indicates the material's minimum ultimate tensile strength. Steels that are offered for sale range in ultimate tensile strength from 450 to over 1200 MPa.

As it is common, stronger DP steels have lower ductility. Also, stronger DP steels have greater springback problems.

Table 3 presents basic properties of some commercial DP steels.

Table 3 - Basic mechanical properties of some DP steels (ArcelorMittal n.d.)

	$Rp_{0.2}$ **[MPa]**	R_m **[MPa]**	A_t **[%]**
(CR) DP450 TD	280-340	450-530	>27
(CR) DP500 RD	300-380	500-600	>25
(CR) DP600 RD	330-410	600-700	>21
(CR) DP780 Y500 RD	500-600	780-900	>13
(CR) DP980 Y700 RD	700-850	980-1100	>8
(CR) DP1180	900-1100	>1180	>5

2.5.4 Springback

Compared to the conventional steels, the design of stamped parts and stamping tools is complicated by the new DP steels, leading to new issues. One of them is springback, which is one of the biggest causes of rejection in plastically deformed parts. It causes a change in geometry of a part, at the end of its deformation process, when it is free from the action of stamping tools that acted on it (Stadnicki and Wróbel 2015).

It is generally known that springback results from uneven stress distribution over the component's cross section and that it is directly related to the cyclic plastic deformation that occurs during forming of DP steels. Throughout the majority of forming operations, various sections experience cyclic plastic deformation, such as bending and straightening along tool radiuses and passing through drawbeads. The Bauschinger effect, which invariably occurs in such forming circumstances (i.e., in loading-reverse loading settings), is another factor to take into account. It causes the hardening behavior to differ significantly in forward and reverse loading and it directly affects springback (Tisza and Lukács 2015).

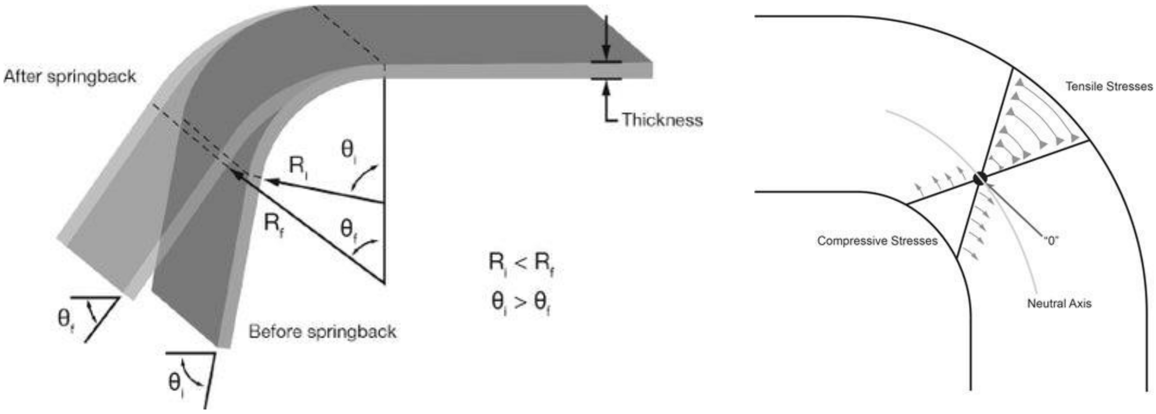

Figure 49 - Springback phenomenon (Tisza and Lukács 2015).

This springback phenomenon is more severe in AHSS than structural steel (the stronger the material, the greater the magnitude of springback, Figure 50). Thicker sheets also tend to be more affected by springback since they can accumulate more stresses (Jadhav, Schoiswohl, and Buchmayr 2018). It was also observed that springback increased as the tool radius and die gap increased (Davies 1981).

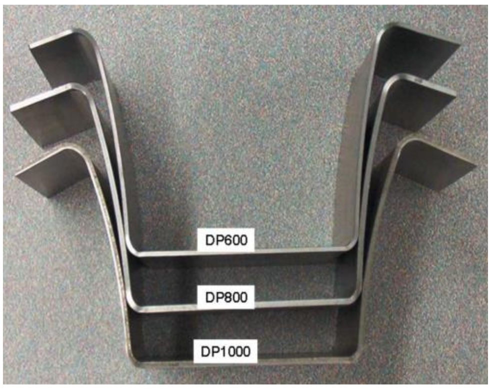

Figure 50 - Springback phenomenon in the same component made in DP600, DP800 and DP1000 (Peng, Koç, and Wenner 2008).

Therefore, among the parameters that influence the most the occurrence of springback are the mechanical properties of the material, like its strength or its Young’s Modulus, the geometry of the tools, like the tool radius or the die gap, and the blankholder force. The initial shape of the material, namely its thickness, the desired geometry, and the stamping conditions, like lubrication, temperature or interface-friction conditions, are also important parameters (Jadhav, Schoiswohl, and Buchmayr 2018).

By affecting the geometry of the stamped parts, the dimensional and geometrical accuracy of the finished component is compromised, see Figure 51. As a result, the industry faces several practical problems: first, prediction of the geometry of the final part with springback and second, the design of the appropriate tools to compensate for this effect. The springback phenomenon can appear in three types when considering the geometry of the product and the forming regime (Figure 51): angular change, sidewall curl, and twist. Also, a combination of these effects can occur (Dezelak et al. 2014).

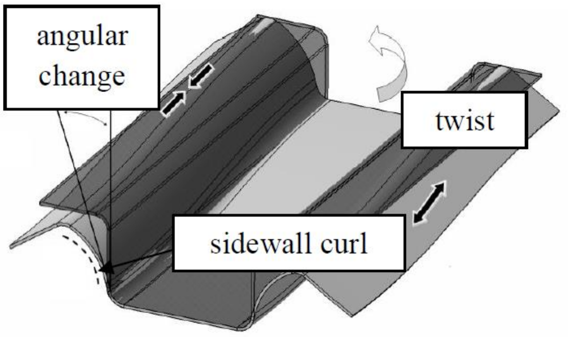

Figure 51 - Types of springback: angular change, twist and sidewall curl (Dezelak et al. 2014).

The springback problem has traditionally been solved by time- and money-consuming trial-and-error techniques. However, using FE simulation tools, designers are now able to save time and money by simulating the stamping process with increasing levels of accuracy and forecast a springback value. This enables the die's predesigned working surfaces to be adjusted in order to account for springback, called springback compensation (Stadnicki and Wróbel 2015).

In order to understand how springback compensation works let us assume that the shape of the working surface of the die is denoted by N, an element vector of nodal coordinates $\bar{\boldsymbol{s}} \in \boldsymbol{R}^N$, and the shape of the stamped part by M, an element vector of nodal coordinates $\bar{\boldsymbol{u}} \in \boldsymbol{R}^M$, whereas vectors $\bar{\boldsymbol{s}}_{nom}$ and $\bar{\boldsymbol{u}}_{nom}$ define the nominal state resulting from the geometric models of the CAD project. Let the function $\bar{\boldsymbol{u}} = \Omega(\bar{\boldsymbol{s}})$ transform the stamped part surface onto the working surface of the die. If the stamped part material is perfectly plastic, the stamped part obtained at the end of the stamping simulation will have the shape postulated in the CAD design $\bar{\boldsymbol{u}}_{nom} = \Omega(\bar{\boldsymbol{s}}_{nom})$. However, because of the springback of the stamped part material, in reality it will be $\bar{\boldsymbol{u}}_{nom} \neq \Omega(\bar{\boldsymbol{s}}_{nom})$. The determination of the shape of the die working surface, which compensates this effect, is therefore a task of optimization involving the determination of corrected die working surfaces $\hat{\boldsymbol{s}}$, in which the objective function is minimized:

$$e(\bar{\boldsymbol{s}}) = \| \bar{\boldsymbol{u}}_{nom} - \Omega(\bar{\boldsymbol{s}}) \| \longrightarrow min \tag{2.10}$$

where ‖ ‖ is the Euclidean norm.

For optimal solutions $\hat{\boldsymbol{s}}$, it should be $e(\bar{\boldsymbol{s}}) = \bar{\boldsymbol{0}}$. However, due to the nonlinearity and complexity of the problem, we shall accept the corrected shape which is an approximation of the optimal solution. It is worth noting at this point that solutions leading to the penetration of nodes of the die working surface model into the stamped part surface model are unacceptable (Stadnicki and Wróbel 2015).

3 Numerical modelling of sheet metal forming processes

The concept of virtual manufacturing has been established to improve industrial performance, as it is one of the most effective means of reducing manufacturing times and enhancing product quality. As a component of the virtual manufacturing process, numerical simulation of metal forming processes contributes significantly to decrease lead times.

Nowadays, the finite element approach is the most popular numerical technique for simulating sheet metal forming operations. The constitutive models and forming limit curve models that are incorporated into the framework of simulation programs used in industry affect their correctness (Banabic et al. 2010).

The proper material model, which includes the proper plastic yield criteria and the flow rule, serves as the starting point for the analysis. It is well recognized that the yield criterion has a substantial effect on the predicted strain and stress distribution and is also crucial for predicting strain localization and fracture (Eggertsen and Mattiasson 2010).

3.1 Constitutive material models

Constitutive models are ubiquitous in scientific research and manufacturing processes as a means of gaining a deeper understanding of certain physical events. The basic objective of material constitutive models is to replicate reality as closely as possible under various assumptions and criteria, depending on the model's final objective and application domain. The reference of this chapter is the work of (Amaral 2020) unless other indication is given.

In recent years, tremendous efforts have been devoted to the development of new constitutive models or the modification of existing models that mathematically capture the many sheet metal behaviors, from hardening to damage, without ignoring anisotropy. The advent of new sophisticated materials whose behavior differs from those already well understood and whose inaccuracy in characterizing the mechanical behavior is clear, contributes to this necessity. However, the accuracy of the findings derived from the numerical simulation is dependent on the characterization of the mechanical properties of the materials, among other things.

Three elements are needed in order to describe the plastic behavior of a material in a general stress state: a yield criterion that expresses a relationship between the stress components at the moment when plastic 'yielding' occurs, an associated flow rule that states the relationship between the components of the strain-rate and stress, and a hardening rule that describes the evolution of the initial yield stress during the forming process (Banabic et al. 2010). Besides that, to simulate a manufacturing process, it is also necessary to establish a failure criterion. As it is imaginable by now, the possible combinations are numerous, see Figure 52.

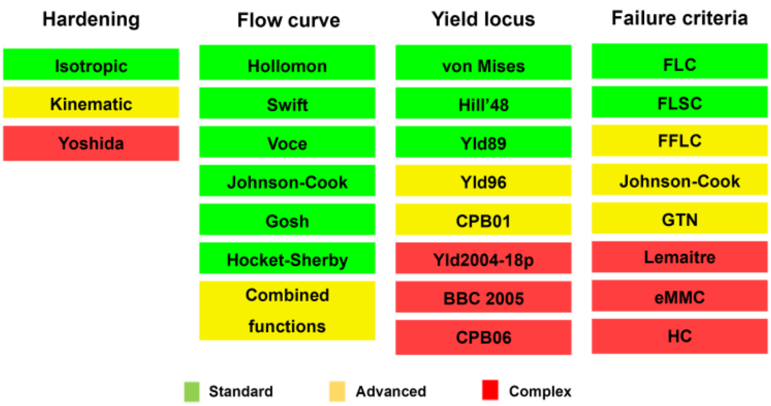

Hardening	Flow curve	Yield locus	Failure criteria
Isotropic	Hollomon	von Mises	FLC
Kinematic	Swift	Hill'48	FLSC
Yoshida	Voce	Yld89	FFLC
	Johnson-Cook	Yld96	Johnson-Cook
	Gosh	CPB01	GTN
	Hocket-Sherby	Yld2004-18p	Lemaitre
	Combined functions	BBC 2005	eMMC
		CPB06	HC

🟩 Standard 🟨 Advanced 🟥 Complex

Figure 52 - Implementation complexity of different constitutive models with respect to the main purpose (Amaral 2020).

Using specialized computer-aided engineering (CAE) software, appropriate material models, and complicated FEM models are required for the modelling of advanced high-strength steel sheet stamping processes. In fact, the engineering design of vehicle body elements frequently results in the creation of issues that are difficult to resolve and require a considerable amount of time (Stadnicki and Wróbel 2015).

3.1.1 Hardening behavior

In general, a different stress level from the initial condition is required for the progression of plastic deformation, which is dependent on the amount of plastic deformation imposed on the material. This process, known as hardening, describes how the yield surface evolves as the plastic deformation develops.

The multi-axial stress condition for the occurrence of plastic deformation is defined by the yield criterion which is a function that represents the yielding condition for all stress situations. It can be characterized generally as:

$$\Phi = f(\boldsymbol{\sigma}) - \sigma_Y(\varepsilon_p) = 0 \tag{3.1}$$

This relationship indicates that yielding takes place when the effective stress $f(\boldsymbol{\sigma}) = \bar{\sigma}$, which is a scalar function of the state of stress, reaches a critical value σ_Y, which is a function of the effective plastic strain ε_p. The function $\sigma_Y(\varepsilon_p)$ is often derived from a curve of uniaxial stress versus plastic strain.

Figure 53 illustrates the models typically employed to characterize the hardening behavior of materials during plastic deformation, detailed on the left and summarized on the right.

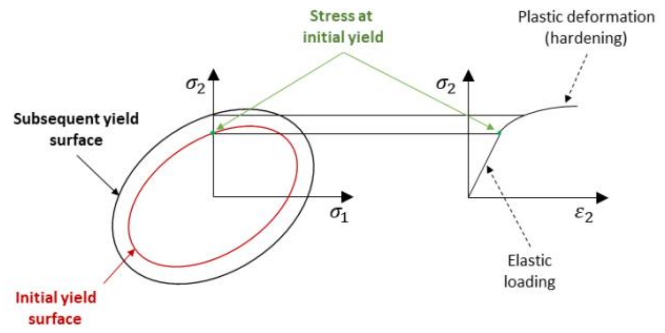
Stress at initial yield
Plastic deformation (hardening)
σ_2
σ_2
Subsequent yield surface
σ_1
ε_2
Elastic loading
Initial yield surface

(a) Isotropic hardening

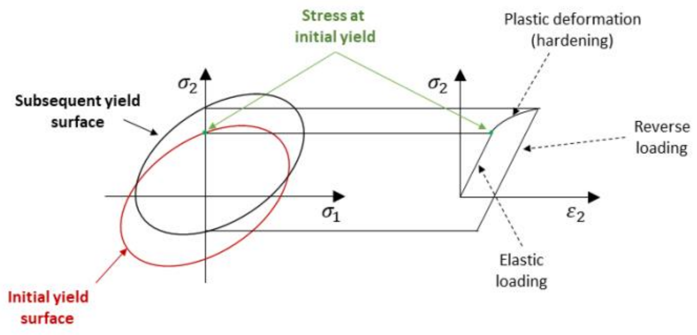
Stress at initial yield
Plastic deformation (hardening)
σ_2
σ_2
Subsequent yield surface
Reverse loading
σ_1
ε_2
Elastic loading
Initial yield surface

(b) Kinematic hardening

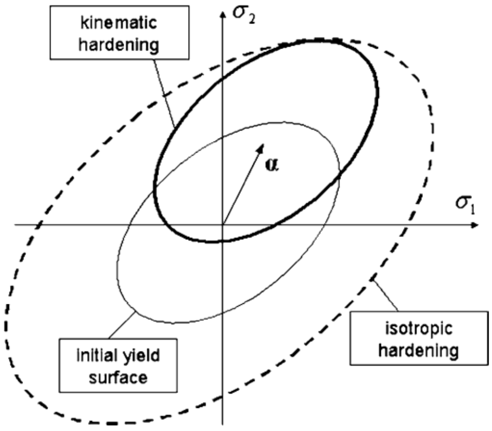
kinematic hardening
σ_2
α
σ_1
initial yield surface
isotropic hardening

Figure 53 - Isotropic and kinematic hardening (Amaral 2020), (Banabic et al. 2010).

Figure 53(a) represents a material undergoing hardening, as the yield surface increases with loading. The term for this sort of hardening is isotropic hardening. It is characterized by a yield locus that expands uniformly without altering shape. In this model of hardening, it is assumed that the initial tensile and compression stresses are identical, so the stress asymmetry that emerges for different deformation trajectories, such as the Bauschinger effect, can be disregarded.

The second model, depicted in Figure 53(b), is characterized by the fact that the subsequent yield surface maintains its shape and dimensions, but undergoes rigid body translations in the plane $\sigma_1 - \sigma_2$. For this reason, it is referred to as kinematic hardening. In instances where the Bauschinger effect is significant, such as when there is a sudden inversion of the strain path, this sort of hardening is applied. This is uncommon in plastic deformation processes, where deformation paths are often monotonic and strain levels are extremely high.

There are, however, theories of hardening that come from a combination of isotropic and kinematic hardening such as the Yoshida-Uemori law:

$$\sigma_Y = (1-\mu)[Y + R_{sat}(1 - e^{-m\varepsilon_p})] + \mu\left[C(\varepsilon_0 + \varepsilon_p)^n\right] \tag{3.2}$$

or the ThyssenKrupp Extrapolation method

$$\sigma_Y = \alpha\left[C(\varepsilon_0 + \varepsilon_p)^m\right] + (1-\alpha)[\sigma_{sat} - (\sigma_{sat} - \sigma_i)e^{-a\varepsilon_p}] \tag{3.3}$$

The Yoshida–Uemori constitutive model has been widely applied to simulations of springback since it has into account several effects that occur during bending and unbending of the sheet metal. It is based on a non-linear, two-surface kinematic hardening strategy and can predict the majority of complex hardening behaviors during load reversal (Figure 54), namely: the Bauschinger effect (a), the effect of transition from elastic to plastic state (b), the hardening effect (c), and the effect of final weakening (d).

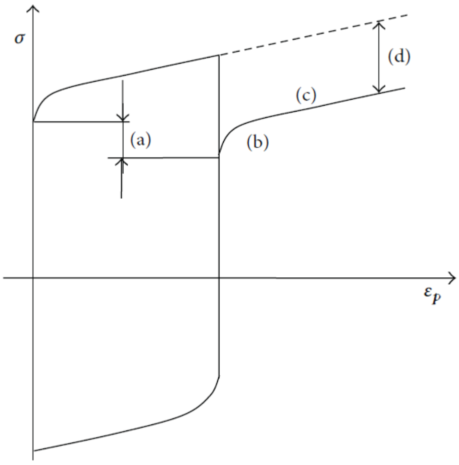

Figure 54 - Complex hardening behaviors during load reversal (Stadnicki and Wróbel 2015).

Some common isotropic hardening laws, with several material parameters, are:

- Ludwick

$$\sigma_Y = \sigma_0 + K\varepsilon_p^n \tag{3.4}$$

- Hollomon

$$\sigma_Y = K\varepsilon_p^n \tag{3.5}$$

- Voce

$$\sigma_Y = A - B(1 - e^{-C\varepsilon_p}) \tag{3.6}$$

- Swift

$$\sigma_Y = C(\varepsilon_0 + \varepsilon_p)^m \tag{3.7}$$

- Ghosh

$$\sigma_Y = C(\varepsilon_p + \varepsilon_0)^m - D \tag{3.8}$$

- Hockett-Sherby

$$\sigma_Y = \sigma_{sat} - (\sigma_{sat} - \sigma_i)e^{-\alpha\varepsilon_p^p} \tag{3.9}$$

- Swift/ Hockett-Sherby

$$\sigma_Y = (1-\alpha)\left[C(\varepsilon_0 + \varepsilon_p)^m\right] + \alpha\left[\sigma_{sat} - (\sigma_{sat} - \sigma_i)e^{-\alpha\varepsilon_p^p}\right] \tag{3.10}$$

- Swift/ Voce

$$\sigma_Y = (1-\alpha)\left[K(\varepsilon_0 + \varepsilon_p)^n\right] + \alpha[A - B(1 - e^{-C\varepsilon_p})] \tag{3.11}$$

According to previous studies, the Swift rule is more suitable for describing the behavior of materials that display isotropic hardening without saturation, which is more applicable to steels than to aluminum alloys.

In contrast, the Voce law is better suited to describing the behavior of materials that display isotropic hardening with saturation. This law applies better to aluminum alloys.

The combination of these two laws (Swift and Voce) makes it possible to characterize the mechanical behavior of a material with a high initial hardening behavior and saturation at greater levels of plastic strain.

The Swift and Hockett–Sherby combined formula has been used to describe the hardening behavior of some dual-phase steels. It is in good agreement with the flow curve of the tensile test of 1.0 mm thick DP1000 (Wu-rong et al. 2011).

The choice of the hardening behavior of the material is of extreme importance and the limitations of the model implemented must be known. Implementing a kinematic hardening model causes a higher material displacement than isotropic hardening. It is shown by several studies that the isotropic hardening underestimates the springback of the part considered, while the kinematic hardening model with standard parameters overestimates the springback in certain areas (Prexl et al. 2010), (Firat et al. 2013).

3.1.2 Yield criteria for anisotropic materials

To describe the plastic behavior of a sheet metal material for any general stress state, a yield criterion should be considered, which allows the identification of the transition moment from the elastic to the plastic regime. It was previously seen that the yield criterion is generally given by the Equation 3.1.

In the principal stress three-dimensional space, this function is represented by a three-dimensional surface, within which the material exhibits an elastic state ($\Phi < 0$) and, if on the surface, a plastic state ($\Phi = 0$). The yield surface can be defined using a variety of models. Typically, for sheet metal forming only the components of stress acting on the blank surface are considered relevant, i.e., plane stress conditions are considered, with $\sigma_{zz} = \sigma_{xz} = \sigma_{yz} = 0$. As a result, the representation is reduced to a bidimensional yield curve in the major stress plane.

Another important point that is needed in plasticity is the stress and strain-rate components relationship, being given by a flow rule, which can be associated (AFR) or non-associated (NAFR).

3.1.2.1 Anisotropy

Anisotropy characterizes the greater or lesser tendency of a given material to deform in a particular preferred direction to the detriment of the others. Anisotropic materials can then be defined as materials that present different mechanical properties according to the direction in which they are requested. On the contrary, the so-called isotropic materials always exhibit the same behavior regardless of direction.

This property is particularly influenced by the manufacturing process, the crystallographic texture, the percentage of chemical elements, and the thermal and mechanical treatments.

As a result of their crystallographic structure and the peculiarities of the rolling process, sheet metals typically display a notable anisotropy of mechanical properties. In fact, the rolling process creates a specific anisotropy characterized by the symmetry of the mechanical characteristics in three orthogonal planes. This type of mechanical behavior is known as orthotropy. The orthotropy axes are the intersection lines of the symmetry planes. The orientation of rolled sheet metals is as follows (see Figure 55): rolling direction (RD), transverse direction (TD), and normal direction (ND).

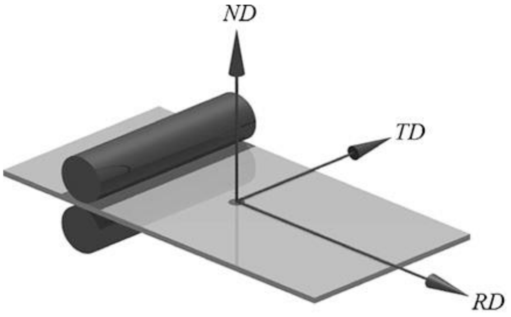

Figure 55 - Definition of the RD, TD and ND.

A metric known as the Lankford parameter or anisotropy coefficient measures the variance of their plastic behavior with direction. This coefficient is derived by uniaxial tensile tests on strip-shaped sheet specimens. Having in mind the condition of volume constancy, the anisotropy coefficient r is defined by:

$$r = \frac{\varepsilon_2}{\varepsilon_3} = -\frac{\varepsilon_2}{\varepsilon_1 + \varepsilon_2} \tag{3.12}$$

where ε_1, ε_2 and ε_3 are the strains in the length, width and thickness directions. If $r = 1$ the material is isotropic. If $r > 1$ the width strains will be dominant (the thinning resistance is more pronounced) and if $r < 1$ the thickness strains will dominate.

The average of the r-values obtained for different directions in the plane of the sheet metal represents the so-called coefficient of normal anisotropy r_n:

$$r_n = \frac{r_0 + 2r_{45} + r_{90}}{4} \tag{3.13}$$

being r_0, r_{45} and r_{90} the values of r at specimens cut along directions at 0°, 45° and 90° relative to the rolling direction in the plane of the sheet metal.

Another used measure is planar anisotropy Δr, which is related to the earring amplitude:

$$\Delta r = \frac{r_0 - 2r_{45} + r_{90}}{2} \tag{3.14}$$

The experimental research has proved that the yield surfaces are not symmetric in the biaxial region. This fact is also a consequence of the plastic anisotropy. In order to give a quantitative description of such a behavior, the so-called coefficient of biaxial anisotropy r_b has been defined as:

$$r_b = \frac{\varepsilon_2}{\varepsilon_1} \tag{3.15}$$

If the material is isotropic the coefficient will be 1. The more pronounced is the anisotropy, the farther is the coefficient from unity. This parameter is a direct measure of the slope of the yield locus at the balanced biaxial stress state.

3.1.2.2 Principal of normality

To find the constitutive equations of the plastic domain for a specific material, it is important to establish a relationship between the stresses and the strain increment knowing that the plasticity criterion specifies the combination of stresses that initiate the plastic flow.

Decomposing the stress increment vector, $d\boldsymbol{\sigma}_{ij}$, in tangential $d\boldsymbol{\sigma}_{ij}^{t}$ and normal $d\boldsymbol{\sigma}_{ij}^{n}$ directions relative to the yield locus (Figure 56), it appears that the tangential component of the stress vector gives a neutral loading condition without associated plastic deformation (case of purely plastic material). In contrast, the normal component will produce the plastic strain increment $d\boldsymbol{\varepsilon}_{ij}^{p}$ perpendicular to the yield surface, which can be mathematically stated as:

$$d\boldsymbol{\varepsilon}_{ij}^{p} = d\lambda \frac{\partial g(\boldsymbol{\sigma}_{ij})}{\partial \sigma_{ij}} = \begin{cases} d\lambda = 0, if\ \Phi < 0 \\ d\lambda > 0, if\ \Phi = 0 \end{cases} \tag{3.16}$$

where $g(\boldsymbol{\sigma}_{ij})$ is the plastic potential function, $d\lambda$ is a plastic multiplier and depends on the loading history, and $\frac{\partial g(\boldsymbol{\sigma}_{ij})}{\partial \sigma_{ij}}$ is a vector normal to the yield surface at the considered loading point.

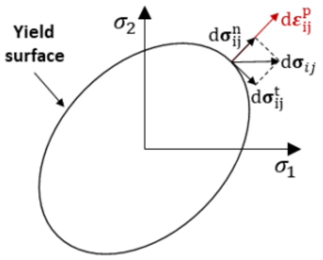
Yield surface
σ_2
$d\sigma_{ij}^{n}$
$d\varepsilon_{ij}^{p}$
$d\sigma_{ij}$
$d\sigma_{ij}^{t}$
σ_1

Figure 56 - Representation of stress and plastic strain increment direction applied to the von Mises yield surface (Amaral 2020).

For the purpose of defining the increment of the plastic strain rate, $d\boldsymbol{\varepsilon}_{ij}^{p}$, an associate flow rule (AFR) illustrated in Figure 57(a) is used, which determines the flow direction. This can also be called the principle of normality.

Adopting an AFR means that the yield and the plastic potential surfaces are considered as described by the same functions, $f(\boldsymbol{\sigma}_{ij}) = g(\boldsymbol{\sigma})$.

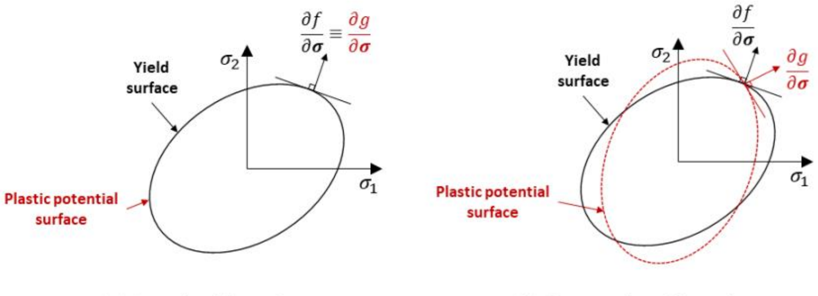
$\frac{\partial f}{\partial \boldsymbol{\sigma}} \equiv \frac{\partial g}{\partial \boldsymbol{\sigma}}$
Yield surface
σ_2
σ_1
Plastic potential surface
$\frac{\partial f}{\partial \boldsymbol{\sigma}}$
$\frac{\partial g}{\partial \boldsymbol{\sigma}}$
Yield surface
σ_2
σ_1
Plastic potential surface

(a) Associated flow rule (b) Non-associated flow rule

Figure 57 - Different types of plastic flow directionality (Amaral 2020).

Although it is not used in this work, there is also the possibility to adopt a non-associated flow rule (NAFR) when the anisotropy cannot be predicted. This can improve the accuracy of the material characterization by considering different function for the yield and the plastic surfaces, $f(\boldsymbol{\sigma}_{ij}) \neq g(\boldsymbol{\sigma})$.

3.1.2.3 Yield criteria for isotropic material

Some very famous models are known for isotropic materials (Banabic et al. 2010):

- Tresca

$$max\{|\sigma_1 - \sigma_2|, |\sigma_2 - \sigma_3|, |\sigma_3 - \sigma_1|\} = \sigma_y \tag{3.17}$$

  where σ_1, σ_2 and σ_3 are the principal stresses and σ_y is the initial yield stress. This criteria states that the material passes from an elastic to a plastic state when the maximum shear stress τ_{max} reaches a critical value.

- Huber-von Mises

$$(\sigma_1 - \sigma_2)^2 + (\sigma_2 - \sigma_3)^2 + (\sigma_3 - \sigma_1)^2 = 2{\sigma_y}^2 \tag{3.18}$$

  This criteria states that the material passes from an elastic to a plastic state when the elastic energy of distortion reaches a critical value that is independent of the type of the stress state.

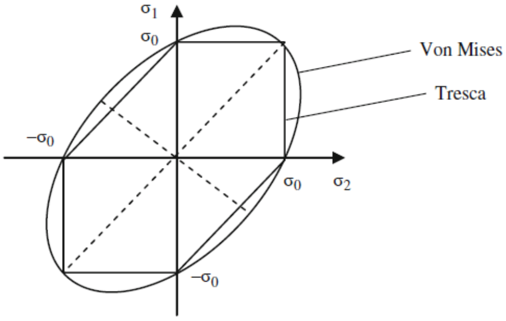

Figure 58 - Tresca and von Mises yield surfaces.

3.1.2.4 Yield criteria considering anisotropy

Regarding anisotropic materials, from the many models for plane stress and strain that are published in the literature, the most frequently utilized in practice when it comes to anisotropic materials are:

- Hill (Hill 1948) known as Hill 48 criteria:

$$\bar{\sigma}^2 = \sigma_{xx}^2 - \frac{2r_0}{1+r_0}\sigma_{xx}\sigma_{yy} + \frac{r_0(1+r_{90})}{r_{90}(1+r_0)}\sigma_{yy}^2 + \frac{r_0+r_{90}}{r_{90}(1+r_0)}(2r_{45}+1)\sigma_{xy}^2 \tag{3.19}$$

  where r_0, r_{45} and r_{90} are the Lankford coefficients characterizing anisotropy, oriented towards the direction of rolling, diagonal and transverse determined in a uniaxial tensile test. In order to define the yield under plane stress condition, these three mechanical parameters are needed. The Hill 48 criteria is still widely used since the small number of parameters included in the yield functions have a direct physical meaning.

  However, due to this mathematical simplicity, this model cannot accurately describe the planar distribution of both the uniaxial yield stress and the uniaxial coefficient of plastic anisotropy and it cannot capture the biaxial yield stress.

- Barlat and Lian (Barlat and Lian 1989) known as Barlat 89 criteria:

$$2\bar{\sigma}^M = a|k_1 + k_2|^M + a|k_1 - k_2|^M + c|k_2|^M \tag{3.20}$$

where

$$k_1 = \frac{1}{2}(\sigma_{xx} + h\sigma_{yy}) \text{ , } k_2 = \sqrt{\left(\frac{\sigma_{xx} - h\sigma_{yy}}{2}\right)^2 + p^2\sigma_{xy}^2} \text{ , } h = \sqrt{\frac{r_0(1+r_{90})}{[(1+r_0)/r_{90}]}} \text{ ,}$$

$$a = 2 - c \text{ , } c = 2\sqrt{\frac{r_0 r_{90}}{(1+r_0)(1+r_{90})}} \text{ , } p = \frac{\sigma_0}{\sigma_p}$$

where σ_0 is a yield strength at bidirectional stretching at $\sigma_{xx} = \sigma_{yy}$ and σ_p is a yield strength at unidirectional stretching and M=6 for steel. This criterion is very flexible since only four parameters are needed although they do not have a physical meaning and the parameter p is not easy to identify.

- Banabic, Aretz, Comsa and Paraianu (Banabic et al. 2005) known as BBC2005 criteria:

$$\bar{\sigma} = [a(\Lambda + \Gamma)^{2k} + a(\Lambda - \Gamma)^{2k} + b(\Lambda + \Psi)^{2k} + b(\Lambda - \Psi)^{2k}]^{\frac{1}{2k}} \tag{3.21}$$

where $k \in \mathbb{N} \geq 1$ and $a, b > 0$ are material parameters and Λ, Γ and Ψ are functions of further material parameters, L, M, N, P, Q and R, as well as the components of the Cauchy stress tensor.

$$\Gamma = \left(L\sigma_{xx} + M\sigma_{yy}\right) \text{ , } \Psi = \sqrt{\left(Q\sigma_{xx} - R\sigma_{yy}\right)^2 + \sigma_{xy}\sigma_{yx}} \text{ ,}$$

$$\Lambda = \sqrt{\left(N\sigma_{xx} - P\sigma_{yy}\right)^2 + \sigma_{xy}\sigma_{yx}}$$

This criterion is part of a group of advanced anisotropic yield criteria since it is more complex than the others in order to be applicable to the more recent materials like AHSS for example. Being more complex implies more input parameters which are not always easy to get. To define this criterion nine material parameters are needed, eight of them need to be determined through experiments. The exponent k depends on the crystallographic structure of the material. Standard values of k=3 and k=4 for body-centered cubic (BCC) and face-centered cubic (FCC) materials, respectively, are recommended by the authors of the model.

3.1.2.5 Choice of yield criteria

The current state-of-the-art in anisotropic plasticity modeling is rather muddled since several other yield criteria in addition to the ones mentioned above are still in use. The following are the most crucial considerations that must be made while selecting the yield criterion (Banabic et al. 2010):

- The yield locus, the uniaxial yield stress, and the uniaxial coefficient of plastic anisotropy can all be predicted accurately.
- The computation is quick and simple to apply in numerical simulation software.
- Flexibility and generality of the yield criterion.
- Number of mechanical parameters needed by the identification procedure and the difficulties associated with their experimental determination.
- Robustness of the identification procedure.
- User-friendliness of the yield criterion.
- Acceptance of the yield criterion in the scientific/industrial community.

3.2 Simulation of cutting and stamping processes

The constant reduction in the development time of new product series requires the development and intensive use of simulation tools. These numerical modelling tools had a great development in the 90's and Portugal has followed the state of the art in this area.

Currently, through the constant improvement of the forecasting quality of the processing models and the performance of computers, it is possible for simulation systems to predict the effects of changes in process parameters with increasing reliability. Therefore, these simulation systems allow for shorter development times and at the same time increased process confidence.

It is possible to reproduce the complete manufacturing process on computer before actually performing it. Process simulation is oriented towards three main objectives: verification of the possibility of achieving an existing manufacturing concept, verification of product properties and optimization of the manufacturing process.

The use of simulation is particularly important in the first steps of projecting a stamped component. The prediction of defects can, from an early stage, be taken into account to optimize the stamping tool, avoiding alterations after it is built. This represents significant savings of time and money.

In the last decade, computer-aided design systems applied to thin sheet metal forming processes have emerged, mainly in the automotive industry. These systems seek, through simulation, to eliminate the empirical iterative error correction process, replacing it with simulation processes that provide answers about the feasibility of executing a given component, without a prototype having been built. In addition, all the data relating to the geometry of the model used during the design phase are subsequently used, both in the simulation phase and in the tool manufacturing phase. The comparison between the traditional and the current process flow is represented in the diagrams of Figure 59 (Dias dos Santos, Ferreira Duarte, and Barata da Rocha 2005).

The current commercial FE codes are based on several formulations. In terms of the mathematical formulation of the equilibrium equations, they might be static or dynamic, and explicit or implicit in terms of the temporal integration approach (Hongzhi and Zhongqin 2000).

Until the appearance of AutoForm, the software market was ruled by dynamic-explicit codes. Examples of codes in use include general-purpose codes like LS-DYNA and ABAQUS/Explicit and specialized codes like PAM-STAMP and OPTRIS. The static-implicit FE codes were more frequently utilized in academic circles, with a few exceptions such as INDEED in the German automobile sector and MTLFORM at Ford Motor Company. However, contrary to the tendency, a research initiative at ETH in Zurich led to the creation of AutoForm, a highly specialized code for stamping simulations. This FE code, which is based on the static-implicit method, incorporates several cutting-edge techniques to improve stability and computing efficiency, putting it on par with the best-in-class dynamic-explicit codes.

These commercial stamping software programs have undergone constant development over the past years to produce outcomes that are more consistent and robust. The stamping FE codes now include new material models as a result of the efforts of various authors. The graphical user interfaces (GUI) have also advanced greatly from throughout the years. Moreover, additional capabilities were added to accommodate the changing demands and expectations of the contemporary automobile industry (such as blank design, die design, process planning, and cost estimates) (Pimentel et al. 2018).

Regardless of the commercial software used, there are a lot of output results or variables that are of extreme importance to the automotive industry. Among those are the estimation of the punch forces, the draw-in, the principal strains distribution, the formability, the springback, and the computational cost.

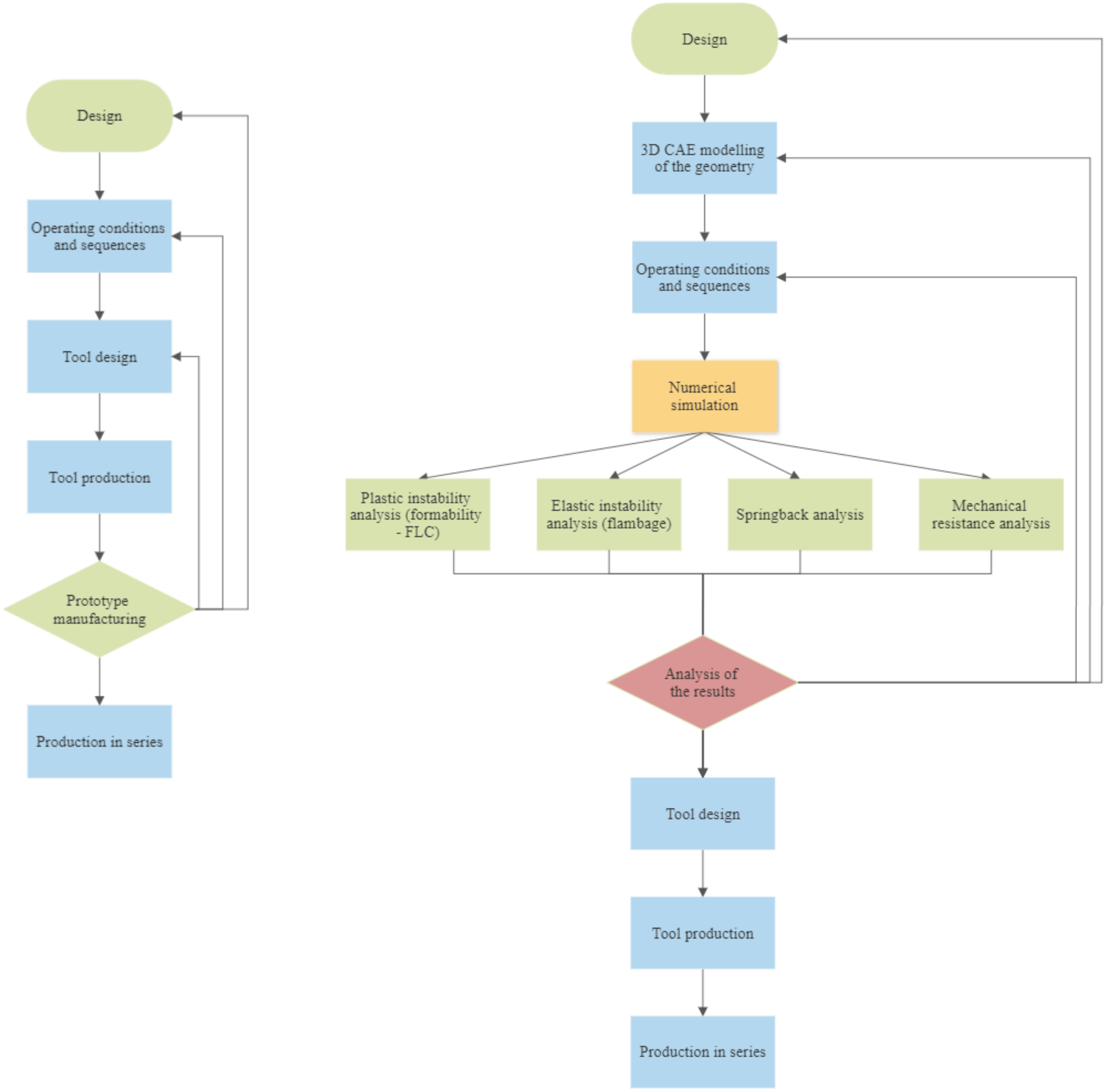
Design
Operating conditions and sequences
Tool design
Tool production
Prototype manufacturing
Production in series
Design
3D CAE modelling of the geometry
Operating conditions and sequences
Numerical simulation
Plastic instability analysis (formability - FLC)
Elastic instability analysis (flambage)
Springback analysis
Mechanical resistance analysis
Analysis of the results
Tool design
Tool production
Production in series

Figure 59 - Process flow before and after the use of numerical simulation.

Correctly defining the punch forces is important because finding a stamping press that can handle the load and energy demands is highly dependent on having all the forming and cutting forces for each stage predicted correctly. By employing draw-in optimization, the ideal blank size and geometry may be determined, helping to reduce the need for raw materials and prevent process instabilities like wrinkles and ruptures. Regarding formability, it was already described the importance of knowing the most requested strain paths given by the FLC. Similarly, the importance of accurately predicting springback was previously stated. Finally, when it comes to computational cost it should be minimized since the timeframes for projects involving the design and development of stamping tools are getting shorter in the automotive sector and also, every issue that occurs on the production line needs to be fixed right away (Pimentel et al. 2018).

To summarize, the principal characteristics of a trustworthy and effective software for numerical simulation of sheet metal include: the ability to simulate enormous plastic and elastic strains of big sections in a short amount of time, automated sheet remeshing for places with high strains and tensions, precise forecasts of strains and pressures, use of a suitable local necking or fracture criterion (major cause of part rejection), accurate prediction of springback (another major cause of part rejection), the ability to include the initial residual stresses existing in the material, the capacity to employ a plastic anisotropy yield criterion for combined isotropic and kinematic hardening for sheet metal plastic behavior, as well as microporosity development and growth throughout the plastic deformation process, the potential of employing a mathematical model for changing friction with normal pressure and sliding distance and roughness progression with straining, prediction of the evolution of surface roughness and microstructure during formation, the ability to adjust the blank hold pressure and temperature throughout the stamping operation (Bressan et al. 2010).

Overall, several studies show that the software available present similarly accurate results. However, AutoForm may offer additional modules, such as AutoForm Sigma and AutoForm Compensator, to enhance stamping die design with accurate springback compensation and presents a greater virtual productivity because of its pre/post processing environment and features. This is probably why it is likely the most used software in automotive industry.

3.2.1 AutoForm presentation

AutoForm is a specific numerical calculation application that, using the finite element method, allows to predict the stress states and strains to which a plate is subjected during a process of sheet metal forming. It is particularly designed to simulate the formability of components for the automotive industry. These procedures undoubtedly entail nonlinear analysis in thin sheets that undergo finite or large deformations. The software is based on an implicit method and assumes a plane stress condition, only the central plane of the sheet is loaded as a result of using triangular, tridimensional elements with a Lagrangian formulation.

Generically, it can be said that this tool can be used to develop the necessary and appropriate tools for a certain part having the final piece as the starting point, to obtain a part and proceed to the respective simulation starting from the tools, and also to change an existing part or tool, before or after its simulation, so as to improve the quality of the part.

Gestamp Cerveira uses this powerful simulation tool in order to obtain a result very close to what actually happens in the stamping of a particular part, thus managing to anticipate problems, reduce costs and even develop alternative solutions, guaranteeing their quality, trying to avoid that parts go to production without due prior study, avoiding unnecessary costs. However, it is important to remind that the accuracy of a simulation depends on the quality of the input data, which should be as representative as possible of the actual process to be studied, namely regarding geometries, material properties, and process variables.

The software will be presented in this subchapter according to the online software manual available for the R10 version (AutoForm® 2021), the same used in this work, and some summary information already gathered by Marzia (2020).

The simulation process in AutoForm is sequentially divided into 7 modules distributed, in order to define all the steps involved in the stamping process, regarding both the stamped part and the tools used. The modules that make up this process are as follows:

- Part – Import the CAD model of the part to be studied, define the geometry, the positioning of the part, the material of which it is made and its thickness.
- Plan – Indicate the operations, as well as the steps of the stamping process that the part will suffer.
- Die Face – Define the boundary conditions of the geometry.
- Blank – Create the initial sketch of the part.
- Process – Organize the tools that will act on the part.
- Simulation – Indicate simulation parameters and simulate.

- Evaluation – Analysis of the results.

After completing the simulation, it is possible to analyze different parameters that come out as results of the simulation. Each step in the sequence can be independently studied and optimized as a separate solution (Fedorko, Urbánek, and Rund 2017).

3.2.2 Implicit solution

The integration strategy employed by the program is an implicit time integration technique based on the solution of the static equilibrium. In other words, it disregards any dynamic forces and treats the analyzed problems as quasi-static. The following equilibrium equation is resolved for the time $t + \Delta t$ in each iteration to find nodal displacements:

$$^{t+\Delta t}\boldsymbol{R} - {}^{t+\Delta t}\boldsymbol{P} = \boldsymbol{0} \tag{3.22}$$

where the internal and external forces, respectively, are represented by **R** and **P**. Equilibrium is needed at time $t + \Delta t$, whereas a state of equilibrium is assumed at time t. Since time does not directly factor into the formulation of implicit methods, the time steps are essentially increments of displacement. Using a Taylor series, the equilibrium equation is resolved as follows:

$$\boldsymbol{K}(\hat{\boldsymbol{u}})\Delta\hat{\boldsymbol{u}} - \boldsymbol{P}(\hat{\boldsymbol{u}}) = \boldsymbol{0} \tag{3.23}$$

being **K** the stiffness matrix, $\hat{\boldsymbol{u}}$ the vector of nodal displacements and $\Delta\hat{\boldsymbol{u}}$ the unknown displacement increment.

This formulation's key benefit over the other, more widely used method, the dynamic explicit method, is that it is unconditionally stable. As a result, the defined time steps can be much greater without leading to instabilities. The size of the time step is limited only by the convergence behavior and the desired accuracy of the solution. Since the explicit technique is conditionally stable, the accuracy of the solution cannot be guaranteed for larger time steps than the critical one. This results in a requirement for very short time steps.

Also, there are no restrictions on the spatial discretization. Large elements can be combined in the mesh with very small elements, particularly when using the adaptive refinement, without the calculating time being affected by the size of the smallest element.

The implicit method's improved stability does, however, have a drawback. An iterative procedure must be used to linearize and solve a set of non-linear algebraic equations for each increment, which increases the CPU's workload and memory requirements. Strong changes in contact constraints, for instance, is another factor that might contribute to convergence issues with extremely large increments. Nonetheless, this technique does not place any limitations on the spatial discretization, which is a crucial factor in the many applications for which it is chosen (Zienkiewicz, Taylor, and Zhu 2005).

In order to improve the effectiveness of the implicit solution, special functionalities are continuously being implemented in AutoForm. For example, efficient formulation of the elastic-plastic shell and thick shell elements and fast direct solver ensure that calculation time and memory requirements are only moderately increased in relation to the bending enhanced membrane (factor 3 - 5). Also, effective automatic time step control ensures that the contact constraints are only moderately changed from one increment to the next. A time step as large as possible is selected so that the effects on the calculation accuracy are negligible on the calculation accuracy and generally cause no convergence problems.

3.2.3 Finite elements

This software uses triangular, tridimensional elements with a Lagrangian formulation. These triangular elements are widely employed due to their simple formulation.

They are incredibly versatile, allowing for local refinement, and are ideal for creating non-structured meshes. In other words, the coarse and finer mesh zones may be distinguished clearly from one another. Zones exhibiting significant gradients of deformation and/or stress, such as areas with strong curvature, should unavoidably be discretized using smaller-sized elements. With no discernible loss in accuracy, the utilization of a combination of finer and coarser mesh sections optimizes computing time and memory usage.

Considering the generic triangular bidimensional element (for simplicity) presented in Figure 60, with nodal degrees of freedom, u_i^e and v_i^e, with $i = 1, 2, 3$. The displacement field can be defined by the shape functions, N_i^e, and the nodal degrees of freedom as follows:

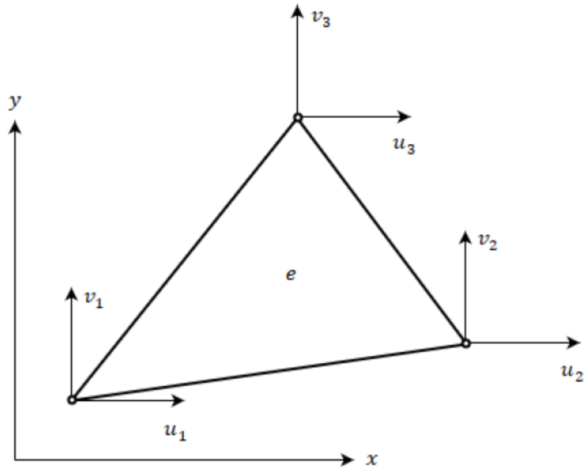

Figure 60 – Generic triangular elements and its displacements.

$$u = \begin{Bmatrix} u(x,y) \\ v(x,y) \end{Bmatrix} = \begin{bmatrix} N_1^e & 0 & N_2^e & 0 & N_3^e & 0 \\ 0 & N_1^e & 0 & N_2^e & 0 & N_3^e \end{bmatrix} \begin{Bmatrix} u_1^e \\ v_1^e \\ u_2^e \\ v_2^e \\ u_3^e \\ v_3^e \end{Bmatrix} \tag{3.24}$$

where, considering linear interpolation, the shape functions are:

$$N_i^e = \frac{1}{2A^e}(\alpha_i + \beta_i x + \gamma_i y) \tag{3.25}$$

being $\alpha_i = (x_j y_k - x_k y_j)$, $\beta_i = (y_j - y_k)$ and $\gamma_i = (x_k - x_j)$, where x_i and y_i are the spatial coordinates of the nodes $(i = 1, 2, 3)$. The area of the finite element can be obtained based on the following determinant:

$$A^e = \frac{1}{2}\, det \begin{bmatrix} 1 & x_1 & y_1 \\ 1 & x_2 & y_2 \\ 1 & x_3 & y_3 \end{bmatrix} = \frac{(x_2 - x_1)(y_3 - y_1) + (x_1 - x_3)(y_2 - y_1)}{2} \tag{3.26}$$

From continuum mechanics, the infinitesimal deformation tensor is given by:

$$\boldsymbol{\varepsilon} = \begin{Bmatrix} \varepsilon_{xx} \\ \varepsilon_{yy} \\ \varepsilon_{xy} \end{Bmatrix} = \begin{Bmatrix} \dfrac{\partial u}{\partial x} \\ \dfrac{\partial v}{\partial y} \\ \dfrac{\partial u}{\partial y} + \dfrac{\partial v}{\partial x} \end{Bmatrix} \tag{3.27}$$

so, the strain field can be obtained by:

$$\boldsymbol{\varepsilon} = \begin{bmatrix} \frac{\partial N_1^e}{\partial x} & 0 & \frac{\partial N_2^e}{\partial x} & 0 & \frac{\partial N_3^e}{\partial x} & 0 \\ 0 & \frac{\partial N_1^e}{\partial y} & 0 & \frac{\partial N_2^e}{\partial y} & 0 & \frac{\partial N_3^e}{\partial y} \\ \frac{\partial N_1^e}{\partial y} & \frac{\partial N_1^e}{\partial x} & \frac{\partial N_2^e}{\partial y} & \frac{\partial N_2^e}{\partial x} & \frac{\partial N_3^e}{\partial y} & \frac{\partial N_3^e}{\partial x} \end{bmatrix} \begin{Bmatrix} u_1^e \\ v_1^e \\ u_2^e \\ v_2^e \\ u_3^e \\ v_3^e \end{Bmatrix} \tag{3.28}$$

Defining the matrixes of the partial derivatives of the shape functions as:

$$\boldsymbol{B}_i = \begin{bmatrix} \frac{\partial N_i^e}{\partial x} & 0 \\ 0 & \frac{\partial N_i^e}{\partial y} \\ \frac{\partial N_i^e}{\partial y} & \frac{\partial N_i^e}{\partial x} \end{bmatrix} = \frac{1}{2A^e} \begin{bmatrix} \beta_i & 0 \\ 0 & \gamma_i \\ \gamma_i & \beta_i \end{bmatrix} \tag{3.29}$$

The compact form of the deformation matrix is $\boldsymbol{\varepsilon} = \boldsymbol{B}\boldsymbol{u}^e$, with:

$$\boldsymbol{B} = \frac{1}{2A^e} \begin{bmatrix} \beta_1 & 0 & \beta_2 & 0 & \beta_3 & 0 \\ 0 & \gamma_1 & 0 & \gamma_2 & 0 & \gamma_3 \\ \gamma_1 & \beta_1 & \gamma_2 & \beta_2 & \gamma_3 & \beta_3 \end{bmatrix} \tag{3.30}$$

Several FE formulations for membrane and shell elements are available in AutoForm. There is just one of the first type available: Bending Enhanced Membrane (BEM). Three formulas are taken into consideration for the second: thick shell (TS), recommended for coining and ironing processes, composite shell (CS), specific to deal with composite materials, and elasto-plastic shell (EPS).

Being this work focused on steel blanks of small thickness, the choice is between BEM and EPS formulations. Compared to the shell element, which has five degrees of freedom per node - three translations and two rotations - the membrane element has three translational degrees of freedom per node. Therefore, simulation times can be shortened by using membrane elements. Complex parts, however, exhibit deformed regions that undergo bending and unbending processes. By using membrane elements, precision is compromised, as well as the presence of geometric details with relatively small radii. As a result, the shell element is the best option because it can incorporate the bending effects thanks to its rotational degrees of freedom.

3.2.3.1 Elasto-Plastic shell element

A shell element traduces a combination of a membrane and a plate element. Each one of the different shell formulations that have been proposed over the years has specific pros and cons. These types of elements can be considered the most complete 3D formulations, having up to six degrees of freedom per node. The shell element implemented in AutoForm seems to be a combination of a membrane element that has a specific formulation (Waldemar Kubli 1995) with a plate element (Katili 1993).

A node of the Elasto-Plastic Shell element has five degrees of freedom: three translations towards the two tangent vectors and the normal vector, and two rotations with the tangent vectors as the axis of rotation. The approximation of both translations and rotations is carried out with the help of the linear shape functions.

In order to determine the stress and strain, the stiffness matrix is evaluated using a trapezoidal Lobatto integration technique, which can be used when taking into account a different number of integration points over the blank thickness. The software only ever takes into account one mid-plane point. AutoForm offers two predetermined options for the through-thickness direction: either 5 or 11 integration points.

In a springback prediction analysis of a U-rail (a benchmark from Numisheet'93), Banabic demonstrated that when employing 5 integration points or more, the findings were already stable (Banabic et al. 2010). It's interesting to note that after 9 points, there were no noticeable improvements, and at 13 points, the computing time began to significantly climb.

In order to ensure a fair balance between accuracy and computational cost, AutoForm advises using 11 points because doing so enables the capture of stress gradients coming from bending effects, which are ultimately the primary source of springback. Also, this improves the precision in the computation of stress and strain in the sheet's top and bottom layers.

3.2.3.2 Mesh refinement or adaptive mesh

Large displacements are an integral aspect of stamping procedures. This causes a continual change in the needs for the calculation mesh throughout the simulation, as the zones requiring finer elements are shifted. This issue could be resolved by the consistent creation of sufficiently fine elements across the entire sheet. Nevertheless, complicated parts would therefore require millions of elements, which would break the fundamental criteria sought in a stamping simulation software: simplicity, accuracy, and computational efficiency. The alternative is adaptive modification of the mesh during the calculation (W. Kubli and Reissner 1995).

There are several mesh adaption techniques, but they can be broadly divided into two groups: h- and p-refinement. In general, h-refinement alters the size of the elements according to the situation, decreasing it for greater accuracy or increasing it for other purposes. On the other hand, for particular elements, p-refinement keeps the size of the interpolation polynomial while increasing the order. There are three common techniques for h-refinement: element subdivision, mesh regeneration, or node reallocation (also known as r-refinement). The first merely enriches the mesh by dividing it using the already-existing pieces and boundaries. During the subsequent cycle, the second builds a whole new, finer mesh.

Unlike the r-refinement approach, which does not modify the amount of elements but instead modifies the position of the nodes, both of these methods allow for refinement and de-refinement (Zienkiewicz, Taylor, and Zhu 2005).

To execute realistic simulations in a reasonable amount of time, AutoForm automatically refines and coarsens the mesh: the initial mesh on the sheet blank is automatically formed with a small number of elements, ranging from a few hundred to a few thousand. During the calculation, these fundamental elements are subdivided recursively based on specific criteria. Hence, it is entirely conceivable to construct several thousand elements from a single element. If minor elements are no longer necessary in a particular area, they are automatically merged into bigger ones. In contrast to the case with linear problems, the criteria for refinement do not consist of so-called error estimators. In a geometrically highly nonlinear forming problem, it is crucial that the complicated shapes of the tools may be accurately represented. AutoForm uses the following criteria for this reason:

- Curvature – at strongly-curved locations finer elements are essential to represent the geometry correctly.
- Contact – if small sections of the tools penetrate into large elements, then these are refined so that the section in the sheet is correctly represented.
- Strain gradients – this corresponds to the linear problem's error estimator. For major gradients finer elements are required to keep the discrete error of the finite-element method sufficiently small.

Using this method, it is possible to acquire a suitably precise description of even the largest problems at an acceptable level of computational expense and with an acceptable amount of storage space (W. Kubli and Reissner 1995).

AutoForm divides or joins triangular elements using the element subdivision h-method, employing an algorithm designed to take into consideration a set of criteria to support the choice. As the element is divided, this approach assigns a refinement level of 0 to the initial element size and raises it. Figure 61 depicts this process in diagram form. The element is divided into four parts while moving from one level to the next. This can continue until the user-defined maximum level of refinement is reached, increasing the local density of the mesh in the process. By consolidating four elements into one, the contrary occurs when the refining level is no longer required. The level 0 can be restored by doing this repeatedly. The refinement process will begin before any geometrical characteristics are encountered thanks to the software's technique.

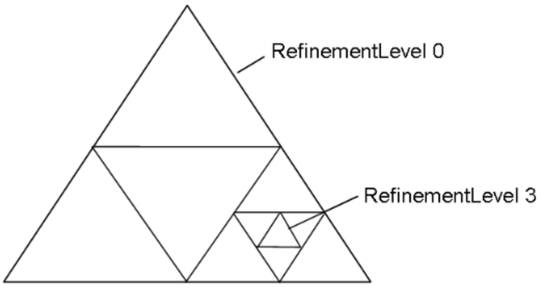

Figure 61 - Refinement levels in AutoForm software.

The user has complete control over the initial maximum element size, the maximum refinement level, the radius penetration, and the maximum element angle using the program. The size associated with refinement level 0 is determined by the initial maximum element size that is chosen. Choosing a smaller element size causes the mesh to be finer overall right from the start of the simulation. The allowed penetration, p, between the sheet and the tools in curvature zones is determined by the radius penetration. The maximum element angle, α, is the maximum angle that an element can make with respect to a 90º radius. The control parameter maximum element angle defines the maximum enclosed angle between two adjacent elements: if the value for the control parameter maximum element angle is exceeded, the element is refined. The control parameter contributes to the generation of sufficient elements in order to have a precise representation if the mesh in the simulation must represent very small radii. It limits the very minimum of elements that can be used to create that radius. Figure 62 shows how these parameters are displayed. It is important to note that these parameters are dependent on one another, with the stricter one dominating the other.

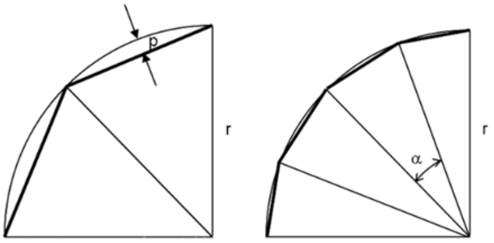

Figure 62 - Refinement scheme in AutoForm software.

The tangential refinement is an additional parameter that deserves to be mentioned. In contrast to the others, it is an on-or-off option that increases the refining range by 2.5 times the blank's thickness. It aids in a more accurate representation of the stress gradient that surrounds regions of significant curvature.

3.2.3.3 Adaptive time step

The time step taken during the simulation is optimized with respect to accuracy and computing time. In a given increment the time step must be small enough to capture the deformation in the sheet during forming. On the other hand, if little deformation takes place, the time step can be increased in order to decrease the total number of increments. Therefore, the time step adaptively changes through the simulation.

The time step is controlled by the parameter Max Material Displacement which is the maximum size of a time step (increment) in a process step. Advanced time step control can be enabled by using the following parameters: Min Tool Displacement, Max Tool Displacement, End Tool Displacement Step, number of End Tool Displacement Steps.

3.2.4 Tools and support types

Figure 63 depicts the design process for FE models in the AutoForm system. The die surface, including the addendum and binder, is designed in accordance with the structure of the automotive component. The addendum is intended to connect the outside profile of the part smoothly, resulting in a uniform force on the die surface during the stamping process.

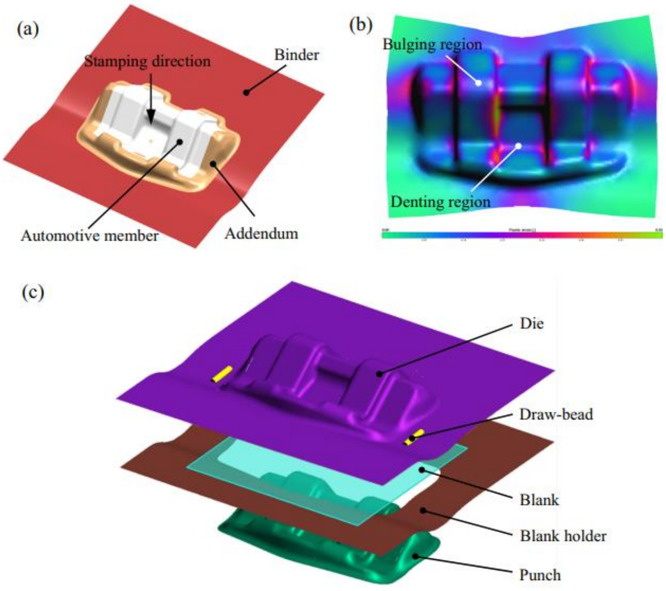

Figure 63 - Design process of FE models in AutoForm (Liao et al. 2015).

In addition, the addendum face is meant to facilitate further operations, such as trimming. To prevent metal sliding and wrinkling, the binder face is produced by offsetting and extending the profile of the addendum. The shape is smooth and simple in terms of geometry, such as a flat and ruled surface.

It is common to define four types of tools: ram, bed, binder ram, and cam. The ram tools are all that are associated with the upper die set. The bed tools are associated with the lower die set. The binder ram tools only apply to double action presses and are associated with the binder ram. Finally, the cam tools travel in a different direction than the press stroke.

The necessary tools can be generated in AutoForm software using the extensive functionalities or they can be individually imported from a CAD program.

AutoForm provides the user with a variety of control options and support types for the process tools. They can be rigid, regulated by force, or by gap. Attached to the ram or bed of the press, rigid tools have extremely high rigidity and low theoretical deformation. Typically, this option is used to replicate the punch or die. Force-controlled tools are designed specifically for blankholders or pads. The specified force is applied, and tool lifting is prohibited. If the initial force is insufficient to counteract the sheet's reaction force, the force delivered to the tool is automatically increased to prevent the sheet from lifting up. During simulation, the force may also increase if necessary. This type of control is quite beneficial. It can be used to establish the minimal blankholder force required to maintain tool closure throughout the forming process.

Gap controlled tools, as their name suggests, maintain a specified distance between the selected tools. This occurs, for instance, when the procedure employs spacing blocks. Note that no binding pressure is exerted when this support is utilized. The gap regulated tool is deemed stiff when EPS is used.

The definition of force and gap-controlled tools includes the choice of an opposing tool and the cushion stroke. The latter represents the tool's distance from its fully closed position at the end of the process. This distance excludes the closing step of the blankholder.

The binder model outlines the transfer of forces to the blank. In other words, it reflects the behavior of components such as gas cylinders, cushion pins, hydraulic columns, etc. that provide force to the tools. There are three distinct methods available in the software: uniform loading, columns, and cushion pins. Uniform loading ensures uniform application of binder pressure. According to the AutoForm user manual, this substantially simplifies the analysis, as the application point of the binder force may be unknown. Columns are intended to represent the distribution of binder pressure induced by individual punctual forces, such as those exerted by cylinders. Local regions of the binder where these forces are defined are regarded as rigid. In addition, the opposing tool must likewise be rigid for this model to be selectable. To locate cushion pins, analogously to columns, a point of application must be given. Yet, this model applies and maintains the total force for the entire tool, regardless of the number of selected pins.

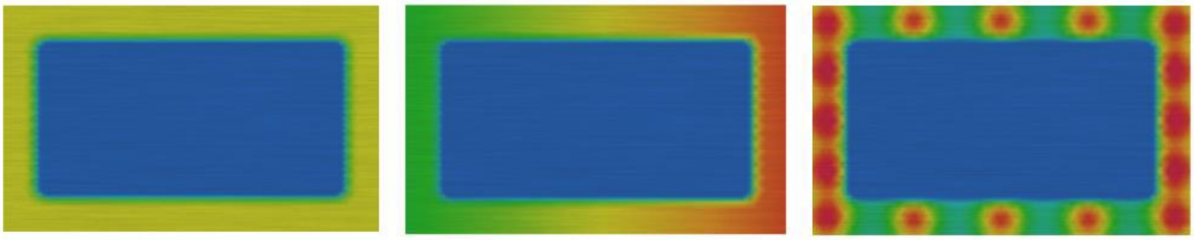

Figure 64 - Rectangular cup with uniform pressure (left), columns (middle) and with cushion pins (right).

3.2.5 Contact and friction

Tribology plays an important role in the process of sheet metal forming. In the tribological behavior of sheet metal forming, the surface roughness, quantity of lubricant, forming speed, blank-holder-force, and other parameters involved in the forming process are integrated. The friction state has an effect on the product's surface quality, tool life, process efficiency and stability (Jadhav, Schoiswohl, and Buchmayr 2018).

In AutoForm, contact is managed by a search algorithm that detects if any node of the sheet penetrates the tools in order to rectify the position of the nodes. Using the penalty method, the contact constraints are determined. The algorithm is governed by two parameters that are not user-defined. The maximum penetration tolerance specifies the maximum acceptable nodal penetration. The distance error defines the lowest estimated distance for contact. Also, the user must specify which side of the sheet, upper or lower, each tool will contact. The search for contacts will not function on the unselected side. For EPS, the software utilizes the current sheet thickness to detect minor gaps caused by, for instance, material thinning.

Lubrication conditions can be defined both globally (for all tools, for all operations) and locally (for individual operations or tools). By defining the friction condition locally, each operation or tool can have a different lubrication condition definition.

Friction is calculated based on the Coulomb’s dry friction law to describe friction conditions between the sheet and tool surfaces.

$$cof = \frac{F_R}{F_N} \tag{3.31}$$

where cof is the coefficient of friction, F_N is the normal force, and F_R is the friction-induced shear force.

The friction shear stress can be obtained with the effective normal stress or pressure, σ_N, applied on the same contact area as:

$$\tau_R = cof\ \sigma_N \tag{3.32}$$

The cof depends on the combination of sheet and tool materials, as well as the lubricant used throughout the process. Yet, although friction is of key importance, it is currently not considered in detail in stamping simulations being the current industrial standard to use a constant (Coulomb) coefficient of friction, cof. This value can be affected by variables such as sliding velocity, contact pressure, and even the direction in which the friction force is applied. It can even be used a User Defined Friction Law.

3.2.6 Material generator and editor

The user can build a material file from start or modify an existing one using the specific material generator in AutoForm. This interface is presented in Figure 65 as an example. The material's class, specific weight, Young's modulus, Poisson's ratio, volumetric heat capacity, and conductivity must be disclosed, among other general characteristics. The constitutive model's yield criterion, hardening law, and forming limit curve should then be defined using the data acquired from the experimental tests or from the software library.

The plastic behavior of sheet metals with typical plastic anisotropy is, as it was seen before, described by the yield locus. The punch force, strain distribution, and localization for punch stretching operations are influenced by the yield surface shape and the plastic anisotropic parameter. Through the FLC, it is specified the maximum amount of local necking or cracking that can occur in the deformed sheet.

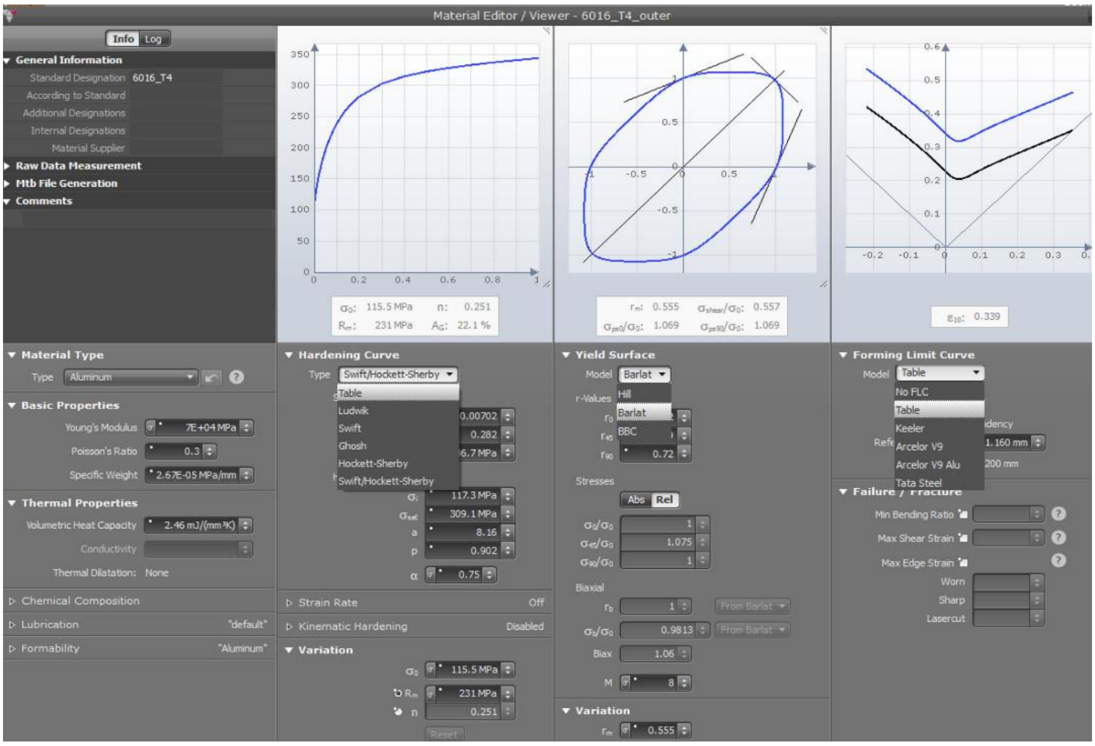
Material Editor / Viewer - 6016_T4_outer

General Information
Standard Designation 6016_T4

σ_0: 115.5 MPa n: 0.251
R_m: 231 MPa A_G: 22.1 %

r_m: 0.555 σ_{shear}/σ_0: 0.557
σ_{ps0}/σ_0: 1.069 σ_{ps90}/σ_0: 1.069

ε_{10}: 0.339

Material Type
Type Aluminum

Basic Properties
Young's Modulus 7E+04 MPa
Poisson's Ratio 0.3
Specific Weight 2.67E-05 MPa/mm

Thermal Properties
Volumetric Heat Capacity 2.46 mJ/(mm³K)
Conductivity
Thermal Dilatation: None

Chemical Composition
Lubrication "default"
Formability "Aluminum"

Hardening Curve
Type Swift/Hockett-Sherby
0.00702
0.282
6.7 MPa
σ_i 117.3 MPa
σ_{sat} 309.1 MPa
a 8.16
p 0.902
α 0.75

Strain Rate Off
Kinematic Hardening Disabled

Variation
σ_0 115.5 MPa
R_m 231 MPa
n 0.251

Yield Surface
Model Barlat
r-Values
r_{90} 0.72
Stresses
σ_0/σ_0 1
σ_{45}/σ_0 1.075
σ_{90}/σ_0 1
Biaxial
r_b 1 From Barlat
σ_b/σ_0 0.9813 From Barlat
Biax 1.06
M 8

Variation
r_m 0.555

Forming Limit Curve
Model Table
1.160 mm
200 mm

Failure / Fracture
Min Bending Ratio
Max Shear Strain
Max Edge Strain
Worn
Sharp
Lasercut

Info
Log
Raw Data Measurement
Mtb File Generation
Comments
According to Standard
Additional Designations
Internal Designations
Material Supplier
350
300
250
200
150
100
50
0
0.2
0.4
0.6
0.8
1
0.5
-0.5
-1
0.6
0.4
0.3
0.2
0.1
-0.2
-0.1
Table
Ludwik
Swift
Ghosh
Hockett-Sherby
Swift/Hockett-Sherby
Hill
Barlat
BBC
r_0
r_{45}
Abs
Rel
No FLC
Table
Keeler
Arcelor V9
Arcelor V9 Alu
Tata Steel
Refe
idency
Reset

Figure 65 - AutoForm material editor layout (Jadhav, Schoiswohl, and Buchmayr 2018).

3.2.6.1 Hardening law

The initial flow stress and the strain hardening are critical for the ductility and strength behavior. The Hardening Curve, or Flow Curve, describes the hardening behavior of a material in response to an applied load. AutoForm requires the true (or logarithmic) stress as a function of true (or logarithmic) plastic strain measured in the direction of rolling (longitudinal direction).

In order to approximate the observed hardening or flow curves for each material, the previously referred phenomenological models are frequently used. The collected data from tensile tests (sometimes combined with Biaxial data) can be used to define these. They capture the non-linear increase of stress with plastic deformation that happens for the majority of metals, including steel.

Besides that method, AutoForm determines the flow curve in two other possible ways: by approximation or by a table of real stress-strain data points.

Although both methods rely on the data points produced by tensile tests, the table and approximation methods follow similar procedures. When directly interpolating the points, the table requires information for up to 50 pairs of these points in an ASCII file that has been previously chosen by the user, however the approximation can take up to 100000 pairs in a .dat file format. The Swift/Hockett-Sherby approximation's parameters are then automatically determined. The user can adjust the weight factor α or add extra details, like the yield stress, to improve the fit of the curve. Since it is relatively easy to get a table with data from a tensile test, this is usually the chosen method.

The hardening behavior can be accurately defined in AutoForm using also kinematic hardening. By default, the software takes into account an isotropic hardening rule which means that in the principal stress plane, the yield curve will accordingly extend in all directions after yielding. This happens because it is not common to have the experimental data to describe kinematic hardening. However, kinematic hardening can be activated by indicating the type of material that is being used: mild steel, TRIP steel, CP steel, HSS, Al 5 series, or Al 6 series. The AutoForm software has already pre-defined models for these classes of materials. Alternatively, the user can define its own model by introducing the required parameters: the transient softening rate κ, stagnation ratio ξ, Young's reduction factor γ, Young's reduction rate χ, and reversal strain ε_{rev}.

3.2.6.2 Yield criterion

The yield surface defines the transition from the elastic to the elastic-plastic region in multi-axial stress space. Once a point reaches the yield surface, the material begins to plastically deform.

Although typically drawn in three dimensions ($\sigma_x, \sigma_y, \sigma_z$), in forming simulations it is generally assumed that the third component σ_z (through sheet thickness stress) is so small in comparison with the in-plane stresses, as to be safely ignored. For this reason, it is typical to see the yield surface defined in two dimensions.

To define the yield surface, models by Tresca, von Mises, Hill, Barlat, and Banabic are frequently employed. von Mises and Tresca consider an isotropic material. However, due to the production of sheet metal, it is usually necessary to consider anisotropy. The anisotropic yield surface can be accurately defined in AutoForm using the Hill 48, Barlat 89, and Banabic (BBC 2005) yield criterion, described in a previous subchapter. Sheet metals are regarded as orthotropic in an anisotropic yield function.

Barlat and Hill only require the plastic anisotropy coefficients r_0, r_{45}, and r_{90} from the experiments, which may be calculated using regular tensile testing. A standard M-value is also required for Barlat, but it is usually predetermined and only varies based on the kind of material, for example, the standard is 8 for aluminum and 6 for steel (Nilsson 2019).

BBC requires plastic anisotropy as well as three distinct yield stress values σ_0, σ_{45}, and σ_{90}. These values are determined through tensile testing. The BBC model's need for biaxial data to function is both an advantage and a challenge. The biaxial data can be obtained using the bulge test and the LDH-test. Not all industries have access to these tests because they are not required for commonly used material models. BBC also requires an M-value (Nilsson 2019).

It has been shown by some researchers that the BBC yield criterion is the only one of the three criteria that can give acceptable springback results in all directions because it is the only one able to describe the measured strain values accurately. The other two criteria work in general quite well, as long as the loading direction coincides with the rolling direction. However, if the sheet is aligned in another direction, acceptable results cannot be guaranteed with the two simpler models (Eggertsen and Mattiasson 2010). Moreover, the Hill 48 model usually overestimates both the punch force and the formability of the material (Banabic et al. 2010).

Having said that, it becomes clear that the BBC 2005 is the model that more completely and accurately describes the behavior of the materials. Nevertheless, it is the model that requires more input parameters. So, an equilibrium between accuracy and the number of parameters available should be achieved.

A new model implemented in the latest versions of AutoForm is the Vegter model. However, because it is not usually used in the company, there was no further research on this model.

Figure 66 summarizes the inputs necessary to define each of these models.

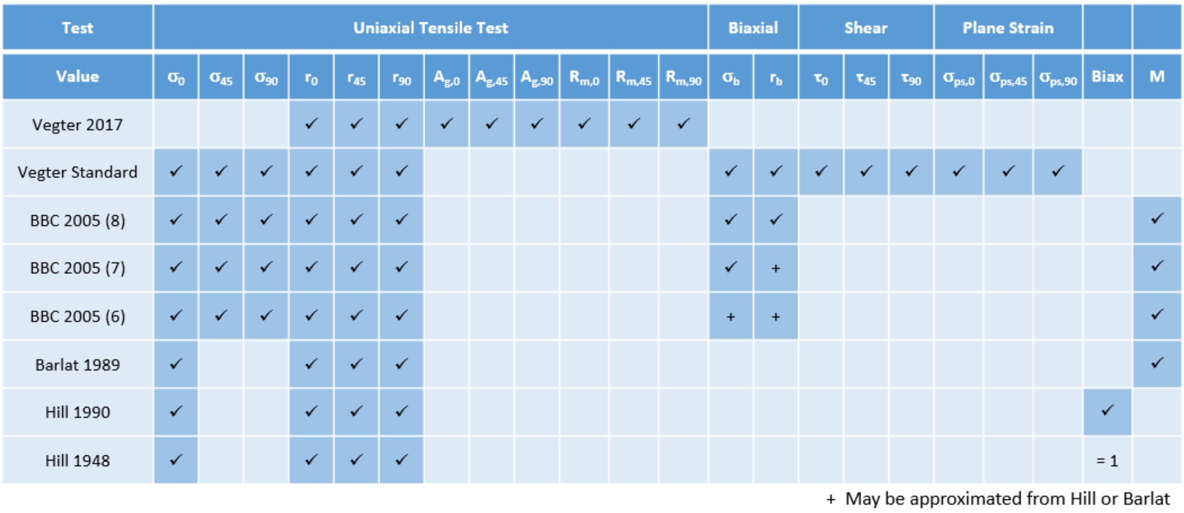

Test	Uniaxial Tensile Test												Biaxial		Shear			Plane Strain				
Value	σ_0	σ_{45}	σ_{90}	r_0	r_{45}	r_{90}	$A_{g,0}$	$A_{g,45}$	$A_{g,90}$	$R_{m,0}$	$R_{m,45}$	$R_{m,90}$	σ_b	r_b	τ_0	τ_{45}	τ_{90}	$\sigma_{ps,0}$	$\sigma_{ps,45}$	$\sigma_{ps,90}$	Biax	M
Vegter 2017				✓	✓	✓	✓	✓	✓	✓	✓	✓										
Vegter Standard	✓	✓	✓	✓	✓	✓							✓	✓	✓	✓	✓	✓	✓	✓		
BBC 2005 (8)	✓	✓	✓	✓	✓	✓							✓	✓								✓
BBC 2005 (7)	✓	✓	✓	✓	✓	✓							✓	+								✓
BBC 2005 (6)	✓	✓	✓	✓	✓	✓							+	+								✓
Barlat 1989	✓			✓	✓	✓																✓
Hill 1990	✓			✓	✓	✓															✓	
Hill 1948	✓			✓	✓	✓															= 1	

+ May be approximated from Hill or Barlat

Figure 66 - Input variables necessary to define the yield criteria models.

3.2.6.3 Forming limit curve

The FLC is, as it was seen before, commonly utilized in sheet metal applications to anticipate failure. The curve displays the maximum values of the principal strains ε_1 and ε_2 as measured at material failure. The Nakazima test, the hydraulic bulge test, and the Marciniak test are among the various methods offered for determining the forming limit curve (see ISO 12004-2).

Despite being practical and useful, this strategy has drawbacks. The primary one is that the strain patterns depicted by these tests are nearly linear and do not involve elastic recovery. Thus, this sort of FLC is considered static. Its use in the analysis of complex forming processes, such as deep drawing, can produce inaccurate results. The AutoForm software introduces then the concept of an Advanced FLC to mitigate this problem.

To define the traditional FLC there are many theoretical models like the Swift’s model, the Hill’s model, the M-K and H-N models, Keeler model, and the MMFC model. But only a few options of defining the FLC are available on AutoForm.

AutoForm provides some FLC-definition options. Similarly to the hardening law, the user can enter a table with 50 principal strain pairs. Alternative methodologies include the Keeler and Arcelor V9 models.

The Keeler model is only recommendable for low carbon steels (mild and HSLA, but not DP nor IF) and the input has to be defined from the tensile data in the 90° direction. The Arcelor V9 FLC model is used for steels having a tensile strength ranging from 260 to 1500 MPa and sheet thicknesses ranging from 0.5 to 3.5 mm.

Due to the limitations of the FLC for the prediction of failure in specific situations, additional failure criteria are available to the user. Parameters like the maximum surface strain (maximum true / logarithmic surface strain prior to the formation of surface cracks of a sample bent through 180° around a known radius; determined from the 3-Point Bend Test, conducted to ISO-7438), the maximum uniaxial strain (local true / logarithmic strain at fracture under uniaxial tensile loading; maximum edge true strain for an edge in pristine condition; it can be experimentally measured by using a notched / hole tensile test), and maximum shear strain (value of True / Logarithmic Shear Strain at the critical level of Shear Stress for pure shear) can be introduced in the material model.

3.2.7 Formability results

The correct interpretation of simulation results is the basis for a successful development of virtual forming processes. AutoForm provides a logical workflow for the evaluation of results. The first requirement, and most important in this study, is the analysis of formability, namely the appearance of wrinkles and splits. Afterwards, the software also helps optimizing the blank size, surface condition, and springback.

Many output results can be obtained using AutoForm but only some will be referred since only those were extracted and relevant for this case study. Some of the non-mentioned ones are curvature, wear, surface cracks, surface quality, draw-in, skid lines, etc. Elementary results can be seen like stresses and strains.

3.2.7.1 Formability and traditional FLC

The result variable formability shows the computed results considering the strain state in the strain based linear Forming Limit Diagram (Traditional FLD). It gives a quick survey of the formability of the part. The areas which show tendencies for failure are represented by the different colors in the main display.

Necking is accurately predicted using traditional FLC only if: the deformation mode stays the same during the whole forming step (linear deformation/ proportional loading, i.e., the ratio between both principal strains remains constant), the deformation is predominantly stretching (bending radius is large), and the material is not compressed in the thickness direction (single sided contact, plane stress).

Failure (definition in Figure 67) is used for the basic evaluation of the formability. It is defined as the ratio of the current major strain in an element and the major strain on the FLC.

The result variable Max Failure (definition in Figure 68) is defined as the ratio between the maximum major strain computed at an element and the major strain of the strain based Forming Limit Curve (strain based FLC) for the same minor strain.

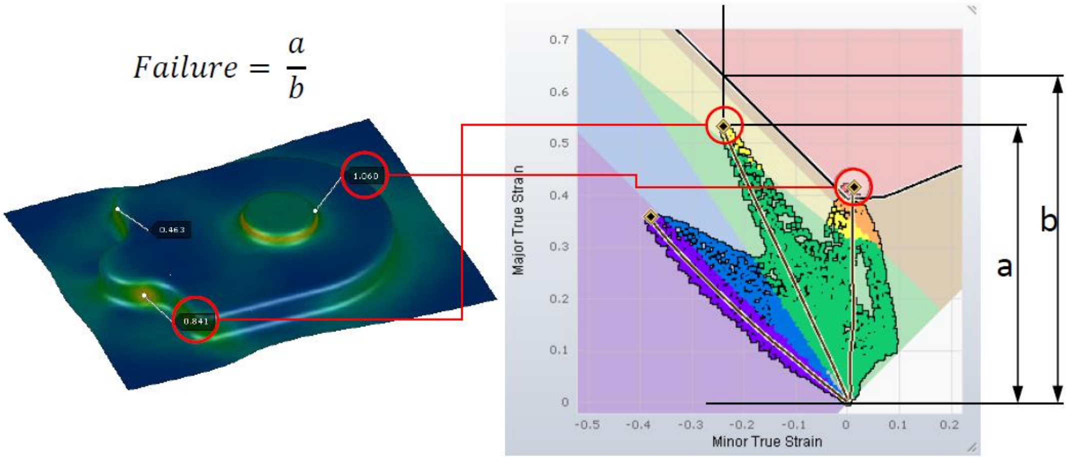

$$Failure = \frac{a}{b}$$

Figure 67 - Definition of the AutoForm parameter failure.

This implies that cracks may be anticipated at a value of 1.0 or more and that successful plastic deformation may be anticipated at values smaller than 1.0. It is important to remember that the FLC is determined by the assumption of linear deformation paths. Therefore, in areas of non-linear deformation paths the result variable Max Failure may be used only to obtain a qualitative indication of the potential for failure. In such areas it is possible to consider Max Failure together with the knowledge of the strain paths of the elements in question.

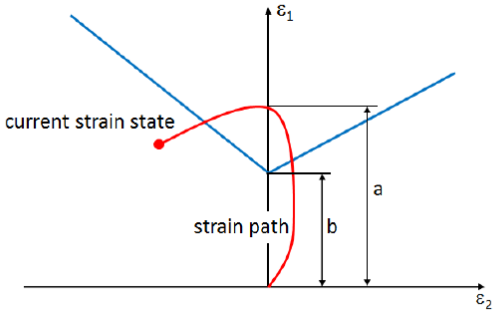

$$Failure_{Max} = \frac{a}{b}$$

Figure 68 - Definition of the AutoForm parameter max failure.

3.2.7.2 Advanced formability and advanced FLC

The Advanced FLC extends the traditional FLC to realistically model nonlinear deformation, bending effects, and the effect of through thickness stress. Therefore, the position of the points is the same as in the traditional FLC but the color of the markers corresponds to the prediction of the advanced models. Therefore, the color of the point and the color of its background may not match. The Advanced FLC is the recommended criteria to analyze splits.

In order to use the new advanced FLC diagram, the user must consider the color of the points as a reference for the state of stretching of the sheet, the background color being related only to the curve generated by the traditional FLC, without the corrections due to the deformation history.

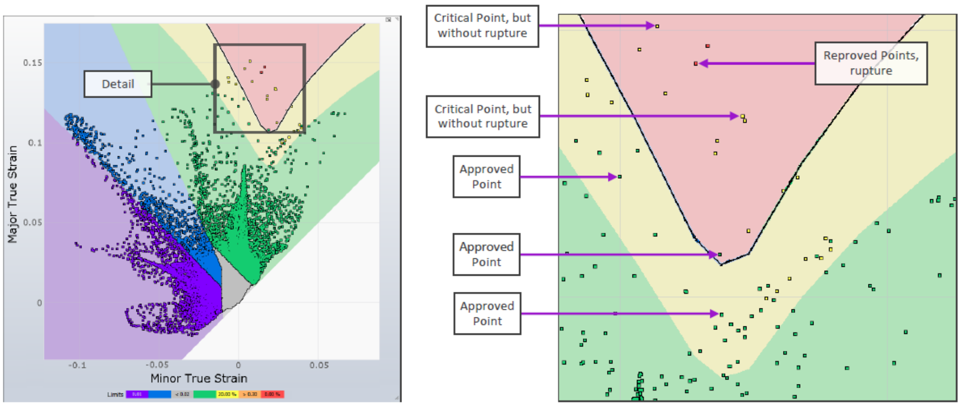

Figure 69 - Visual explanation of the advanced forming limit curve concept.

The colors used in this case study to represent the strain state of the sheet on the Advanced Formability result variable have the following meaning:

- Thickening (purple): Elements that present increase on the thickness and presents a minor strain bigger than 1% (0.01). This area of the FLC is defined as the area where the absolute value of minor strain is higher than an absolute value of major strain. Also, the line that separates the blue and purple areas of the FLC has an angle of 45°.
- Compression (blue): The compression area represents strain states caused by stress states that include compression. The line that represents the border between the blue and the green area refers to the uniaxial tensile test (in which minor stress is 0). The slope of this line depends on the mean r value of the material.
- Insufficient Stretching (grey): Elements that present less than 2% present of thinning (< 0.02) and a minor strain smaller than 1% (0.01).
- Safe (green): Elements that are not in risk of necking, do not present a thinning bigger than 30% (0.3), present a thinning bigger than 2% (0.02), do not present compression, and do not present thickening.
- Nonlinear Risk of Splits (yellow): Elements that are in risk of necking by experimenting more than 80% of their strain capacity. To consider uncertainties, this yellow area consists of a safety margin that is defined in the FLC.
- Excess Thinning (orange): Elements that present more than 30% of thinning (> 0.3). In the FLC a line of 45° indicates strain states of constant thinning. So, the parameter excessive thinning separates an orange coloured area in the FLC which lays above the 45° line that crosses the vertical axis at the defined acceptable thinning.
- Nonlinear Splits (red): Elements that fall above the FLC or that during a nonlinear strain path enter this zone. This area is meant to visualize the failure due to cracks.

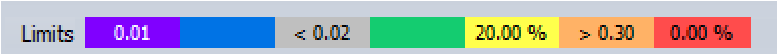

Figure 70 - Color scale of the advanced forming limit curve.

3.2.7.3 Wrinkles and potential wrinkles

The wrinkles result variable is based on a geometric evaluation of wrinkles, represented in Figure 71. If wrinkles occur geometrically the elements of the sheet become colored according to color scale. The color of maximum wrinkles is kept even if the wrinkles disappear because of closing tools at the end of the forming process.

To calculate wrinkles, the maximum curvature of the sheet at concave areas (relative to the tool) is checked. If there is tool contact all along the concave area it is assumed to be a geometry feature. If there is no contact in concave areas, it is assumed to be a wrinkle. The value of this result variable is dimensionless, and it is calculated by the following formula:

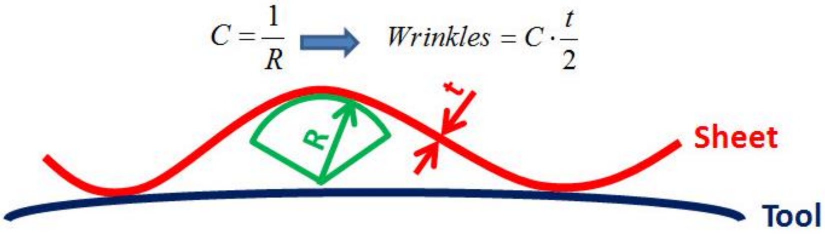

Figure 71 - Definition of the AutoForm parameter wrinkles.

Potential Wrinkles is one of the post variables in AutoForm which aims at assessing the tendency of wrinkling and help designers to avoid the defects of wrinkling during the stage of die design. Potential Wrinkles is just one of the variables to measure the magnitude of compressive stress. If the value is greater than 0, that means there is compressive stress and possibility of wrinkles; the larger the value is, the more serious the tendency to wrinkling. If the value equals 0, there is no compressive stress and the wrinkling will be impossible to take place in such area.

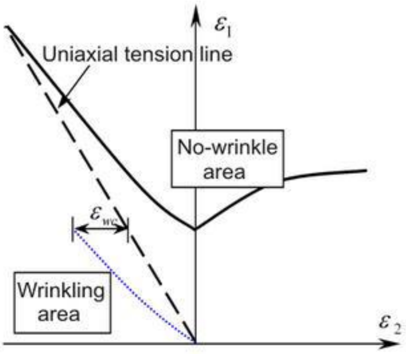

Figure 72 - Definition of the AutoForm parameter potential wrinkles.

3.2.7.4 Thickness variation

The thickness variation can be seen through two different variables: thinning or thickness. The first is the relative thickening or thinning in relation to the original thickness. The second is the final thickness obtained. In AutoForm thinning conforms to engineering strain. However, for other purposes it is used the true strain. It is very common to refer the strain state which is the combination of the two principal strains (minor and major).

For the complete description of the strain state, the strain in the thickness direction of the sheet has also to be considered in addition to the plane strains. Constant volume is assumed for the forming of an element in AutoForm.

3.2.7.5 Edge cracks

Edge cracks is the material failure initiated at the edge of the sheet and it cannot be predicted by using the FLC. The initiation of edge cracks depends on the quality of the trimming or blanking tool and the material used.

Laser cutting or piercing using a worn steel will lead to a different initial damage state in the sheet edge and therefore will influence the moment in time when the crack will actually start to form. It is also known from literature that high strength steels, stainless steels and aluminum are more sensitive to failure due to edge cracking whereas most of low strength steel and medium strength steels are not sensitive to edge cracks.

Therefore, the edge cracks results are dependent on the definition of a fracture curve based on the theory of the Hosford Coulomb model. This model takes into account four significant points of fracture that can be inserted in the material model of the material in AutoForm: Max Biaxial Strain (1) (coupled with Max Uniaxial Strain in the HC model), Max Surface Strain (plane strain) (2), Max Uniaxial Strain (3), and Max Shear Strain (4).

These points can be estimated by AutoForm based on the type of material and the FLC.

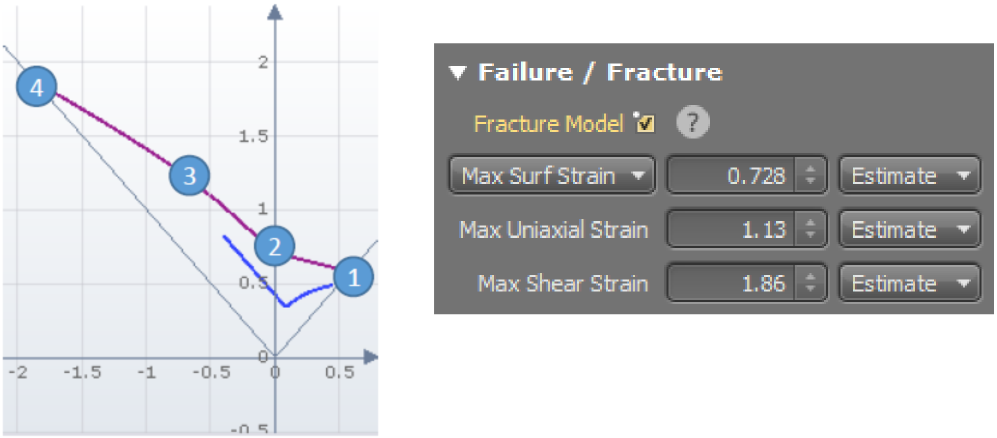

Fracture Model ☑

Max Surf Strain 0.728 Estimate

Max Uniaxial Strain 1.13 Estimate

Max Shear Strain 1.86 Estimate

Figure 73 - Necessary input parameters to determine edge cracks in AutoForm.

Another three values of true strain must be specified in order to represent different state of edge quality: worn steel, sharp steel and laser cut. These values are maximum edge strains obtained using different tools and they can be obtained using a hole expansion test (ISO 16630). However, a more practical way is suggested by AutoForm. Since a rough edge leads to cracking a little bit earlier than the FLC indicates due to the notching effect, the critical strain (Max Edge Strain) can be assumed to be a little bit lower than the strain at the uniaxial stress state. Therefore, the value for laser cut can be estimated as 95% of the FLC uniaxial stress state, the sharp steel 70% of the same value, and the worn steel 50%.

The value of Edge Cracks is calculated referring to the shifted Fracture Model for each increment. The total amount of Edge Cracks is the sum of the result of each increment.

3.2.8 Springback results

If the tools open at the end of an operation, the part is released and the springback takes place. In AutoForm, Measuring Equipment is used to simulate springback at the end of the process. The behavior of the part between individual operations of the forming process can be calculated by adding Free Springback functionality at the end of each operation or by using Inter-OP Measurements. Such an approach may be needed to determine a suitable strategy for Springback Compensation.

Real Measurement functionality provides the most realistic way to simulate a well-defined clamping fixture. Gravity effects are included and various types of elements of the measuring support can be defined. Compared to other Springback options, real measurement can simulate positioning of the part on the measuring fixture before actual clamping is taking place. Locating can be done on single-sided clamps or tool surfaces.

Constrained Springback can also be used to simulate a well-defined clamping fixture with or without gravity effects. Compared to Real Measurement, positioning of the sheet in the measuring support and sequential clamping is not simulated.

Fixed Boundary Conditions are suitable for evaluation of full, not over-constrained, springback with or without gravity effects. The main characteristic feature of this option is that during springback analysis, all possible rigid body motions of the part can be blocked with the minimum number of constraints. Therefore, the functionality can typically be used to determine the Minimum Clamping Concept for subsequent Springback Compensation. In some cases, FBCs can also be used when it is not possible to define kinematically stable support with clamps and pilots.

Free Springback offers the simplest way to define springback operation and it is usually the most used. Minimum user input is required, since automatic constraints are applied to fix the part in space. Gravity effects are not simulated in case of free springback.

The results available to quantify springback are material displacement, distance from reference, displacement from reference, and material deformation. The result variables dealing with a Reference Geometry show how much the sheet after springback diverge from the reference.

4 Industrialization of an automobile dual-phase steel component

4.1 Description and characterization of the component

The stamped component under study in this work is a DP980 steel component which is part of a major project in Gestamp Cerveira. All the parts in the left side of Figure 74 are made in the company and it is possible to see how they fit in the structure of the car in the right side of the same figure. Each component is represented in a different color and the component under study is highlighted. From all the parts produced in the company for this project, this component was the most challenging one because it was the one that involved more iterations in order to optimize the geometry of both the part and the tool to make it feasible.

Each press stroke produces both the right and left parts which are perfectly symmetrical. Each is mounted on the respective side of the car. They are called EXT SILL INR, to which the acronym LH/RH is added if it corresponds to the left- or right-hand part, respectively.

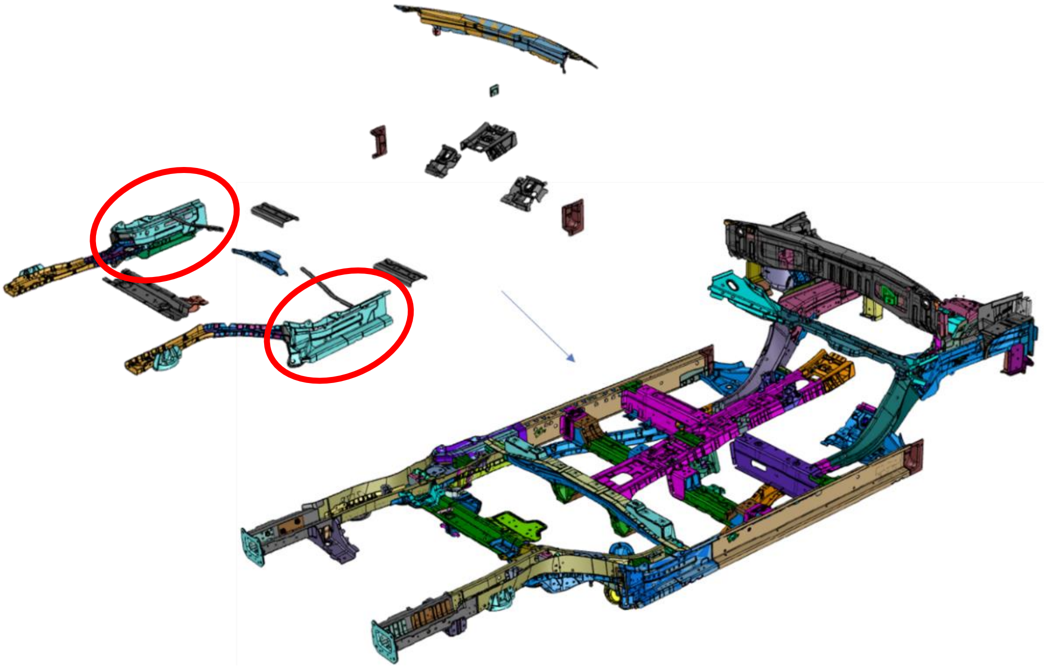

Figure 74 - Components from a project of a car model, highlighted those produced in Gestamp Cerveira and highlighted the component under study.

This part is internally classified as a regulation part (R) and is therefore identified by the symbol below. This internal classification allows to distinguish between safety parts (S), regulation parts, safety and regulation part (S/R) and none of them. Being a S part means that it corresponds to a part or assembly whose failure is likely to cause a risk to passengers in a vehicle and/or people in the vicinity. A R part is subjected to prescriptions established and imposed by an administration whose violation may lead to sanctions: fine, sale ban, etc.

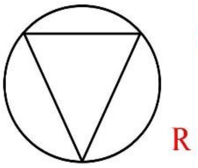

Figure 75 - Symbol that identifies a regulation part.

The DP980 steel that composes the component has the following admissible chemical composition.

Table 4 - Chemical composition of DP980.

Element	***C***	***Mn***	***Si***	***P***	***S***	***Al***	***Ni***	***Ti***	***Mo***	***Cr***
Admissible range [%]	<0.1	<2.8	<0.4	<0.02	<0.008	<0.25	<0.05	<0.05	<0.2	<0.4

The alloy elements in DP steels have different types of purposes. Carbon (C) strengthens the martensite and determines the phase distribution, also acting as an austenite stabilizer. Silicon (Si) promotes ferrite transformation and manganese (Mn) is a ferrite solid solution strengthener. Niobium (Nb) promotes finer grains and a more homogeneous distribution on DP microstructure, resulting in a higher strength and better ductility.

Being almost the strongest DP steel on the market, it is estimated that this steel has a percentage of martensite of about 50%, providing it with a major strength but also a relatively low ductility.

Regarding coating, the material is coated with quality G10/10 which means that the sheet is galvanized on both sides with a thickness of 10 μm with the following composition.

Table 5 - Chemical composition of the coating.

Element	***Zi***	***Al***	***Fe***
Quantity [%]	94.4	0.6	5

This DP steel is one of the strongest on the market. However, that also means that is one of the less ductile. It has greater martensite content and lower average grain size. Allied with a 1.2 mm thickness, it can be foreseen high springback and probability of cracks in the most solicited zones.

Regarding mechanical properties, according to the client, they should respect the values in the Table 6 in the longitudinal direction of the coil, i.e., the rolling direction.

Table 6 - Basic mechanical properties in RD of DP980.

Property	$Rp_{0.2}$ **[MPa]**	R_m **[MPa]**	A_t **[%]**	**E [GPa]**	***v***
Admissible range	590-740	980-1130	>10	210	0.3

In Figure 76, both 3D drawings of the left- and right-hand parts are displayed and in Figure 77 the final main dimensions of only the right part are shown. During the industrialization process, the geometry or dimensions of the parts have been adapted so that the stamping process was optimized and the tolerances met. However, the thickness of the part and consequently the coil, was imposed from day one as 1.2 mm. Each of the parts weights 1.26 kg.

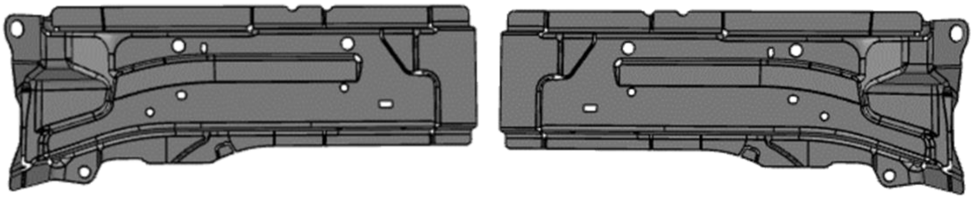

Figure 76 - Pair of parts of the component under study.

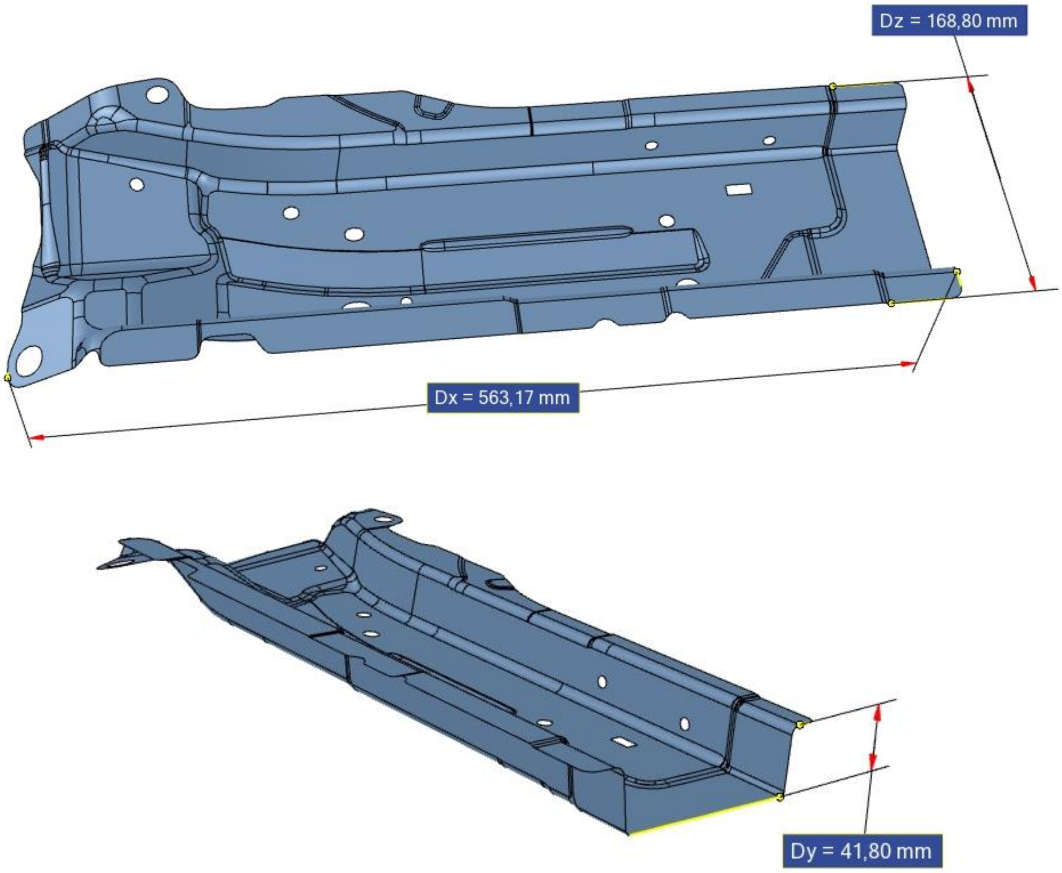

Figure 77 - Main dimensions of the RH component.

When consulting Gestamp, the client indicated a desired annual production volume of 117 365 pairs of parts. Nowadays the average daily production is about 589 pairs, which gives an annual production of 132 525 pairs. This does not mean that this number of parts is produced each day, it is just an indicative average number. In this case, the parts are produced on average each month with a cadence of about 16 strokes per minute.

4.2 Industrialization process of the component

After the initial negotiations between Gestamp Cerveira and its clients, when a new project is adjudicated, the industrialization process begins. This process consists of the preparation needed to produce the desired component in series regarding the necessary tool and control gauge.

The process starts with the search for a supplier for the tool and the control gauge. After the validation of the strip, a supplier for the coil is also sought.

The construction of the tool has several midterm validations, that can involve visits to the tool maker factory, and there are several steps that must be taken. The first is a feasibility study that includes the project of the strip and numerical simulations of the process to optimize certain aspects to prevent future problems in production. Although simulation helps reducing the iterations needed to the construction of the tool, a permanent dialogue is kept between Gestamp, the tool maker and even the client in order to optimize constructive details.

Before the final validation, several test productions must be done. Small lots are produced both in the tool maker factory using laser cut flat contours and in Gestamp. At least three productions are done in Gestamp before final validation of the tool. These productions are fundamental to correct possible errors and to optimize some process variables.

The construction of the control gauge is also very complex and also requires validations. This control gauge is a way to guarantee quality and repeatability of the produced components right after being produced and it allows the worker to see if the component is meeting tolerances, both dimensional and geometrical. Of course that in complex parts it is impossible to check every tolerance in the control gauge and that is why each part is periodically 3D measured.

After the final reception and validation of both the tool and the control gauge, the component is ready to start being produced in series.

4.2.1 Feasibility study

This is the first phase of every project. The objective at this stage is to determine whether the parts can be manufactured using stamping technologies, and, if so, to build and analyse the entire production process.

This first approach consists of defining the production process, that is, establishing the production steps necessary for the manufacture of a given part. Thus, after this initial step, a representative strip of the process is constructed. Most decisions at this stage are based on experience from previous projects and when the project starts it is just indicative since it suffers alterations throughout the industrialization process.

Simultaneously, stamping simulations are carried out, according to the defined strip, in order to determine the feasibility of the previously described process and, if necessary, rethink it again in order to obtain an optimized process.

At the end of this initial study, the type and size of the tool are defined based on the complexity of the process and the dimensions of the strip (width, step, and number of operations) as well as the necessary force that directly affects the selection of the press.

4.2.1.1 Study of the strip

After a brief analysis of the geometry of the part and taking into account the dimensions of the press tables at Gestamp Cerveira, it was decided to make both hands of the part on the same tool, reducing the cost per stroke. These decisions avoid the need for two different tools and the occupancy of two presses at the factory when in production.

Considering the dimensions of the part and the production rate communicated by the customer of 117 365 pairs of parts per year, a progressive tool was chosen as the production process. In this kind of tool, the cutting and stamping operations are performed sequentially and the part remains attached to the strip until the last step through the side rails avoiding the use of lateral clamps needed in transfer tools. A progressive tool is generally beneficial to the client since it is cheaper overall. Transfer tools are slower and are only considered when complex geometries need to be achieved like deep draws or geometries that imply rotating the part. Also, in a transfer tool the trims can be done after stamping, assuring trim position tolerances of ±0.5, which are not required in the present case.

In this way, the process of drawing the strip must start by generating the flat contour of the part. This will give an idea of the width of the band and the step, factors that also limit the usage of a certain press. To perform this study, a specialized software is used: FormingSuite. This software allows the determination of the geometry of the contour and its layout on the strip, namely using grids, optimizing the MUC. After importing the geometry to the software, it gives the general dimensions of the contour, Figure 78.

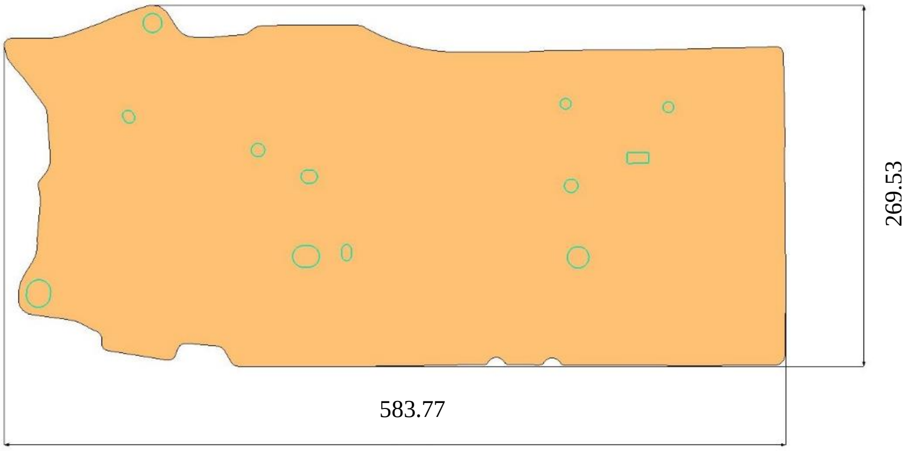

Figure 78 - Main dimensions of the sketch/format that will originate the stamped component.

It is not only possible to obtain the format but also to define the production layout, that is, the arrangement of the flat contours in the sheet metal strip. That said, the layout indicated in Figure 79 is the most suitable for the process since it presents the best MUC, maintaining feasibility, meaning that scrap production is minimized.

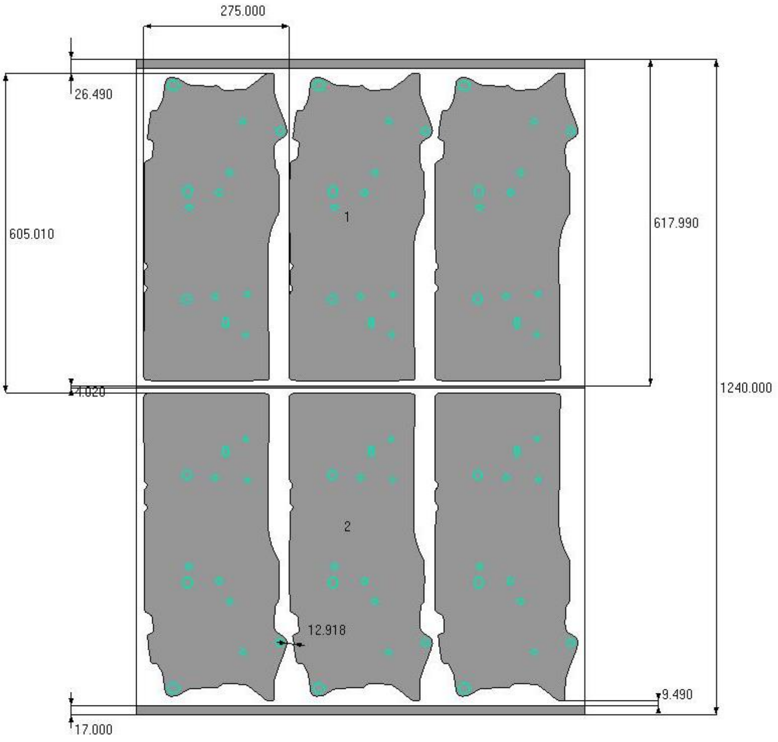

Figure 79 - Optimal layout suggested by FormingSuite.

Given the large size of both parts and in order to better control the position of the strip on the tool, it was defined that the strip would have to have side rails. Thus, with this characteristic, it is possible to guarantee the position of the sheet in the tool as well as to control its deformation during stamping, since the part is fixed at both ends. Besides the side rails, both hands are also connected to each other in the centre of the strip. If extra guidance and positioning was required, it could also be used a central rail. However, in this case the side rails are enough. A good positioning is guaranteed by the pilots, five during the initial trims and three during the next steps.

In addition to the side rails, an aspect to be taken into account is the connection of these to the parts. Considering the geometry, it is observed that the connection cannot be rigid since the stamping processes will change the contour dimensions. In this case, since there are not very deep draws but there is the need for the blank to move, the use of a S shaped harmonium joint is the most suitable option, as it not only keeps the sheet in the desired position, but also allows the necessary flow.

This configuration allows the strip to have a material usage coefficient of 78.5%, that is, 21.5% of the initial coil is discarded as scrap. This value is considered good in this industry.

$$MUC = \frac{P_p}{W \times S \times T \times \rho} \times 100 = \frac{1.26 + 1.26}{1240 \times 275 \times 1.2 \times 7.85 \times 10^{-6}} \times 100 = 78.5\%$$

Considering the characteristics described, the final dimensions of the strip are shown in Figure 80.

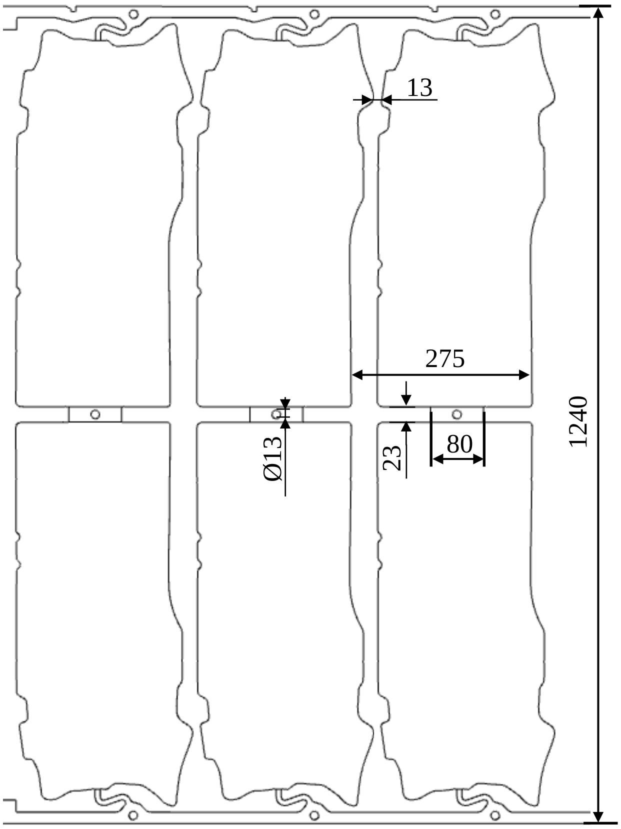

Figure 80 - Main dimensions of the strip and distances between parts.

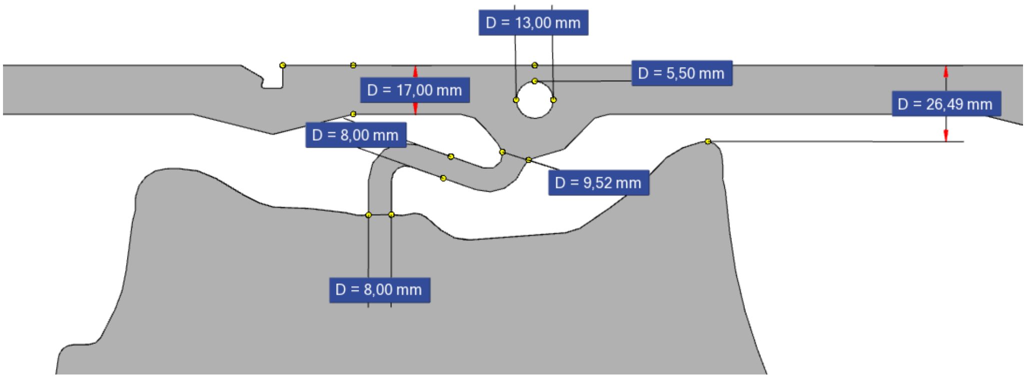

Figure 81 - Main dimensions of the harmonium connections between the parts and the side rails.

Regarding the connection between the side rails and the parts, their dimensions are indicated in Figure 81 according to the internal standards of Gestamp referred before. These connections respect the diameter of the pilot holes (13 mm), the width of the side rails (17 mm), the minimum width of the harmonium connection close to the part and the rail (min 8 mm), the width of the rest of the harmonium (min 4 mm). Not displayed but also respected are the minimum distance of 6 mm between part and rail and the minimum distance between parts of 6 mm.

As shown in Figure 80, a step of 275 mm and a width of 1240 mm were defined. The step is the distance that goes from one point of the part to the homologous point of the next part in the strip in a progressive tool. Taking into account the thickness of the sheet and the length of both parts, the grid dimensions were considered as described in Figure 81, width of 17 mm, pilot holes with 13 mm of diameter and minimum harmonium thickness of 8 mm. The separation between symmetrical parts was considered to be rectangular 80x23 mm having also a pilot hole.

Then, and after this choice, it is necessary to define the order of the stamping and trimming operations. In an industrial context, as is the case, there are a series of standard procedures that are necessary and mandatory for all parts, such as component identification through a coined code and logo as well as trims on the sheet for positional control. In this way, in addition to the essential forming steps for the geometry of the part, it is necessary to consider more steps.

Figure 88 shows the stages of this process. It is important to refer that the strip suffered alterations during the industrialization process and the final iteration is the one here presented.

- Step 1 – First of all the component is identified through three coined codes. One indicating the number of the week and year of production, which identifies the batch. Other with the logo of the client, the car manufacturer. And the last identifying the reference of the component. The left- and right-hands, identified in Figure 76 have different references.
- Step 2 – Five pilot holes are made in the plate that will help with positioning in the steps that follow. A small notch is also made in the side of the strip, with the aim of controlling the advance of the sheet through a mechanical sensor placed in step 3. Besides the pilots, the rails and this mechanical sensor at the beginning of the tool, there is also an inductive sensor at the end of the strip. The slide of the press moves downwards only if these two sensors are actuated.
- Steps 3, 4, 5 and 6 – In these steps, the sheet is progressively trimmed according to the previously defined contour. However, this cut is not made in a single operation due to the extreme complexity of constructing cutting punches with large dimensions. The trims are made in separate operations and using individual punches and dies. This means that if a punch or die must be replaced or repaired, the fix-up time is shorter, and the costs are lower. Another limitation to the size of the punches are the cutting tools available on the shop floor, namely the electro erosion tool, as its working area is only 300x300 mm, thus limiting the geometry of the punches. If the dies and punches are to be independent and if their shape is limited to simple geometries due to machining costs, then it is impossible to have all these elements in the same step.

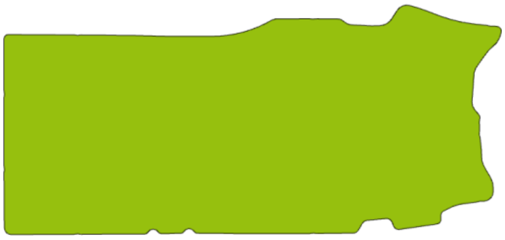

Figure 82 - Resultant geometry after step 6.

- Step 7 – It is in this step that the stamping process begins, in which the general geometry of the parts is stamped. In this way, the contour is trampled in the central area by a binder element and the outer shapes are stamped.

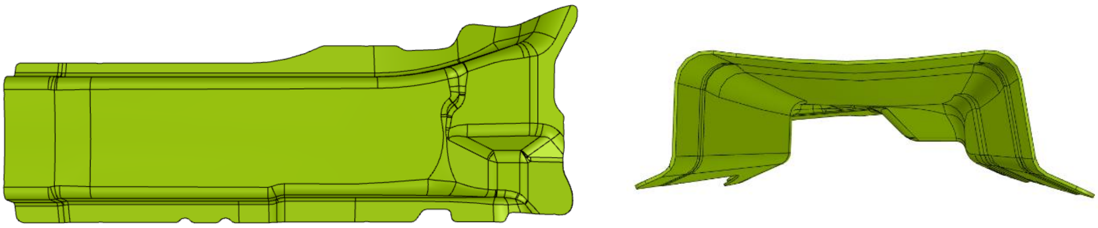

Figure 83 - Resultant geometry after step 7.

- Step 8 – This step is free, which means that no operation is performed. However, it is necessary for the tool to have this free step since its space is partly occupied by the elements of the previous and next stations, namely the stamping punches and dies.
- Step 9 – In a crash forming operation, the remaining shape is given to the parts, namely the geometries in the central zone of the parts. The exterior flaps are also put in their final position.

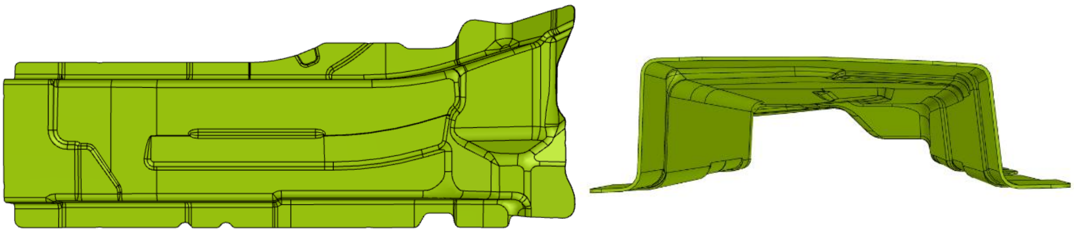

Figure 84 - Resultant geometry after step 9.

- Step 10 – In this station, the idea was to carry out a calibration on the posterior side of the parts. The main objective of this stage was causing small deformations to the parts after the final stamping in order to correct geometries that were not correctly defined after the first stamping stages. However, in the current process, since the springback compensation and the tool dimensioning were well defined, this step acts like a free step, i.e., the calibration elements are present in the tool but they are not causing any further plastic deformation to the part. The same is valid for the step 12.
- Step 11 – This is the punching stage where most of the holes are punched. It is usually made an effort to punch all the holes in the same step in order to guarantee quality in terms of positioning and repeatability. In this particular case, only the holes that need to be punched by movable overhead cams are left to a posterior step and for not being done at the same time as the others are the most prone to miss the position tolerance and therefore are the most frequently controlled in the control gauge.

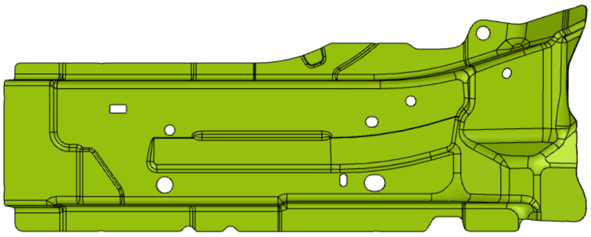

Figure 85 - Resultant geometry after step 11.

- Step 12 – This step is similar to the step 10. However, in this station, the calibration was designed for the anterior side of the parts.
- Step 13 – In this step the parts are slightly rotated so that two movable overhead cams can be responsible for punching the two holes close to the side rails, one on each side.

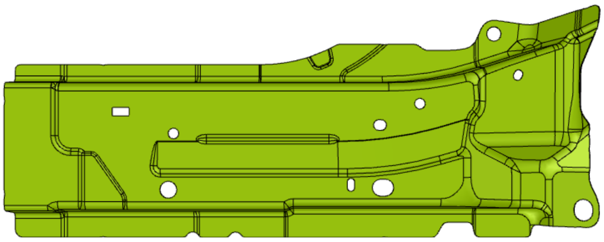

Figure 86 - Resultant geometry after step 13.

- Step 14 – In the last step, the parts are separated from the side rails using movable cams and from each other. The two remaining pairs of holes are punched using another two overhead cams.

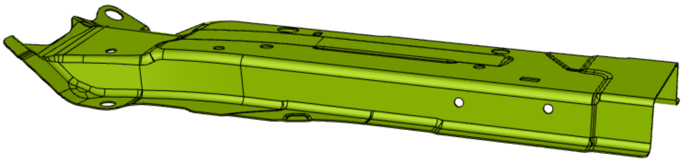

Figure 87 - Resultant geometry after step 14 (final geometry).

Even before the definition of this sequence, after a first look at the part geometry, it is also defined that it will be stamped with the flaps facing downwards. This happens for mainly two reasons. The first and most important is due to the holes made using overhead cams. If the flaps were facing upwards the scrap that results from these holes would be trapped in the part. The second reason is that if the flaps were facing upwards the stamped shape would be given by the binder and not the punch, overloading the gas springs that connect the binder to the upper shoe.

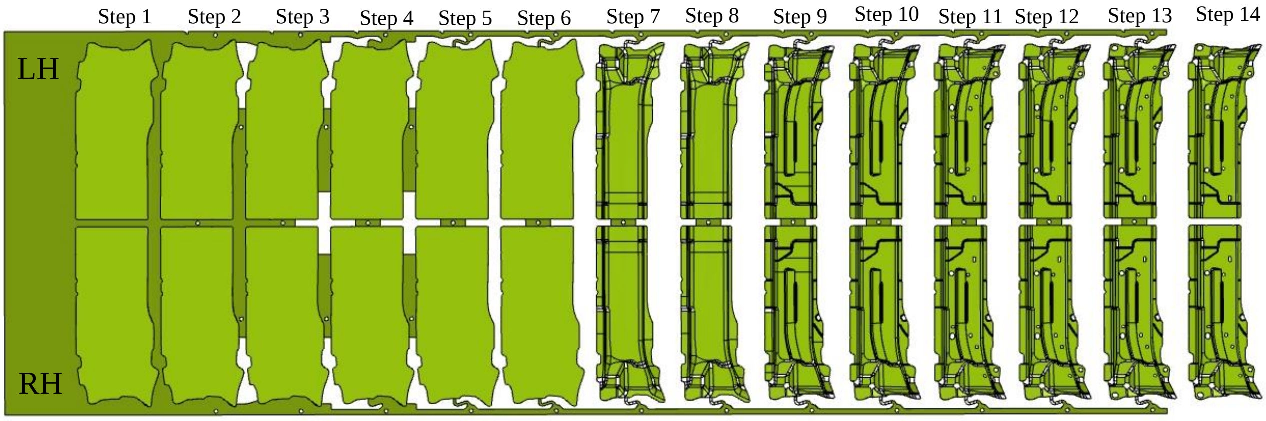

Figure 88 - Complete stamping strip of this component.

Since the strip is composed of 14 steps and each step corresponds to 275 mm, the total length of the strip is 3850 mm.

4.2.1.2 Simulation in AutoForm of current process

The blank was discretized with EPS elements, with 11 integration points through the thickness (EPS-11 type elements). The mesh refinement control parameters used are the ones given by default by the software and they are listed in Table 7, which also resumes the control parameters for the tools. The maximum number of iterations was considered 40 and the convergence tolerance 0.5.

Table 7 - Simulation parameters to input in AutoForm.

Element	***Parameter***	***Value***
Mesh refinement	Radius penetration	0.22 mm
	Max element angle	22.5º
	Initial max element size	20 mm
	Min element size	0.31 mm
	Number of initial elements	6937
	Max refinement level	6
	Master element size	40 mm
	Tangential refinement	off
Tools control	Max material displacement	2.2 mm
	Min tool displacement	1.87 mm
	Max tool displacement	5.5 mm
	End tool displacement step	0.5 mm, in the 3 final steps

The component is cold stamped, so the temperature effects can be neglected. So, the forming process is assumed to be isothermal, and no thermal expansion occurs. Therefore, the material parameters related to its behavior with temperature are defined but not used to obtain any result in the simulation.

It is used a simple Coulomb’s dry friction law not dependent from direction, pressure, or velocity. Therefore, the only parameter that is needed is the cof which was considered 0.15 parallel to rolling direction.

All dies and punches were considered rigid. The non-rigid tools, binders and cushions/pads, were considered force controlled with the default recommended stiffness of 50 MPa/mm with uniform loading condition.

Regarding the material, it was considered the model used by the tool supplier (which was slightly adapted from the AutoForm library). Therefore, the elementar properties, hardening curve, yield surface and forming limit curve were defined.

The material was defined as a high strength steel with a Young’s modulus of 210 GPa and a Poisson’s ratio of 0.3.

It is possible to see in Figure 89 the true stress-strain hardening curve that was defined through a table. Kinematic hardening is considered using the pre-defined model for high strength steel.

The yield surface is based on the BBC 2005 model, the one that has been proven to give better results regarding springback. The parameters used for this model are described in Table 8 and the resulting surface is represented in Figure 89.

Regarding the forming limit curve, it was also defined through a table that was in the AutoForm library and it is shown in Figure 89.

Table 8 - Parameters for the BBC 2005 model to characterize the yield surface of DP980.

	r_0	r_{45}	r_{90}	r_b	σ_0 [MPa]	σ_{45}/σ_0	σ_{90}/σ_0	σ_b/σ_0	M
DP980	0.76	0.96	0.76	0.915	767.4	0.9726	0.9992	0.99	6

Theoretically, the stronger the material (high yield and ultimate tensile strengths), the lower its elongation and the higher the risk of cracks. Therefore, the model should be set to the highest yield and tensile strengths and lowest elongation referred in Table 6. That is already accomplished in this model. It even considers a slightly worse case.

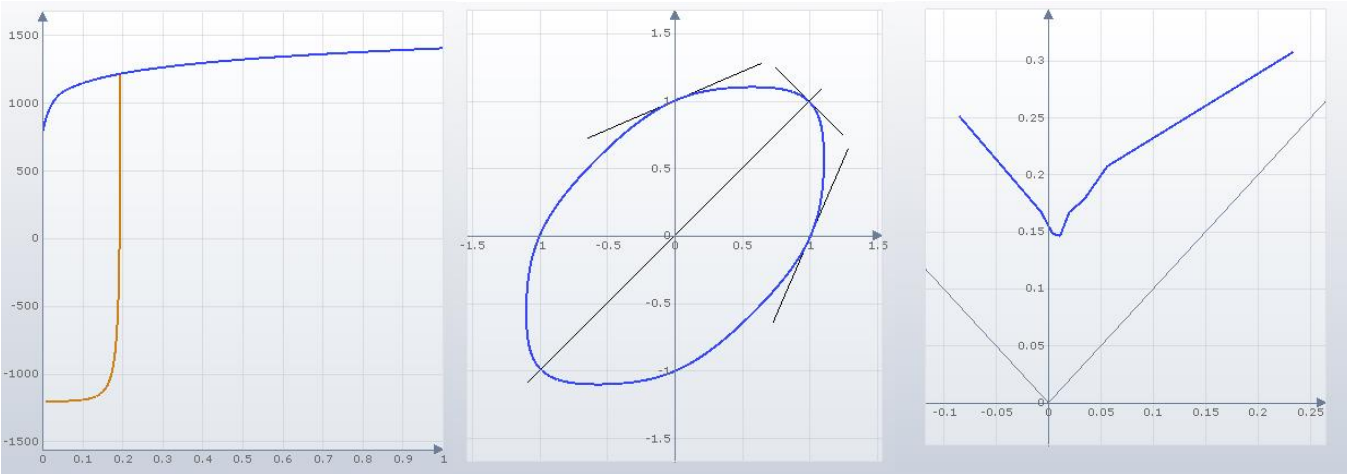

Figure 89 – Hardening law (left), yield surface (middle) and FLC (right) of DP980.

After importing the geometry, selecting the rolling and stamping direction, and correctly defining the material model, it is necessary to define which sequence of operations leads from the initial blank until the final geometry. In this case, it was not considered the complete final geometry, namely the holes punched using cams, since the most important steps to evaluate formability and risk of splits are the forming ones. The simulation was also performed only for the left-hand part since the tools and consequent results are symmetrical.

Even so, the number and type of operations necessary to obtain the geometry have to take into account the thickness, material and complexity of the component. Of course that this stage is highly dependent on former experience.

The first operation is defined as an aggregation of the first six steps described in the strip. This means that the trims that originate the blank are performed in one go, contrary to what happens in the tool. However, for simulation purposes, this simplification has a minimal influence on the results, and it avoids having many steps. Thus, the final format is obtained, in the operation called T-20.

As it was defined above, the stamping of the component is carried out in two moments, the first one where the exterior shape is formed (F-30) and the second one, where the central shapes are formed and the exterior flaps are given its final shape (F-40). These operations correspond to the steps number 7 and 9 of the strip.

After the stamping operations, it follows T-50 where all of the holes except from the ones that are made with cams are punched, an operation that evaluates free springback M-60, the separation T-70 and again a final evaluation of springback M-80. Included in operations F-30 and F-40 are also intermediate evaluations of springback.

These operations described are represented in Figure 90.

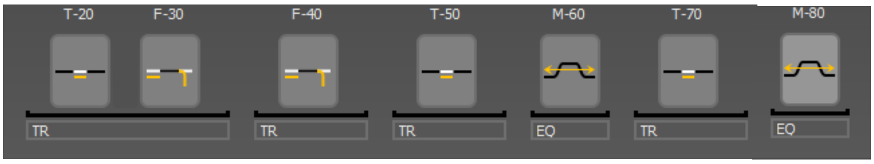

Figure 90 - Sequence of AutoForm operation to model the manufacturing process of the component.

After defining which operations are needed and in what order, the tools have to be designed or imported, Figure 91. In this case it was used the geometry of the compensated tool for operation F-40 which was given by the tool maker, according to the already implemented project. All the others were not compensated. These tools are designed so that their effect on the part is similar to what happens in the real one but it does not mean that geometrically they are identical. Therefore, some processes can be simplified without lowering accuracy.

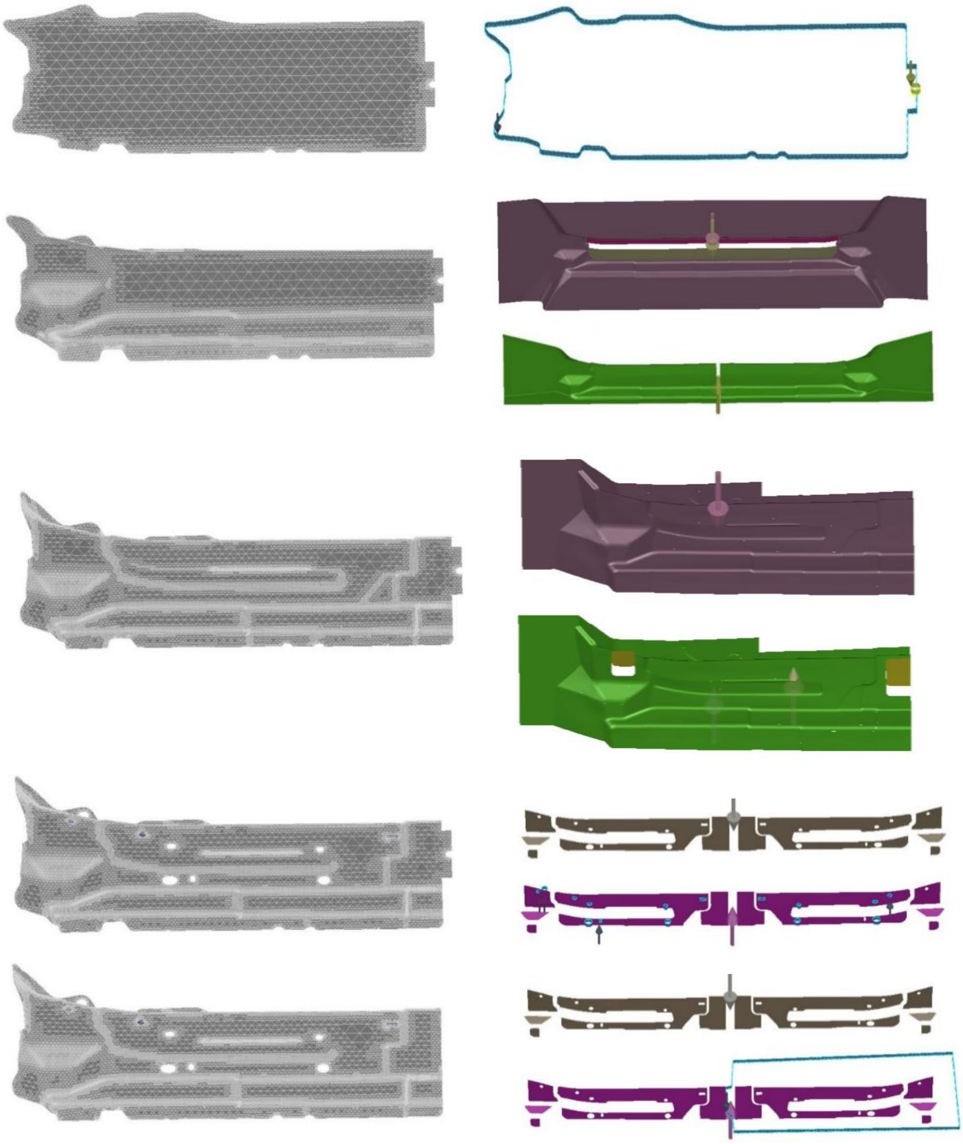

Figure 91 - Meshed geometries in each operation (left) and correspondent tool (right).

The first tool corresponds to a cutting tool responsible for transforming the sheet into the format with the desired shape. It also punches the pilot hole that is present between the left- and right-hand parts.

The part is then first stamped by the second tool. This tool is composed of a die, present in the lower part of the tool, and a punch and binder, present in the upper part of the tool. The binder, represented in yellow, moves down firstly, trampling the central area of the part so that when the punch moves down it can form the exterior of the part.

The second and final stamping operation is made using the third tool which is composed of a die and a cushion on the lower part of the tool and a punch on the upper part. This is a crash forming operation which means that the part is not restrained by a common binder. The cushion contacts the blanket first as some sort of pilot for positioning. Then, the punch moves down forming the blank against the die giving it its final shape.

The fourth and fifth tools are cutting tools, represented by blue contours.

According to the geometries available from the tool maker, some of the tools are represented for both hands of the part and others just for the hand that is being simulated.

The sequence of geometries obtained in AutoForm are illustrated in Figure 92.

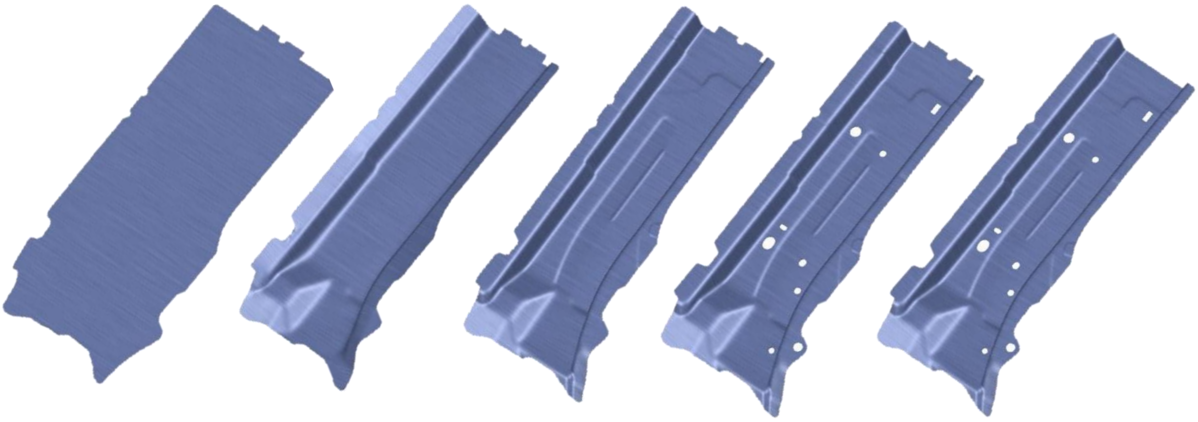

Figure 92 - Sequence of geometries obtained after each AutoForm operation.

Having all the tools designed, the next step is to run the simulation with the referred parameters and analyze the results. There are several outputs available to be analyzed: FLC along the process to access formability, thinning and splits, thickening and formation of wrinkles, edge cracks, strains, displacements, etc. All these results can be evaluated at each time step. The most important results when industrializing a product are the ones related to formability namely the appearance of cracks, wrinkles, excessive thinning or thickening.

Therefore, regarding formability, in Figures 94 and 95 are represented the advanced formability results for operations F-30 and F-40, focusing the critical zone where the cracks appear. Accompanying these results, the advanced FLCs are also represented for those stages, displaying several points over the FLC defined in the material model (Figure 93).

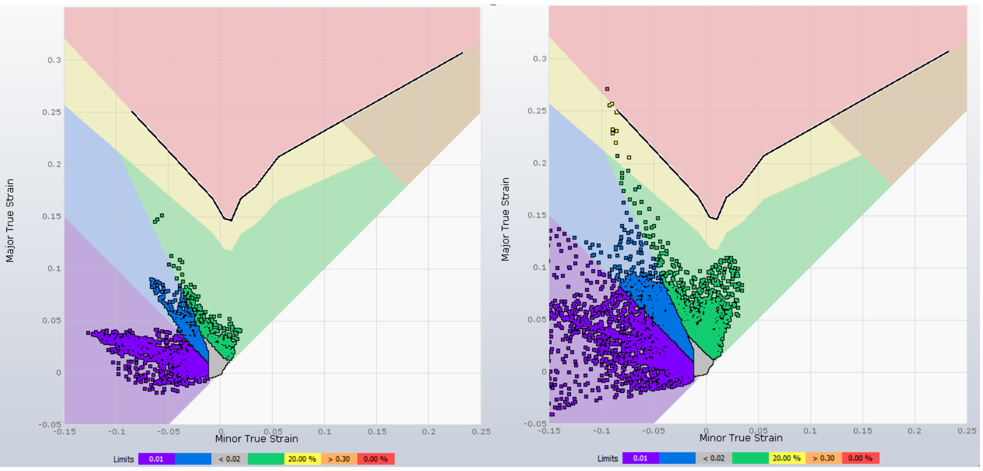

Figure 93 - Dispersion of points over the FLC after operations F-30 (left) and F-40 (right).

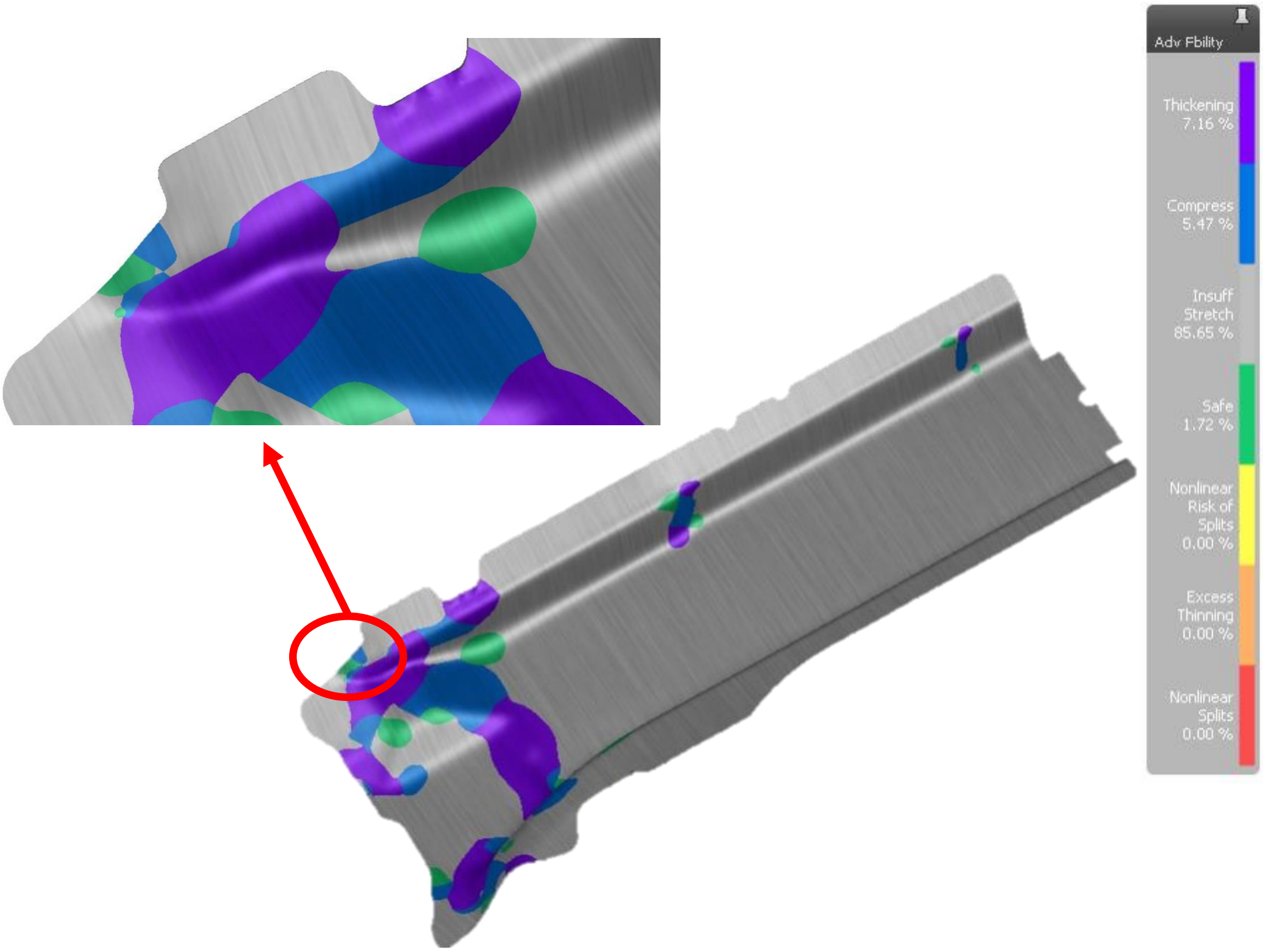

Figure 94 - Advanced formability results after F-30.

After operation F-30 there are not yet signs of cracks since there are no points having risk of splits, excessive thinning, or splits, meaning that there are no yellow, orange or red areas. All the points are located under the FLC with a reasonable safety coefficient. Therefore, there are not critical zones yet. In the purple areas, where there is accumulation of material, i.e., thickening, there can be the formation of wrinkles. However, that is just a possibility, that should also be analyzed, but that is usually not an alarming situation.

Regarding the critical zone, there are no signs of cracks yet. This may indicate that the step where these cracks are formed is the second stamping operation and not the first. In the highlighted area, AutoForm also gives the visual indication of the formation of wrinkles in the purple zone close to the edge. These wrinkles exist in the produced parts nowadays and they were even worse in earlier stages of the industrialization process. They do not compromise the part's assembly or function and they were approved by the client.

After operation F-40, it can be confirmed that it is in this step that the cracks appear. Despite being a very low percentage (<0.01%), some points are colored red in the FLC indicating nonlinear splits. These points are represented in the highlighted critical zone by a red area. This red area is located exactly where the cracks occur, indicating that the simulation is part correct. It is not fully correct since it would mean that all the produced parts would have splits and, as it will be verified, it is not the case.

In a regular industrialization process, these results would be alarming, and the tool would not be made or approved until the simulation considered the part feasible. However, due to delays or short deadlines, the tool maker produced the tool as it was simulated regardless of these results. The fact is that no cracks occurred during the validation process of the tool.

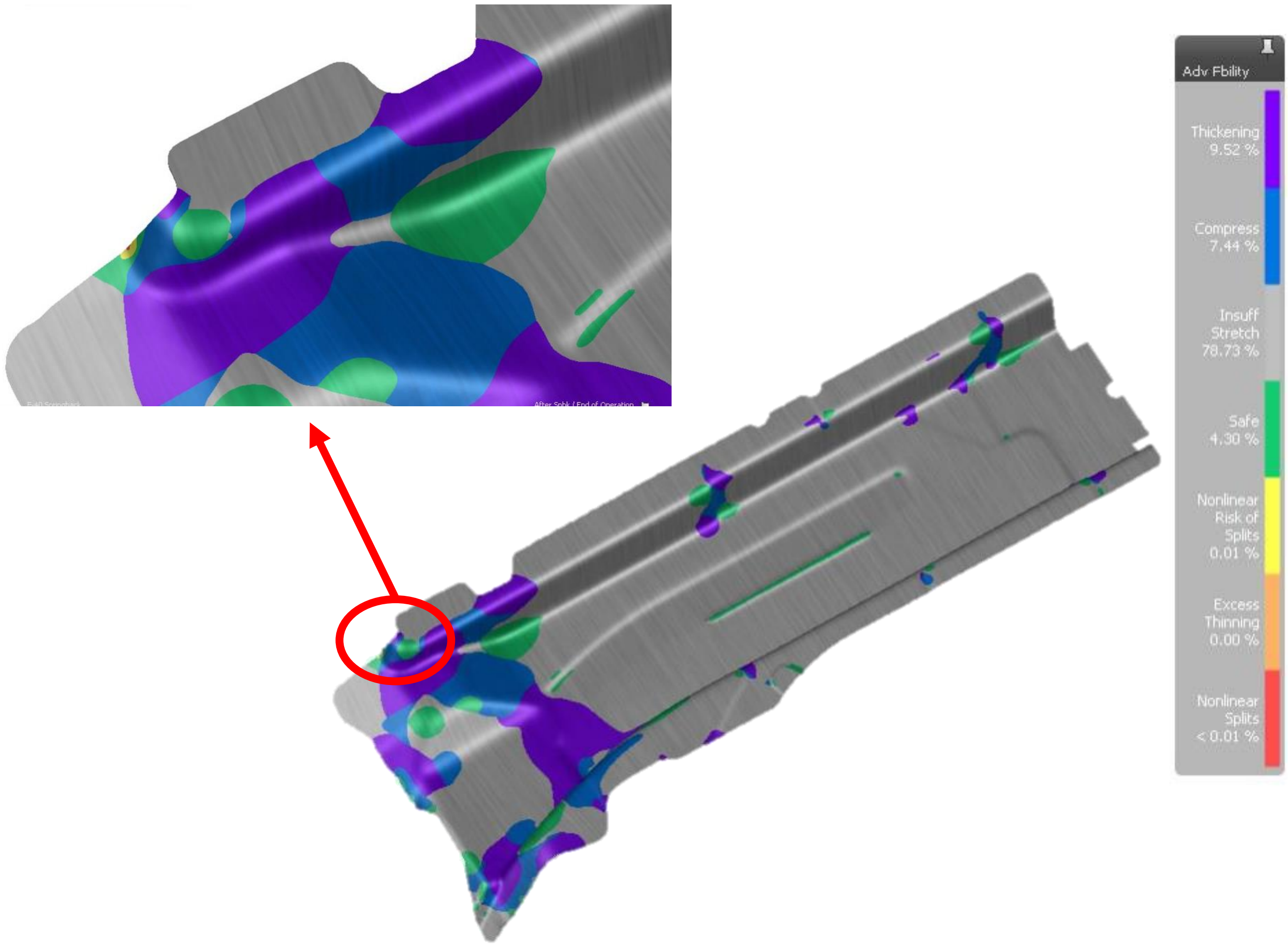

Figure 95 - Advanced formability results after F-40.

These two stamping operations were the critical steps, meaning that if there were to appear cracks, it would happen in one of these. The final formability results, after all the process, are presented in Figure 96 and very few alterations can be stated.

The results related to springback are of extreme importance particularly for the tool maker because he needs to care about compensating the tools for high springback if that is the case. However, these results should be analyzed in order to predict problems or even suggest alterations during the industrialization process.

Springback results in Figure 97 are analyzed using displacements. They are critical in the stamping operations. Nevertheless, the operations M-60 and M-80 were created to measure springback after punching and separating, respectively. Therefore, springback results will be represented for F-30, F-40 and after T-50 and T-70. It is important to note that this simulation was done using the geometry of the compensated tool in F-40 which means that the displacements are given having the compensated tool as reference. This means that, in this case, the tool was made so that after the displacements caused by springback (6.888 mm max and -6.562 mm min), the part had the correct shape. The tool in F-30 was not compensated because it only makes sense to compensate one tool, the one where it is being given the blank its final shape.

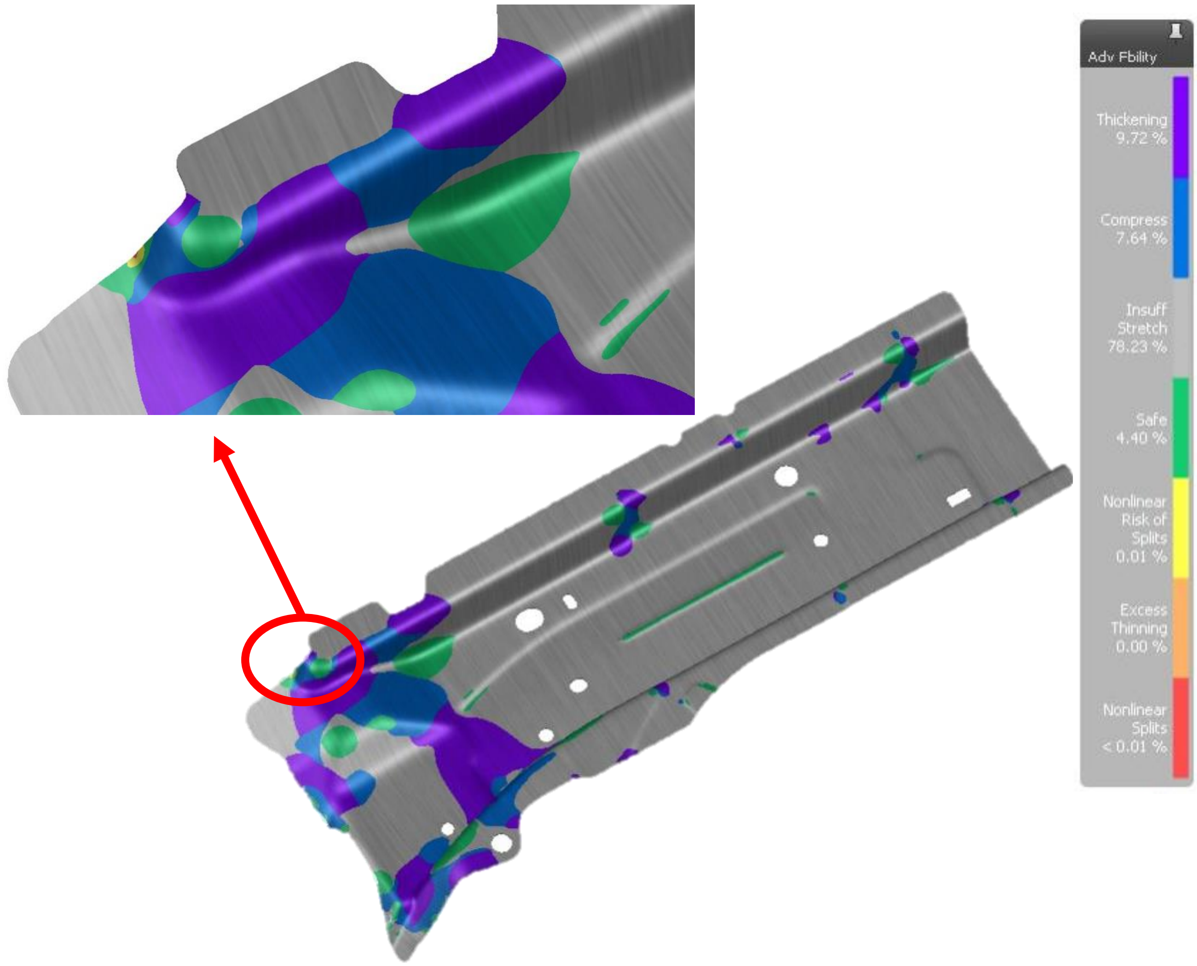
Adv Fbility
Thickening 9.72 %
Compress 7.64 %
Insuff Stretch 78.23 %
Safe 4.40 %
Nonlinear Risk of Splits 0.01 %
Excess Thinning 0.00 %
Nonlinear Splits < 0.01 %

Figure 96 - Final advanced formability results.

In essence, the values indicated measure the displacement suffered by the point after the moment the tool is removed. Therefore, it compares the geometry before springback and after springback, whether or not the tool is compensated. If the tool with which the simulation was done is already compensated, that means that the geometry after springback is already very close to the desired geometry.

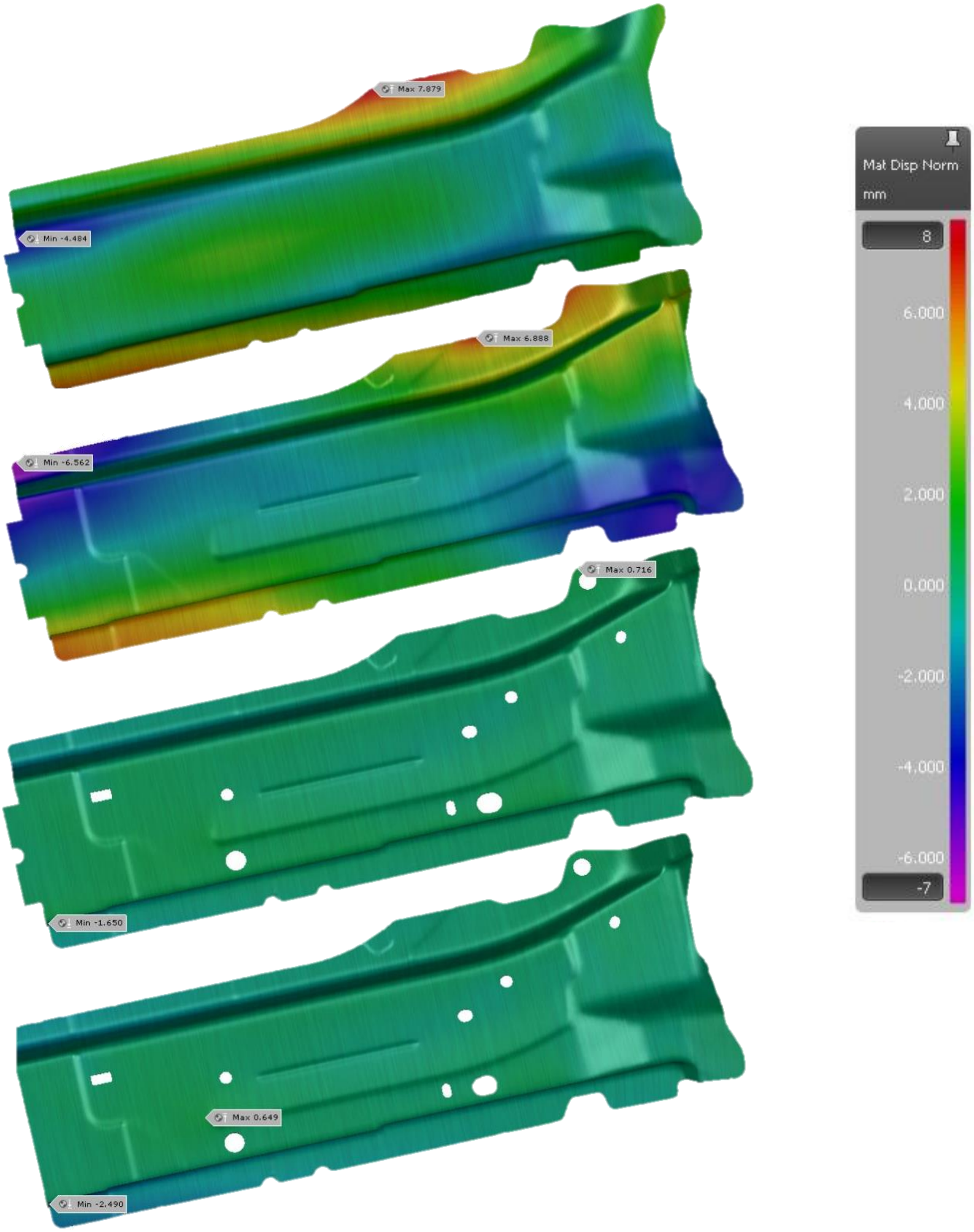

Figure 97 - Springback results after each operation.

Figure 98 shows the difference between the geometries before (meshed) and after springback, evidencing the twist springback that occurs in both steps F-30 and F-40.

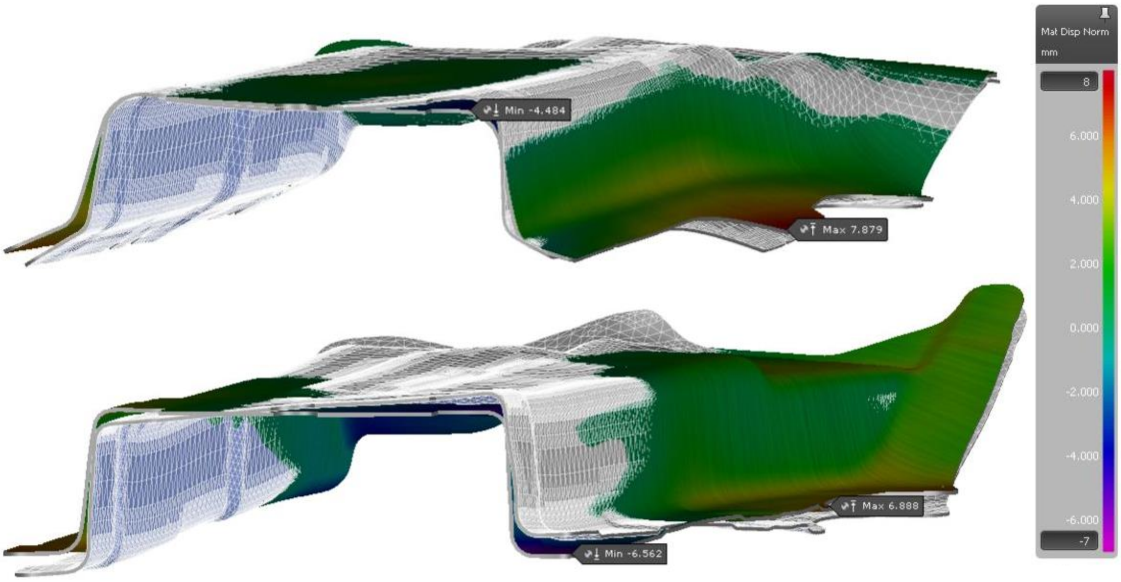
Mat Disp Norm
mm
8
6.000
4.000
2.000
0.000
-2.000
-4.000
-6.000
-7
Min -4.484
Max 7.879
Max 6.888
Min -6.562

Figure 98 - Geometries before and after springback in operations F-30 and F-40.

Even with the compensated tool, the geometry after springback is not the exact desired geometry. The comparison between the perfect desired geometry (meshed) and the one obtained is shown in Figure 99. This means that full compensation was not achieved, being A elevated about 1.5 mm in relation to the desired geometry and B lowered about 1 mm. However, the desired and the obtained geometries practically coincide, being that maximum difference of 1.5 mm acceptable as long as it is just in minimal areas which is the case.

Overall, the final springback results are acceptable as it can be confirmed in the analysis of the part in the control gauge and 3D measuring reports.

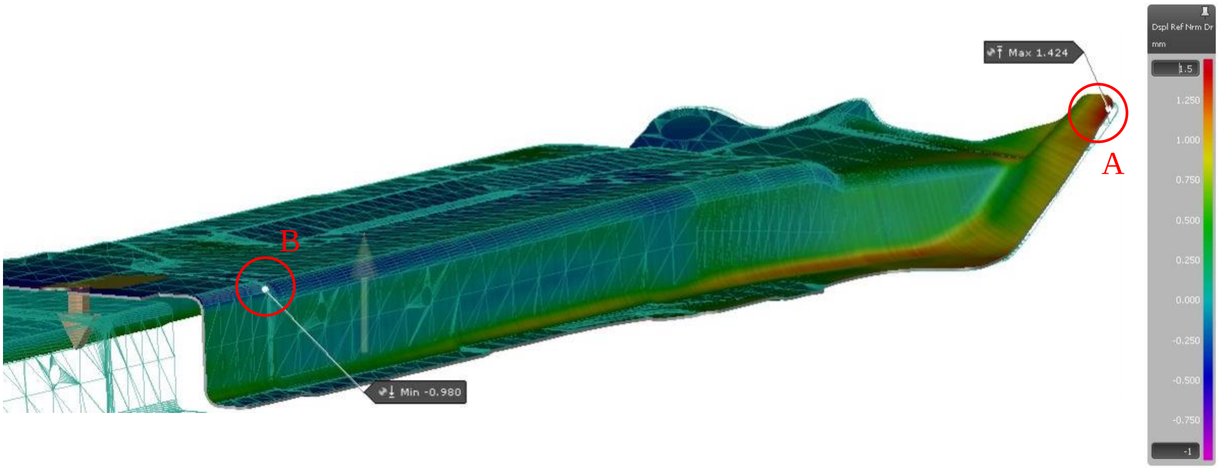
Dspl Ref Nrm Dr
mm
1.5
1.250
1.000
0.750
0.500
0.250
0.000
-0.250
-0.500
-0.750
-1
Max 1.424
A
B
Min -0.980

Figure 99 - Final deviation from the desired geometry.

Regarding other important but somehow complementary results, in Figure 100 is the thickness variation which shows that during forming some areas thin, losing until 0.2 mm, and others thiken up to 0.3 mm. An analisis related to the formation of wrinkles is also displayed in Figure 100. In the same figure, it is also the edge cracks results. A value for this variable over 1.2 is usually problematic.

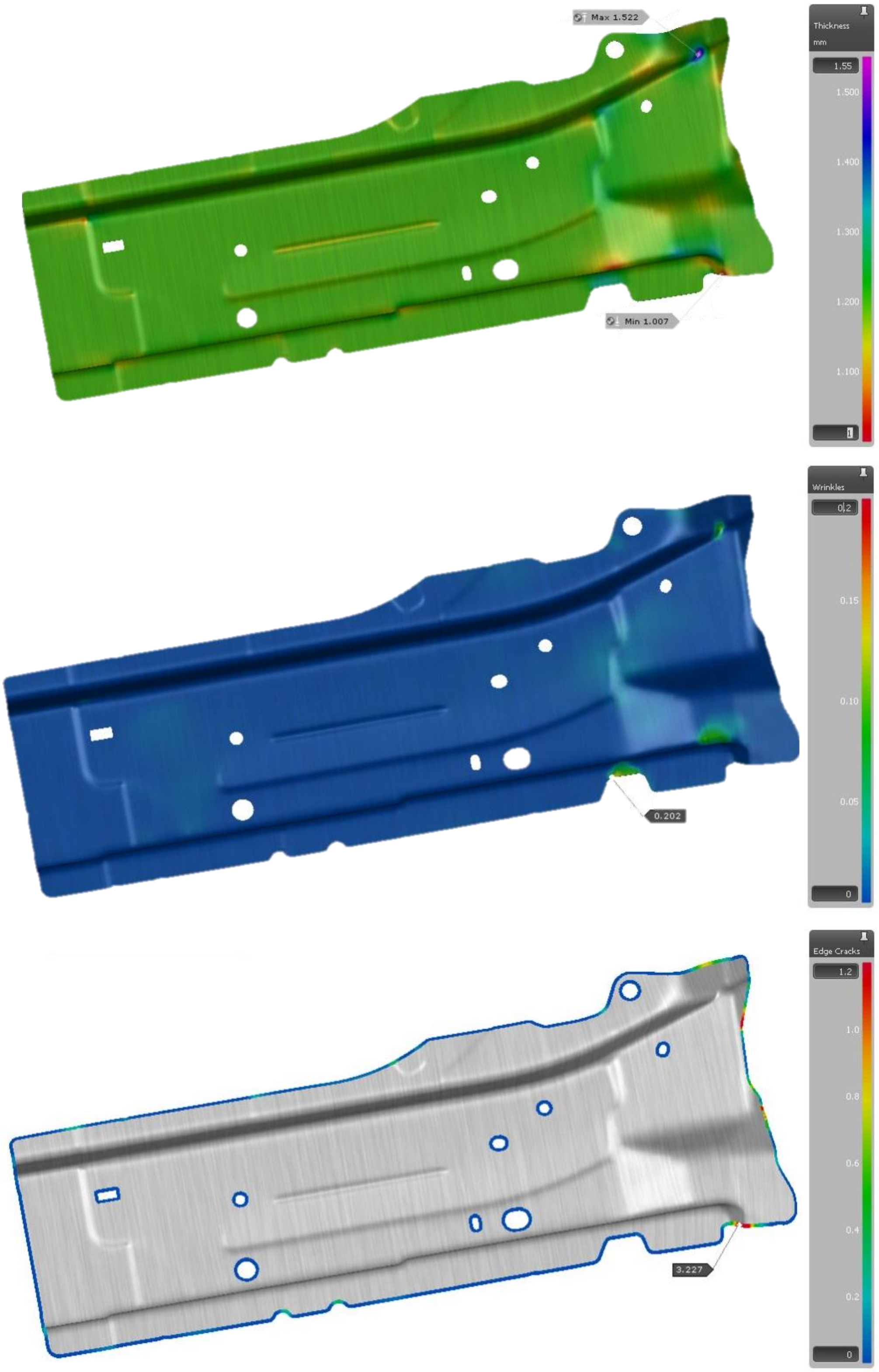
Max 1.522
Min 1.007
Thickness
mm
1.55
1.500
1.400
1.300
1.200
1.100
Wrinkles
0.2
0.15
0.10
0.05
0
0.202
Edge Cracks
1.2
1.0
0.8
0.6
0.4
0.2
0
3.227

Figure 100 - Complementary results: thickness variation, formation of wrinkles, and edge cracks.

These results point to the occurrence of cracks where they are actually appearing, Figure 101. As well as for the already mentioned wrinkles in the maximum point indicated in Figure 100.

Nevertheless, as it was already briefly stated, what is seen in reality does not correspond directly to the simulations. According to those, it would be expected that all parts presented cracks, both in the right- and left-hands. Actually, in spite of these results, during the validation phase in the industrialization process no cracks were detected and therefore it was assumed that the results of the simulation were not 100% accurate and that the tool would produce non-defected parts since the red area in Figure 96 was extremely small and could be derived of some imprecision in a numerical input parameter.

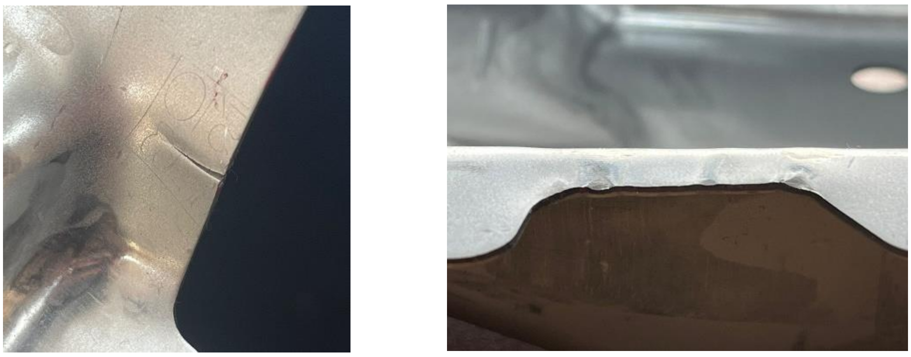

Figure 101 - Existing defects in the stamped parts.

In Table 9 are the approximate forces calculated by AutoForm in each operation. It is important to note that these forces correspond only to one hand of the component and since both hands are made at the same time the press must be chosen according to the double of these values. Other important thing to highlight is that the holes that are punched by cams are not considered and therefore the force needed for that operation is not included in the calculated force.

Table 9 - Necessary forces for each operation.

Operation	***Force [kN]***	***Force [ton]***
T-20	1620	165
F-30	635	65
F-40	1295	132
T-50	525	54
M-60	-	-
T-70	260	27
M-80	-	-
Total	4335	443

Taking into account the equipment available at Gestamp Cerveira, it is necessary to choose the press for the processes in the production of this component. Knowing that the tool selected for this process is a progressive one, it is necessary to choose, among the progressive presses at Gestamp Cerveira, which one is the most suitable for this production. In this way, the factors that limit the choice of the press are essentially two, the first being the necessary effort and the second the dimensions of the table of the press.

Knowing that the defined strip has a width of 1240 mm, a length of 3850 mm and that the effort required to obtain the final geometry is more than 886 ton, it is concluded that this tool will have to work in a press of 1250 or 1500 ton. Here, the choice of the 1500 ton press relies on the fact that it is a servo press, which allows for higher production rates.

4.2.2 Project of the tool

The tool is, logically, built from the strip defined in the feasibility study. However, during the industrialization process, anticipating some problems that may occur in production, some small alterations can be done to the production process and consequently to the strip. In this section, the described tool will be the final one, currently used. The number of positions in the tool corresponds to the previously defined number of steps, fourteen, as well as their order. Thus, it can be generally divided into 3 major modules, that can even be physically independent (in the present case the tool is made by 2 not physically independent modules, the stamping and punching are part of the same):

- Trimming – area where all the cuts that define the blank outline are progressively done, as well as the pilot holes for guiding the strip along the tool and the notch for the mechanical sensor. It is also in this area that the references of the parts, the customer's logo, and the date of manufacture of the batch are coined. It corresponds to the steps 1 to 6.
- Stamping/forming – area where mechanical work is performed on the blank in order to obtain the desired final geometry. It is in this module that the part gets its shape. It corresponds to steps 7 to 9 although the calibration steps could also be part of this area.
- Punching/Separation – area in which all the holes are punched and, finally, the separation of the part. It corresponds to steps 11 to 14.

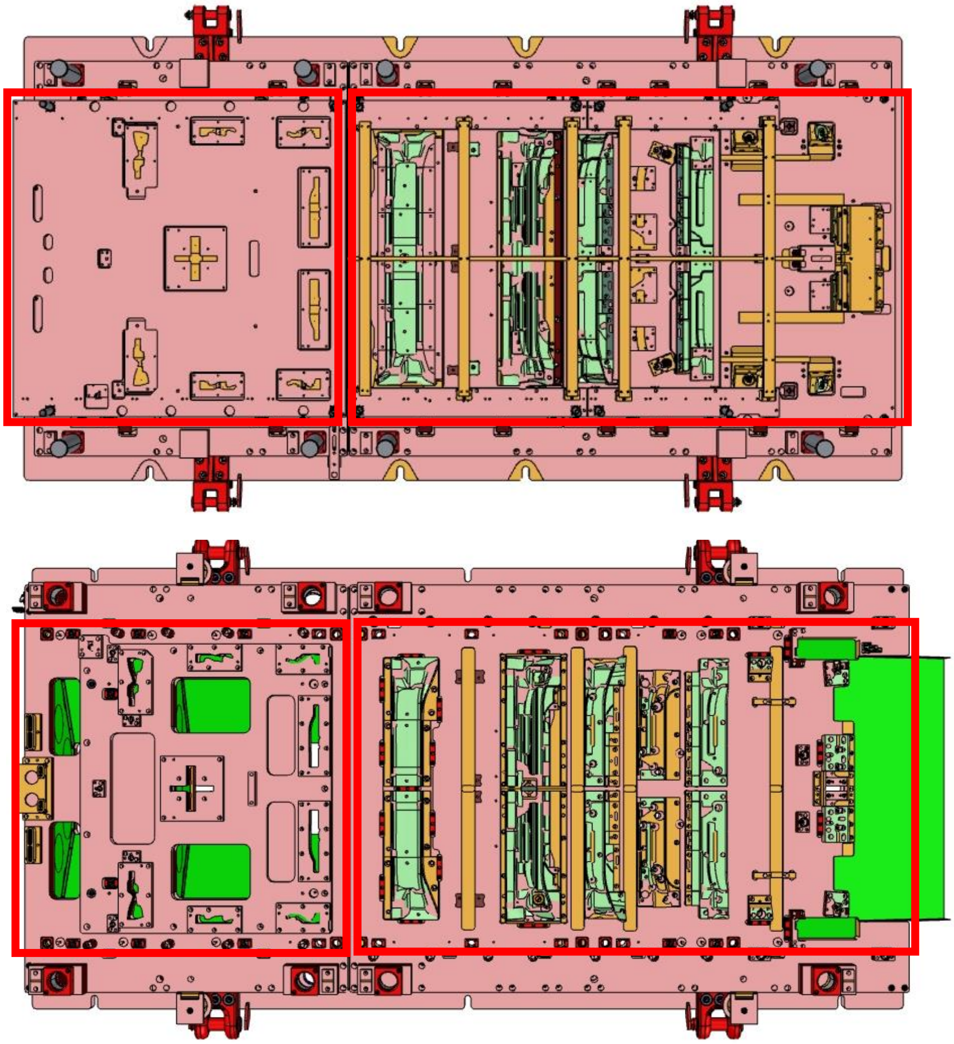

Figure 102 - General sectors of the stamping tool: trimming zone and stamping/punching/separation zone.

Considering the process defined in the strip and the simulation of the stamping process the total necessary force was calculated. This force obviously restrains the press to be used. However, other factors like the size of the strip and consequently the tool are crucial. In Figure 103 the main dimensions of the tool are presented: 4200 mm length, 2120 mm width and 1149.5 mm height (in the bottom dead center). According to the press and its table dimensions, maximum dimensions for the tool are set. In the case of the selected press for this part (1500 ton servo press) the table dimensions are 6000 mm length and 2400 mm width.

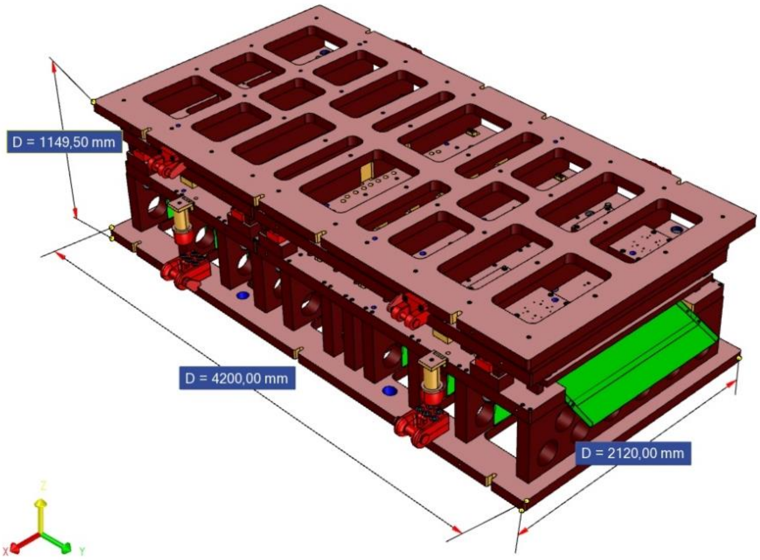

Figure 103 - Main dimensions of the tool in bottom dead center.

The most important constructive details, functions and materials of the tool and its components will be detailed next. Although each company has its own standards when it comes to stamping tools, the main features and elements are similar to those found around the world in stamping companies from the automotive industry.

Next, the most important components and construction details are referred and described.

The lower part of the tool is displayed in Figure 113. Its most important components are:

- 1 – Lifting flanges: they are the elements where the crane rings are attached to transport the tool between the press and the warehouse. They consist of a fixed part (in red) and a mobile part (pin with safety ring) which is inserted into the crane rings.
- 2 – Positioning holes: a pair of holes on each side of the tool, one circular and one oblong to ensure correct positioning (correct stamping direction).
- 3 – Lower clamping shoe: 76 mm thick steel plate (imposed by Gestamp Cerveira) whose main function is to fix the lower part of the tool to the press table. The indentations for quick centering and tool fixing are located here. Attached to this shoe are the transport handles and the props. It also supports the scrap guides. It can be seen in Figure 103 that this plate has several holes to reduce the weight of the tool.
- 4 – Props: they are 100 mm thick steel blocks, and their main function is to increase the height of the tool while maintaining the rigidity of the set. As it can be seen in Figure 103, similarly to what happens in the lower and upper shoes, the props have holes to reduce the overall weight of the tool.
- 5 – Storage supports (resting system for storage): are cylindrical rubber elements that are rotated upwards when the tool is removed from the press and placed in the respective warehouse. The resting system makes sure that none of the gas cylinders are activated, guaranteeing a gap of about 40 mm. It also allows another tool to be placed on top in order to optimize the occupied space.
- 6 – Indentations for fixing and positioning: they are notches in the lower clamping shoe that provide a fast first positioning of the tool on the press table.

- 7 – Exit ramp: ramp at the end of the tool to facilitate the exit of finished components. This prevents that these components get stuck and interrupt the production flow.
- 8 – Lower shoe: it is a plate where all the other elements that make up the lower part of the tool are coupled and has a thickness of 95 mm. The cutting and stamping dies, columns for secondary guiding of the lifting plate, sleeves for primary guiding columns, the inductive sensor that indicates the end of the strip, etc. are attached to it. Along with the upper shoe, it is considered a fixed component.

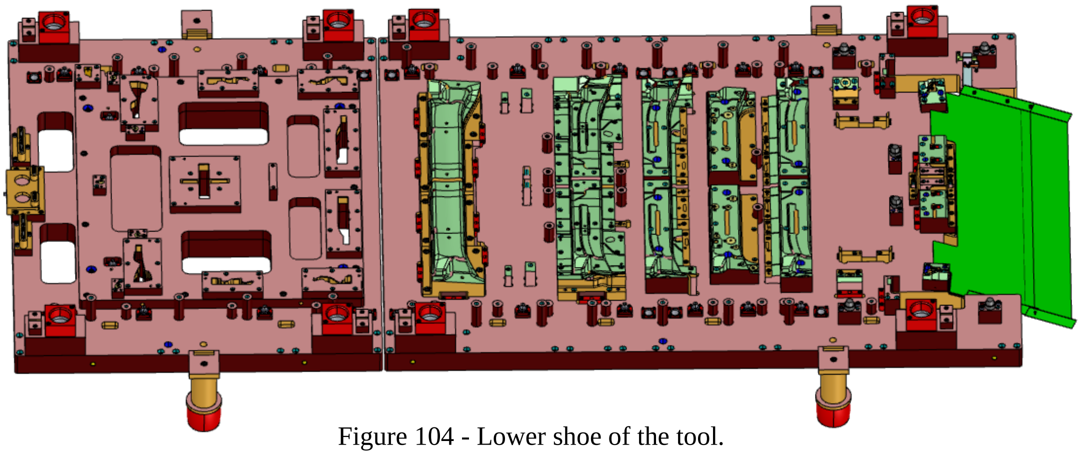

Figure 104 - Lower shoe of the tool.

- 9 – Lifter plate: this plate has the function of keeping the sheet metal higher than the dies and other elements in the lower shoe, allowing the strip to slide over them as it is required in a progressive tool. A closer detail to this element is given in Figure 105. It is considered a movable part of the tool and its operation is based on gas springs (pneumatic cylinders charged with gas), Figure 105, which lower this plate when the upper part of the tool is forced against it. It is made up of lateral rulers or strip guides that ensure the movement of the sheet between them in the productive direction, by secondary guide columns that guarantee the verticality of the up and down movement of the lifter plate, stoppers that limit the maximum course of the lifter plate, and the step sensor. This is also where the series start line (number 10) is located.
- 10 – Start line: This is the line where the beginning of the coil must be placed at the start of production and must obey certain rules such as not intersecting any cutting punches, not generating unbalanced stampings and that incomplete parts are not produced.

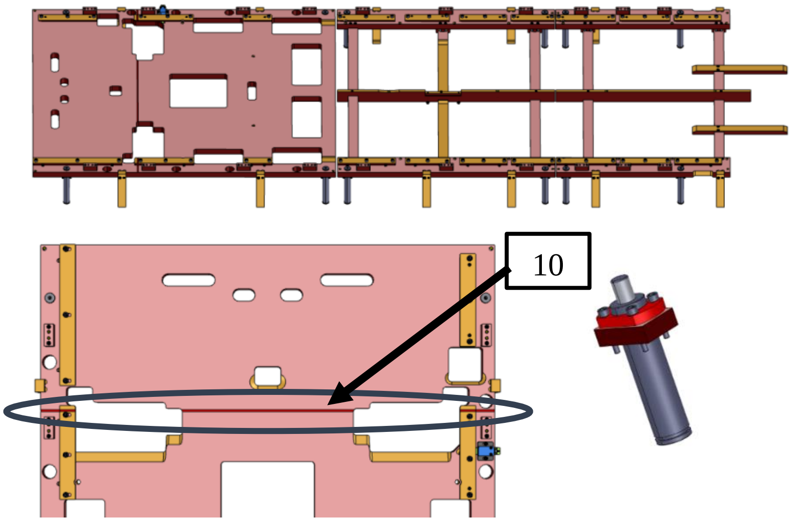

Figure 105 - Lifter plate, gas spring, and start line.

- 11 – Sleeves for primary guiding: they house the guide columns that slide in them, maintaining the correct position of the upper part of the tool relative to the lower one. These generally use bronze reactions with graphite applications as a solid lubricant.
- 12 – Trim dies: they are, along with the punches, responsible for cutting the sheet. Whenever possible, they are presented as a parallelepiped, facilitating machining operations during tool manufacture and maintenance. In the center they have an opening with the desired shape for the cut. This opening has vertical walls in the first 5 mm of the punch (dimension varies depending on the thickness of the sheet) and, in the rest of the walls, an inclination with an angle of 1.5º in order to optimize the exit of scrap, avoiding its accumulation in the tool (Figure 106). They are fixed to the die retainer with screws and two off-centered dowels in order to ensure that no die is mounted in an incorrect position.
- 13 – Die retainer: plate fixed to the lower shoe responsible for holding the dies.

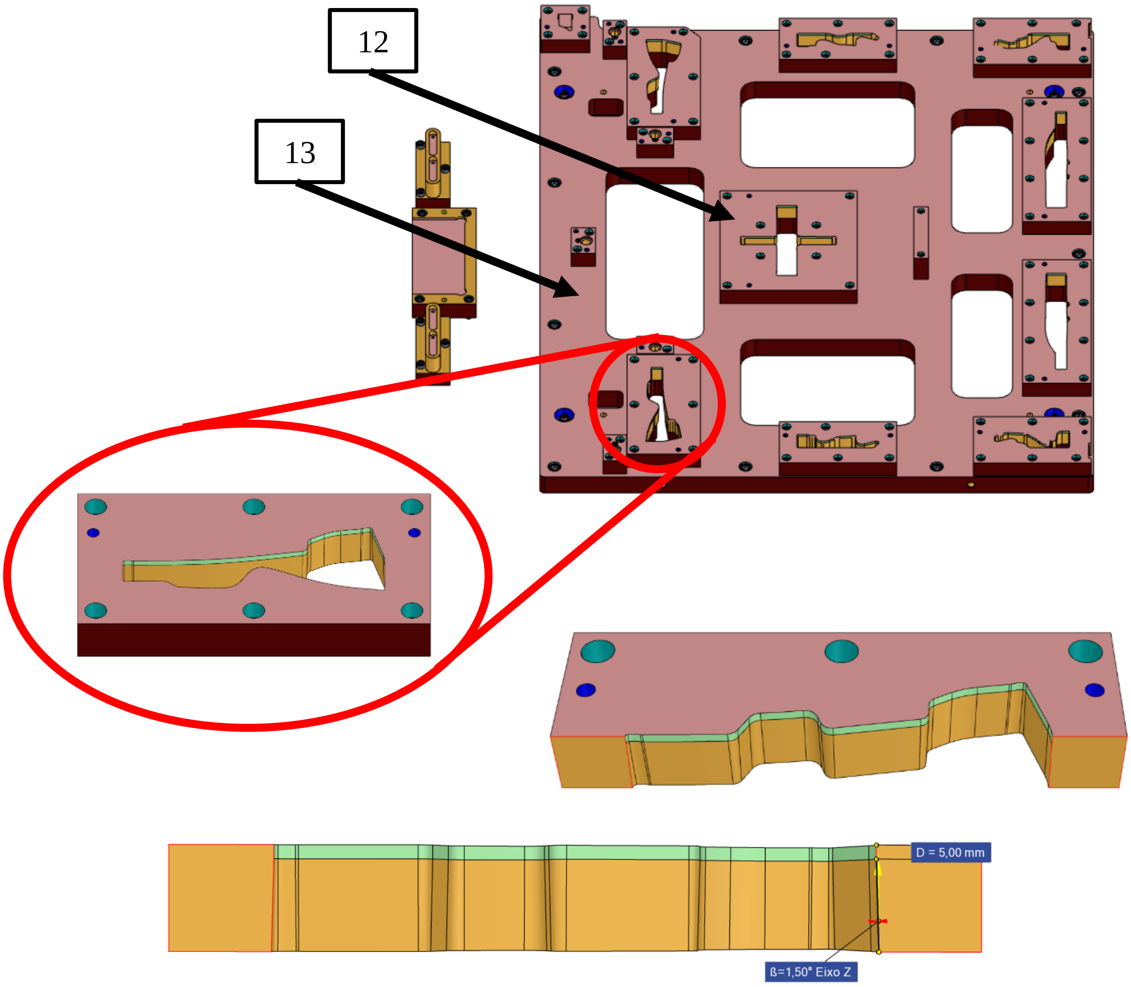

Figure 106 - Trim dies and die retainer.

- 14 – Stamping dies: they are the dies responsible for giving shape to the components alongside with the stamping punches. These are the tool components that usually need to be compensated for springback. In this case, the compensated zone corresponds to step 9, where the geometry gets its final shape (interior and exterior) and the values of springback were excessive (Figure 107 illustrates the compensation where it is seen that the sheet suffers twist springback).
- 15 – Calibration dies.

- 16 – Punching dies.

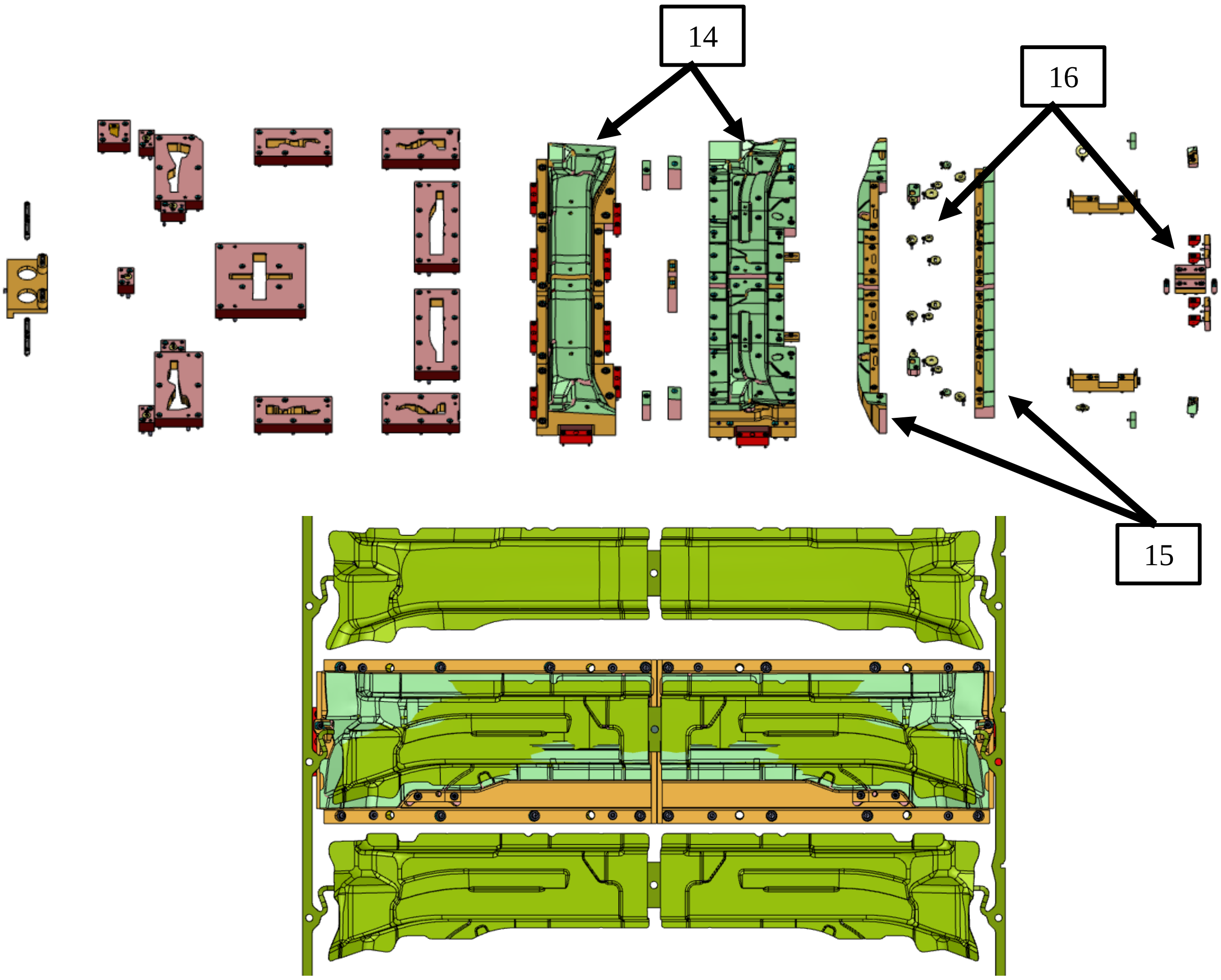

Figure 107 - Dies present in the tool and focus on the compensated stamping die.

- 17 – Stoppers: they are the elements that limit the movement of the lifter plate when it rises, during the opening movement of the tool.
- 18 – Step sensor: mechanical sensor that only when activated allows the press to stroke. This assures, along with several other redundant methods, the correct positioning of the strip. It detects a notch done in the previous step on the edge of the strip.

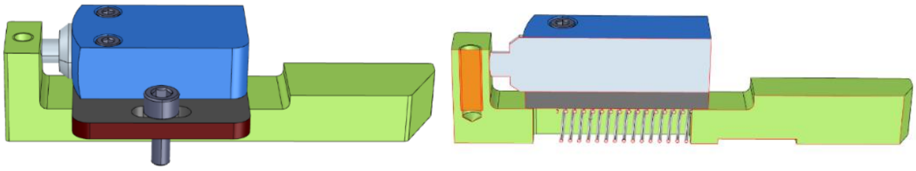

Figure 108 - Step sensor.

- 19 – End of strip sensor: inductive sensor that detects the presence of the strip at the end of the tool. Similarly to what happens with the previous sensor, the press only strokes if this sensor is actuated. When the strip gets to this sensor, it hits the sensor in the direction of the arrow (Figure 109) and the sensor detects its presence.

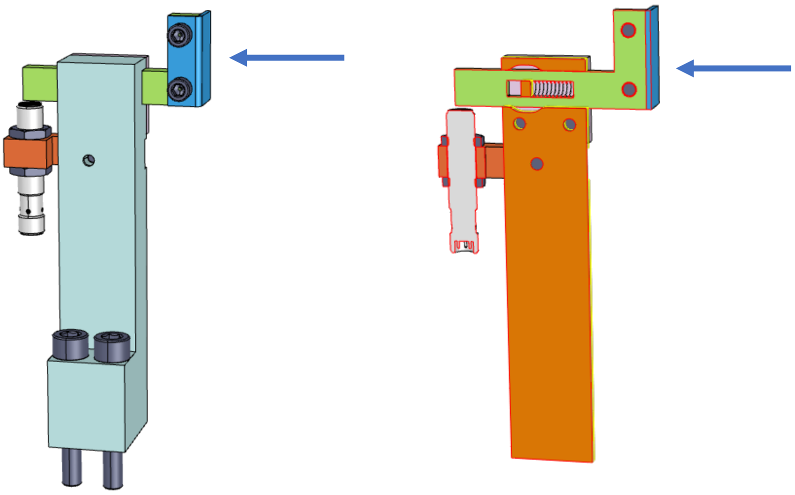

Figure 109 - End of strip sensor.

- 20 – Coining type holders: these elements allow the coining of the batch number, reference and the customer's logo on the parts. The character holders can be easily accessed in order to change the batch number characters.

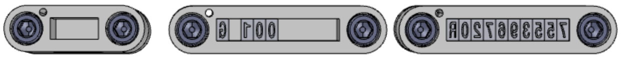

Figure 110 - Type holders.

- 21 – Strip guides: they have the function of guiding and keeping the strip in the correct position. The strip guides control the movements in the direction perpendicular to the productive one, that is, they do not let the grid exceed the lateral limits. The side rails are part of the strip and guide it through the strip guides. They also prevent the strip from shrinking in that direction, that is, they do not allow the plate to flow towards the center, during stamping. In Figure 111 it is possible to see how the side rails slide in the strip guides. The highlighted zone shows an inclination created to smoothen the entrance of the side rails in the strip guides.

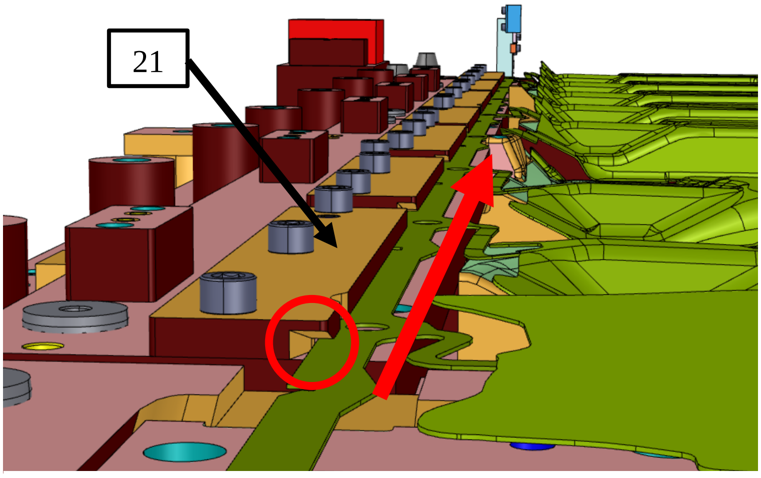

Figure 111 - Strip guides.

- 22 – Scrap guides: they are steel plates that gather the resulting scrap from trimming and punching operations and guide it to the scrap tunnels.

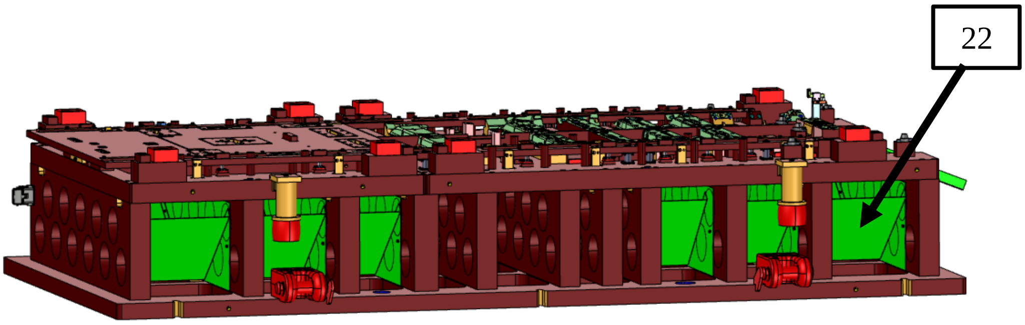

Figure 112 - Scrap guides.

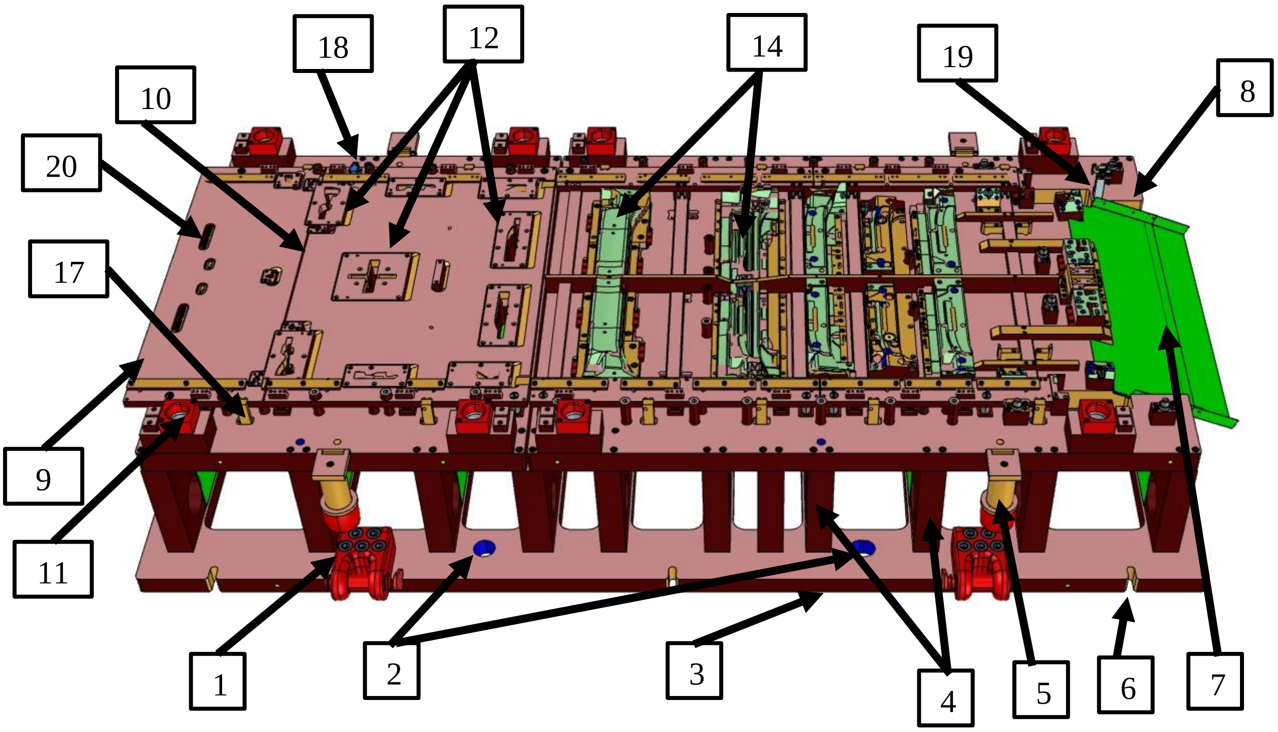

Figure 113 - Lower tool.

Regarding the upper part of the tool (Figure 118) the most important elements are described below.

- 23 – Primary guiding columns: these elements are the main responsible for aligning the top with the bottom part of the tool.
- 24 – Upper clamping shoe: this plate is fixed to the upper part of the press table by means of claws that enter the notches present in it. Like the lower clamping shoe, the lifting flanges are also tightened on this element. It can be seen in Figure 103 that this plate has several holes. These reduce the weight of the tool on the one hand and provide easy access to the standardized punches that can be that way easily replaced on the other hand.
- 25 – Upper props.
- 26 – Upper shoe: it is on this plate that all the other elements belonging to the upper part are mounted.

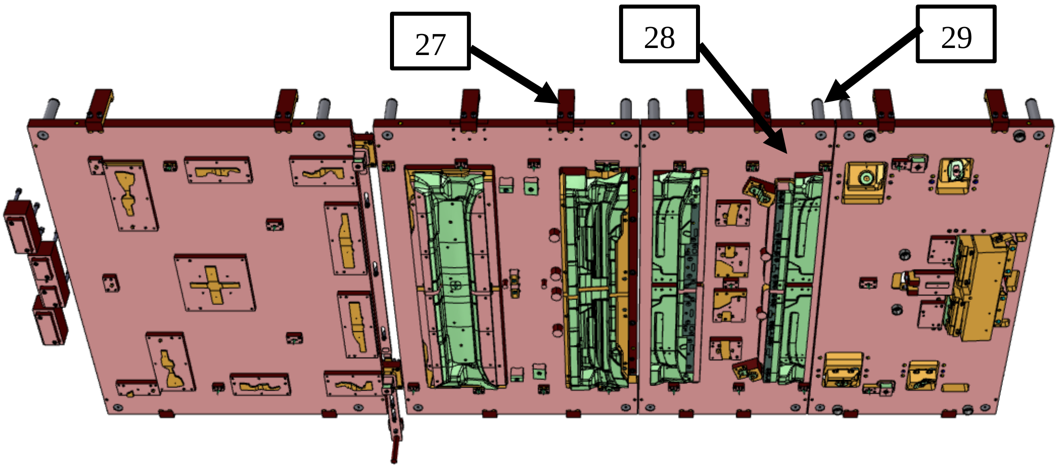

Figure 114 – Stripper plate.

- 27 – Stoppers: they are the elements that limit the movement of the stripper plate when it moves down, during the opening movement of the tool.
- 28 – Stripper plate: this plate holds all the binders/pads/blankholders and pilots, Figure 114. It is divided into several parts in order to facilitate both manufacturing and maintenance. Like the lifter plate, this is also a movable element whose movement is also due to the gas cylinders placed between it and the upper shoe, it is guided by the secondary guiding columns and the stroke limit is imposed by the stoppers placed at the edges.
- 29 – Secondary guiding columns: these elements are responsible for aligning the stripper plate with the upper shoe.
- 30 – Resting stoppers: elements where the storage supports rest.

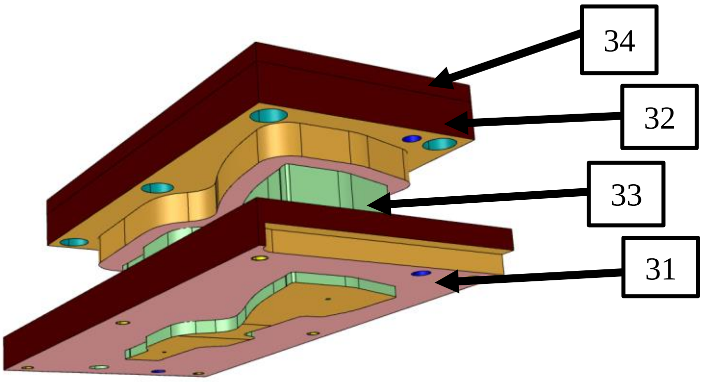

Figure 115 - Trimming punch (cuts critical zone).

- 31 – Binders/pads/blankholders: their main function is to step on the sheet on the perimeter of the cut or the stamped shape. According to the type of operation, the name changes from blankholder in the case of a deep draw to binder or pad in the case of more simple stamping operations or trims.
- 32 – Punch retainer: it is the plate that is fixed to the upper shoe and holds the punches.
- 33 – Trimming punches: elements responsible for the cut. Their geometries are dictated by the shape of the cuts. Their function is to cut the plate according to the desired shape.
- 34 – Reactions/shock plate: it is the plate that separates the upper shoe from the punches and punch retainers. Its function is to absorb the impacts from the punches and distribute them across the upper shoe.

- 35 – Stamping punches: elements responsible for the geometry of the part. Their function is to give the plate its shape.

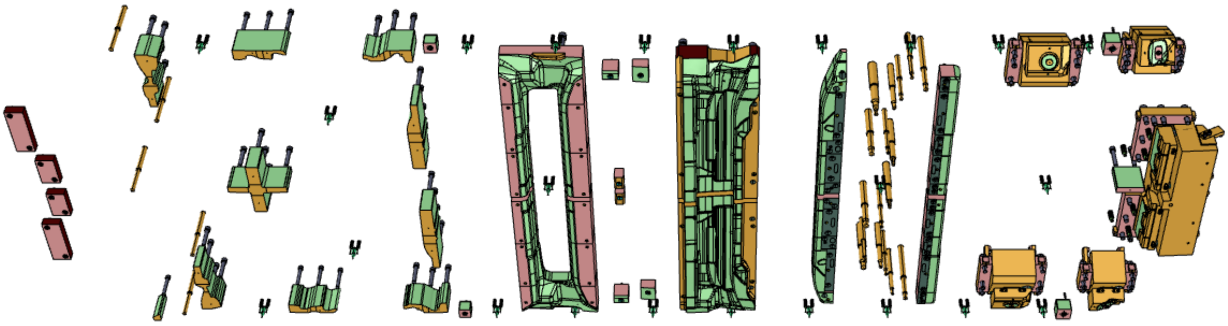

Figure 116 - Punches present in the tool.

- 36 – Pilots: small cylinders with a conical end, visible in Figure 117. Their function is to enter the pilot holes of the sheet just before a stroke. Entering the respective hole, it guarantees the correct positioning of the sheet in the tool.

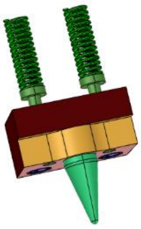

Figure 117 - Pilot.

- 37 – Guillotine activator: it is an element that has the function of activating the punches of the guillotine. Its normal position is retracted. However, it can be activated in order to facilitate the separation and removal of the strip after a production.
- 38 – Cams.

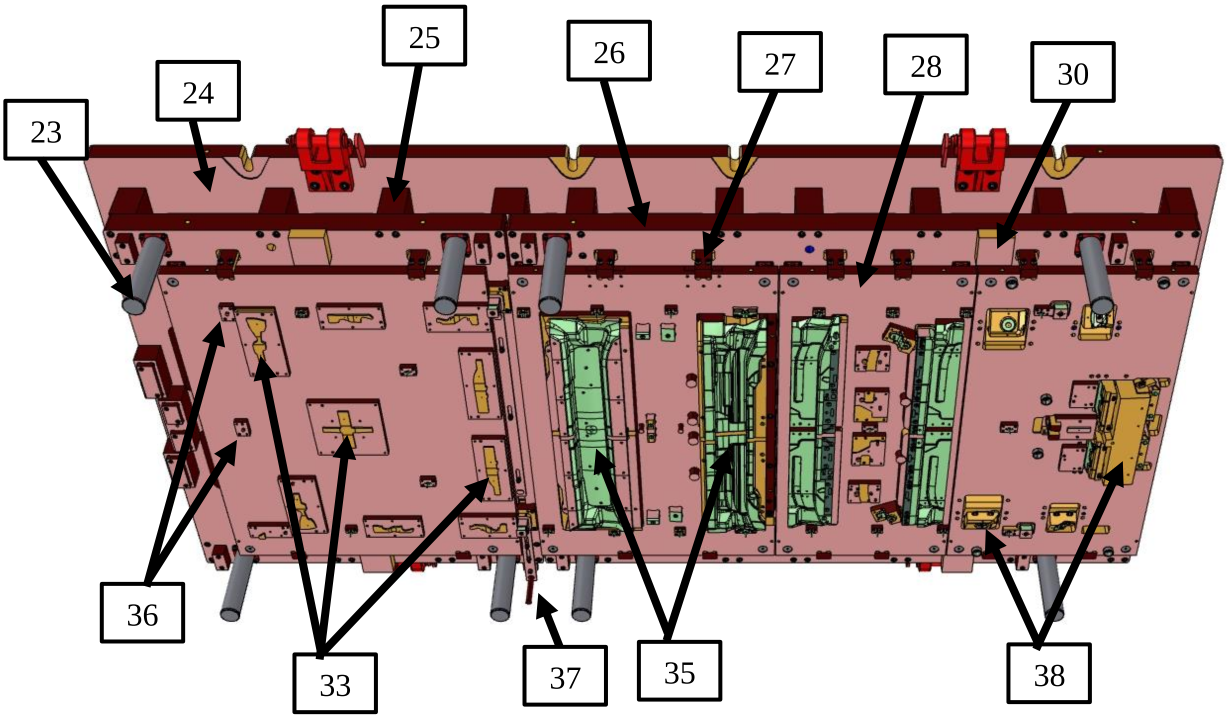

Figure 118 - Upper tool.

The general functioning of the tool is divided into four cyclic moments, common to the double acting tools, as it was previously seen.

4.2.3 Project of the control gauge

After studying the production process and the tool, it is important to be able to check if the part is within the tolerances predefined by the customer in a regular basis. For that, firstly, it is necessary to carry out a visual analysis of the part, in which the following parameters are analysed: dimensions and numbers of the holes, flatness or position of surfaces and possible hindrances to future assembly.

After a careful and detailed visual analysis, a second analysis, this time in a control gauge must be performed. This control tool is designed according to the part geometry and tolerance specifications, which are imposed by the client. Each control gauge is specifically designed for a component or pair of components according to the desired tolerances and it is not possible to use the same to analyse other parts. Similarly to the tool, the project of this control gauge is influenced by the alterations of the component's geometry during the industrialization process and it is only validated after production tests and measurements. Therefore, the tolerances, geometries and drawings refer to the final geometry.

For the construction of the control gauge, the first consideration to be made is to decide which one of the two faces of the part will be controlled, that is, which of the faces is facing up and down (the one that faces downwards is said that lays on the template of the control gauge). This decision, in most cases, is only influenced by the thickness direction of the component, i.e., the reference face on which the thickness is given is facing downwards because, if in the future there is a thickness change, this face does not suffer any changes.

In this case, analysing the component that is being studied, it has been decided to produce one control gauge to control both the left and right parts and to place them in the control gauge with the flaps facing upwards (+ side on the template, - side facing upwards). This happens because it is the + or red side that contacts and is fixed to the rest of the car structure. One day, if the thickness has to be altered, the red side remains unchanged and only the blue side moves.

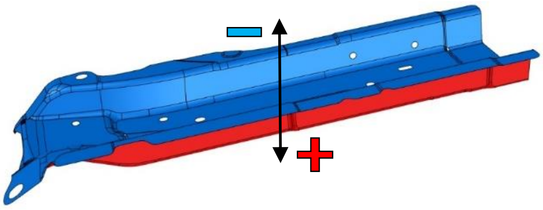

Figure 119 - Orientation of the component in the control gauge.

After correctly positioned on the template of the control gauge, and to carry out a good analysis on it, it is important to determine points on the part that serve as a guide of orientation or reference. These points make sure that the part remains fixed in the required position, restraining all degrees of freedom.

To position the parts on the control gauge two holes are used, one called primary (B in Figure 120) that fixes displacements in the plane of the template, which pilots the position, and another called secondary (C) which, after piloting the part, restrains further in-plane movement, i.e. rotation. After these two means of control have been placed, the part is placed in the correct position.

However, in spite of being in the right position, the part is not yet completely fixed. It is yet necessary to fix the part in the axis perpendicular to the template preventing small vertical movements or oscillations, namely in the areas that are relatively far from the reference points, especially in the case of large components.

Consequently, it is necessary to fix the part in a vertical plane at these points, defined by the client as the points A1, A2, A3 and A4. For this, three clamps were enough (only three points are needed to define a plane) but here four are used.

It is important to note that Figure 120, where these reference fixing and positioning points are indicated, represents an assembly of components, the one that is being studied and another that is not covered here. It is common practice that the client establishes tolerances for assemblies. Also, during this subchapter the analysis will be done for only one of the parts because they are completely symmetrical.

After fixing the part, the next step is to proceed to its evaluation. In this evaluation, the positions of surfaces, holes, trims, welded components, among others, are analyzed. These controlling points or areas are defined by the client.

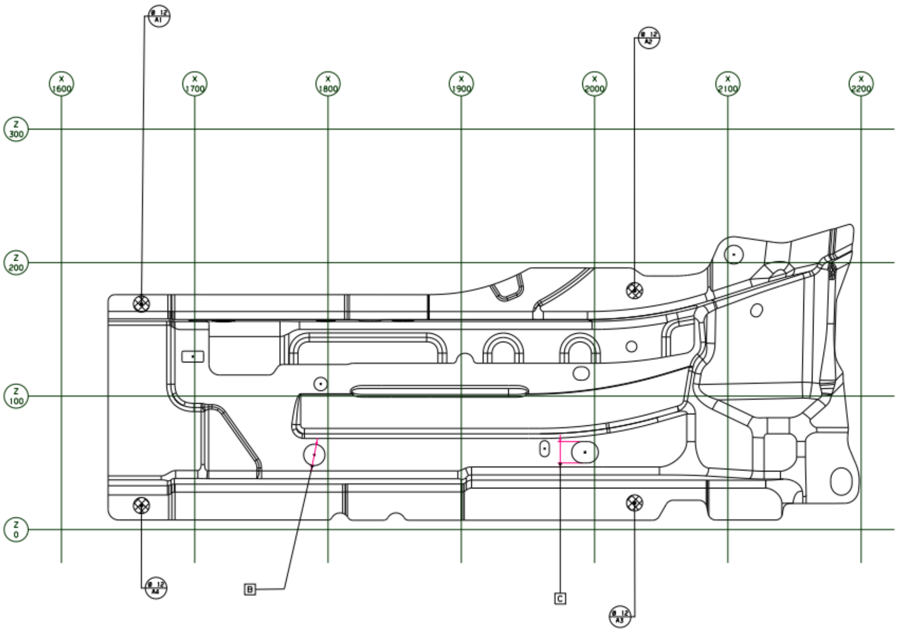

Figure 120 - Identification of the references fixing and positioning points.

Several pin gauges can be used to check if the tolerances are being met being the most common used the go/no go (G/NG) gauges. This evaluation method is very useful because it can be used by any worker as long as he has adequate training. Another advantage is the size of the control gauge, which is generally small (depending on the size and weight of the components) and allows for good mobility as well as storage. It can also be placed next to the press where the part is being produced, thus allowing immediate evaluation, avoiding taking the parts somewhere else, and also the early detection of any problem and instantaneous interruption of the production process.

The most common tolerances and those used to control this part are surface, flatness and location. Figure 121 exemplifies the meaning of a location or position tolerance.

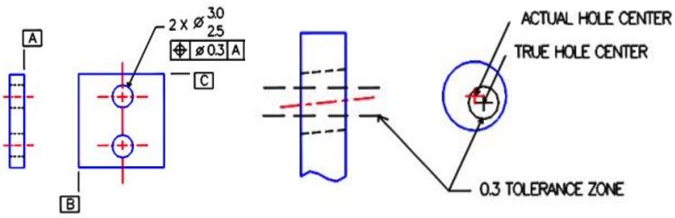

Figure 121 - Location tolerance (eMachineShop n.d.).

Figure 122 provides the same information for the surface tolerance.

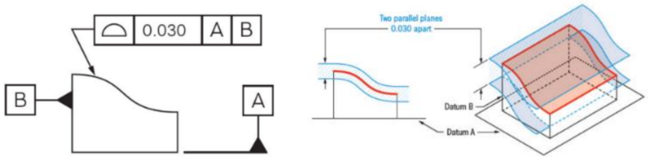
0.030
A
B
B
A
Two parallel planes
0.030 apart
Datum B
Datum A

Figure 122 - Surface tolerance (GD&TBasics n.d.).

Figure 123 illustrates an example of a flatness tolerance.

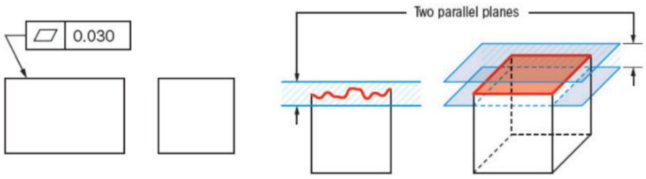
0.030
Two parallel planes

Figure 123 - Flatness tolerance (GD&TBasics n.d.).

Figure 124 shows the part with the indications of the holes that must be analyzed.

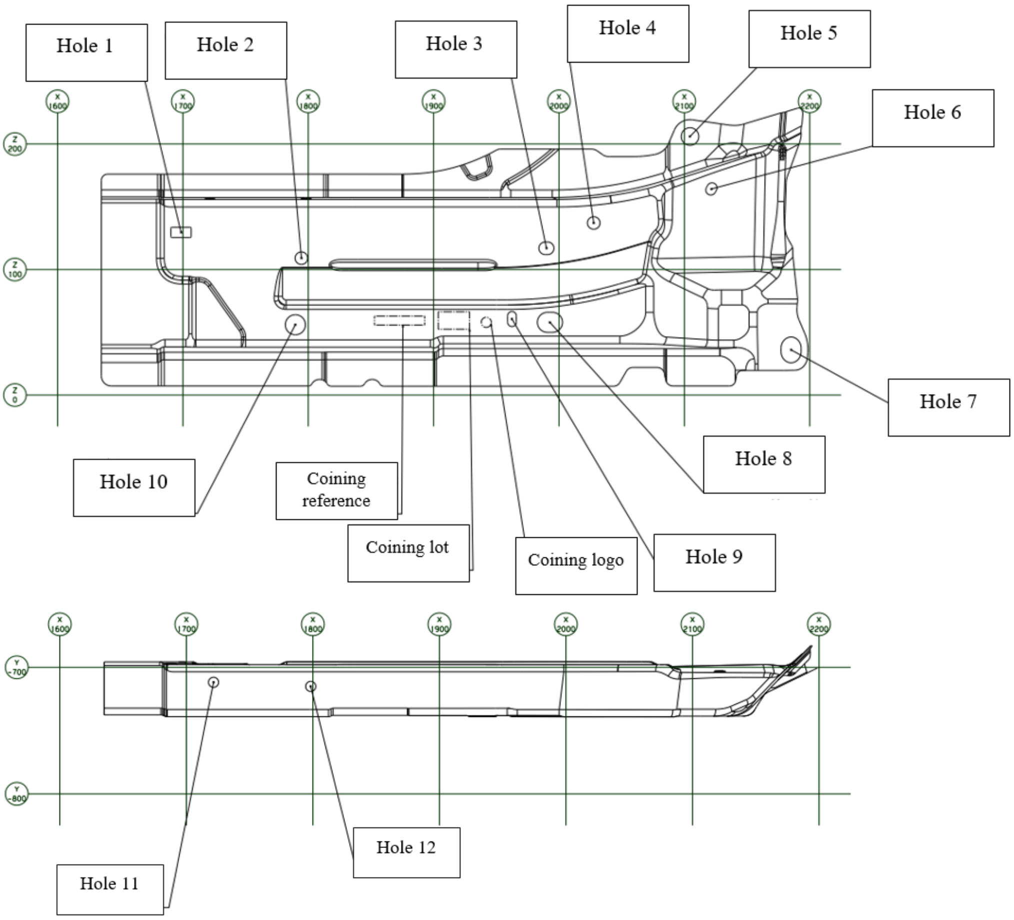
Hole 1
Hole 2
Hole 3
Hole 4
Hole 5
Hole 6
Hole 7
Hole 8
Hole 9
Hole 10
Hole 11
Hole 12
Coining reference
Coining lot
Coining logo
X 1600
X 1700
X 1800
X 1900
X 2000
X 2100
X 2200
Z 200
Z 100
Z 0
Y -700
Y -800

Figure 124 - Holes to be analysed.

The tolerances that must be controlled during the analysis of the holes and therefore have to be taken into account in the construction of the control gauge are listed in Table 10. The acronym DFN, meaning *Définition Numérique*, refers to the initial numerical definition of the part, that is, the CAD model of the part. This means that the location of a hole can vary in relation to the position that the part presents in its initial geometry depending on the limit shown in the table.

Table 10 - Tolerances to be controlled when analysing the holes.

Hole	***Tolerance***	***Nominal value [mm]***	***Lower limit [mm]***	***Upper limit [mm]***
Hole 1	Width of rectangular hole	8.2	-0.15	+0.01
	Length of rectangular hole	16.2	-0.15	+0.01
	Location	DFN	-0.5	+0.5
Hole 2	Dimension	Ø10	-0.05	+0.2
	Location	DFN	-0.5	+0.5
Hole 3	Width of oblong hole	10	-0.05	+0.2
	Length of oblong hole	12	-0.15	+0.4
	Location	DFN	-0.5	+0.5
Hole 4	Dimension	Ø10	-0.05	+0.2
	Location	DFN	-0.5	+0.5
Hole 5	Dimension	Ø14	-0.05	+0.2
	Location	DFN	-0.5	+0.5
Hole 6	Width of oblong hole	8	-0.05	+0.2
	Length of oblong hole	10	-0.15	+0.4
	Location	DFN	-0.5	+0.5
Hole 7	Width of oblong hole	17.8	-0.05	+0.2
	Length of oblong hole	20.5	-0.15	+0.4
	Location	DFN	-0.5	+0.5
Hole 8	Width of the secondary hole	16	-0.05	+0.2
	Length of the secondary hole	20	-0.15	+0.4
	Location (length)	DFN	-0.5	+0.5
Hole 9	Width of oblong hole	7	-0.05	+0.2
	Length of oblong hole	12	-0.15	+0.4
	Location	DFN	-0.5	+0.5
Hole 10	Dimension of the primary hole	Ø16	-0.05	+0.2
Hole 11	Dimension	Ø8	-0.05	+0.2
	Location	DFN	-0.5	+0.5
Hole 12	Dimension	Ø8	-0.05	+0.2
	Location	DFN	-0.5	+0.5

After analyzing the holes, a volume analysis is then carried out, taking into account certain regions of the part where a special care is needed in this regard. As each zone of the part can have a different volume, or the respective ranges of tolerance can also be different from each other, each zone is analyzed independently of the others, as it can be seen in Figure 125. A closer look allows to see that the position tolerances were defined in the beginning of the industrialization process over a geometry that is not the final geometry: area 2 is missing the notch that was done to reduce the wrinkled area. However, these tolerances remained for the current geometry.

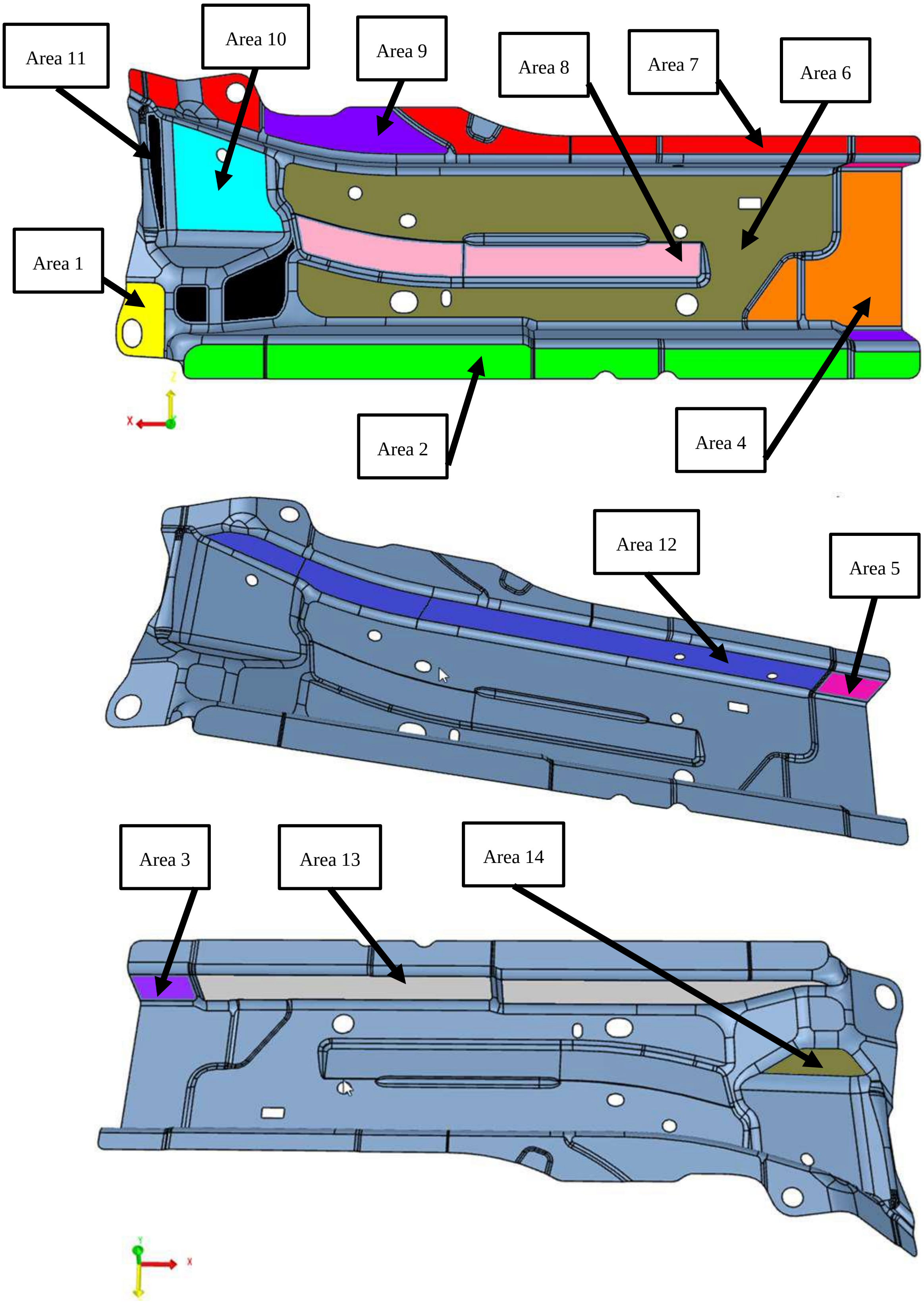
Area 11
Area 10
Area 9
Area 8
Area 7
Area 6
Area 1
Area 2
Area 4
Area 12
Area 5
Area 3
Area 13
Area 14

Figure 125 - Areas to be analysed.

Table 11 - Tolerances to be controlled when analysing the areas.

Location	***Tolerance***	***Lower limit [mm]***	***Upper limit [mm]***
Area 1	Surface	-0.5	+0.5
Area 2	Surface	-0.5	+0.5
Area 3	Surface	-0.5	+0.5
Area 4	Surface	-1	+1
	Flatness	0	0.7
Area 5	Surface	-0.5	+0.5
Area 6	Surface	-1	+1
	Flatness	0	0.7
Area 7	Surface	-0.5	+0.5
Area 8	Surface	-0.5	+0.5
Area 9	Surface	0	+1.4
Area 10	Surface	-0.5	+0.5
Area 11	Surface	-0.5	+0.5
Area 12	Surface	-0.7	+0.7
Area 13	Surface	-0.5	+0.5
Area 14	Surface	-0.5	+0.5
Contour	Trim	-1	+1
Areas 12 & 13	Distance between areas	-1	+1

All the areas or lines that are not controlled by the previously listed tolerances have to comply with the general tolerances imposed by the client according to Figure B1 in Annex B. When 3D measuring the parts some extra points besides those ruled by the specific tolerances are also measured in order to check if they are complying with the general tolerances.

The analysis of the part begins even before it is placed on the control gauge. There are three types of control of a part in this stage. The first one is visual and in which, firstly, the absence of burr, deformations, lack of material or the presence of cracks is checked. Next, the presence of the engraved batch number, reference and logo is checked, and finally check the presence of all twelve holes.

The next control method is still done with the component out of the control gauge, and it aims to check the size of the holes using the hexagonal G/NG.

Finally the quality control is done with the part positioned on the control gauge. Thus, the first step involves correctly positioning the part on the control gauge with the clamps opened. Afterwards, the primary gauge is placed followed by the secondary one. With these gauges it is ensured that the part is in the right position to start the analysis. Then, the clamps are closed, and the positioning gauges, primary and secondary, are removed. From this stage on, a series of checks begins with the gauges corresponding to the different characteristics already mentioned above.

An analysis that in recent years has been widely used in control gauge control involves removing one of the fastening clamps (identified by the detent support in orange in Figure 127). After the initial analysis with all the clamps in position, one of them is released and it is done a new measurement of volumes of some predefined zones considering a wider tolerance. This method is adopted when using metals with high springback, as their behavior vary depending on whether they were fixed at three or four points.

Further, from time to time, with a defined periodicity, a part is measured in the 3D machine to compare the position with the original CAD model with great precision. In Table 11 it is possible to find a tolerance for the trim line which refers to the outline of the part. However, the gauge to control this feature is not part of the control gauge. It is generally accepted that this parameter is only controlled by the 3D measurement.

In Figure 126 below the control gauge is represented with a pair of parts on it with right hand one correctly positioned and with the position of the holes being controlled.

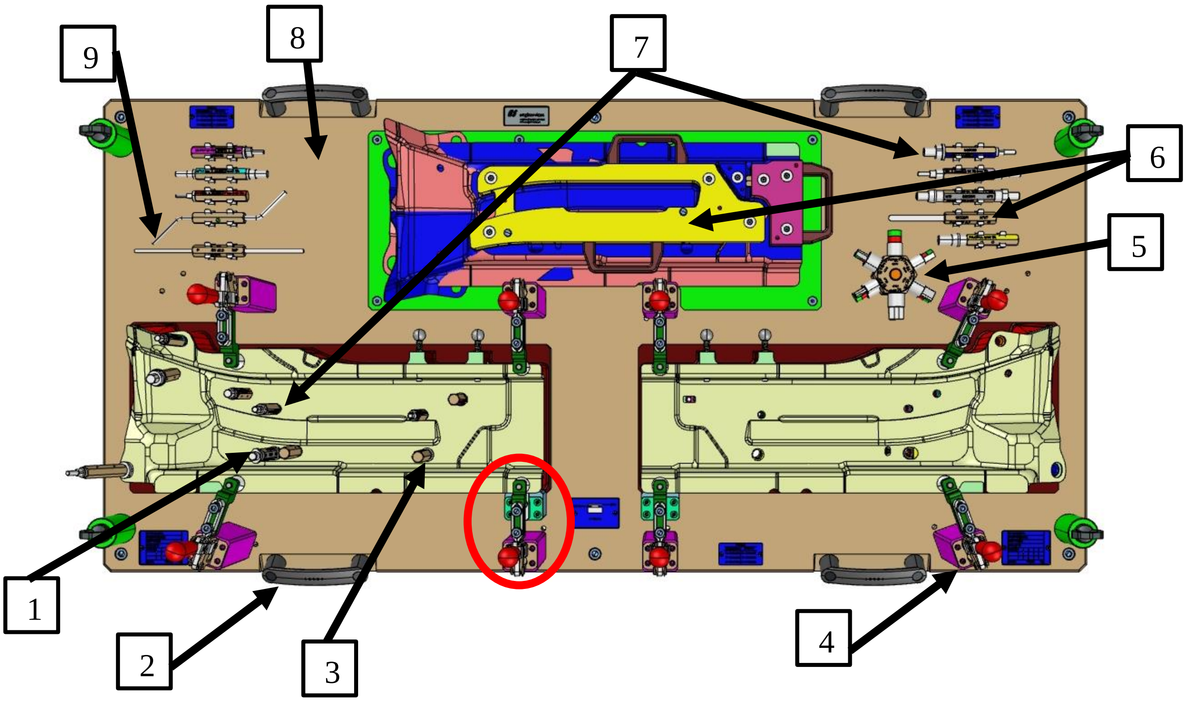

Figure 126 - Control gauge for a first quality control of the components.

Table 12 - Components of the control gauge.

Number	***Description***	***Number***	***Description***
1	Secondary pin gauge	***6***	Gauges for flatness control
2	Lifting flange	***7***	G/NG gauges for position control of the holes
3	Primary pin gauge	***8***	Base plate
4	Fixation clamp	***9***	G/NG gauges for volume control
5	G/NG gauge for dimensional control of the holes	***10***	Template

The zone highlighted in Figure 126 is detailed in Figure 127 where it can be seen the mechanism that allows the removal of the fourth clamp in a second volume control with a greater tolerance.

Through an intuitive color code, the workers can easily see where they should use each gauge. The gauges to control the dimension of the holes and the surface tolerances are of the type go/no go which means that if it fits the tolerance is achieved and if it does not the part is out of tolerance. The gauges to control the position of the holes are different, if they cannot fit the hole, the position tolerance is not fulfilled. Finally, to check the flatness of a surface two components are needed, a major block of steel with the shape of the area to be controlled that is magnetic to couple with the desired area and a gauge that must not pass in the gap between the block and the part to make sure the tolerance is met.

Closer looks at some of the pin gauges are given in Figure 128. Besides these, it can also be seen in Figure 127 a highlighted zone where the position control of the side holes, made with cams in the last step, is done using fixed elements in the control gauge that just need to be pushed.

All the elements in the control gauge that do not contact with the part, for example the base plate, are made of aluminum which is why it is relatively light, in this case 140 kg. However, to avoid wear, the parts that contact with the part are made of steel.

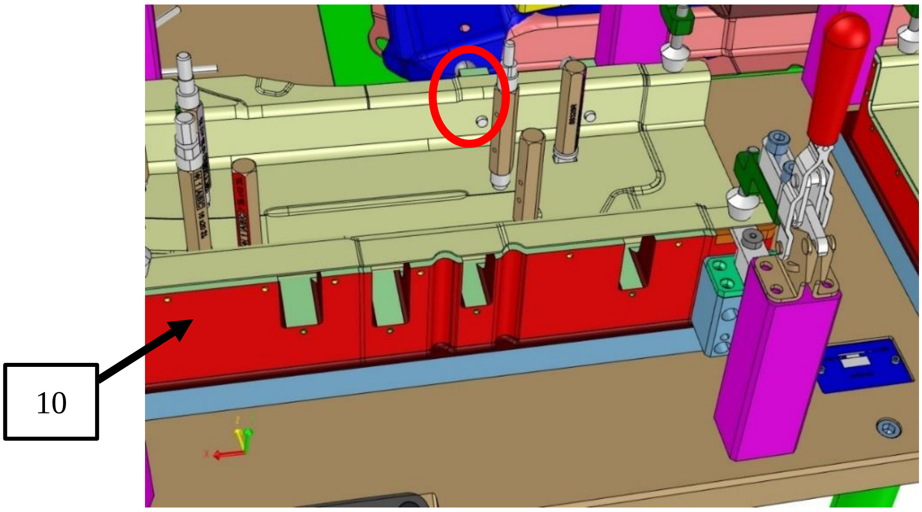

Figure 127 - Closer look at some control gauge details.

It is clear that some zones cannot be controlled using this control gauge because of complex geometric features, being the volume tolerance of area 11 is one example. However, this first quality control is essential to avoid the production of large quantities of defected parts.

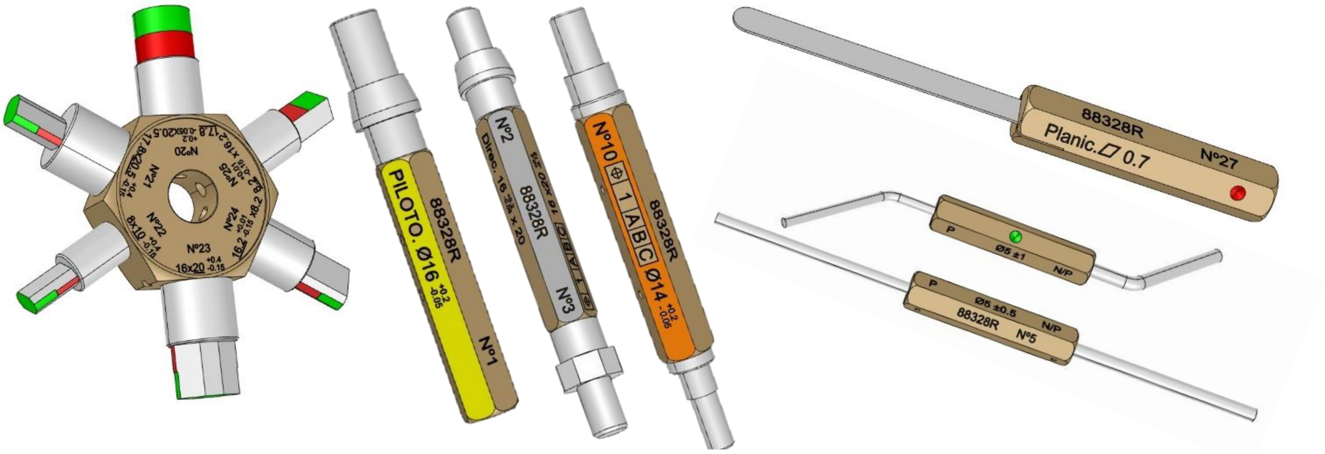

Figure 128 - Pin gauges used to control dimension and position.

4.3 Problem in production

After being in production for about six months the client presented a complaint due to the presence of cracks at the edge of the right-hand part exactly where the simulation predicted (Figure 129). This complaint was received by Gestamp in October 2022. After checking all the stock available at the company and also at the client's warehouse, it was estimated that the cracked parts consisted of 2% of the total.

From October 2022 forward the productions were all monitored in order to understand what was going on, moreover all the parts produced were and kept being checked twice before being sent to the client: once immediately when they come out of the press and once again in the so-called classification zone.

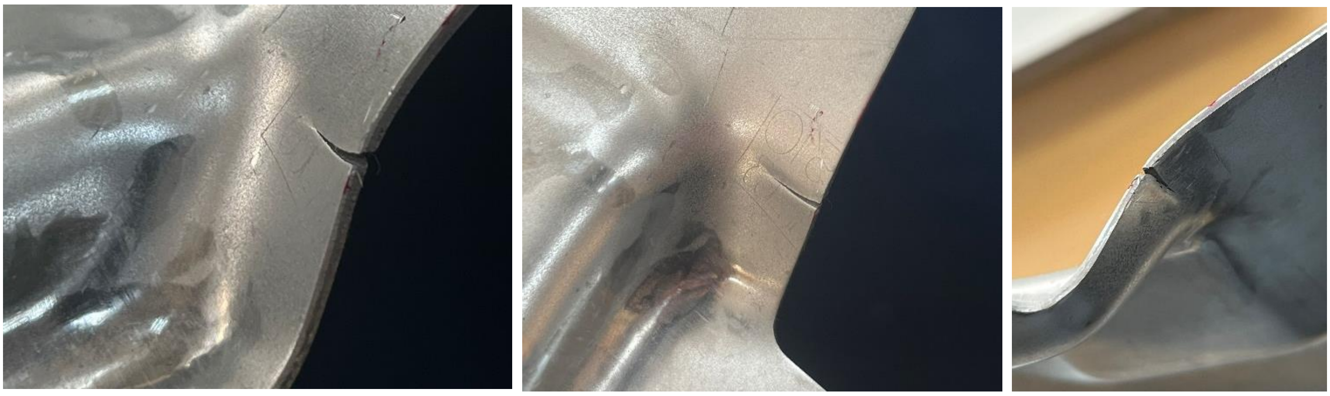

Figure 129 – Close look at the cracks that appear in the component under study.

The particular aspect in the appearance of these cracks, revealed during this phase, is the pattern and frequency when it occurs. Despite being parts completely symmetrical, made using punches and dies also completely symmetrical, made at the same time with the same sheet coil, the number of cracks found in the right-hand part is significantly larger than the cracks found in the left-hand part. There is not also a time coherent pattern in the appearance of cracks which means that the frequency is not greater in the beginning, middle or close to the end of production, it is arbitrary. This indicates on the one hand that it is not a problem of wear or heat and on the other hand that it is probably related to point changes in the sheet related to the sheet production process.

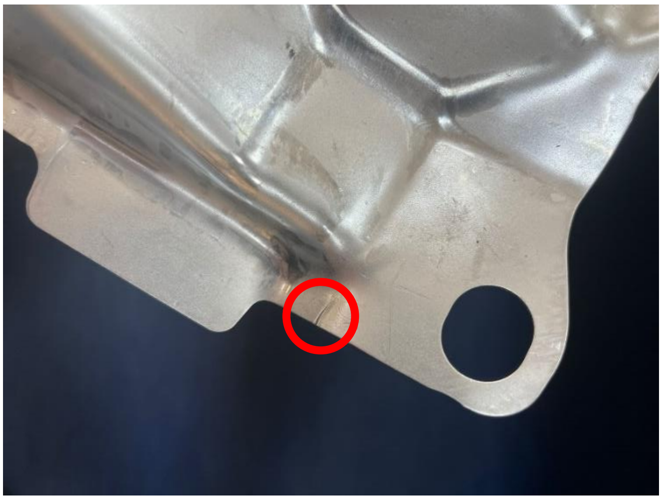

Figure 130 - Location of the crack in the component.

Nevertheless, the most robust way to deal with the situation is generally to intervene in the tool and make it proof against fluctuations in sheet properties. This happens because even if the frequency of appearance of cracks is related to fluctuations of properties, these properties can even so be within the admissible range. This is corroborated by the AutoForm simulations that, in fact, revealed the existence of cracks. It is important to note that when it is said “intervene in the tool”, only small alterations are done so that the tolerances are still met.

Trying to quickly solve the problem, the first action that was taken was softening the stamping radii, keeping everything between tolerances, a common procedure performed in situations like this and that aims to reduce local thinning. This alteration was performed in the second stamping operation. A schematic illustration of this process is shown in Figure 131, where the red represents the previous geometry and the green the new one. This first monitored production was in the 21st October 2022 and in 3800 strokes (3800 pairs of parts) appeared 24 cracks all in the right-hand, which correspond to 0.6% of scrapped parts. Although it seems a small percentage, the costs that this represents to the company are very high. First of all because there has to be an extra worker involved in the production process in the classification zone and secondly because of the scrapped parts themselves that represent money being thrown away.

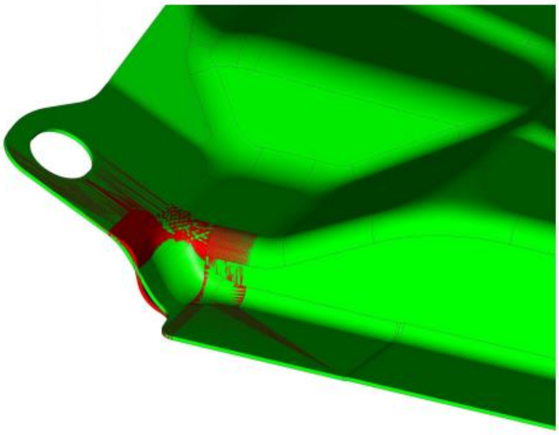

Figure 131 - Smoothened radii implemented as an attempt to reduce the cracks.

Since there was just a slight change, it was decided for a second production to smoothen the radii even more. However, in just 240 strokes, 14 cracks appeared one of them in the left-hand. It was decided to stop the production after that because it was clear that either the properties of this coil were very unfavorable, or the alteration only made it worse. At this point, it was clear that the problem was not only on the right-hand side.

Verifying that smoothing the radii did not work, it was decided that something extra needed to be done but not yet jump into a complaint to the sheet supplier for lack of evidence of its responsibility. It was decided to intervene again in the tool, namely in the first stamping stage close to the critical area of the part. It was tried to approximate the geometry to the final one so that the second stamping operation was not so violent. That is in accordance with the simulation since the results from the first stamping operation still gives some leeway. This included an operation in all that zone modifying the radii and the flap close to the crack zone. Initially that flap was progressively bent in the two stamping steps. The intervention was made so that in the first stamping operation the flap was already very close to its final position (see Figure 132). This means that before this alteration, all of the lateral flap (colored red) was on the same plane. With this alteration, after the first stamping operation, the smaller flap close to the critical zone is already very close to its final position.

Nevertheless, this intervention was apparently a failure. The productions that followed consisted of iteratively perfecting this alteration. These corrections were done by adding and removing material according to experience from other similar problems. The fact is that after these alterations, from the production of the 21st November onwards, the results returned to the beginning, meaning that in these three productions the number of cracks found was similar to the beginning and therefore the problem remained.

After all these iterations, the tools mainly from the first stamping operation (due to the alterations to the flap) were very crafted and geometrically different from the original project o the tool.

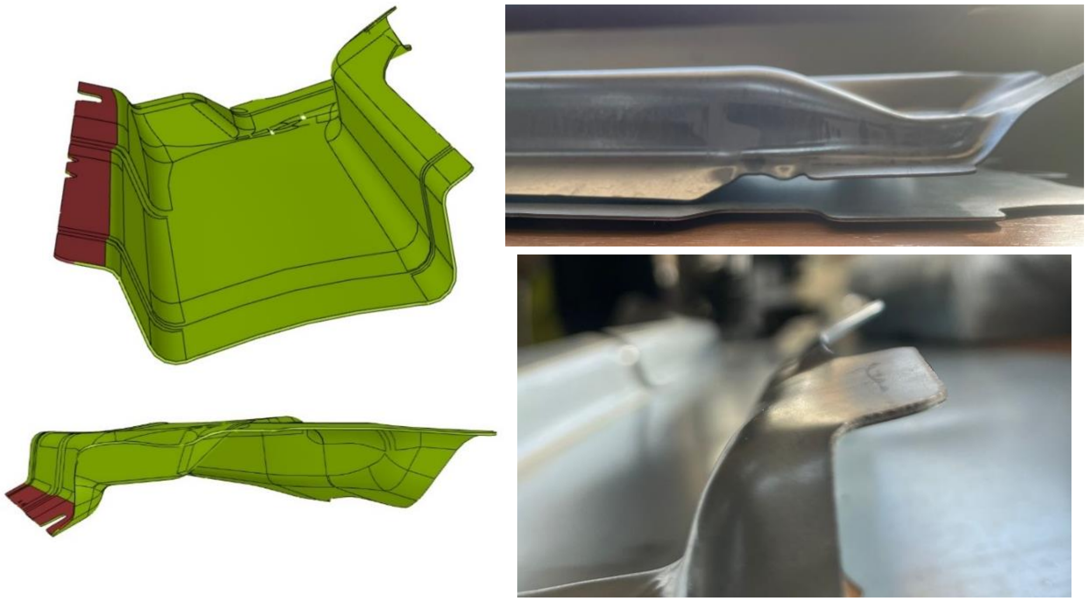

Figure 132 - Attempt to eliminate the cracks by approximating geometry resultant from the first stamping to the final geometry.

Table 13 summarizes the actions taken in each production and the number of cracks found in each hand in each production.

Assuming that every single punch and die are symmetric (except for the ones involved in positioning and guiding) and that all the performed alterations are in theory beneficial, it seems likely that there are in fact differences between coils. An asymmetry in properties between sides of the same coil is also questionable since there are significantly more right-hand cracked parts. Besides that, the last two productions, where no alterations were done to the tool, also suggest a difference in sheet properties between coils.

Table 13 - Attempts to reduce the cracks until the beginning of this study.

Date	***21/10/2022***	***28/10/2022***	***08/11/2022***	***14/11/2022***	***21/11/2022***	***09/01/2023***	***01/02/2023***
Strokes	***3800***	***240***	***420***	***4989***	***3251***	***6198***	***5825***
Action	***Geometry (radii)***	***Geometry (radii)***	***Geometry (flap)***	***Geometry (flap correction)***	***Geometry (flap correction)***	***No action***	***No action***
RH	24	13	135	168	28	7	48
LH	0	1	0	0	0	2	0
Percentage of cracks	0.63%	5.83%	32.14%	3.37%	0.86%	0.15%	0.82%

Summing up, in the beginning of this work, the situation remained as it had first started. However, now the tools in the first stamping step are different and the radii in the critical zone are also a little different in the second stamping step. These alterations were only done on the right part of the tool, the left one is exactly how it is in the project.

5 Experimental and numerical characterization of the material

To improve the accuracy of the simulation and to rule out a possible asymmetry of properties between sides and between coils the material was studied in more depth.

Firstly, there was made a comparison between material models keeping the hardening curve and forming limit curve but altering the yield criterion. This comparison was done in order to check for significant differences regarding formability results.

Then, uniaxial tensile tests were performed in four sheet pieces from both sides of two different coils. This material characterization can contribute to the rectification of parameters of the material model including the hardening law and yield criterion. However, it is not possible with the equipment available to determine the r-values, input parameters usually necessary.

5.1 Comparison between material models in AutoForm results

In the previous chapter it was used the material model indicated by the tool maker to run the simulations. It consisted of a hardening law and a FLC in the form of tables, which correspond to experimental data, and a BBC 2005 model for the yield surface.

Maintaining the tables that define the hardening law and the FLC, it was analysed the influence of the model used for the yield surface in the advanced formability results. This will be used to determine which material model will be used in the upcoming simulations that will help deciding on the implementation of solutions to fix the problem.

5.1.1 Barlat 89

As previously stated, when presenting the models, Barlat 89 model only needs four input variables: the anisotropy coefficients in three directions (0º, 45º and 90º) and the M value.

Therefore, the values of these variables were the same as those used in the BBC 2005 model, presented in Table 14.

Table 14 - Parameters for the Barlat 89 model to characterize the yield surface of DP980.

	r_0	r_{45}	r_{90}	M
DP980	0.76	0.96	0.76	6

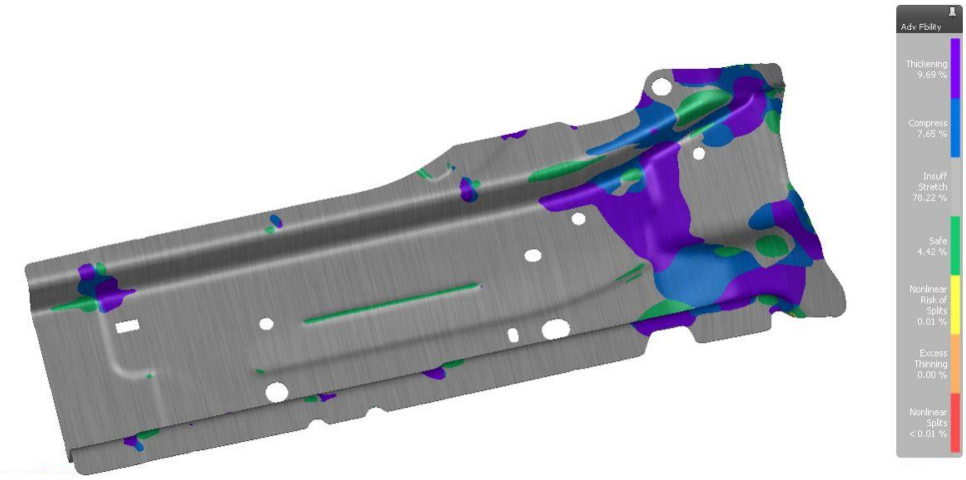

Figure 133 - Advanced formability final results using the Barlat 89 material model.

The points of the resultant geometry over the FLC are presented in Figure 134, and they represent only the most critical points (that are close to the yellow/red border). The remaining results regarding advanced formability (presented in Figure 133), edge crack, thickness, and springback (in Annex C) are very similar.

Figure 134 compares the critical points using the BBC 2005 model (left) that was used before and the Barlat 89 model (right). As it was seen before, the position of the points is not relevant compared to its colour in the Advanced Formability results. Therefore, in spite of the points being closer to the red zone using the Barlat 89 model, the colour of the points is the same in both models. There are 0.01% of yellow points and <0.01% of red points, exactly the same percentages as before.

It is also important to note that the total CPU time decreased in about 4%, from 11.8 to 11.3 minutes.

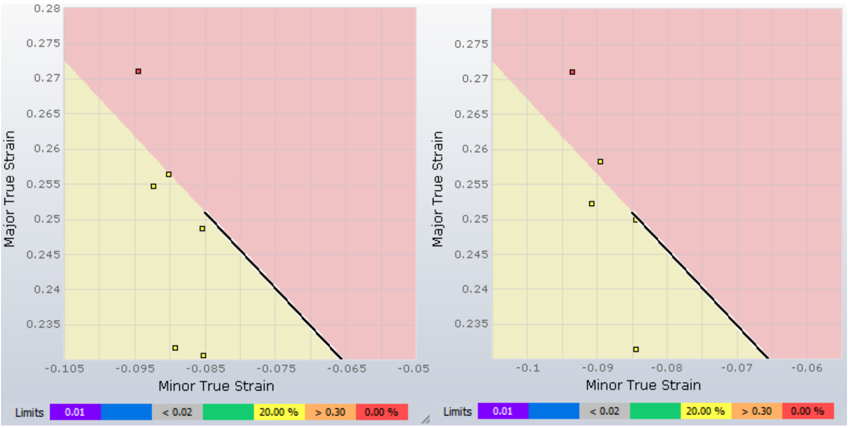

Figure 134 - Dispersion of the critical points over the FLC considering the BBC 2005 (left) and the Barlat 89 (right) criteria.

5.1.2 Hill 48

The Hill 48 model is the simpler one. It only requires three input variables, the anisotropy coefficients, which were considered the same as before, according to Table 15.

Table 15 - Parameters for the Hill 48 model to characterize the yield surface of DP980.

	r_0	r_{45}	r_{90}
DP980	0.76	0.96	0.76

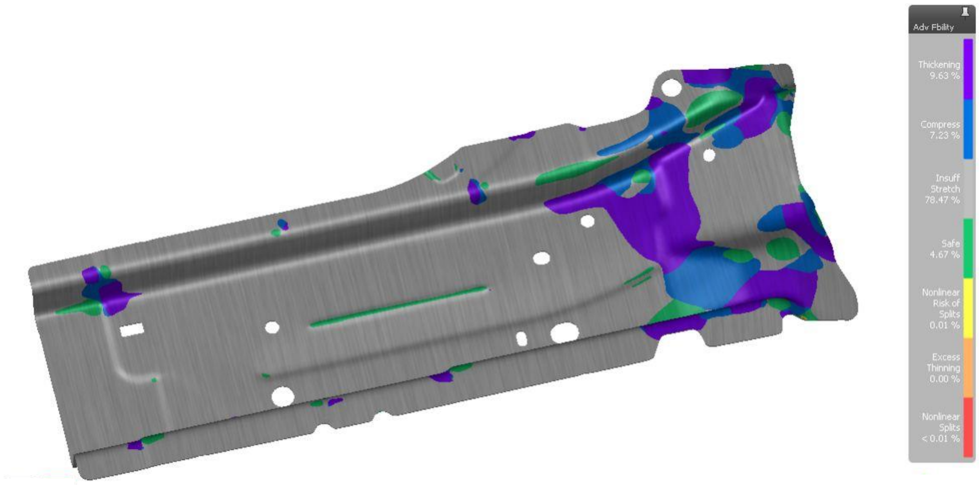

Figure 135 - Advanced formability final results using the Hill 48 material model.

The Advanced Formability results are presented in Figure 135 and the most critical points of the resultant geometry over the FLC in Figure 136. The remaining results are also very close to those obtained using BBC 2005 and presented in Annex C.

Figure 136 compares the critical points using the BBC 2005 model (left) that was used before and the Hill 48 model (right). Regarding these points, there are barely any differences between models.

Like in both previous simulations, there are 0.01% of yellow points and <0.01% of red points.

The total CPU time decreased in about 9%, from 11.8 to 10.7 minutes.

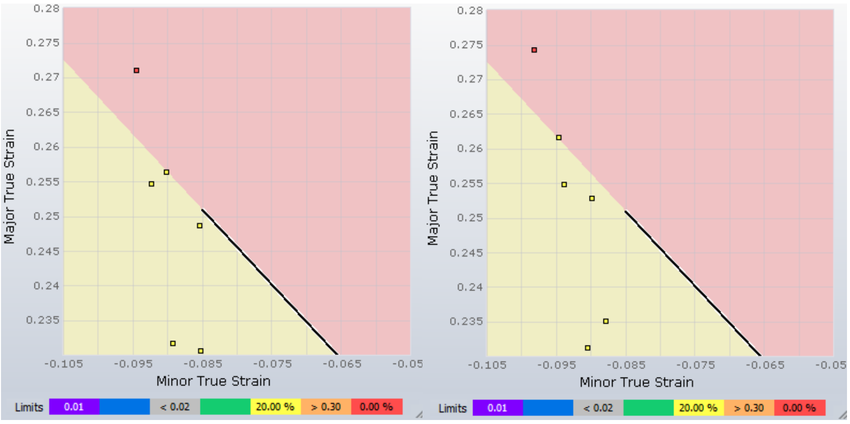

Figure 136 - Dispersion of the critical points over the FLC considering the BBC 2005 (left) and the Hill 48 (right) criteria.

5.1.3 Conclusions of the numerical characterization

The differences in the results of formability and other variables are not so abrupt as it could be expected when looking at the difference in complexity of the inputs of the models. The BBC 2005 model is considered in the literature the most accurate model, mainly regarding springback.

Regarding Advanced Formability and the risk of splits, the models present exactly the same results. This result is the most important to assess the risk of splits.

Some advantages could rise using of the Barlat 89 model namely the reduction in total CPU time (from 11.8 to 11.3 minutes) and the reduction in memory consumption (from 321.9 MB to 312.2 MB) or the Hill 48 criterion because of the same reasons. However, since no significant differences regarding formability were observed, and following the literature review, the yield criteria will remain the BBC 2005, the most complex and with more inputs.

5.2 Experimental characterization of the material

A common experimental test used to ascertain the basic mechanical characteristics of materials is the uniaxial tensile test. The material's modulus of elasticity, coefficient of Poisson, yield strength, ultimate tensile strength, elongation after rupture, and anisotropy coefficients (important in the case of metal sheets due to the manufacturing process) are the most pertinent among these characteristics. The r-values were not calculated in this study.

The typical procedure for uniaxial tensile tests is to apply a constant strain rate monotonically until the material fractures. To capture and define a particular behavior of the material, the test can be run at various strain rates and stress levels using techniques like numerous loading cycles and rest intervals.

The experimental test is conducted at a steady pace, which causes the material to get harder with increasing elongation and increases the applied force to the specimen. The extensometer, which must be positioned in the region of the specimen's useable length, must record the evolution of the material's elongation.

In order to characterize the material and trying to identify possible differences between coils and between sides of the same coil, 24 tensile tests were carried out according to ISO 6892-1 (IPQ 2012). Three distinct loading conditions were tested (different directions in relation to the rolling direction), on specimens from 2 different coils and from both left and right sides of the coils. To ensure repeatability, 2 specimens of each direction of each coil and of each side were tested. There were therefore four pieces of sheet (two sides from two coils) and from each of the pieces were machined six specimens resulting in four groups as the one represented in Figure 137. All the specimens were machined according to the indicated standard with the dimensions indicated in Figure 137. Table 16 contains information about the test's experimental setup.

Table 16 - Test parameters.

Loading directions	3
Nr of experiments for each direction	2
Nr of coils	2
Nr of sides	2
Crosshead speed (grip)	5 mm/min
Data acquisition	20 Hz
Clip gage initial length - l_0	50 mm
Temperature	22º
Relative humidity	70%

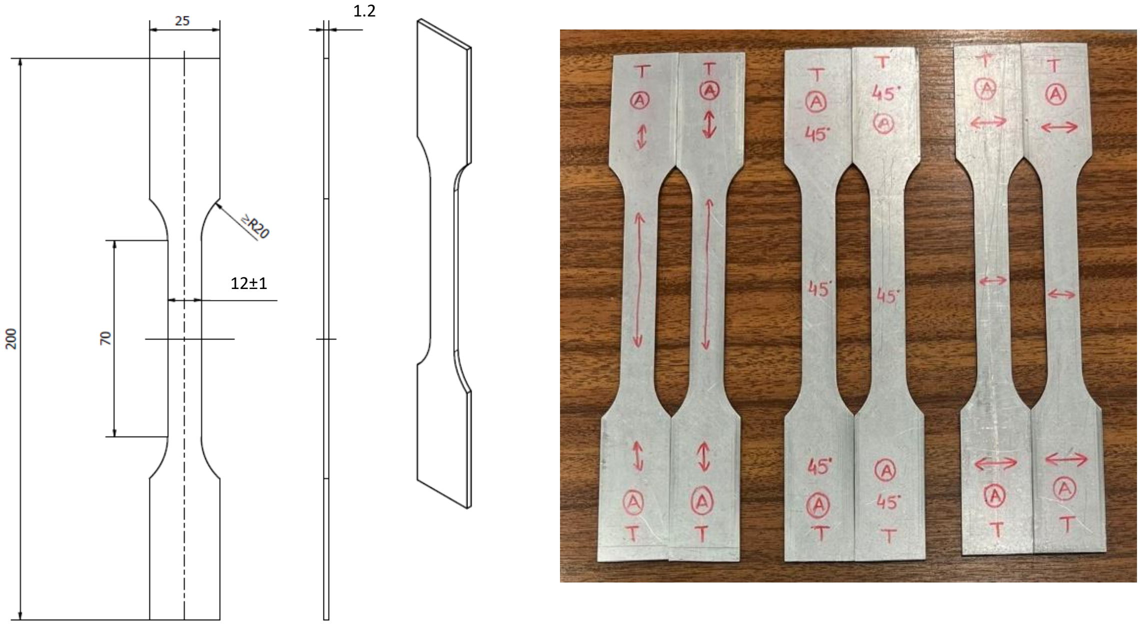

Figure 137 - Dimensions of the specimens (left) and group of specimens before testing (right).

The specimens were tested at room temperature quasi-statically with a constant crosshead speed, until the material rupture on a 100 kN servo-hydraulic testing machine (MTS 810). For the acquisition of elongation in the uniform section of the specimen, and therefore measurement of corresponding strains, an extensometer with an initial length of 50 mm was used. The equipment is represented in Figure 138.

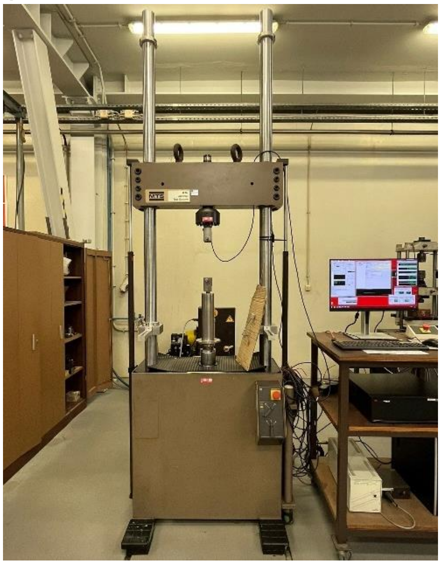

Figure 138 - Uniaxial tensile test machine used.

Only one result out of the two specimens tested is shown in the next figures to make the analysis of the stress-strain flow curves resulting from the uniaxial tensile tests performed clear and simple. Annex D contains all the data, including results from the 24 tests that were conducted and the repeatability observed. It is also relevant to point out that due to a machining mistake it could not be guaranteed that all specimens had the same cross section area. Therefore, the Force-Strain curves were transformed into Stress-Strain curves using the area of each cross section measured using a caliper.

Although the results obtained from the two specimens of each sheet are close, several other specimens from the same sheets should be tested to properly statistically treat the data. It is not possible to determine which one of the two results is closer to the real properties of the sheet. Therefore, it was arbitrarily chosen one of the two as a representative to present the graphic results. Afterwards, the average properties of both specimens are represented in Table 17.

5.2.1 Comparison between sides of the same coil

Attempting to compare the left and right sides of the coils, the results for both sides were plotted in the same graph for each direction. This was done for both coils, one that produced worse production results (0.82% of cracked parts, responsible for the production of 1st February), and one that produced better production results (0.04% of cracked parts, responsible for the production of 15th February, after the implementation of solution 1, that will be presented in the next chapter). It was an attempt to check if the coils are asymmetric in terms of their mechanical properties and consequent plastic behaviour. If that could be proven, it was a reasonable explanation to the different frequency of cracks in symmetrical parts.

Figure 139 contains the graphs that compare for the rolling direction, diagonal, and transverse, the left and right sides of both coils tested. On the left are the results from the coil that produced more cracked parts (0.82%) and on the right are the results from the coil that produced only 0.04% of cracked parts.

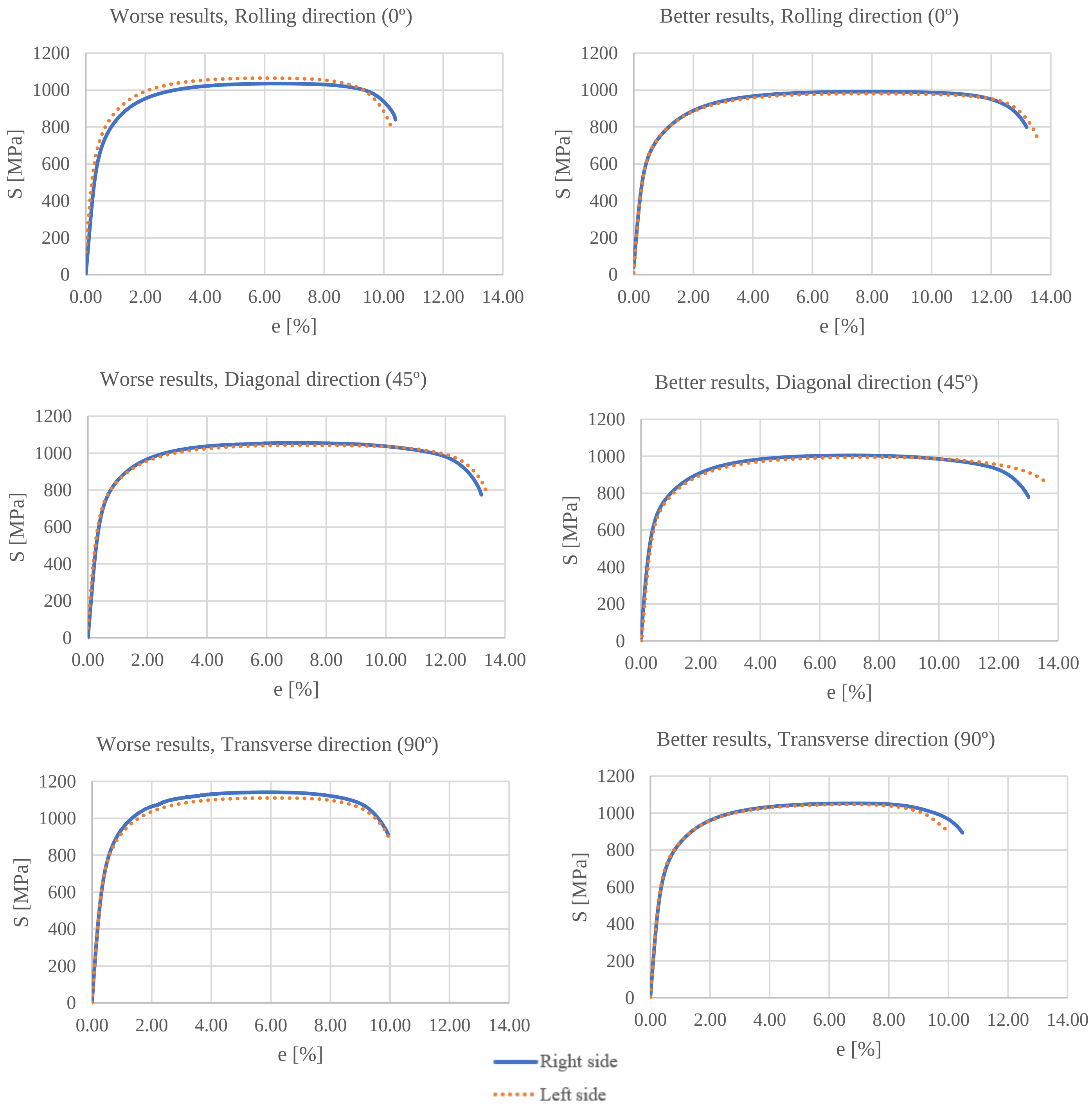

Figure 139 - Experimental results that compare the left and right sides of the two coils.

For both coils there seems to be no difference between sides. The curves resultant from the uniaxial tensile tests in the same direction on both sides essentially coincide. Therefore, there are not significant differences from the left to the right side of the same coil in any of the tested directions.

It is possible to verify that the obtained engineering stress-strain curves become almost flat for maximum force, thus meaning a reduced strain hardening, after an initial stage of high hardening behavior, at initial yielding.

Moreover, it is already possible to see a tendency for the sheet to present lower total elongation but higher strength in transverse direction. In opposition, for the diagonal direction the elongation is higher.

5.2.2 Comparison between coils

The next analysis consists of comparing the same sides of different coils for each direction. This will allow to quantify the variation of the properties from one coil to another and check how these properties can be influencing the appearance of cracks. Moreover, all the data will also be used to analyse how close are the measured mechanical properties to the upper and lower admissible limits. This analysis can only be performed for the rolling direction since those are the only listed by the client.

On the left side of Figure 140 are the graphs that compare the left side of both coils and on the right side are the graphs that compare the right side of both coils.

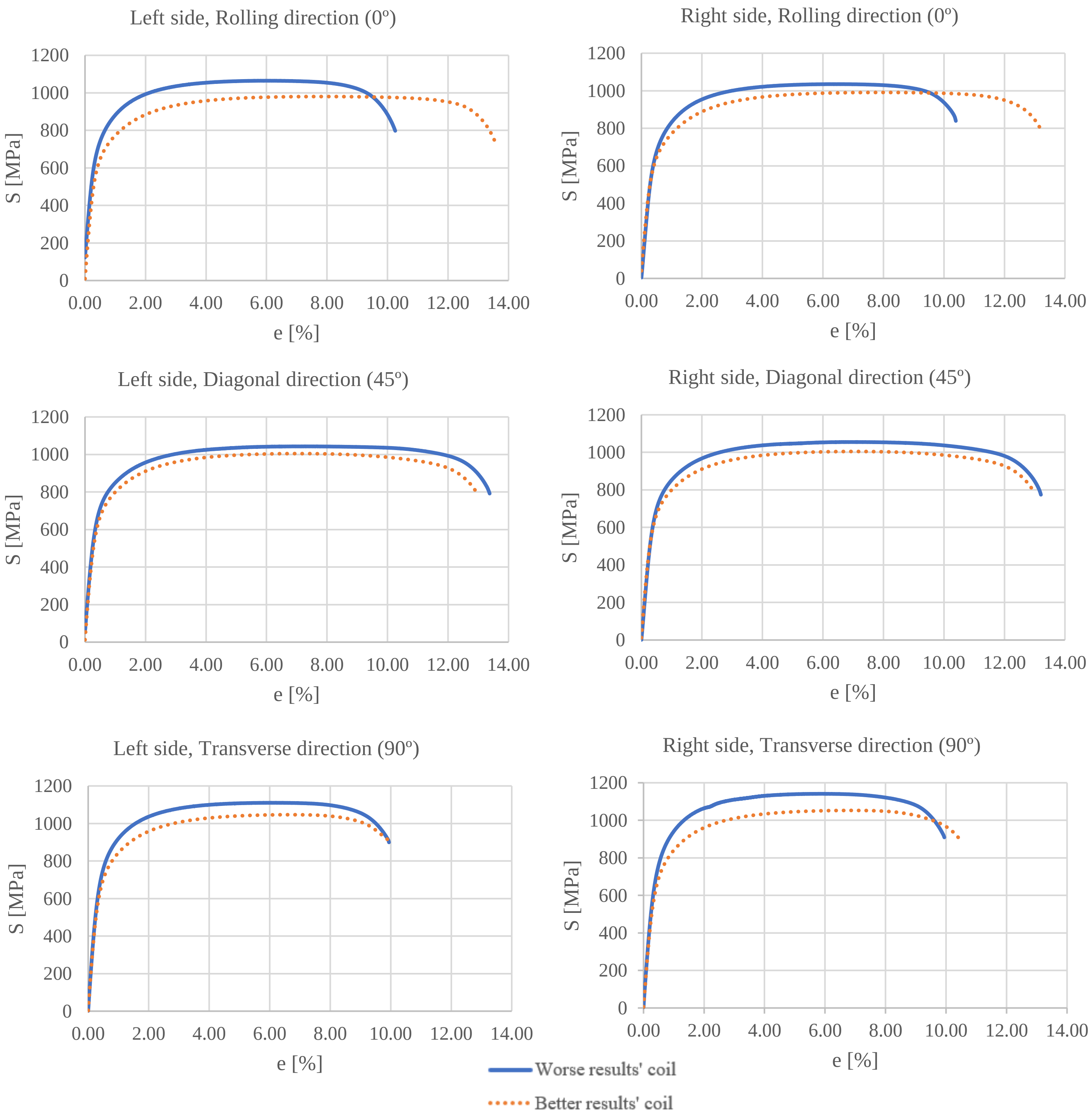

Figure 140 - Experimental results that compare both coils from specimens of the same side.

The difference between coils is clearly visible, particularly in the rolling direction. The coil that produced a lower percentage of cracks (better results' coil) presents significantly higher total elongation and slightly lower resistance. Regarding the diagonal and transverse direction, the tendency of better production results (less cracks) being associated with lower strength is verified.

The experimental results for the right side follow the same tendencies observed in the left side. In the rolling direction it is notorious that the total elongation is much higher for the coil that presented better production results. Also, the resistance of this coil, namely yield and ultimate tensile strengths, is lower than the coil that produced worse production results. For the other directions, these differences are not so abrupt but the tendency for the coil that had better production results to have lower resistance is kept.

5.2.3 True stress-strain curves and hardening law

To properly define the material, AutoForm requires, as it was already seen, a hardening curve that describes the hardening behavior of the material in the rolling direction. This curve should, according to the AutoForm manual, be represented as a true stress-strain curve preferably until a value of $\varepsilon_p = 1$. This is recommended since during the forming process biaxial strain conditions may occur that are significantly higher than those measured in the uniaxial tensile test.

The true stress-strain curves obtained in the tests as well as the curve used in the project simulation are plotted in Figure 141.

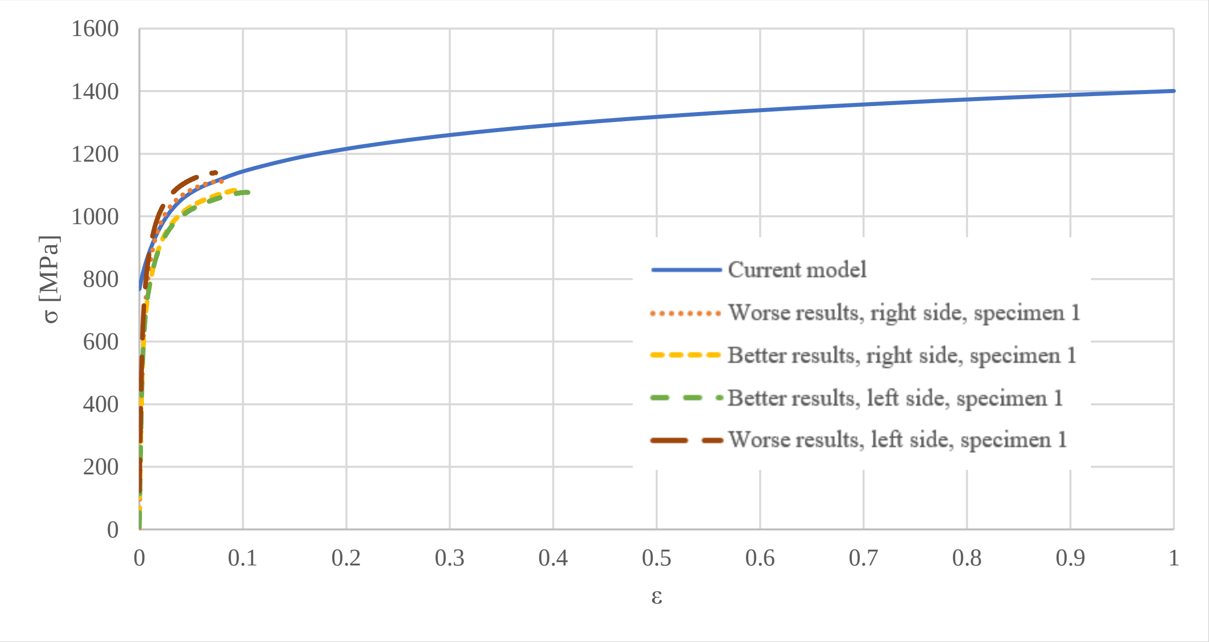

Figure 141 - True stress-strain curves from the current model and obtained in the experimental tests.

The current model seems to fit properly the hardening behavior of the material. Only one set of conditions (the left side of the coil that produced more cracked parts) is apparently more severe regarding the properties that most influence forming.

The results from the experimental tests can be used to alter the hardening curve in the material model in two ways: manually alter the current model by defining parameters like the yield strength, ultimate tensile strength, and total elongation, or import the data from the test that represents the most severe results, use the approximation option to determine the parameters for the Swift / Hockett-Sherby hardening law and extrapolate until $\varepsilon_p = 1$.

5.2.4 Conclusions of the experimental characterization

The results showed overall good repeatability. There was only one test that could not be used to determine total elongation since necking and consequent rupture occurred outside of the gage measurement length. This happened in one of the specimens from the right side of the coil that produced better results for a direction of 90º. All the specimens can be seen after rupture in Figure 142. The letters scripted in the specimens stand for: A – right side of the worse results' coil, B - right side of the better results' coil, C – left side of the better results' coil, D - left side of the worse results' coil.

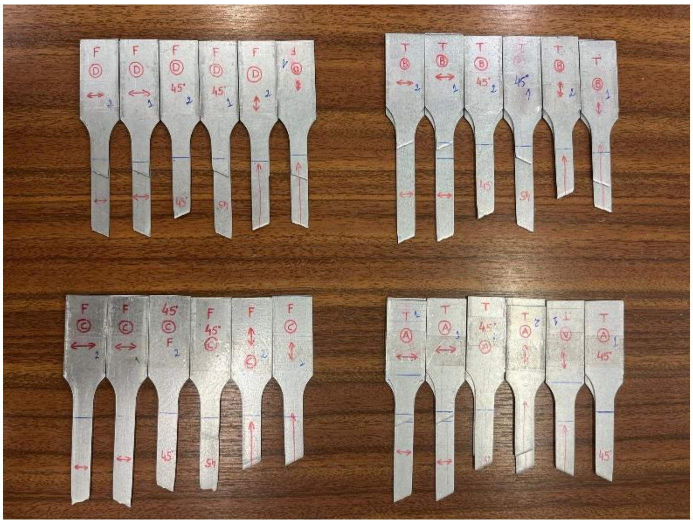

Figure 142 - Tested specimens after rupture.

Table 17 summarizes the results obtained for all the conditions tested. The numerical values of the mechanical properties represent an average of the properties of both specimens tested in those conditions.

Table 17 - Average mechanical properties obtained in the experimental results.

Coil	Side	Angle	$Rp_{0.2}$ [MPa]	Rm [MPa]	A_t [%]	E [GPa]
1/Feb **Worse results (high % of scrapped parts)**	Left	0º	758.6	1058.0	10.6	192
		45º	736.0	1039.1	12.5	190
		90º	798.9	1116.4	9.8	215
	Right	0º	776.0	1053.7	10.4	189
		45º	747.9	1056.9	13.9	190
		90º	809.1	1145.4	9.9	219
15/Feb **Better results (low % of scrapped parts)**	Left	0º	657.8	969.4	13.8	190
		45º	686.7	996.8	13.6	173
		90º	723.3	1043.1	9.6	201
	Right	0º	673.4	994.9	13.6	178
		45º	693.5	1005.2	13.3	188
		90º	720.9	1054.0	10.5	201

As it can be seen, these results quantitatively state the conclusions that were previously taken. First, there are no significant variations in properties from the left to the right side of the same coil. The variables are in general 1 or 2% different from one side to another.

Secondly, from one coil to another significant differences arise. In the rolling direction, the yield strength, ultimate tensile strength, and total elongation, vary in more than 10% (being the total elongation higher and yield and tensile stresses lower for the coil that produced better results). In the other directions these variations are of about 7 or 8%. The difference is particularly significant regarding elongation (more than 30% difference), a property usually linked to formability. Therefore, this alteration in properties from one coil to another is most likely linked to the appearance of cracks since the lower its elongation and higher the resistance, the lower its formability. This is coherent with the number of cracks found using each coil.

Another aspect that should be analysed is where these properties are located in the admissible range indicated by the client. These ranges are only specified for the rolling direction. According to the previously presented table, the yield strength of the material must be between 590 and 740 MPa, the ultimate tensile strength between 980 and 1130 MPa, and the total elongation must be higher than 10%. Regarding the coil that produced worse production results, the yield strength is above the admissible values, and the ultimate tensile strength and total elongation are very close to the limit of the range. Regarding the coil that produced better production results, the yield strength is within the range, the total elongation is way above the minimum required and the ultimate tensile strength is a little lower than the minimum admissible on the left side of the sheet.

The Young’s modulus calculated through the slope of the elastic zone of the graphs is lower than expected for the rolling and diagonal directions.

To completely describe and model the material behaviour some other parameters needed to be collected. The impact of anisotropy, for example, could not be tested. The test used to obtain this variable is the uniaxial tensile strength. However, an additional extensometer or a digital image correlation (DIC) system that enables optical 3D strain measurements were needed.

The biaxial anisotropy coefficient could be calculated using, for example, the disk compression test (stack test), the bulge test, or the biaxial test (Fedorko, Urbánek, and Rund 2017).

Furthermore, data from some more coils should be obtained so that the results could be treated statistically and properly determine the inputs in the material model. More than editing the material model, the purpose of these tests was to compare the basic mechanical properties between coils and sides of the same coil.

The most important result of this study was the impact of total elongation in the rolling direction on the appearance of cracks. In the coil that produced more cracked parts, this parameter was the minimum value required. Therefore, the low ductility of the material was impacting its formability. In the other coil, that produced better production results, this value was way above the minimum required, providing the steel with greater ductility.

It is clear that to verify these statements all the coils used in the productions should be tested and this analysis performed. Also, a chemical analysis of the coils to quantify the elements present could help find which elements most influence the mechanical properties.

In fact, during the implementation of the solutions detailed in the next chapter it was possible to run tests on one other coil that turned out to be out of the admissible ranges, namely regarding yield strength and elongation. These results were performed in different conditions from the ones described in this chapter. These conditions as well as the results can be consulted in Annex E. The results of the three coils are conclusive regarding the influence of the raw material on the appearance of defective parts.

5.3 Material model edition

As it has been stated, the material model edition is limited by the simple and few experimental tests conducted. The hardening law can be adjusted to the worst-case scenario as well as the coefficients σ_{45}/σ_0 and σ_{90}/σ_0 regarding the yield criterion. For a complete and accurate edition more types of tests and more samples should be tested so that the results could be properly statistically treated. For example, to correctly model anisotropy, the r-values are essential, and they could not be measured experimentally. Therefore, these values remain the ones from the original material model.

However, considering the worst of the conditions verified in the uniaxial tensile tests, the hardening law was adjusted considering a Swift / Hockett-Sherby approximation according to Figure 143 and Table 18. Also, regarding the coefficients σ_{45}/σ_0 and σ_{90}/σ_0, they were adjusted to the average values of the four representative tests considered in the rolling direction according to Table 19.

Table 18 - Swift/Hockett-Sherby parameters that approximate the worst-case scenario from the tests.

	ε_0	*m*	*C* *[MPa]*	σ_i *[MPa]*	σ_{sat} *[MPa]*	**a**	**p**	**α**
Swift/Hockett-Sherby parameters	0.002	0.114	1570	0.9726	0.9992	47.3	1	0.361

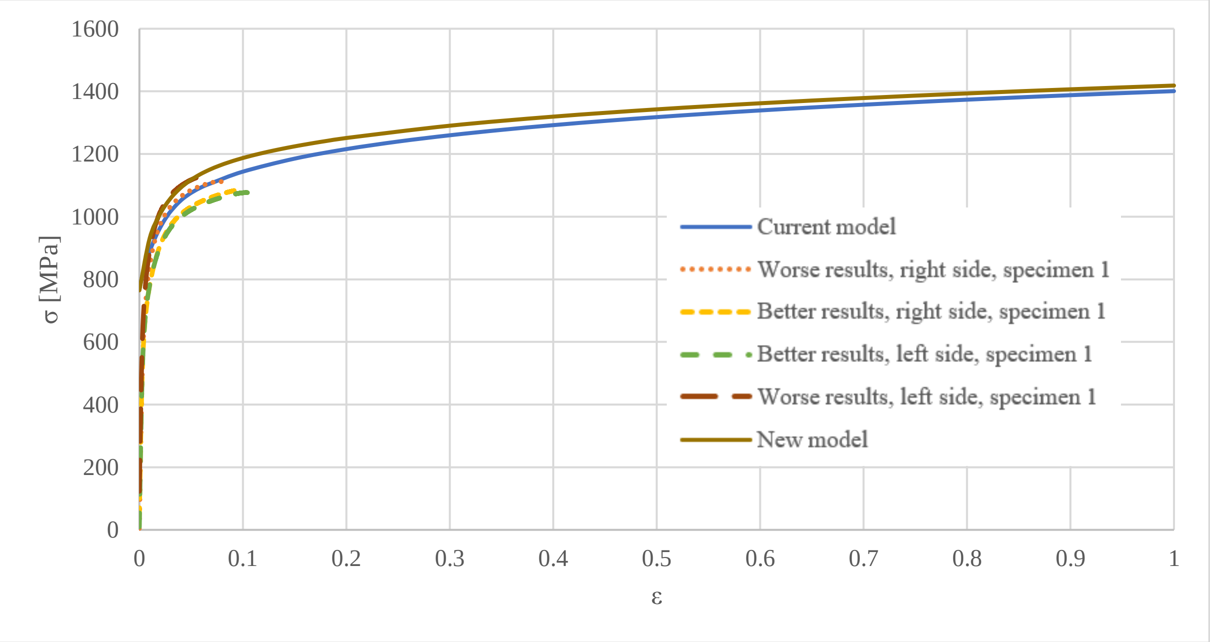

Figure 143 - True stress-strain curves from the current model, the obtained in the experimental tests and the new approximation model.

Table 19 - Important coefficients for the definition of the yield criteria.

	σ_0 [MPa]	σ_{45}/σ_0	σ_{90}/σ_0
Current parameters	767.4	0.9726	0.9992
Experimental parameters Worse results, left	758.6	0.9702	1.0531
Experimental parameters Worse results, right	776	0.9638	1.0427
Experimental parameters Better results, left	657.8	1.0439	1.100
Experimental parameters Better results, right	673.4	1.0298	1.0705
Average experimental results	-	1.0019	1.0666

6 Iterative numerical modelling and experimental implementation for problem solving

After deeply studying the industrialization process of the component and the production problem that was occurring, it was necessary to fix it as quickly as possible in order to avoid classification and associated costs. Several solutions or even combinations of solutions can be implemented in order to accelerate this process.

Since the delivery of parts was not yet being compromised, in order not to accumulate stock, these solutions were only implemented when there was the need to produce and deliver parts. This fact limited the implementation of new solutions to roughly a monthly basis. Some of these solutions could be simulated in AutoForm using the new material model before their implementation to accelerate the process and avoid implementing unfavourable solutions.

6.1 Solution 1: Removal of a label - experimental results

The first attempt, in a production that occurred at the 15th February 2023, was to remove a small label that identified the tool maker and that was by coincidence exactly in the zone of the crack. This label ended up being printed in that critical area creating extra stresses. Figure 144 shows how this label was being marked on the part.

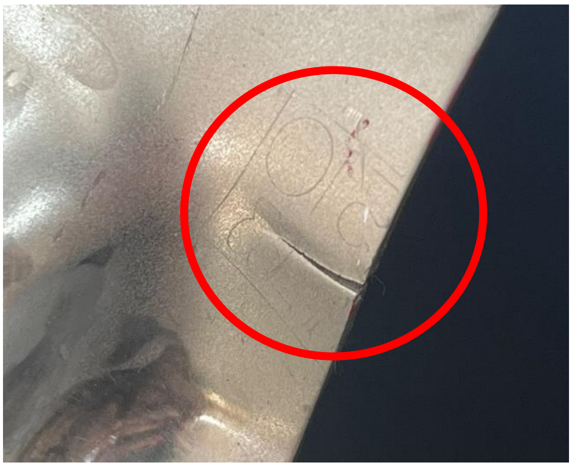

Figure 144 - Label located in the critical zone removed as an attempt to eliminate the cracks.

The only action that was taken was to sand and polish the label (present in the tool) in order to remove it and remove the mark that was adding stresses to that area of the part. It was, however, unlikely that this would solve the situation since, as the simulation showed, that area was already critical without considering the label.

Clearly that this could not be simulated in AutoForm since the label was not printed on the project and consequently it was not present on the imported CAD geometries.

During this production of 5370 pairs of parts, only 2 right-handed parts cracked. This was a tremendous improvement, representing only 0.04% of scrapped parts.

These were very good results. However, visually analyzing the quality of the cutting surface, it seemed far better than the ones from previous productions with the absence of microcracks and a greater relative thickness of the pure shear zone. This, once again, corroborated the thesis of different coils presenting slightly different properties. Since this coil was one of the tested in the previous chapter it was obvious that the good properties influenced the number of cracked parts.

Therefore, although the results were better, it was considered that the quality of this coil was clearly better. Hence it was necessary to keep monitoring the productions and even implementing more alternative solutions.

During this production and due to the good quality of the cutting surface, the cadence was even increased to 18 strokes per minute during some parts of the production.

Table 20 - Cracked parts obtained in the production of 15th Feb after implementation of solution 1.

	15/02/2023	
	5370 strokes	***Percentage***
Action	***Label***	
RH	2	0.04%
LH	0	0%

6.2 Solution 2: Smoothing radius - numerical and experimental results

During the previous production, during the control of the parts in the control gauge it was noticed that it was still possible to slightly increase the radius that define the transition between the flap and the critical zone (red radius in Figure 145, which represents the second stamping compensated punch) and still meet the desired tolerances. This alteration occurred on the right side of the second stamping operation tools since it intends to refine the final geometry.

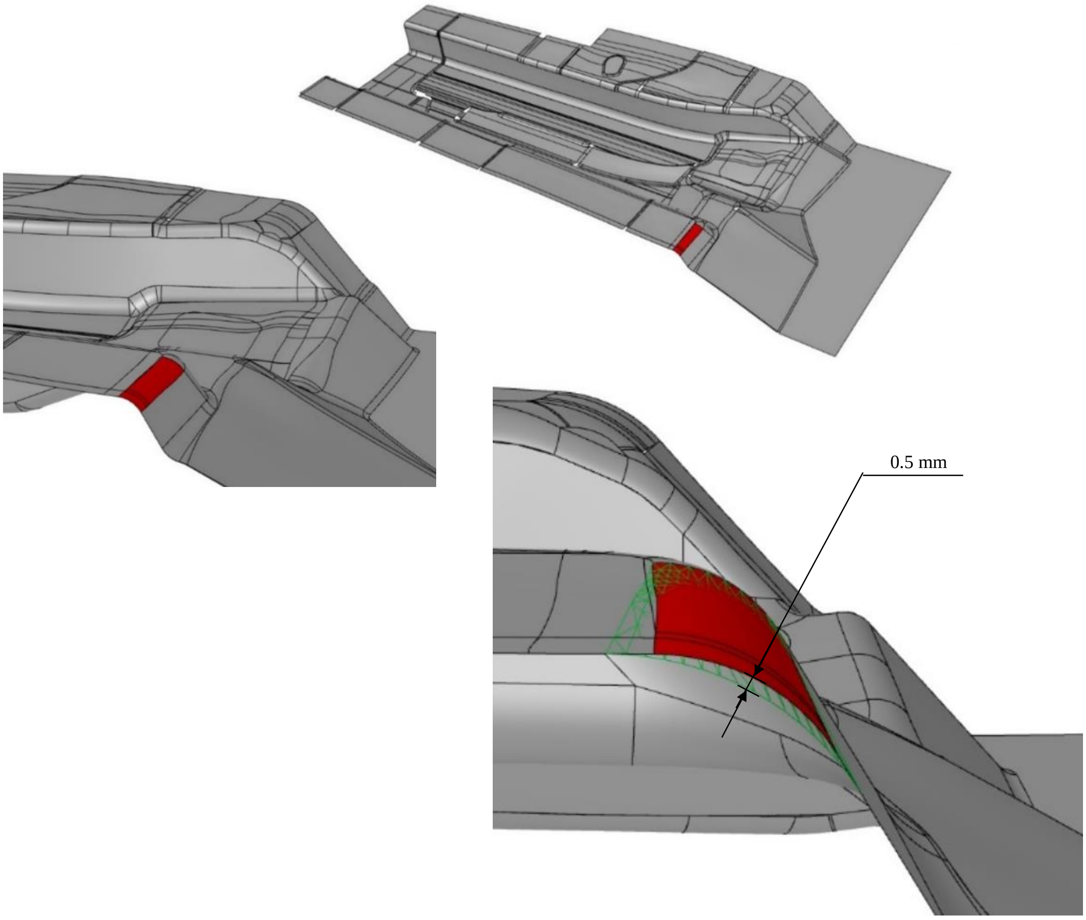

Figure 145 - Second stamping punch with highlighted smoothened radius in the critical zone as an attempt to eliminate the cracks.

Thus, in the production of the 6th March 2023 it was decided to again smoothen only this radius. Looking at Figure 145, it is noticeable that this alteration was very soft, being the maximum distance between the red (before alteration) and meshed green (after alteration) radii of 0.5 mm.

Even being a slight alteration, according to the simulation performed in AutoForm there was already an improvement in the results. Also, it was already an alteration made in several cases similar to this one since it locally reduces the stretching of the sheet. The results of Advanced Formability and the correspondent Advanced FLC are presented in Figure 146.

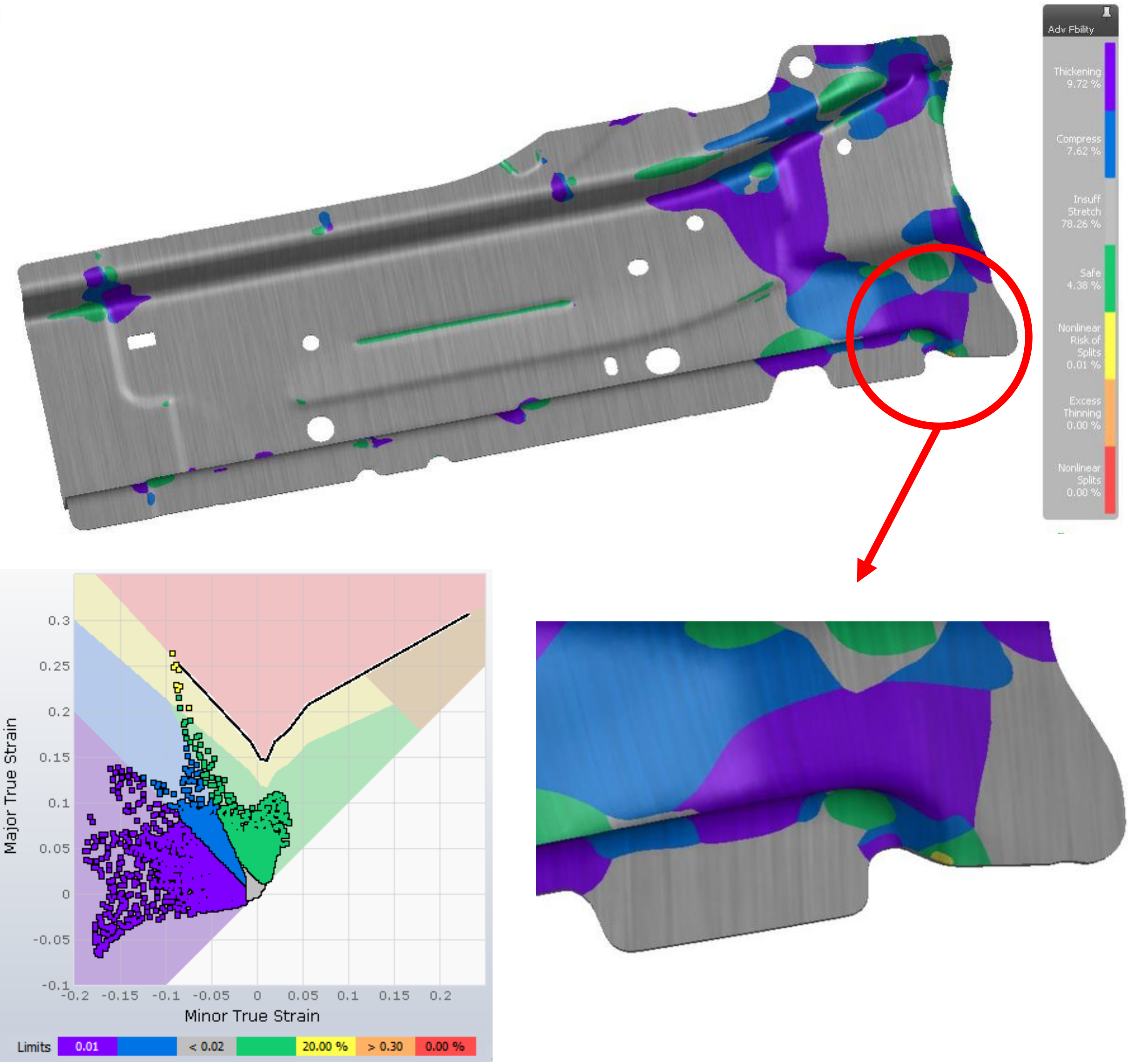

Figure 146 - Advanced formability results and points over the FLC according to new geometry with smoothened radius.

The results from Figure 146 confirm an improvement in relation to the current process. With a smoothened radius close to the critical zone, that zone of the sheet is less solicited and suffers less thinning. Despite this improvement, there are still several yellow points that represent risk of splits.

With this alteration were produced 5359 pairs of parts. On the contrary of what was expected and foreseen by the simulation, it was the greatest percentage of scrapped parts obtained after stabilizing the flap alteration. This production was also a turning point because there was a great percentage of scrapped left-hand parts which had never happened. From the 5359 pairs of parts produced, 3.68% of the right-hand and 0.9% of the left-hand parts had cracks.

Given that the alteration is clearly favorable for the correction of the problem (corroborated by experience and the simulation) and the last production was satisfactory, it is likely that this time the sheet had unfavorable properties. The fact that this time both hands presented cracks (without any alteration on the left side of the tool whatsoever) also indicates that the properties of this coil were more severe. However, no tests could be performed on this sheet and therefore it is not possible to assess if the properties are within the admissible limits.

Despite the already proven possibility of having coils with different properties that can severely affect formability, there is the possibility of having coils with admissible but limit properties. This means that the process must be robust in order to cover this possibility.

Table 21 - Cracked parts obtained in the production of 6th Mar after implementation of solution 2.

	06/03/2023 5359 strokes	***Percentage***
Action	***Geometry (radius)***	
RH	197	3.68%
LH	49	0.9%

6.3 Solution 3: Manufacturing new critical punches and dies on the right side - numerical and experimental results

After all the attempts so far, the right-side of the tool had a considerable amount of welded and machined zones, namely regarding the stamping operations. These alterations did not eliminate the problem and the welded and machined imperfections cannot be accounted for in the simulations. These can thus be introducing unnecessary residual stresses. Therefore, it was decided to manufacture a new original pair of punch and die for the first stamping operation.

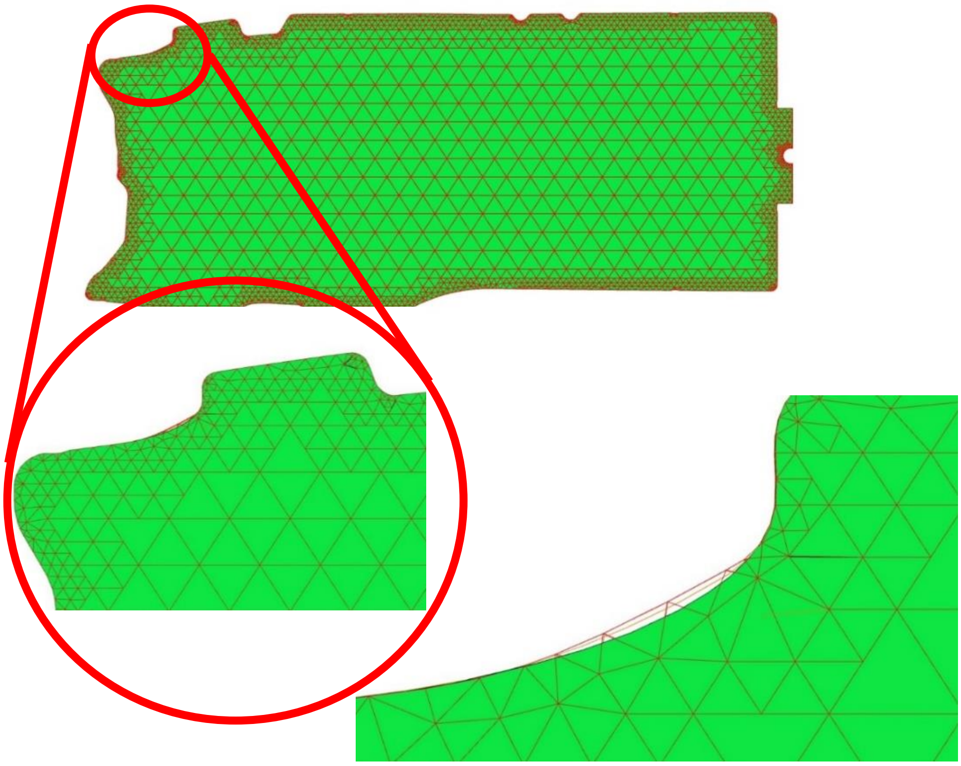

Figure 147 - New sketch geometry cutting more material than necessary as an attempt to eliminate the cracks.

Looking at the Advanced Formability results of the previous simulations, it is possible to see that the critical points were very close to the edge of the part. Therefore, in order to avoid the appearance of these points it was decided to act on the right-hand side of the tool again but this time on the trim punch and die responsible for cutting the critical zone. This action consists in the removal of more material when first cutting the crack zone (step 3 from the strip). Along with this alteration, the gap between punch and die was reduced from about 20% to about 10% to improve the quality of the cutting surface (making the pure sheer zone bigger).

Two different simulations were done removing approximately extra 0.5 mm and 1 mm of material in the critical zone. These alterations can make some points be out of tolerance. However, this is a minor problem and an acceptable risk compared to the cracks. Figure 147 compares the original sketch (red line), the removal of 0.5 mm of material (orange line) and the removal of 1 mm of material (green shape). This last one was the most promising simulation and therefore it was the implemented solution on the right-hand side.

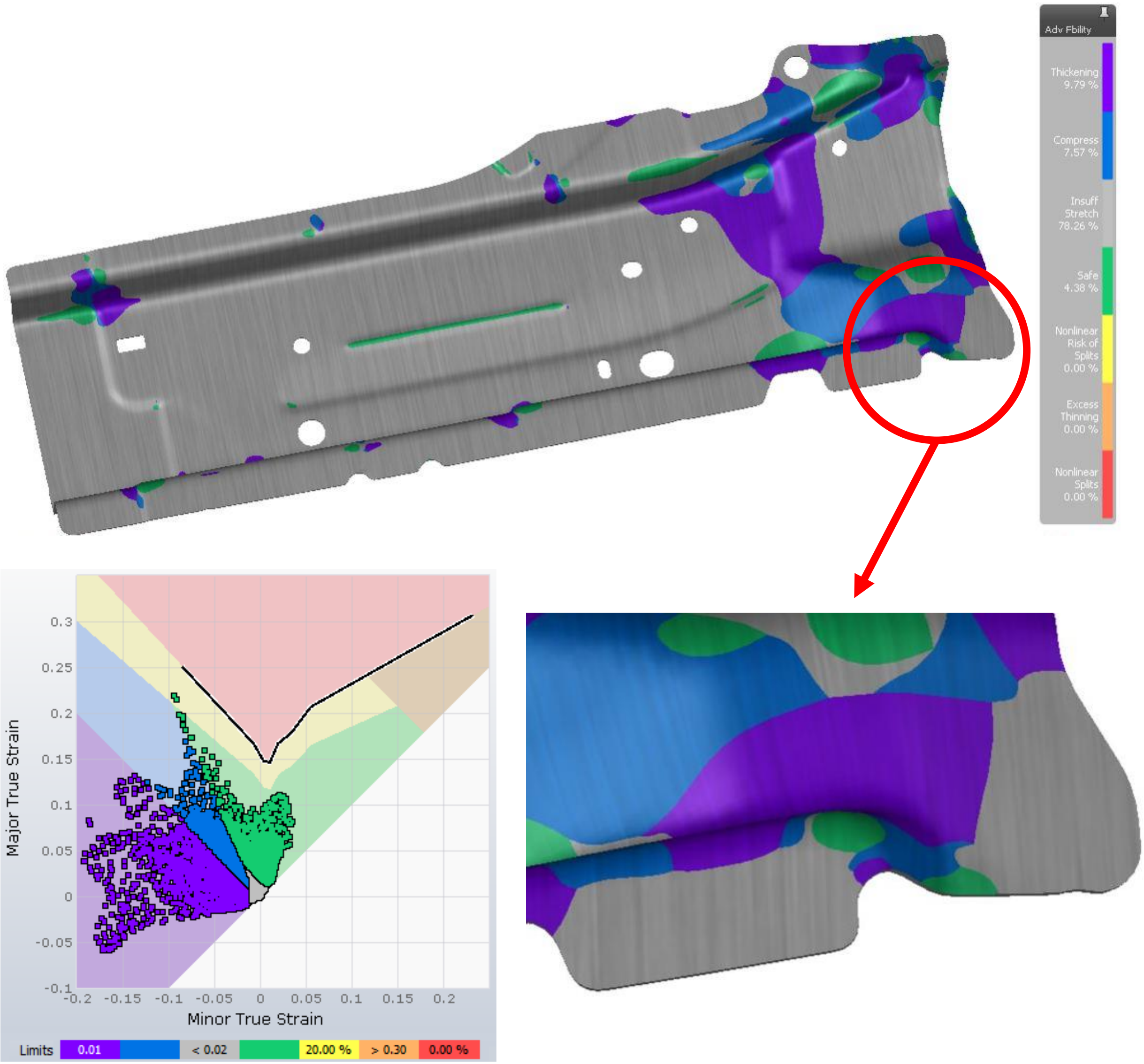

Figure 148 - Advanced formability results and points over the FLC according to new sketch geometry.

Figures 148 represent the Advanced Formability results for the implemented solution, i.e., removing 1 mm in the critical zone. The results of the simulation removing 0.5 mm of material can be found in Annex F.

It can be seen that according to the numerical simulation, this alteration in the geometry of the format eliminates the possibility of cracks. The numerical results considering this alteration were very promising.

Three productions were done with this solution using three different coils. The results of the productions were conclusive regarding the effectiveness of the alterations implemented since the first production produced a lot more cracks on the left side than on the right side. Since the alterations were only done on the right side, these results are coherent. Also, the second and third productions, done in the same exact conditions but using different coils, did not produce any cracked parts. However, it was intriguing to have such large number of cracks in one of the productions firstly because the simulation results did not point that possibility, and secondly because two other productions did not produce any defective part.

Table 22 - Cracked parts obtained in the production of 3rd Apr, 26th Apr and 15th May after implementation of solution 3.

	03/04/2023 ***5150 strokes***	***26/04/2023*** ***3740 strokes***	***15/05/2023*** ***4887 strokes***
Action	***New tools (critical RH trimming and first stamping)***		
RH	10 (0.19%)	0	0
LH	91 (1.70%)	0	0

Trying to understand if there was something wrong with the coil from the 3rd April, it was possible to conduct internal uniaxial tensile tests on samples from this coil. The conditions of the tests and their graphic results are in Annex E. The yield strength and total elongation in the rolling direction are way out of the admissible range as it can be seen in Table 23 that summarizes the results. The very low elongation justifies the high number of cracks even with the implemented improvements.

Table 23 - Mechanical properties of the coil from production of 3rd April.

Side	**Angle**	$Rp_{0.2}$ **[MPa]**	R_m **[MPa]**	A_t **[%]**
Left	0º	752.4	1071.6	7.9
	90º	783.3	1089.4	7.7
Right	0º	744.4	1068.1	7.7
	90º	781.8	1099.1	7.8

Thus, these productions also corroborated the fact that the properties of the coils can vary and can in fact cause a tremendous impact on the number of cracks found. They also proved the positive impact of the implemented alteration since the number of cracks found on the left part was higher than on the right part. Despite the great improvement, the appearance of cracks is not eliminated when the properties of the sheet are unfavorable.

The sheet supplier was warned since it was not complying with the correct properties. However, since it is not common to test the coils, it cannot be guaranteed that all the future coils will have favorable or even admissible properties. Therefore, since appearing coils with properties out of the admissible range is a possibility, it is necessary to take other measures to assure the quality of the component.

6.4 Solution 4: New format with excess material in the critical zone for posterior 3D cutting – numerical results

It is clear at this point that the critical zone where the cracks occur is always at a limit state, i.e., any punctual slight instability can be responsible of originating a crack. This means that the minimal possible alterations to the geometry (that still meet the tolerances) are essentially ineffective because it is possible to have coils with very different properties.

To guarantee a total elimination of the cracks regardless of the properties of the coil, it was studied a much more complex but way more effective solution. The idea is to deeply alter the tool in order to produce a sketch with more material than necessary in the critical area (Figure 149), so that the extra material can be cut to the final shape only after stamping. In that way, even if the cracks appear, they will appear in the material excess that will be posteriorly scrapped.

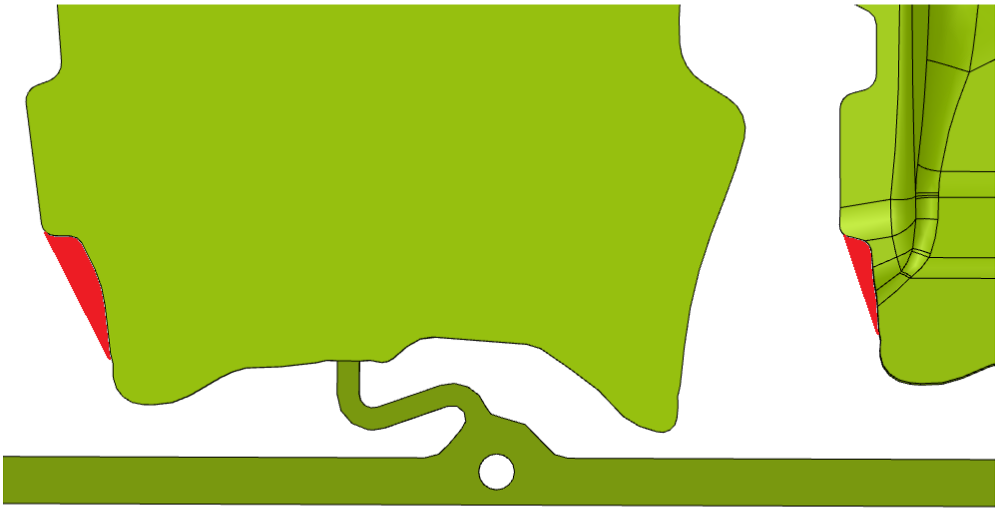

Figure 149 - New sketch geometry leaving extra material than necessary for posterior 3D cutting as an attempt to eliminate the cracks.

It is common to perform this type of operation in a transfer tool (stamping and only afterwards cutting in 3D the final shape). However, in a progressive tool, this type of operation is very complex. Even more when the tool is already done, and it is necessary to find the space to add the new components. Besides that, it is also a solution that usually involves greater maintenance costs.

The most suitable step to implement the 3D cutting tools is in step 11, as represented in Figure 150. It is the ideal step because it is the one with the space available to fit the extra necessary tools. It is also the one that involves minimal alterations to the structural elements of the tool.

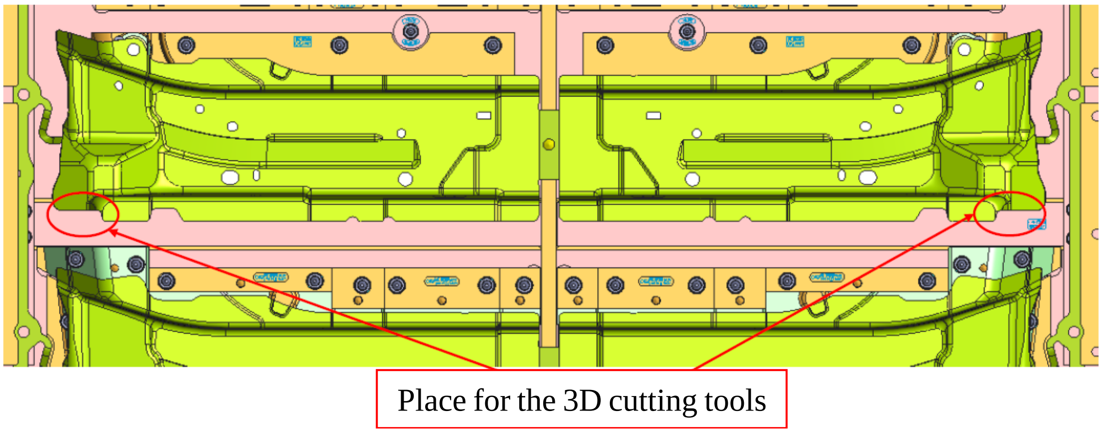

Place for the 3D cutting tools

Figure 150 - Best studied location to implement 3D cutting tools.

Also, performing this 3D trim at the same time that the holes are punched, more dimensional and geometrical accuracy is achieved. This solution also implies an alteration in the tools from the trimming step 3 in order to alter the format, leaving the extra material.

To permanently solve the problem, the alteration will be done for both right and left parts. The second stamping tools will also be minimally altered so that during this stage, the extra material left in the critical zone can follow the material flux, smoothing transitions. This alteration of the second stamping tools is also needed because those from the right side had already been altered in other attempts to fix the problem and therefore could produce burr with the implementation of solution 4. This alteration was studied in the numerical simulations, whose final results are in Figure 151.

As it is visible in that figure, the simulation is promising since not only there is not possibility of cracks but also the critical area is indicated as safe or in compression. This represents a large safety margin. However, even if the cracks appear due to a coil out of the admissible ranges, it is posteriorly cut leaving the component defect free.

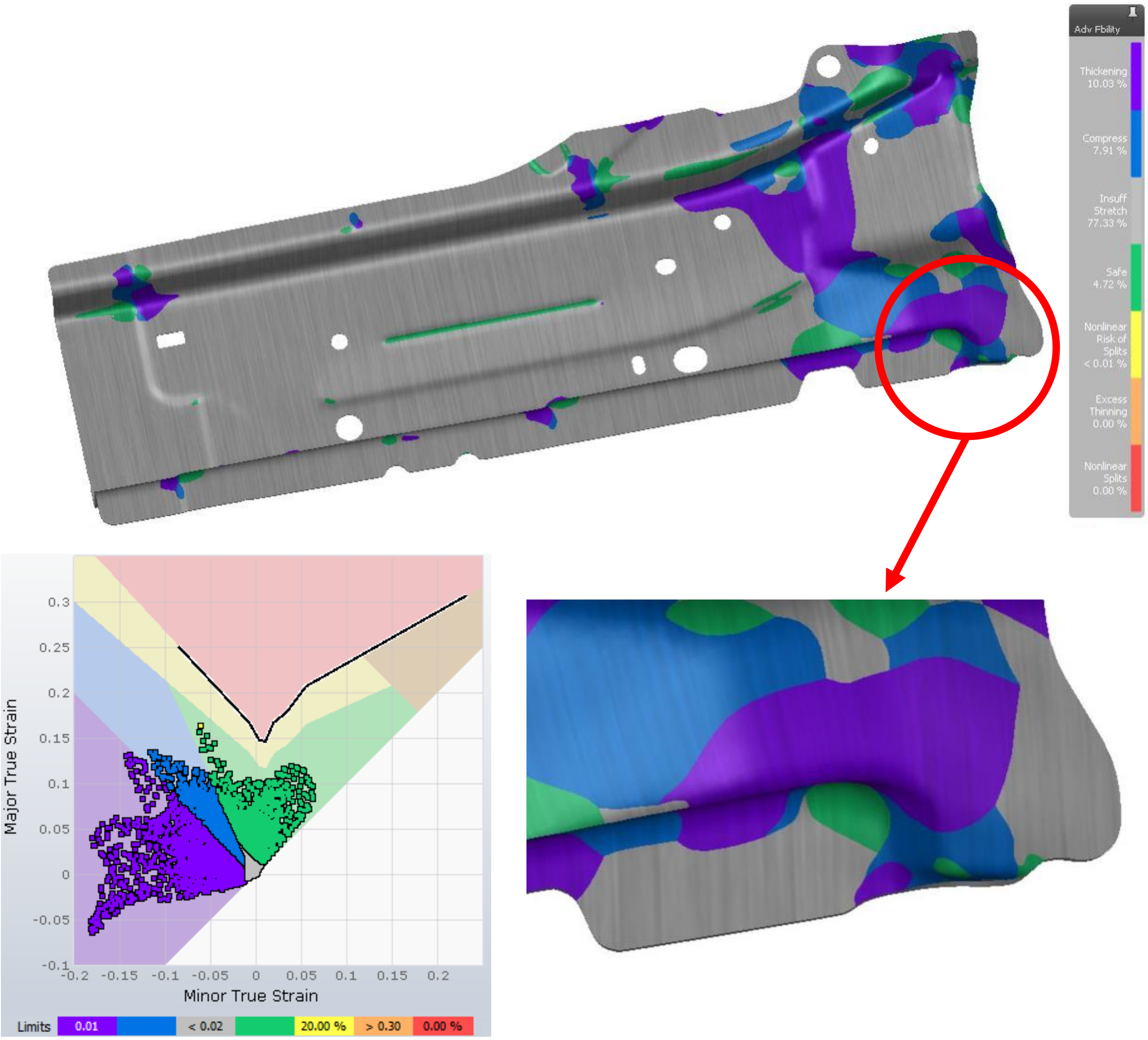

Figure 151 - Advanced formability results and points over the FLC according to defined solution 4.

6.5 Economical impact

Considering a complete elimination of the production problem according to solution 4, the batches of these parts can be removed from the classification zone. This means that they will no longer be checked twice. They will be checked only once by the worker that is storing them as soon as they leave the press.

The alteration proposed in the last sub-chapter is a considerable investment. However, by not going through classification, this investment is justifiable.

Not taking any action to solve the problem, considering an average of 2% cracked and scrapped parts, the company was losing around 14 000€ each year. This value was calculated considering the current annual cadence (132 525 pairs), the selling price of scrap (around 300€/ton), the selling price of the finished parts, the time of classification (around 3 s/part) and its hourly cost (7.5€/h).

The intern and extern alterations of the tool costed around 22 000€. This value considers the total cost of solution 4, which is made outside Gestamp by the tool maker, that is 21 000€. It also considers the intern iterative adjustments: alteration of radii, manufacture of new stamping and cutting punches and dies, alterations in the first stamping operation, etc. The cost of the intern alterations was estimated considering not only the number of hours dedicated and hourly cost of tooling and engineering department personnel, but also the same variables for the use of machines (electro-erosion, turning, milling, and grinding).

Since a project is generally developed for a minimum of 10 years of series life, it is clear that it was much more advantageous to study this problem and do the necessary corrections instead of keeping the batches in classification. The total investment is covered in about 1.5 years, which is a perfectly reasonable time.

7 Conclusions and future work

Stamping technology, as it usually happens in others, has been evolving to adapt to new non static demands. Regarding the automotive industry, safety, sustainability, and comfort are features that continuously need to be incorporated in vehicles while keeping them light. The adaptation of this technology in this particular sector relies mainly on two different fields of study: virtual manufacturing through numerical simulation of the production process as well as new high strength and high formability materials.

The utilization of finite element software in sheet metal forming industry, particularly in the automotive sector, is nowadays indispensable. These numerical tools are used during the development stage for feasibility studies and process optimization to provide the process with robustness and avoid problems or defects during series life. Moreover, even when these undesirable problems occur, software like AutoForm allow a much faster process of problem solving, iteratively testing possible virtual solutions. One of the main objectives of numerical simulation is to predict the material behavior namely regarding the unacceptable defects.

In parallel with the benefits of numerical simulations, new challenges arise due to the complexity of new materials and geometries. A group of these new materials that is now widely spread in the automotive industry is dual-phase steels. Dual-phase steels, as the name suggests, are composed of hard and brittle martensite particles embedded within a soft continuous phase of ferrite. They generally offer a good compromise between strength, weldability, and formability. However, this compromise is less stable for stronger DP steels, for example DP980. Stronger DP steels are usually steels with a greater percentage of martensite, compromising ductility and affecting elongation and consequently formability.

This thesis was focused on taking advantage of numerical simulation, using AutoForm software, to solve a production problem in Gestamp Cerveira. This production problem consisted of the appearance of cracks with an irregular frequency on symmetrical DP980 steel parts made at the same time in the same combined progressive tool. The cracks appear with an irregular pattern between coils and between sides, with a tendency for predominance in the right part.

In order to solve this problem, a first study of the industrialization process was conducted to understand the productive process (sequence of operations displayed in the strip), the simulation of the current process, the functioning principles of the tool, and the required quality parameters.

Afterwards, trying to understand the irregular frequency of the cracks, uniaxial tensile tests were performed on both sides of two different coils in three directions. The results were coherent with what was expected, i.e., the coil that produced more cracked parts was the one with the lowest total elongation and higher yield and ultimate tensile strengths. The experimental results suggest a reasonable justification for the irregular frequency of cracks between coils and also for the possible appearance of more cracks when implementing a solution that would theoretically reduce them. The results of these tests also reject the possibility of asymmetrical properties between left and right sides of the same coil, not justifying the tendency of more cracks on the right part. Several considerations regarding the constitutive models were made and the experimental results contributed to the edition of the model used in the simulations.

Later in the development of this work it was possible to conduct uniaxial tensile tests on another coil whose properties proved to be out of the admissible range, namely its yield strength and elongation. Very low total elongations were measured (around 7.8% instead of the minimum 10% required) justifying that even after some improvements made in the tool there were still appearing cracks.

Still regarding the material model, three different yield criteria (Hill 48, Barlat 89 and BBC 2005) were used and compared mainly regarding advanced formability results, memory and CPU time. The difference in results is barely significant. However, the BBC 2005 was chosen due to its documented improved accuracy.

Under the scope of this work, a sequence of four solutions was proposed to solve the production problem in order to cope with the variation of the mechanical properties of the coils. These solutions were geometric alterations to the tool focusing on the right side, keeping the other process variables unchanged. The fourth and more severe solution focuses on both sides.

Solution 3, that consisted in producing a new trim punch and die for the critical zone to remove an extra 1 mm of material, arose from the fact that previous simulations indicated the appearance of cracks very close to the edge of the format. The simulations done with this alteration indicated a great improvement with no possibility of cracks. Three productions were done with this alteration and the results helped to prove the influence of the raw material. Two out of the three productions produced zero cracked parts. However, the other produced a high percentage of cracks, 0.19% on the right side (where the alterations were done) and 1.77% on the left side (where no alterations were done).

Since the simulations indicated no possibility of cracks it was suspected that the properties of the coils were out of the admissible ranges. To prove that, more uniaxial tensile tests were done. These tests were made on this coil and proved a much lower elongation and higher yield strength than allowed, corroborating the influence of these mechanical properties on formability.

Despite the inconstant properties of the coils and the severe deviations from the imposed limits, there was no guarantee that this situation was not going to be repeated in the future. Therefore, and in order to assure the quality of all the parts during the series life, a more complex solution was proposed, solution 4. It consists in altering the productive process (sequence of operations) itself. Instead of trimming the exact necessary format, stamping, and punching, the alternative is keeping extra material around the critical zone, stamping, 3D trimming the critical zone to its final shape, and then punching. This sequence of operations guarantees the production of defect free parts according to the simulation. But even if they appear in that zone, it is in the extra material zone, which means that they are posteriorly trimmed.

In spite of being the most reliable solution, it is significantly more expensive and complex, involving also more maintenance costs. Thus, it took time to be approved and implemented, not being ready in time to confirm the results. As future work, after the implementation of this solution, two or three productions should be monitored in order to confirm the predictions.

It was of extreme importance for the company to eliminate this production problem since a lot of resources were being spent on monitoring the productions and double checking for cracks all parts individually. The reduction of cracks from around 2% (initial value) to 0 is responsible for a lot of savings for the company not only in avoiding the double inspection before shipping but also in taking this problem out of the engineering department table. After solution 4 is implemented, it is expected that the problem is solved and the parts can be immediately shipped.

This study was mainly focused on the raw material and its influence on the production outcome, i.e., the defects were assumed to derive from varying properties of the coils. Its influence is undeniable according to the experimental tests performed and the productions monitored. However, other process variables like temperature, humidity, and some tool tuning parameters, were assumed constant and may have also played a role in the appearance of cracks. For future reference, to help solving similar situations, a deeper study of the influence of these variables should be carried out.

References

Amaral, Rui Ricardo Loureiro. 2020. "Development of accurate numerical methodologies applied to the stamping of advanced high strength steels and experimental validation." Doctor of Philosophy, Department of Mechanical Engineering, Faculty of Engineering, University of Porto.

ArcelorMittal. n.d. "Dual phase steels." Accessed March 2023. https://automotive.arcelormittal.com/products/flat/first_gen_AHSS/DP.

AutoForm®. 2021. *AutoForm R10 software manual*https://servicecenter.autoform.com/smf10/en (accessed April and May 2023).

Banabic, D., H. Aretz, D. S. Comsa, and L. Paraianu. 2005. "An improved analytical description of orthotropy in metallic sheets." *International Journal of Plasticity* 21 (3): 493-512. https://doi.org/10.1016/j.ijplas.2004.04.003. https://www.scopus.com/inward/record.uri?eid=2-s2.0-6344294741&doi=10.1016%2fj.ijplas.2004.04.003&partnerID=40&md5=3110fe90890cb4fa7fc7384bd783aca1.

Banabic, D., B. Carleer, Dan-Sorin Comsa, E. Kam, A. Krasovskyy, Kjell Mattiasson, M. Sester, Mats Sigvant, and X. Zhang. 2010. *Sheet metal forming processes: Constitutive modelling and numerical simulation*.

Barlat, F., and K. Lian. 1989. "Plastic behavior and stretchability of sheet metals. Part I: A yield function for orthotropic sheets under plane stress conditions." *International Journal of Plasticity* 5 (1): 51-66. https://doi.org/10.1016/0749-6419(89)90019-3. https://www.scopus.com/inward/record.uri?eid=2-s2.0-0024775634&doi=10.1016%2f0749-6419%2889%2990019-3&partnerID=40&md5=9939ea01f16735302b4e71af29d569c4.

Bouaziz, O., H. Zurob, and M. Huang. 2013. "Driving force and logic of development of advanced high strength steels for automotive applications." *Steel Research International* 84 (10): 937-947. https://doi.org/10.1002/srin.201200288. https://www.scopus.com/inward/record.uri?eid=2-s2.0-84885401898&doi=10.1002%2fsrin.201200288&partnerID=40&md5=a92a236bbdab92d6acd850a1f36e5dea.

Bressan, J. D., J. C. Cieto, F. H. Vieira, L. S. B. Bastos, and P. A. M. Rojas. 2010. "A numerical simulation study of deep drawing testing and experimental results of steel sheets, using a comercial software." *International Journal of Material Forming* 3 (SUPPL. 1): 231-234. https://doi.org/10.1007/s12289-010-0749-5. https://www.scopus.com/inward/record.uri?eid=2-s2.0-78651594758&doi=10.1007%2fs12289-010-0749-5&partnerID=40&md5=dd466f8ed9de8183fa1f7f3a5005177e.

Davies, R. G. 1981. "Springback in high-strength steels." *Journal of Applied Metalworking* 1 (4): 45-52. https://doi.org/10.1007/BF02834345. https://www.scopus.com/inward/record.uri?eid=2-s2.0-0019342816&doi=10.1007%2fBF02834345&partnerID=40&md5=86b2e385e50c6f088e27bf6bf6a263cd.

Dezelak, M., A. Stepisnik, I. Pahole, and M. Ficko. 2014. "Evaluation of twist springback prediction after an AHSS forming process." *International Journal of Simulation Modelling* 13 (2): 171-182. https://doi.org/10.2507/IJSIMM13(2)4.261. https://www.scopus.com/inward/record.uri?eid=2-s2.0-

84921816957&doi=10.2507%2fIJSIMM13%282%294.261&partnerID=40&md5=a14db0d72eef3c52e0a24dc686f75d48.

Dias dos Santos, A., J. Ferreira Duarte, and A. Barata da Rocha. 2003. *Corte em Ferramenta*. Edited by INEGI - Instituto de Engenharia Mecânica e Gestão Industrial. Vol. 1.*Tecnologia Mecânica*. Porto: INEGI - Instituto de Engenharia Mecânica e Gestão Industrial.

---. 2005. *Tecnologia da Embutidura - Princípios e Aplicações*. Edited by INEGI - Instituto de Engenharia Mecânica e Gestão Industrial. Vol. 3.*Tecnologia Mecânica*. Porto: INEGI - Instituto de Engenharia Mecânica e Gestão Industrial.

Du, C., X. M. Chen, T. Lim, T. Chang, P. Xiao, and S. D. Liu. 2007. "Correlation of FEA prediction and experiments on dual-phase steel automotive rails." AIP Conference Proceedings.

Eggertsen, P. A., and K. Mattiasson. 2010. "On constitutive modeling for springback analysis." *International Journal of Mechanical Sciences* 52 (6): 804-818. https://doi.org/10.1016/j.ijmecsci.2010.01.008. https://www.scopus.com/inward/record.uri?eid=2-s2.0-77955232129&doi=10.1016%2fj.ijmecsci.2010.01.008&partnerID=40&md5=601a68079dd178c8077a1346ddb2dbe8.

eMachineShop. n.d. "GD&T Position Definition." Accessed April 2023. https://www.emachineshop.com/gdt-position-definition/.

Fedorko, M., M. Urbánek, and M. Rund. 2017. "Prediction of thinning of the sheet metal in the program AutoForm and its experimental verification." IOP Conference Series: Materials Science and Engineering.

Firat, M., E. Karadeniz, M. Yenice, and M. Kaya. 2013. "Improving the accuracy of stamping analyses including springback deformations." *Journal of Materials Engineering and Performance* 22 (2): 332-337. https://doi.org/10.1007/s11665-012-0257-5. https://www.scopus.com/inward/record.uri?eid=2-s2.0-84878528056&doi=10.1007%2fs11665-012-0257-5&partnerID=40&md5=b098cfba48017cd2b93776f4eb3120ac.

GD&TBasics. n.d. "GD&T Symbols Reference Guide." Accessed April 2023. https://www.gdandtbasics.com/gdt-symbols/.

Gestamp Cerveira, Lda. 2021. Gestamp Cerveira - Company Presentation. Vila Nova de Cerveira.

---. 2022. "Gestamp Cerveira - Uma viagem de transformação." *Gestamp Cerveira em Foco*.

---. 2023. Arquivo Gestamp Cerveira. Vila Nova de Cerveira.

Granbom, Ylva. 2010. "Structure and mechanical properties of dual phase steels – An experimental and theoretical analysis." Doctor of Philosophy, Division of Mechanical Metallurgy, Royal Institute of Technology, School of Industrial Engineering and Management.

Güngör, Gönül Öykü. 2019. "Microstructural modelling of dual-phase steels through polycrystalline plasticity at RVE level." Master of Science, Department of Aerospace Engineering, Graduate School of Natural and Applied Sciences of Middle East Technical University.

Hill, Rodney. 1948. "A theory of the yielding and plastic flow of anisotropic metals." *Proceedings of the Royal Society A - Mathematical, Physical and Engineering Sciences* 193 (1033): 281–297. https://doi.org/https://doi.org/10.1098/rspa.1948.0045.

Hongzhi, D., and L. Zhongqin. 2000. "Investigation of sheet metal forming by numerical simulation and experiment." *Journal of Materials Processing Technology* 103 (3): 404-410. https://doi.org/10.1016/S0924-0136(00)00453-2. https://www.scopus.com/inward/record.uri?eid=2-s2.0-0033706654&doi=10.1016%2fS0924-0136%2800%2900453-2&partnerID=40&md5=963c9ecb87cfd1d1f42ae90a1bf57af3.

IPQ. 2012. *NP EN ISO 6892-1. Materiais metálicos. Ensaios de tração, Parte 1: Método de ensaio à temperatura ambiente.*

Jadhav, Sandip, Martin Schoiswohl, and Bruno Buchmayr. 2018. "Applications of Finite Element Simulation in the Development of Advanced Sheet Metal Forming Processes." *BHM Berg- und Hüttenmännische Monatshefte* 163 (3): 109-118. https://doi.org/10.1007/s00501-018-0713-0. https://doi.org/10.1007/s00501-018-0713-0.

Katili, I. 1993. "A new discrete Kirchhoff-Mindlin element based on Mindlin-Reissner plate theory and assumed shear strain fields—part I: An extended DKT element for thick-plate bending analysis." *International Journal for Numerical Methods in Engineering* 36 (11): 1859-1883. https://doi.org/10.1002/nme.1620361106. https://www.scopus.com/inward/record.uri?eid=2-s2.0-0027608520&doi=10.1002%2fnme.1620361106&partnerID=40&md5=9e22533c3f1f92a215d26cf3875d6568.

Kubli, W., and J. Reissner. 1995. "Optimization of sheet-metal forming processes using the special-purpose program AUTOFORM." *Journal of Materials Processing Technology* 50 (1): 292-305. https://doi.org/https://doi.org/10.1016/0924-0136(94)01390-M. https://www.sciencedirect.com/science/article/pii/092401369401390M.

Kubli, Waldemar. 1995. "Prozessoptimierte implizite FEM-Formulierung für die Umformsimulation grossflächiger Blechbauteile." *Prozessoptimierte implizite FEM-Formulierung für die Umformsimulation grossflächiger Blechbauteile*.

Liao, M., J. Liu, Y. Liu, and S. Wang. 2015. "Optimal stamping direction for an automotive part." *International Journal of Advanced Manufacturing Technology* 79 (1-4): 285-297. https://doi.org/10.1007/s00170-015-6826-7. https://www.scopus.com/inward/record.uri?eid=2-s2.0-84938290983&doi=10.1007%2fs00170-015-6826-7&partnerID=40&md5=63d0dda190b82d3400d3c7a3a8fd302f.

Marzia, José António Assunção. 2020. "Influence of the yield criterion in the formability prediction on parts with complex geometry." Master of Science, Departamento de Engenharia Mecânica da Faculdade de Ciências e Tecnologia, Universidade de Coimbra.

Nilsson, Kevin. 2019. "Material modeling in Sheet Metal Forming Simulations - Quality comparison between commonly used material models." Master of Science, Faculty of Mechanical Engineering, Blekinge Institute of Technology.

Ozsoy, M., E. Esener, S. Ercan, and M. Firat. 2014. "Springback Predictions of a Dual-phase Steel Considering Elasticity Evolution in Stamping Process." *Arabian Journal for Science and Engineering* 39 (4): 3199-3207. https://doi.org/10.1007/s13369-013-0910-9. https://www.scopus.com/inward/record.uri?eid=2-s2.0-84899998235&doi=10.1007%2fs13369-013-0910-9&partnerID=40&md5=e5d949eb36c10d4e214786f00acf6f90.

Peng, C., M. Koç, and M. L. Wenner. 2008. "Experimental investigation of springback variation in forming of high strength steels." *Journal of Manufacturing Science and Engineering*

130 (4): 0410061-0410069. https://doi.org/10.1115/1.2951941. https://www.scopus.com/inward/record.uri?eid=2-s2.0-53549090706&doi=10.1115%2f1.2951941&partnerID=40&md5=daaef775e9d8db621deb783d08caa78c.

Pimentel, Anthony Michael Fernandes, José Luís de Carvalho Martins Alves, Nuno Miguel de Seabra Merendeiro, and Diana Maria Faria Vieira. 2018. "Comprehensive benchmark study of commercial sheet metal forming simulation softwares used in the automotive industry." *International Journal of Material Forming* 11 (6): 879-899. https://doi.org/10.1007/s12289-018-1397-4. https://doi.org/10.1007/s12289-018-1397-4.

Prexl, A., M. Golle, H. Hoffmann, S. Kudraß, and M. Wahl. 2010. "Experimental and numerical investigation of forming and springback behavior and the resulting effects on industrial application on a structural part in mass production." AIP Conference Proceedings.

Stadnicki, J., and I. Wróbel. 2015. "Numerical effectiveness of the simulation of an automotive body part stamping." *Advances in Mechanical Engineering* 7 (2). https://doi.org/10.1155/2014/708434. https://www.scopus.com/inward/record.uri?eid=2-s2.0-84993924977&doi=10.1155%2f2014%2f708434&partnerID=40&md5=7e8bfb3d0bd72cc2c2fa6b44d23028b9.

Stamtec, Inc. - Metal Stamping & Forming Equipment. n.d. "Servo Presses." Accessed March 2023.

Tisza, M., and Z. Lukács. 2014. "Springback analysis of high strength dual-phase steels." Procedia Engineering.

---. 2015. "Formability Investigations of High-Strength Dual-Phase Steels." *Acta Metallurgica Sinica (English Letters)* 28 (12): 1471-1481. https://doi.org/10.1007/S40195-015-0346-1. https://www.scopus.com/inward/record.uri?eid=2-s2.0-84969845542&doi=10.1007%2fS40195-015-0346-1&partnerID=40&md5=f35cf0ace3e4e413f89a196f1289e636.

Wu-rong, W., H. Chang-wei, Z. Zhong-hua, and W. Xi-cheng. 2011. "The limit drawing ratio and formability prediction of advanced high strength dual-phase steels." *Materials and Design* 32 (6): 3320-3327. https://doi.org/10.1016/j.matdes.2011.02.021. https://www.scopus.com/inward/record.uri?eid=2-s2.0-79953164526&doi=10.1016%2fj.matdes.2011.02.021&partnerID=40&md5=4a9d92669703616eec8154fccc79ec65.

Zienkiewicz, O.C., R.L. Taylor, and J.Z. Zhu. 2005. *The Finite Element Method: Its Basis and Fundamentals*. Elsevier Science.

ANNEX A: Reference dates and respective achievements in Gestamp Cerveira's history

Table A 1 - Reference dates and respective achievements in Gestamp Cerveira

Dates	***Important achievements in Gestamp Cerveira***
1995	Foundation of the company
1997	Factory opening and beginning of production.
1999	Construction of the scrap tunnels and transportation belts. Creation of the Metrology Laboratory.
2000	ISO 9001 Quality Certification.
2001	Implementation of ERP SAP. Creation of the UAPs.
2002	Construction of "Nave 2"
2003	Installation of the first robotized welding cells. Creation of the chemical products' warehouse.
2004	ISO/TS 16949 Quality Certification. ISO 14001 Environmental Certification. Start of the assembly of pedals. Implementation of automatic threading in press.
2005	Production of the first components in aluminium. Machines and equipment are redesigned in order to be safer. Implementation of automatic welding in press.
2006	Creation of the Metallography Laboratory.
2007	EMAS Certification. Implementation of welding shielding gas network.
2008	Gestamp Portugal becomes independent from Gestamp Vigo.
2009	First chassis components.
2012	Installation of the first 12 500 ton press and the first laser welding cells. Implementation of the software AutoForm.
2013	Name changes from Gestamp Portugal, Lda. to Gestamp Cerveira, Lda. Implementation of remote welding.
2014	"Best Plant" 2014 award by PSA. Oil reutilization system.
2015	"Best Plant" 2015 award by PSA.
2016	"Best Plant" 2016 award by PSA. GME Supplier Quality Excellence Award by GM. Wi-fi system in the tools. Construction of "Nave 3".
2017	"Best Plant" 2017 award by PSA.
2018	Reorganization of operations and logistics spaces.
2019	Installation of a 15.000 ton servo transfer/progressive press.
2021	"Resíduo Zero" Certification. Requalification of the scrap dock.

2022	Development of the Virtual Planner and Virtual Quality Manager software. ISO 45001 Certification. Microsoft PowerBI implementation. Implementation of photovoltaic panels on the roof.

ANNEX B: General tolerances imposed by the client

For the non-mentioned areas or holes, the general tolerances imposed by the client, visible in Figure B1, are applied.

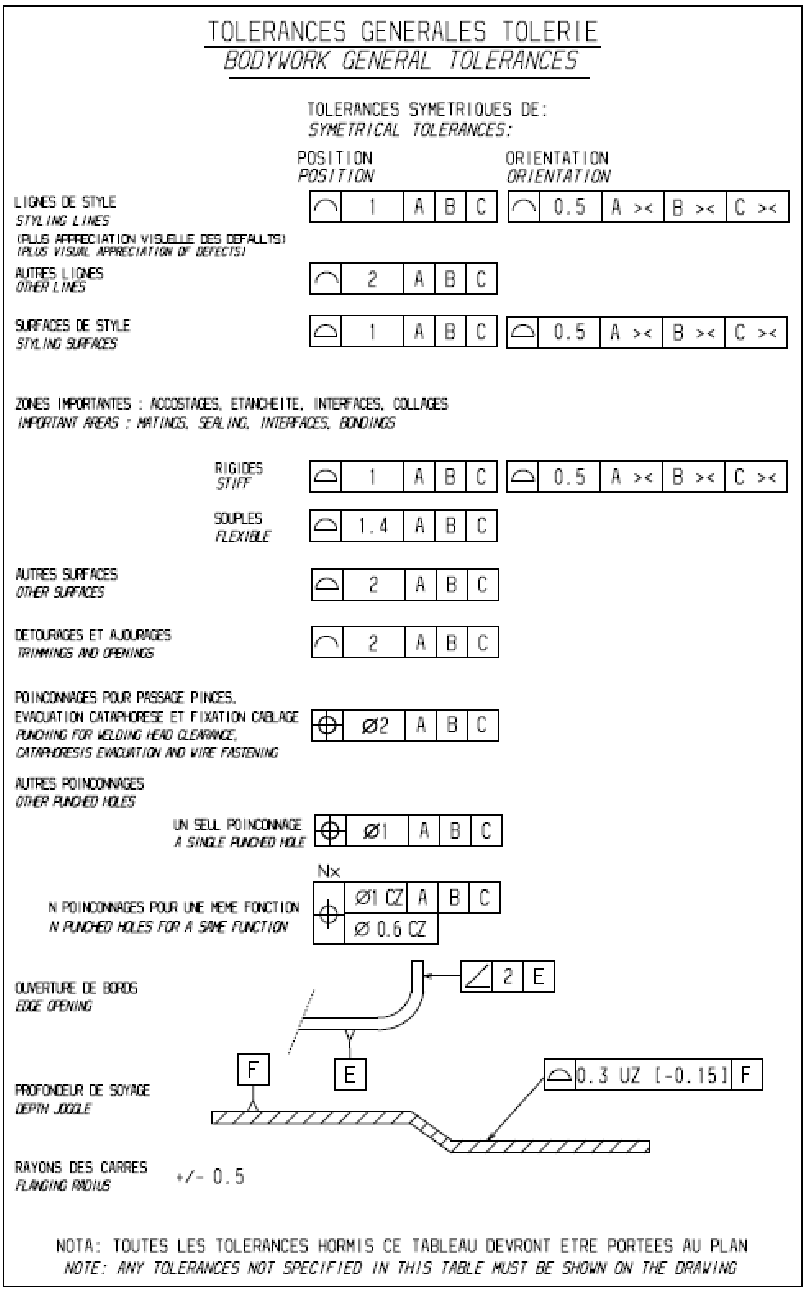
TOLERANCES GENERALES TOLERIE
BODYWORK GENERAL TOLERANCES
TOLERANCES SYMETRIQUES DE:
SYMETRICAL TOLERANCES:
POSITION
POSITION
ORIENTATION
ORIENTATION
LIGNES DE STYLE
STYLING LINES
(PLUS APPRECIATION VISUELLE DES DEFAULTS)
(PLUS VISUAL APPRECIATION OF DEFECTS)
1 A B C
0.5 A >< B >< C ><
AUTRES LIGNES
OTHER LINES
2 A B C
SURFACES DE STYLE
STYLING SURFACES
1 A B C
0.5 A >< B >< C ><
ZONES IMPORTANTES : ACCOSTAGES, ETANCHEITE, INTERFACES, COLLAGES
IMPORTANT AREAS : MATINGS, SEALING, INTERFACES, BONDINGS
RIGIDES
STIFF
1 A B C
0.5 A >< B >< C ><
SOUPLES
FLEXIBLE
1.4 A B C
AUTRES SURFACES
OTHER SURFACES
2 A B C
DETOURAGES ET AJOURAGES
TRIMMINGS AND OPENINGS
2 A B C
POINCONNAGES POUR PASSAGE PINCES, EVACUATION CATAPHORESE ET FIXATION CABLAGE
PUNCHING FOR WELDING HEAD CLEARANCE, CATAPHORESIS EVACUATION AND WIRE FASTENING
Ø2 A B C
AUTRES POINCONNAGES
OTHER PUNCHED HOLES
UN SEUL POINCONNAGE
A SINGLE PUNCHED HOLE
Ø1 A B C
Nx
N POINCONNAGES POUR UNE MEME FONCTION
N PUNCHED HOLES FOR A SAME FUNCTION
Ø1 CZ A B C
Ø 0.6 CZ
OUVERTURE DE BORDS
EDGE OPENING
2 E
E
F
PROFONDEUR DE SOYAGE
DEPTH JOGGLE
0.3 UZ [-0.15] F
RAYONS DES CARRES
FLANGING RADIUS
+/- 0.5
NOTA: TOUTES LES TOLERANCES HORMIS CE TABLEAU DEVRONT ETRE PORTEES AU PLAN
NOTE: ANY TOLERANCES NOT SPECIFIED IN THIS TABLE MUST BE SHOWN ON THE DRAWING

Figure B 1 - General tolerances imposed by the client.

ANNEX C: Results of the simulations of the current process considering the Hill 48 and the Barlat 89 yield criteria

Trying to compare the three different most used yield criteria, several results were analyzed. The simulations were run according to the current manufacturing process and keeping the hardening law and FLC constant. Apart from the advanced formability results, some other can be looked. In Figure C1 it is represented the results for the edge cracks variable. Values over 1.2 are usually alarming. Besides the critical zone where the cracks are currently appearing, two other zones are represented in red.

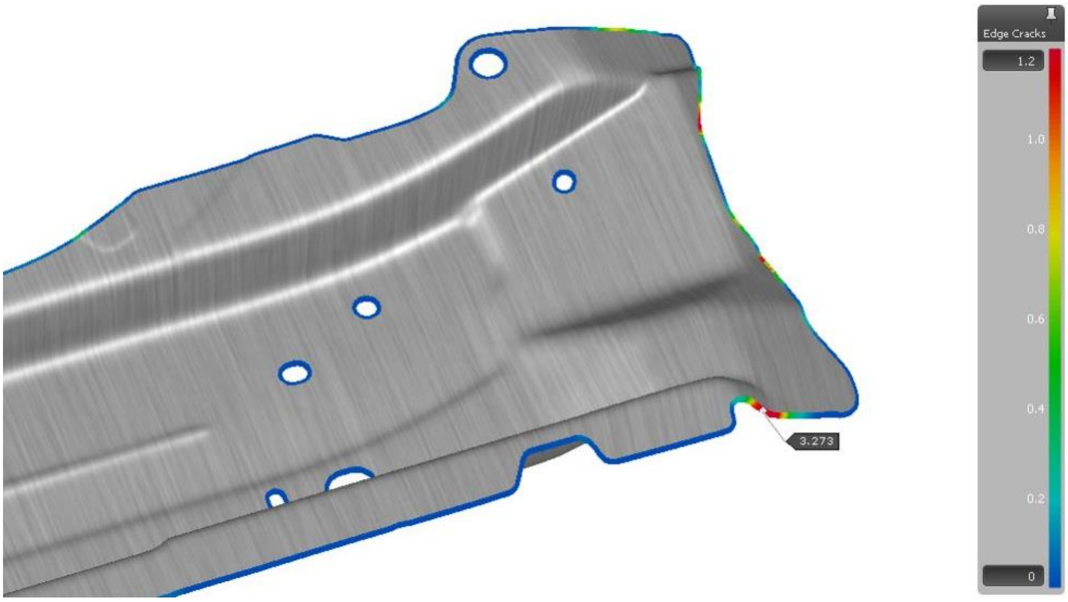

Figure C 1 - Edge crack results of the simulation of the current process considering the Hill 48 yield criterion.

Figure C2 presents the thickness results using the Hill 48 yield criterion.

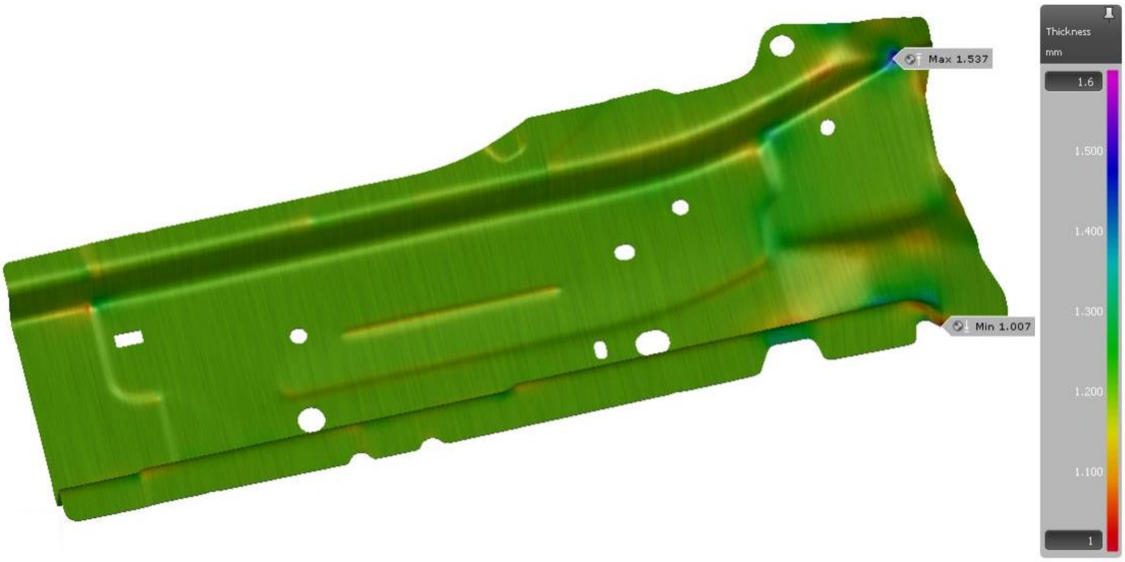

Figure C 2 - Thickness results of the simulation of the current process considering the Hill 48 yield criterion.

Lastly, regarding springback, the results using the Hill 48 yield criterion are in Figure C3.

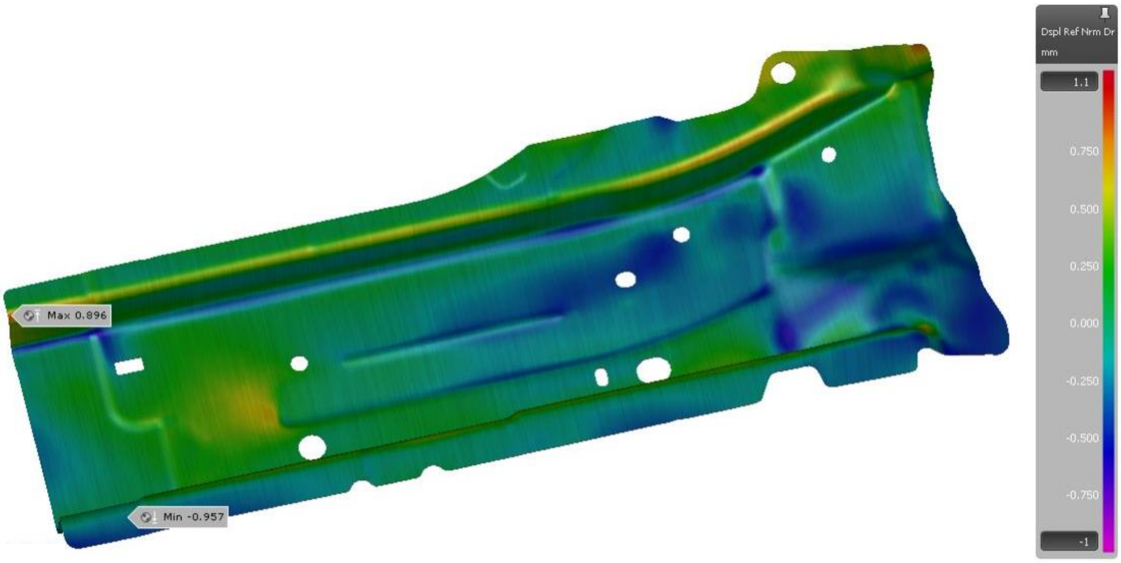
Max 0.896
Min -0.957
Dspl Ref Nrm Dr
mm
1.1
0.750
0.500
0.250
0.000
-0.250
-0.500
-0.750
-1

Figure C 3 - Springback results of the simulation of the current process considering the Hill 48 yield criterion.

When using the Barlat 89 yield criterion the results for the same variables were obtained. Regarding edge cracks, the results are presented in Figure C4.

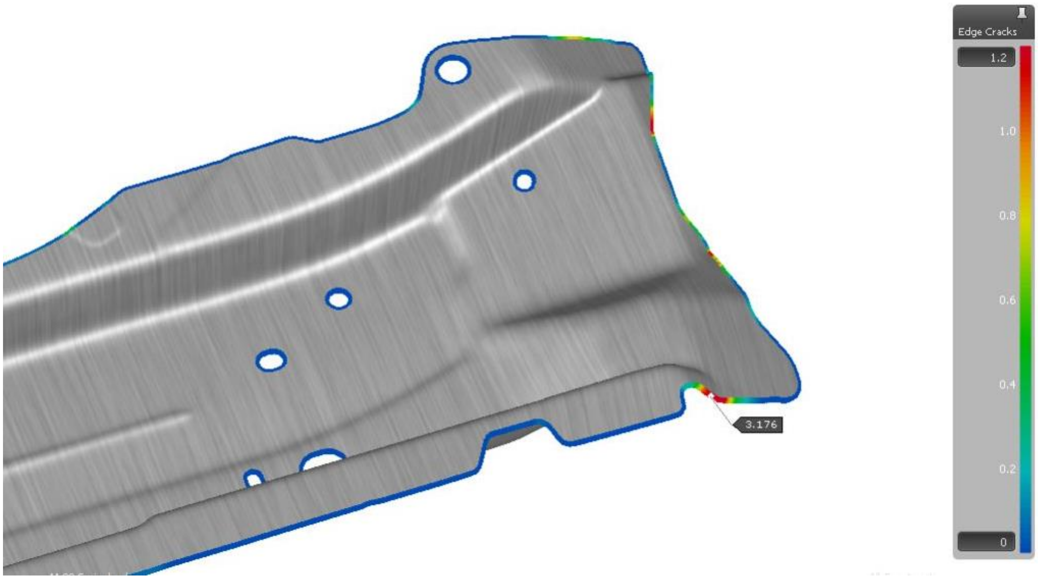
3.176
Edge Cracks
1.2
1.0
0.8
0.6
0.4
0.2
0

Figure C 4 - Edge crack results of the simulation of the current process considering the Barlat 89 yield criterion.

Regarding thickness, the results are presented in Figure C5.

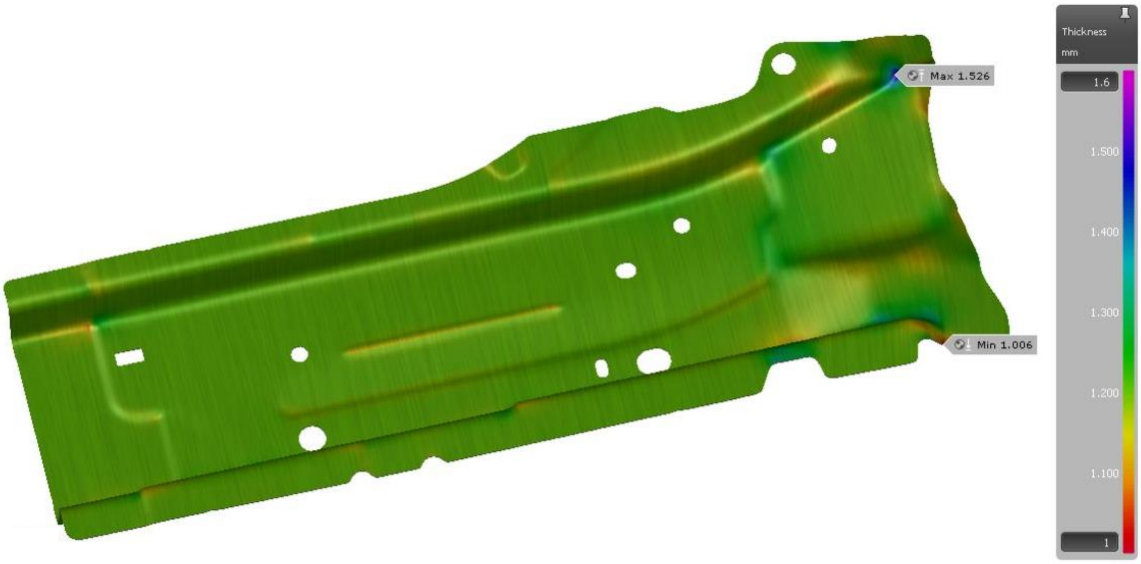
Max 1.526
Min 1.006
Thickness
mm
1.6
1.500
1.400
1.300
1.200
1.100
1

Figure C 5 - Thickness results of the simulation of the current process considering the Barlat 89 yield criterion.

Lastly, Figure C6 depicts the springback results using the Barlat 89 yield criterion. The results are very similar to those obtained using both the Hill 48 and BBC 2005 yield criteria.

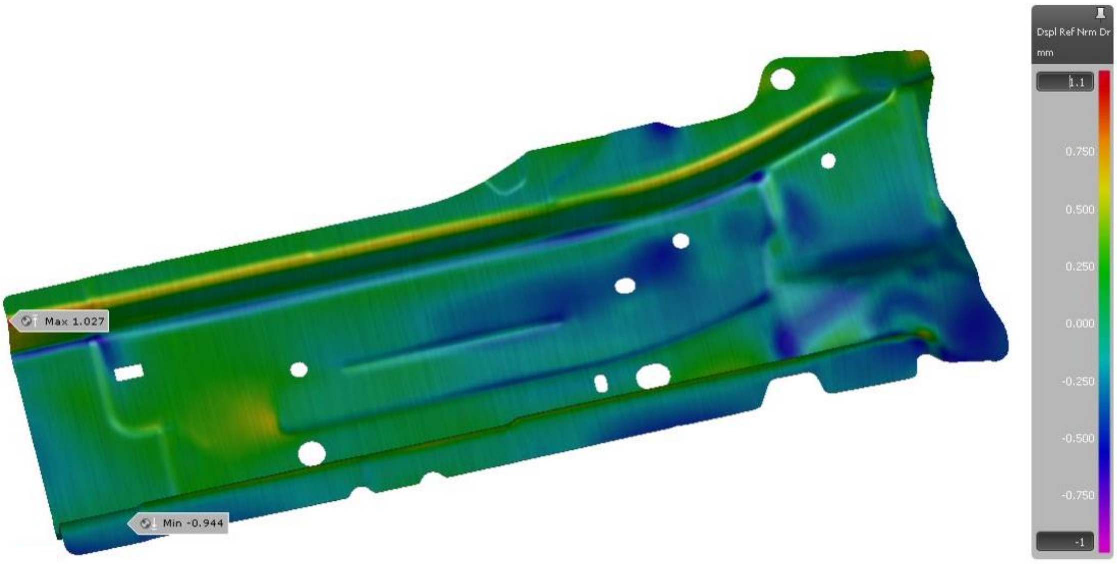
Max 1.027
Min -0.944
Dspl Ref Nrm Dr
mm
1.1
0.750
0.500
0.250
0.000
-0.250
-0.500
-0.750
-1

Figure C 6 - Springback results of the simulation of the current process considering the Barlat 89 yield criterion.

ANNEX D: Experimental results

The specimens were divided into four groups, from A to D. Each group represents a side of one of the coils. The coding of the labels is group followed by the direction relatively to the rolling direction and the number of the specimen (1 or 2, since there were 2 specimens of each).

Regarding group A the results in Figure D1 show good repeatability, i.e., the curves of specimens 1 and 2 of each direction almost coincide except for the diagonal direction.

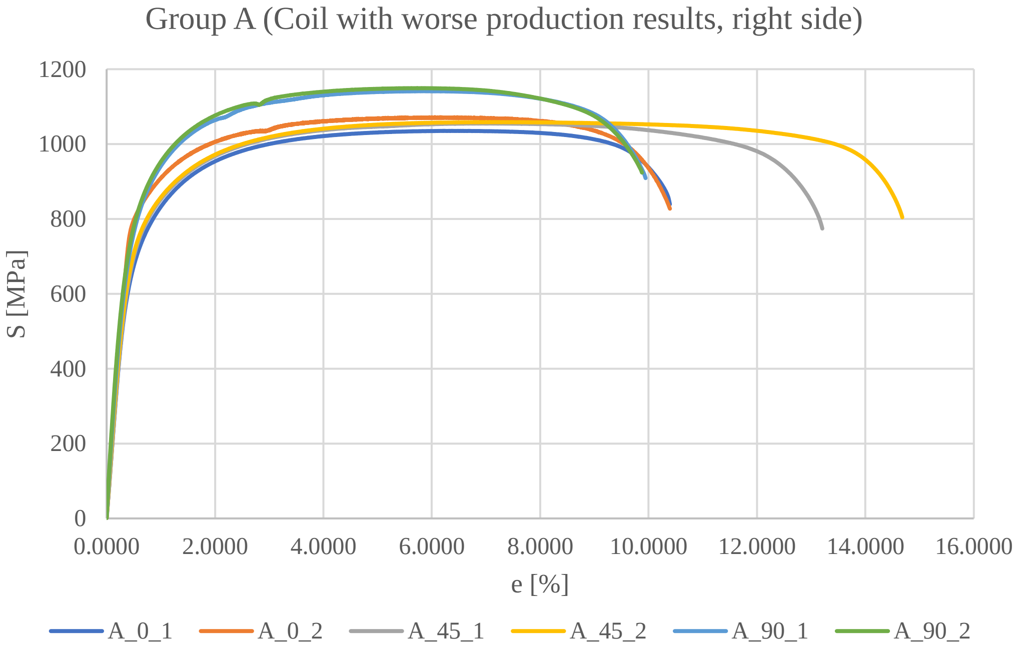

Figure D 1 - Results of the uniaxial tensile tests on the specimens from group A.

Regarding group B, the experimental results are in Figure D2. The B_90_2 test is invalid since the rupture was out of the gage length.

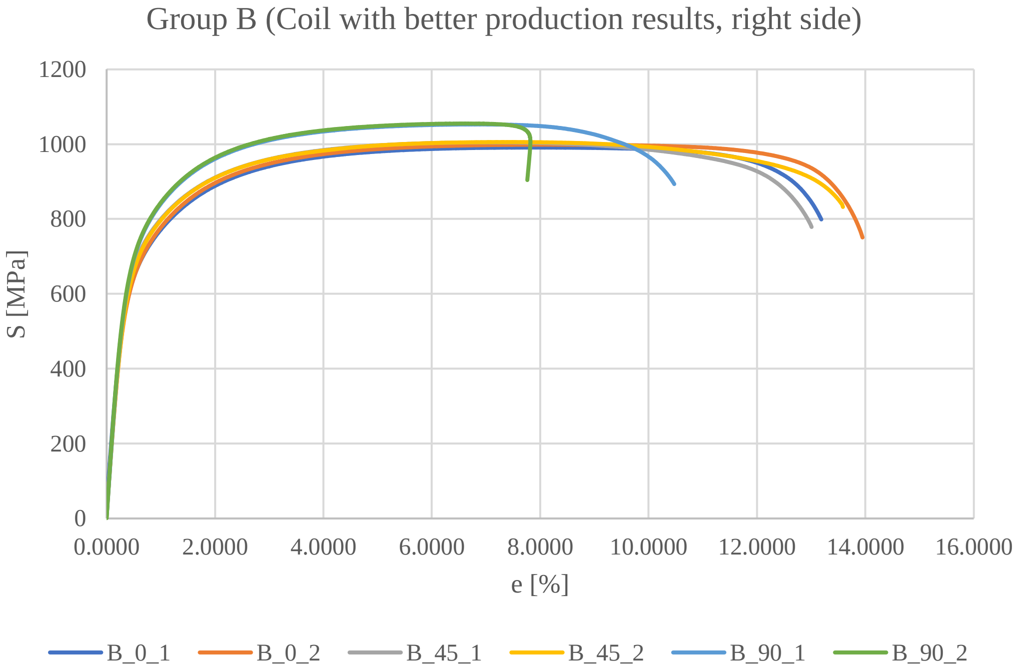

Figure D 2 - Results of the uniaxial tensile tests on the specimens from group B.

Regarding group C, the experimental results are in Figure D3.

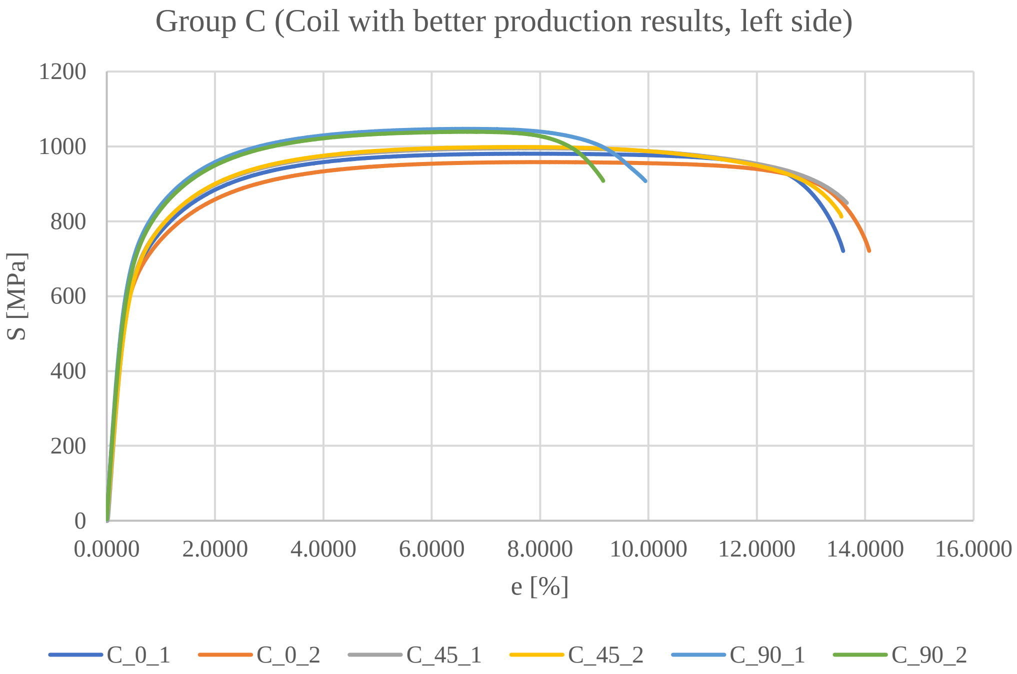

Figure D 3 - Results of the uniaxial tensile tests on the specimens from group C.

Finally, regarding group D, the results are in Figure D4.

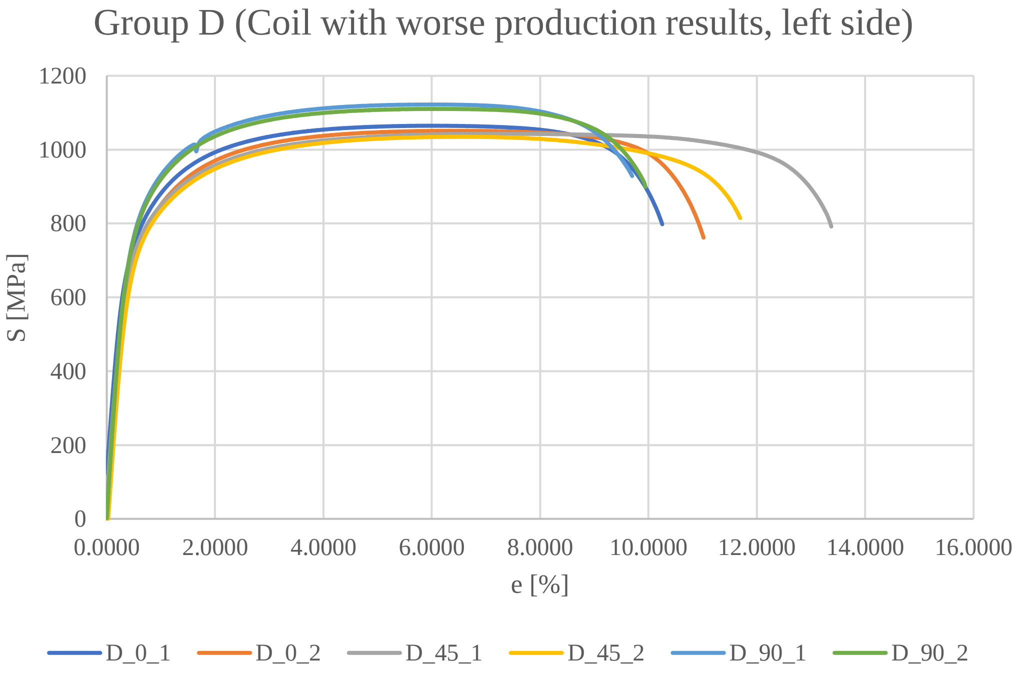

Figure D 4 - Results of the uniaxial tensile tests on the specimens from group D.

ANNEX E: Conditions and results of the uniaxial tensile tests from the coil used in the production of 3rd April

After the implementation of solution 3, a clearly favorable solution that would eliminate the appearance of cracks according to the simulations, it was obtained one production with a high percentage of cracks (0.19% on the right side where the improvements were implemented, and 1.70% on the untouched left side) and two productions with zero cracks without any alteration between them.

Given that results, it was decided to perform uniaxial tensile tests in specimens from the coil of that problematic production. The specimens were cut using an electroerosion machine from the tooling department according to NP EN ISO 6892-1, specimens of type 2 (Figure E1).

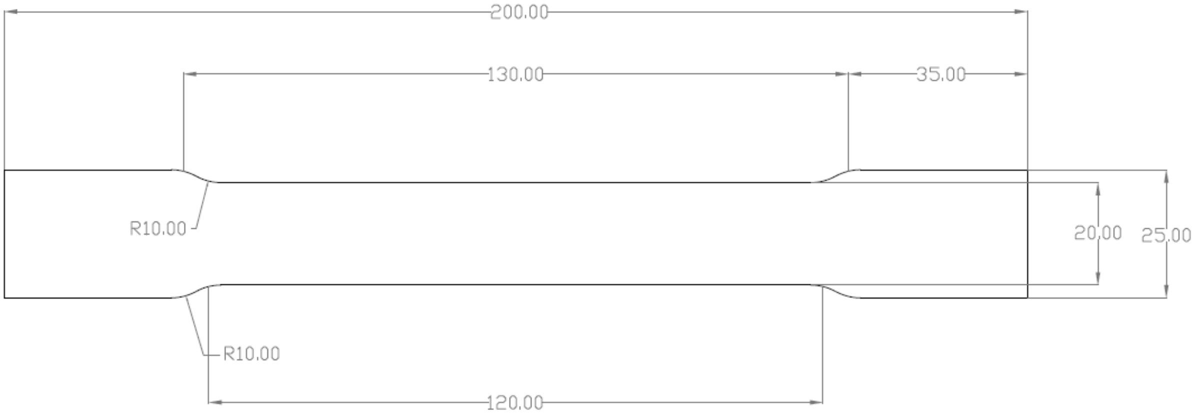

Figure E 1 - Dimensions of the specimen for the uniaxial tensile tests according to NP EN ISO 6892-1.

The machine where the tests were performed is a 150 kN hydraulic testing machine (Figure E2).

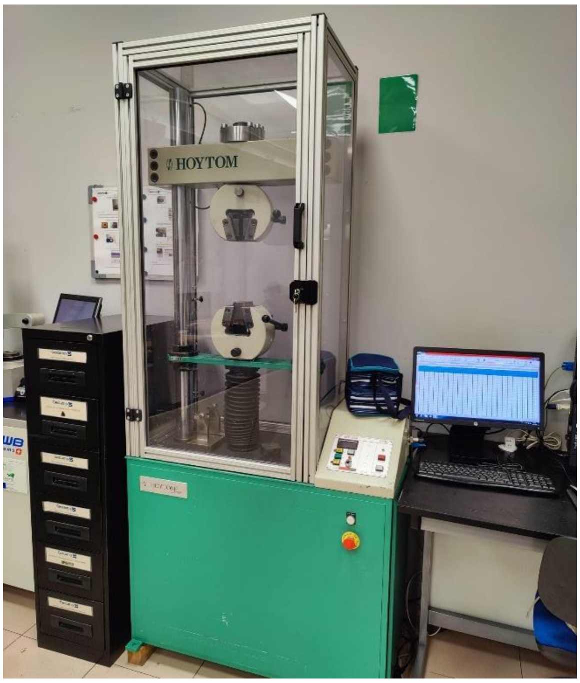

Figure E 2 - Uniaxial tensile tests machine.

Only two directions were tested, 0º and 90º, from both sides of the coil. The conditions in which the tests were conducted are in Table E1.

Table E 1 - Conditions of the uniaxial tensile tests.

Loading directions	2
Nr of experiments for each direction	2
Nr of coils	1
Nr of sides	2
Crosshead speed (grip)	8 mm/min
Data acquisition	20 Hz
Clip gage initial length - l_0	80 mm

Two specimens of each direction and of each coil were tested, the results showed good repeatability, but only one representative test of each is represented in Figure E3.

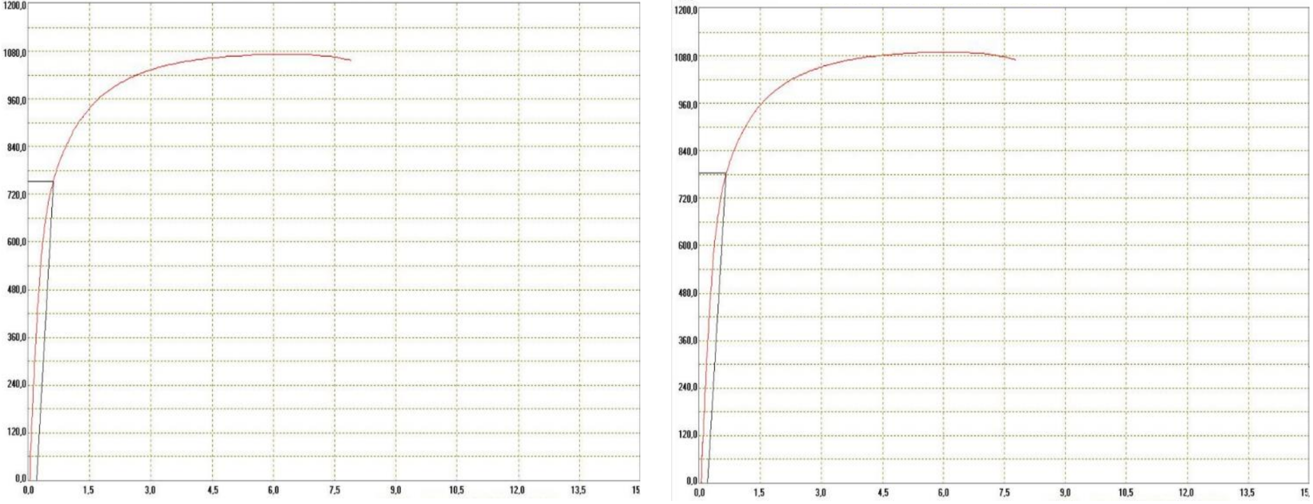

Left side, rolling direction (0º)

Left side, transverse direction (90º)

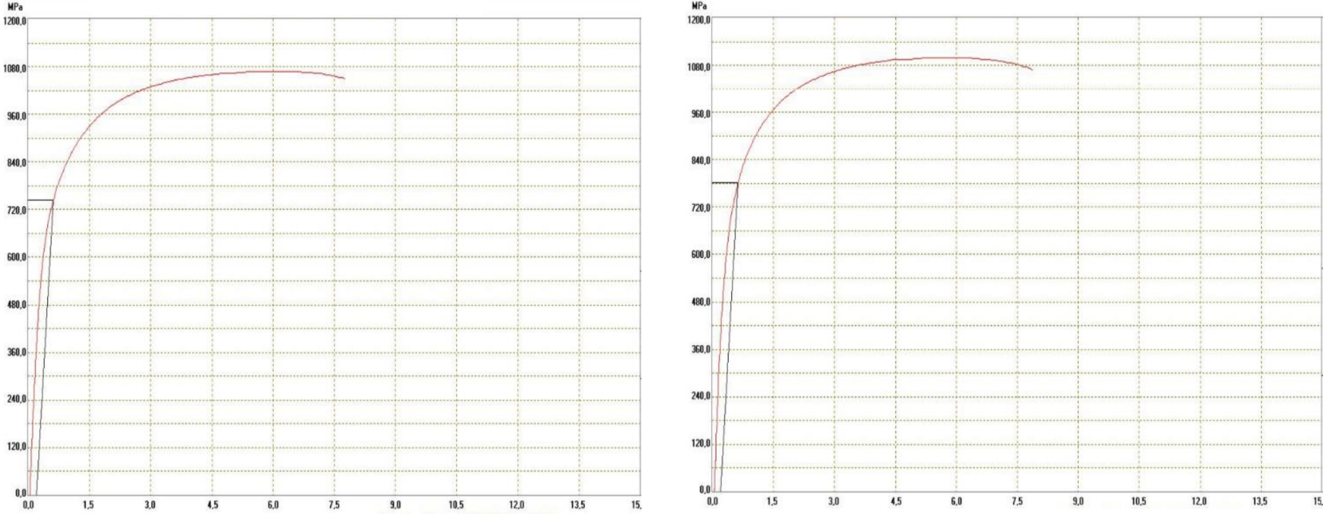

Right side, rolling direction (0º)

Right side, transverse direction (90º)

Figure E 3 - Results of the uniaxial tensile tests performed in Gestamp during the iterative problem-solving phase.

Corroborating the conclusions withdrawn from the experimental results from the other two coils, there seems to be no difference between sides of the same coils. In transverse direction, the yield strength and ultimate tensile strength tend to be higher than in the rolling direction.

This time, the yield strength and total elongation are clearly out of the admissible ranges (590-740 MPa and >10%, respectively).

The specimens after rupture can be seen in Figure E4. Indicated on the specimens are the direction relatively to the rolling direction (0º or 90º), as well as an arrow indicating the rolling direction, and the side of the coil from which they were taken (E – left or D – right).

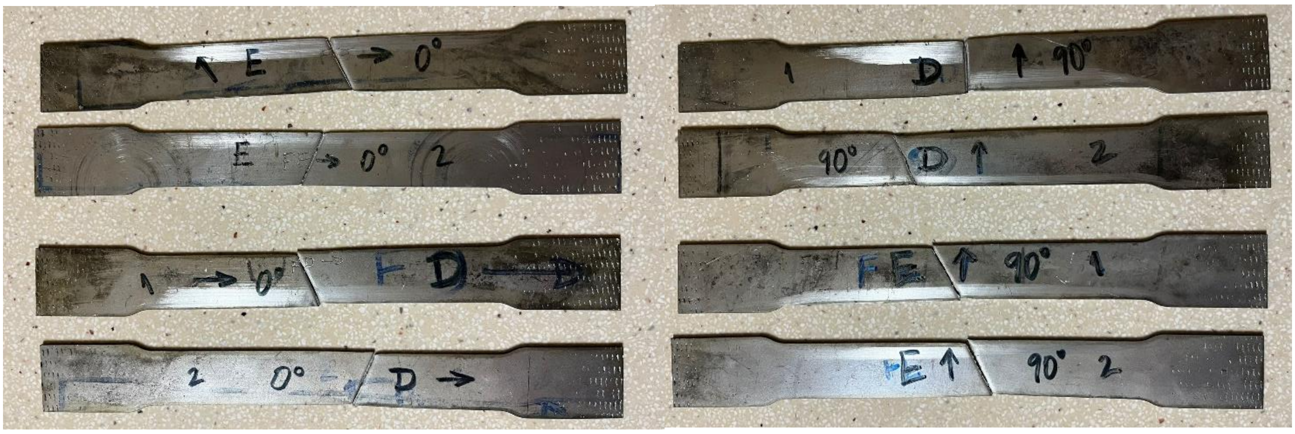

Figure E 4 - Specimens after rupture.

ANNEX F: Results of the numerical simulation with removal of 0.5 mm of material in the critical zone

Trying to optimize solution 3, it was made the simulation removing only 0.5 mm of material instead of the implemented 1 mm. That way the tolerance of the contour would most likely still be met. However, as it can be seen in the advanced formability results shown in Figure F1, there was still the possibility of splits, indicated by the yellow points in the critical zone and over the advanced FLC.

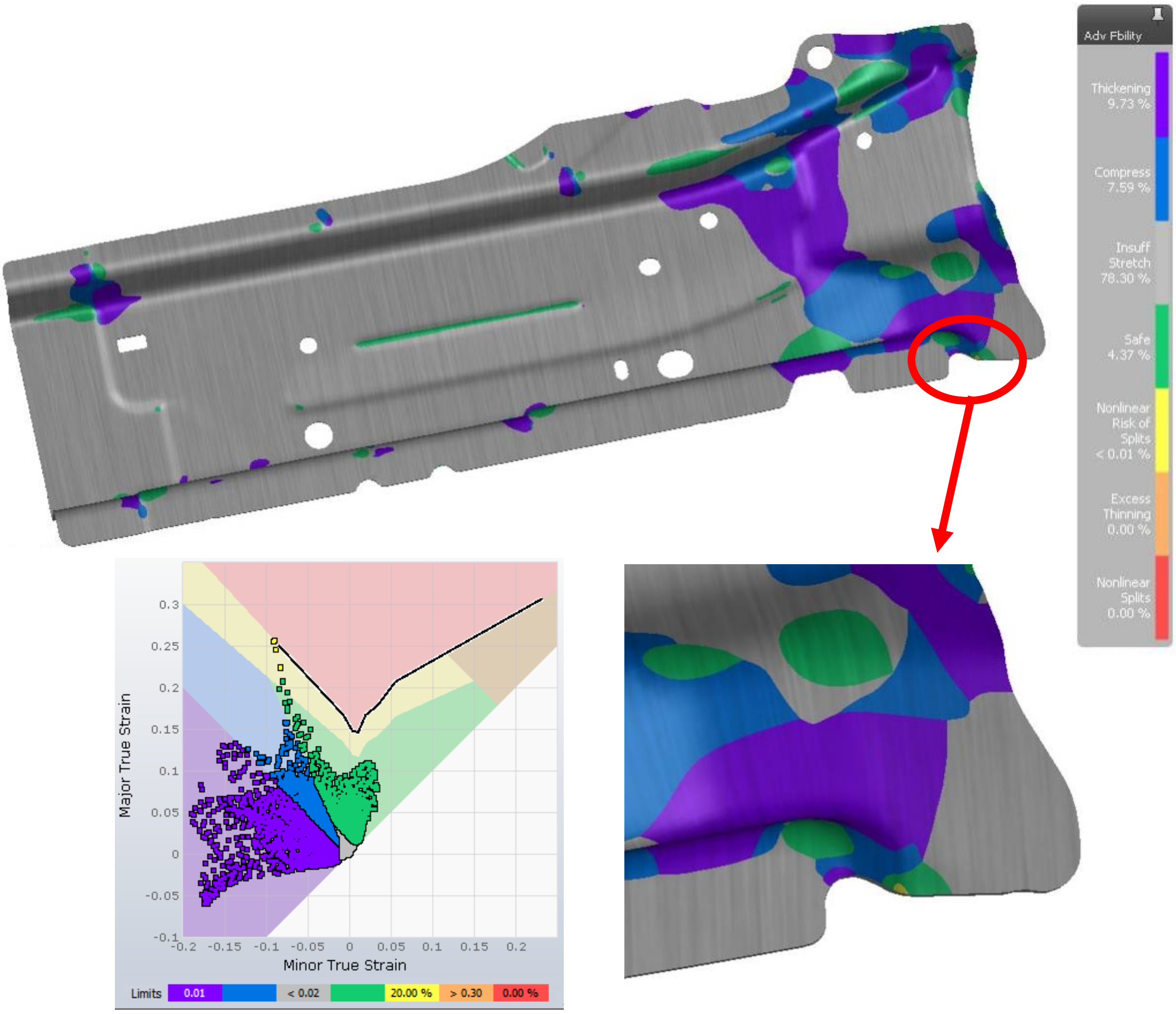

Figure F 1 - Advanced formability results and dispersion of points over the FLC with removal of 0.5 mm of material in the critical zone.